I. Extraterrestrial ^{3}He in the sedimentary record

II. Geochemistry of shield stage lavas from Kauai, Hawaii

Thesis by

Sujoy Mukhopadhyay

In Partial Fulfillment of the Requirements

For the degree of

Doctor of Philosophy

California Institute of Technology

Pasadena, California

2002

(Defended September 18, 2001)

Acknowledgements

I would like to thank Prof. Ken Farley for the invaluable guidance, encouragement, support, and opportunities he provided me as my thesis advisor. I am grateful to Prof. Peter Wyllie for supporting my research and acting as my academic advisor during my first two years at Caltech. I thank Prof. George Rossman for being my academic advisor during the latter part of my stay at Caltech and for engaging me in helpful discussions regarding my research and job search. I am grateful to Prof. Don Burnett and Prof. John Eiler for serving on my thesis committee and for the many helpful discussions and advice. I greatly appreciate the help and advice from Prof. Gerry Wasserburg and Prof. Joe Kirschvink regarding my post graduate career moves and discussions on science in general.

I am grateful for the help I received for my collaborators Dr. Alessandro Montanari (Osservatorio Geologico di Coldigioco, Italy), Dr. S. W. Bogue (Occidental College, Los Angeles, USA,) and Dr. John Lassiter (Max Plank Institute, Mainz, Germany). Dr. Montanari helped with sample collections in the Italian Apennines, and on any queries about the Italian stratigraphic record. Dr. Bogue provided the Kauai samples, and Dr. Lassiter made the radiogenic isotope measurements on the Kauai rocks and I also appreciate the discussions with him on many different aspects of Hawaiian magmatism.

I have enjoyed the numerous interactions, both on and off campus, with Ronit Kessel, Yulia Goreva, Edwin Schauble, Greg Okin, Magali Billen, Emily Brodsky, Liz Johnson, Laura Wasylenki, Matt Prichard, and Anthony Toigo. I thank my colleagues in

the noble gas laboratory, Pete Reiners, Martha House, Dave Shuster, Selene Eltgroth, Lindsey Hedges, and in particular Des Patterson, and Pete Burnard.

I greatly appreciate the support of my parents Elfriede and Dhruba Mukhopadhyay. I am thankful to my brother, Ranjan Mukhopadhyay, for his support in helping me to adjust to Caltech and life in the United States, especially during my first year. Finally, I thank my wife Sarah Stewart, for her constant support and encouragement, and to whom I dedicate this thesis.

Abstract

(I) Extraterrestrial ^{3}He in the sedimentary record

Analyses of ^{3}He, a tracer of interplanetary dust particles (IDPs), in marine carbonates from the Italian Apennines exclude large, long-lived enhancement in the IDP flux between 75 Ma and 39 Ma. These data in combination with previous ^{3}He measurements preclude recurrent comet showers with periods < 38 Myrs. The IDP accretion rate at the K-T boundary (65 Ma) is invariant and has, therefore, been used as a chronometer to estimate the duration of the K-T extinction event. Our calculation suggests that the duration of the boundary event is 10000 ± 2000 years, and the deposition time of the impact ejecta layer is less than 60 years. These results indicate that the mass-extinction at the K-T boundary was catastrophic, ruling out volcanism and sea level changes as important factors and requiring an extremely rapid faunal turnover rate.

Because extraterrestrial ^{3}He is preserved in the sedimentary record for at least 480 Ma, the ^{3}He carrier phase(s) must be chemically stable on the seafloor and resist diffusion over geologic time. Our chemical leaching and step-heating experiments indicate that the carrier phase(s) may be magnetite or more probably associated with magnetite. The association may be in the form of composite grains or nanometer thick rims.

(II) Geochemistry of shield stage lavas from Kauai, Hawaii

We measured He, Sr, Nd, Pb, and Os isotope ratios and major and trace element concentrations in shield lavas from Kauai, Hawaii. The range of ^{3}He/^{4}He ratios (17-28 R_A) measured from the Kauai shield is similar to that reported from Loihi Seamount and

is clearly distinct from other Hawaiian shield volcanoes. These results challenge the prevailing notion that high $^{3}He/^{4}He$ ratios are restricted to the pre-shield stage of Hawaiian volcanism. $^{3}He/^{4}He$ ratios in Kauai shield lavas vary erratically with stratigraphic position and on timescales of 100 years. These variations in $^{3}He/^{4}He$ ratios are correlated with variations in radiogenic isotope ratios, suggesting rapid changes in parental magma composition with time.

Our new geochemical data from Kauai shield lavas require the involvement of a depleted mantle component that is normally sampled only during the post-shield and post-erosional stages of Hawaiian volcanism. In addition, the Kauai data support the existence of a single high $^{3}He/^{4}He$ reservoir in the Earth's mantle and suggest that the proportion of the high $^{3}He/^{4}He$ component in the Hawaiian plume has varied significantly with time. The long-term evolution of the Hawaiian plume and the temporal variability recorded in Kauai lavas cannot be explained by a steady-state cylindrically zoned plume and require more complex time-varying heterogeneities.

Table of Contents

List of Tables

Chapter 1

Chapter 2

Chapter 3

Chapter 4

List of Figures

Chapter 1

Chapter 2

Chapter 3

Chapter 4

Introduction

The noble gases are unique geochemical tracers for studying a variety of processes in the Earth and planetary sciences, including the accretionary history of extraterrestrial material to Earth, irradiation record of lunar regolith and meteorites, geochemical evolution of the Earth's mantle, and formation of the terrestrial atmosphere. In this dissertation, I have investigated two major topics, primarily involving helium isotopes. The first investigation was carried out to understand the accretionary history of interplanetary dust particles (IDPs) from the Maastrichtian (Late Cretaceous) to the Eocene. The second investigation explored the mantle sources involved in Hawaiian magmatism and the geochemical evolution of the Hawaiian plume from a study of shield lavas from Kauai, the northernmost of the main Hawaiian islands.

(I) Extraterrestrial ^{3}He in the sedimentary record

Interplanetary dust particles (IDPs) are tremendously enriched in ^{3}He, compared to terrestrial matter, because of the presence of implanted solar wind helium (e.g., Merrihue, 1964; Nier and Schlutter, 1990). Accumulation of IDPs imparts high helium concentrations and high ^{3}He/^{4}He ratios to many deep-sea sediments, and the ^{3}He/^{4}He ratios can be used to fingerprint the fraction of extraterrestrial ^{3}He in the sediments. The extraterrestrial ^{3}He in sediments is most sensitive to the accretion of IDPs $\leq$ 35 μm because larger IDPs undergo frictional heating upon atmospheric entry and lose their helium (Farley et al., 1997). Like large IDPs, large bodies (> few meters in diameter) are intensely heated and vaporized upon impact and, hence, do not contribute ^{3}He to the sedimentary record. Thus, ^{3}He is a tracer of only the IDP accretion rate and, unlike

platinum group elements (e.g., Os and Ir), does not trace the total extraterrestrial mass flux or the arrival of single large impactors.

IDPs are derived from collisions in the asteroid and Kuiper belts and from active comets. The geologic record of the IDP accretion rate is a powerful tool to investigate major events occurring in the solar system, such as the dynamics and recurrence interval of collisions in the asteroid belt and comet showers (e.g., Farley, 1995; Farley et al., 1998). Alternatively, an invariant IDP accretion rate may be utilized as a constant-flux proxy to estimate instantaneous sedimentation rates (Takayanagi and Ozima, 1987; Marcantonio et al., 1996). Sedimentation rates are important in probing timescales of climate change and biological evolution, but poorly constrained over much of Earth's history, including the past few million years.

Impacts on Earth have played a major role in biological evolution and climate change, although the nature of the impactors is often debated (e.g., Alvarez et al., 1980; Hut et al., 1987). After Alvarez et al. (1980) presented evidence that the mass extinction at the K-T boundary was caused by an impact event, Raup and Sepkoski (1984) argued for a 26 Myr periodicity in mass extinctions. This was quickly followed by claims of a 28-31 Myr periodicity in the terrestrial cratering record, which led to the idea that periodic mass-extinctions are driven by periodic delivery of large impactors (Alvarez and Muller, 1984; Rampino and Stothers, 1984a,b). Because of the uncertainties associated with ages of impact craters, the statistical significance of the periodicity in the cratering record has been debated (e.g., Heisler and Tremaine, 1986; Yabushita, 1992). Nonetheless, a number of theoretical models have been put forward to explain the apparent periodicity in the extinction and cratering record, all of which invoke periodic

modulation of the Oort cloud comet flux (Alvarez and Muller, 1984; Rampino and Stothers, 1984; Hut et al., 1987). While arguments against periodic cometary impacts have been presented (e.g., Weissman, 1985), periodic modulation of the Oort cloud by galactic tides (e.g., Matese et al., 1995) apparently remains a viable mechanism for generating cyclical comet showers.

Farley et al. (1998) demonstrated that an enhanced ^{3}He accretion rate in the Late Eocene was temporally correlated with multiple terrestrial impact features, specifically the Chesapeake Bay and Popigai impact craters, and Ir anomalies in the stratigraphic record. The pattern of ^{3}He flux in the Late Eocene and close temporal association with multiple impacts is most consistent with an enhanced solar system dustiness associated with a comet shower (Farley et al., 1998). ^{3}He is the only known geochemical tool with which to identify the enhanced solar system dustiness characteristic of a large comet shower. Hence, the ^{3}He record in sedimentary rocks can be utilized to document past occurrences of comet showers, a record which would be particularly valuable for supporting or refuting the following ideas: (a) comet showers are periodic and (b) major mass extinction events on Earth are driven by comet showers.

In Chapter 1, measurements of ^{3}He in limestones from the Italian Apennines are presented. In combination with previous data, the new measurements from 75 Ma to 40 Ma provide the first high-resolution and continuous record of the IDP accretion rate from the Maastrichtian to the Late Eocene. The implications of this record for (a) variations in the flux of asteroidal and Kuiper belt IDPs; (b) the nature of the accretionary event at the K-T boundary; and (c) the recurrence interval of comet showers are discussed. Along with ^{3}He measurements, ^{4}He concentrations were also obtained from the limestones. ^{4}He

is a tracer of the temporal changes in flux and composition of terrigenous material and our record indicates the importance of ^{4}He as an indicator of continental weathering rates. Chapter 1 was recently published (Mukhopadhyay et al., 2001a). In Chapter 2, the impact event at the K-T boundary, the cause of the K-T mass-extinction and faunal recovery timescale following the mass-extinction are investigated in more detail. Chapter 2 demonstrates the power of using IDP accretion rates in constraining geologically short (1-100 kyr) events. This chapter was also published recently (Mukhopadhyay et al., 2001b).

The work presented in this dissertation, along with previous studies (e.g., Patterson et al., 1998), demonstrates the retention of ^{3}He in sediments over geologic time. What is the carrier phase(s) responsible for the long-term retention of ^{3}He in seafloor sediments? Determining the carrier phase(s) is important for understanding the long-term ^{3}He retentivity in sediments as a function of different geologic variables such as temperature and redox conditions. Previous experiments on recent sediments have suggested magnetite, and an unknown non-magnetic phase as possible carriers (e.g., Fukumoto et al., 1986; Amari and Ozima, 1988). However, magnetites in IDPs are predominantly formed from breakdown of troilite, olivine, and pyroxene during atmospheric entry heating (Fraundorf et al., 1982; Brownlee 1985), a process that should have resulted in the loss of shallowly implanted solar helium. Primary magnetite in IDPs is either absent or extremely rare ($<<$ 1% by mode; Fraundorf et al., 1982; Brownlee 1985; Bradley et al., 1988). Thus, the suggestion of magnetite as a carrier phase is problematic. In Chapter 3, the host-phase(s) responsible for long-term retention of ^{3}He in the sedimentary record is discussed. The study involves characterizing the chemical and He diffusion properties of the magnetic and non-magnetic fraction of the sediments

ranging in age from 0.5 to 55 Ma. This chapter is currently being prepared for publication.

(II) Geochemistry of shield stage lavas from Kauai, Hawaii

Variations in $^{3}He/^{4}He$ ratios in mantle-derived rocks provide valuable insights into the chemical heterogeneity of the mantle and the degassing history of the Earth (e.g., Kurz et al., 1982, 1983; Kellogg and Wasserburg 1990). Mid-ocean ridge basalts (MORB) removed from influences of hotspot volcanism have relatively uniform $^{3}He/^{4}He$ ratios of 7-9 R_A (where R_A is the $^{3}He/^{4}He$ ratio normalized to the atmospheric ratio of 1.39×10^{-6}), while $^{3}He/^{4}He$ ratios in ocean island basalts (OIBs) are more heterogeneous, varying between 8-37 R_A (Farley and Neroda, 1998 and references therein; Hilton et al., 2000). The uniformity in $^{3}He/^{4}He$ ratios in MORBs suggests a well-mixed mantle source, while $^{3}He/^{4}He$ ratios < 7 R_A in certain OIBs suggest a mantle source with lower time-integrated $^{3}He/(U + Th)$ than MORBs (Graham et al., 1992). Such a characteristic can be reasonably attributed to the presence of subducted material rich in U and Th but poor in ^{3}He.

The origin of $^{3}He/^{4}He$ ratios higher than the MORBs value, however, is more controversial. Hofmann et al. (1986) have suggested that helium is 'decoupled' from other lithophile tracers. They attributed high $^{3}He/^{4}He$ ratios in mantle-derived rocks to helium 'leakage' from the core, although no evidence or mechanism for such a process has ever been provided. Anderson (1993) proposed that high $^{3}He/^{4}He$ ratios are a result of subduction of ^{3}He-rich IDPs within seafloor sediments. However, Allegre et al. (1993) noted that the flux of ^{3}He out of the mantle far exceeds the ^{3}He flux from space, and that

He/Ne systematics of mantle rocks are not consistent with derivation from subducted extraterrestrial material. Further, diffusion measurements suggest that He in IDPs is completely removed within subduction zones (<200 km; Hiyagon, 1994). Thus, subducted ^{3}He-rich IDPs are unlikely to be the source of high ^{3}He/^{4}He ratios in mantle rocks.

Recent acquisition of combined He, Sr, Nd, and Pb isotopic data samples from Hawaii, Galapagos, Iceland, and Samoa have provided compelling evidence that high ^{3}He/^{4}He ratios found in many OIBs (up to 37 R_A) reflect a mantle source with high ^{3}He/(U + Th) (Farley et al., 1992; Graham et al., 1996; Kurz et al., 1996; Hilton et al., 2000). Given the expectation that ^{3}He is more incompatible than U and Th during mantle melting, high ^{3}He/(U + Th) indicates a less degassed mantle reservoir than the MROB source. Because 'bulk-earth' Nd, Sr, and Pb isotope ratios can be produced by mixing of depleted and enriched material, ^{3}He/^{4}He ratios may provide the best evidence for the existence of a relatively primitive undegassed reservoir (e.g., Farley et el., 1992). Demonstrating the existence of a distinct lithophile reservoir with high ^{3}He/^{4}He ratios places fundamental constraints on mantle convection models and on the geochemical evolution of the mantle, because such a reservoir would have to be largely isolated from the MORB source over Earth history (Kellogg and Wasserburg 1990; Kellogg et al., 1998). Hence, it is important to characterize the lithophile composition (e.g., Sr, Nd, Pb isotope ratios) of rocks with high ^{3}He/^{4}He ratios.

The Hawaiian-Emperor chain of volcanoes is one of the best examples of hotspot volcanism, commonly explained by thermal upwelling of deep mantle material (Morgan, 1971). Loihi seamount in the Hawaiian-Emperor chain has amongst the highest ^{3}He/^{4}He

ratios (20-32 R_A) in OIBs, while Hawaiian shield volcanoes have $^3He/^4He$ ratios dominantly < 20 R_A. Two published $^3He/^4He$ ratios of 24 R_A and 25 R_A in shield lavas from Kauai (Rison and Craig, 1983; Scarsi, 2000) suggest that Kauai lavas might have higher $^3He/^4He$ ratios than other Hawaiian shield volcanoes. Therefore, a systematic study of He, Sr, Nd, and Pb isotopic composition of Kauai lavas could better characterize the high $^3He/^4He$ component in the Hawaiian plume. Furthermore, models of the Hawaiian plume are often based on the observation that the oldest tholeiites have the highest $^3He/^4He$ ratios (e.g., Kurz et al., 1995; Kurz et al., 1996; Valbracht et al., 1996), but the helium isotopic data from Kauai suggest that this may not be a universal phenomenon. In addition, understanding the geochemistry of older Hawaiian islands, like Kauai, is important because such studies can provide insights into the long-term evolution of the Hawaiian plume.

In Chapter 4, the geochemistry of shield lavas from Kauai is presented. An integrated approach, using isotope ratios (He, Sr, Nd, Pb) and major and trace element data, is employed to (a) address temporal variations during the evolution of a Hawaiian shield volcano, (b) better characterize the high $^3He/^4He$ component in the Hawaiian plume, and (c) understand how the chemical composition of the Hawaiian plume may have evolved over the past 5 Myrs. Dr. S. W. Bogue (Occidental College, Los Angeles) provided the samples and Dr. J. C. Lassiter (Max Planck Institute, Mainz) made the Sr, Nd, Pb, and Os measurements and the work is currently being prepared for publication.

References

Allegre C. J., Sarda P., and Staudacher T. (1993) Speculations about cosmic origin of He and Ne in the interior of the Earth. *Earth Planet. Sci. Lett.***117**, 229-233.

Alvarez L., Alvarez W., Asaro F., and Michel H. (1980) Extraterrestrial cause for the Cretaceous-Tertiary extinction. *Science* **208**, 1095-1108.

Alvarez W. and Muller R. A. (1984) Evidence from crater ages for periodic impacts on the earth. *Nature* **308**, 718-720.

Amari S. and Ozima M. (1988) Extra-terrestrial noble gases in deep sea sediments. *Geochim. Cosmochim. Acta* **52**, 1087-1095.

Anderson D. L. (1993) Helium-3 from the mantle; primodial signal or cosmic dust? *Science* **261**, 170-176.

Anderson D. L. (1998) A model to explain the various paradoxes associated with mantle noble gas geochemistry. *Proceedings of the National Academy of Sciences USA* **95**, 9087-9092.

Bradley J. P., Sandford S. A., and Walker R. M. (1988) Interplanetary dust particles, in *Meteorites and the Early Solar System* (eds. J. Kerridge and M. S. Mathews), Univ. Arizona Press, Tucson, pp 861-895.

Brownlee D. E. (1985) Cosmic dust: Collection and research. *Ann. Rev. Earth Planet. Sci.* **13**, 147-173.

Farley K. A. (1995) Cenozoic variations in the flux of interplanetary dust recorded by ^{3}He in a deep-sea sediment. *Nature* **376**, 153-156.

Farley K. A. and Neroda E. (1998) Noble gases in the Earth's mantle. *Annu. Rev. Earth Planet. Sci.* **26**, 189-218.

Farley K. A., Natland J. H., and Craig H. (1992) Binary mixing of enriched and undegassed (primitive?) mantle components (He, Sr, Nd, Pb) in Samoan lavas. *Earth Planet. Sci. Lett.* **111**, 183-199.

Farley K. A., Love S. G., and Patterson D. B. (1997) Atmospheric entry heating and helium retentivity of interplanetary dust particles. *Geochim. Cosmochim. Acta* **61**, 2309-2316.

Farley K. A., Montanari A., Shoemaker E. M., and Shoemaker C. S. (1998) Geochemical evidence for a comet shower in the Late Eocene. *Science* **280**, 1250-1252.

Heisler J. and Tremaine S. (1986) The influence of the galactic tidal field on the Oort comet cloud. *Icarus* **65**, 13-26.

Hilton D. R., Thirwall M. F., Taylor R. N., Murton B. J., and Nichols A. (2000) Controls on magmatic degassing along the Reykjanes Ridge with implications for the helium paradox. *Earth Planet. Sci. Lett.* **183**, 43-50, 2000.

Hiyagon H. (1994) Retention of solar helium and neon in IDPs in deep sea sediments. *Science* **263**, 1257-1259.

Fraundorf P., Brownlee D. E., and Walker R. M. (1982) Laboratory studies of interplanetary dust, in *Comets*, (eds. L. L. Wiikening), University Arizona Press, Tucson, pp 383-409.

Fukumoto H., Nagao K., and Matsuda J. (1986) Noble gas studies on the host phase of high $^{3}He/^{4}He$ ratios in deep-sea sediments. *Geochim. Cosmochim. Acta* **50**, 2245-2253.

Graham D. W., Jenkins W. J., Schilling J. G., Thompson G., Kurz M. D., and Humphris S. E. (1992) Helium isotope geochemistry of mid-ocean ridge basalts from the South Atlantic. *Earth Planet. Sci. Lett.* **110**, 133-148.

Graham D. W., Castillo P. R., Lupton J. E., and Batiza R. (1996) Correlated He and Sr isotope ratios in south Atlantic near-ridge seamounts and implications for mantle dynamics. *Earth Planet. Sci. Lett.* **144**, 491-503.

Hofmann A. W., Jochum K. P., Seufert M., and White W. M. (1986) Nb and Pb in oceanic basalts – new constraints on mantle evolution. *Earth Planet. Sci. Lett.* **79**, 33-45.

Hut P., Alvarez W., Elder W. P., Hansen T., Kauffman E. G., Keller G., Shoemaker E. M., and Weissman P. R. (1987) Comet showers as a cause of mass extinctions. *Nature* **329**, 118-126.

Kellogg L. H. and Wasserburg G. J. (1990) The role of plumes in mantle helium fluxes. *Earth Planet. Sci. Lett.* **99**, 276-289.

Kellogg L., Hager B. H., and Van der Hilst R. D. (1999) Compositional stratification in the deep mantle. *Science* **283**, 1881-1884.

Kurz M. D., Jenkins W. J., Schilling J. G., and Hart S. R. (1982) Helium isotopic systematics of ocean islands and mantle heterogeneity. *Nature* **297**, 43-47.

Kurz M. D., Jenkins W. J., Hart S. R., and Clague D. A. (1983) Helium isotopic variations in volcanic rocks from Loihi Seamount and the Island of Hawaii. *Earth Planet. Sci. Lett.* **66**, 388-406.

Kurz M. D., Kenna T. C., Kammer D. P., Rhodes J. M., and Garcia M. O. (1995) Isotopic evolution of Mauna Loa volcano: A view from the submarine southwest rift zone,

in *Mauna Loa revealed* (eds., J. M. Rhodes and J. P. Lockwood), American Geophysical Union Monograph 92, 289-306.

Kurz M. D., Kenna T. C., Lassiter J. C., and DePaolo D. J. (1996) Helium isotopic evolution of Mauna Kea Volcano: First results from the 1-km drill core. *J. Geophys. Res.* **101**, 11781-11791.

Marcantonio F., Anderson R.F., Stute M., Kumar N., Schlosser P., and Mix A. (1996) Extraterrestrial ^{3}He as a tracer of marine sediment transport. *Nature* **383**, 705-707.

Matese J. J., Whitman P. G., Innanen K. A., and Valtonen M. J. (1995) Periodic modulation of the Oort Cloud comet flux by the adiabatically changing galactic tide. *Icarus* **116**, 255-268.

Merrihue C. (1964) Rare gas evidence for cosmic dust in modern Pacific red clay. *Ann. N.Y. Acad. Sci.* **119**, 403-411.

Morgan W. J. (1971) Convection plumes in the lower mantle. *Nature* **230**, 42-43.

Mukhopadhyay S., Farley K. A., and Montanari A. (2001a) A 35 Myr record of helium in pelagic limestones from Italy: Implications fro interplanetary dust accretion from the early Maastrichtian to the middle Eocene. *Geochem. Cosmochim. Acta* **65**, 653-669.

Mukhopadhyay S., Farley K. A., and Montanari A. (2001b) A short duration of the Cretaceous-Tertiary boundary event: Evidence from extraterrestrial Helium-3. *Science* **291**, 1952-1955.

Nier A. O. and Schlutter D. J. (1990) Helium and neon isotopes in stratospheric particles. *Meteoritics* **25**, 263-267.

Patterson D. B., Farley K. A., and Schmitz B. (1998) Preservation of extraterrestrial 3He in 480-Ma-old marine limestones. *Earth Planet. Sci. Lett.* **163**, 315-325.

Rampino M. R. and Stothers R. B. (1984a) Terrestrial mass extinctions, cometary impacts and the Sun's motion perpendicular to the galactic plane. *Nature* **308**, 709-712.

Rampino M. R. and Stothers R. B. (1984b) Geological rhythms and cometary impacts. *Science* **226**, 1427-1431.

Raup D. and Sepkoski J., 1984. Periodicity of extinctions in the geologic past. *Proc. Nat. Acad. Sci.* **81**, 801-805.

Rison W. and Craig H. (1983) Helium isotopes and mantle volatiles in Loihi Seamount and Hawaiian Island basalts and xenoliths. *Earth Planet. Sci. Lett.* **66**, 407-426.

Scarsi P. (2000) Fractional extraction of helium by crushing of olivine and clinopyroxene phenocrysts: Effects of the 3He/4He measured ratio. *Geochim. Cosmochim. Acta* **64**, 3751-3762.

Takayanagi M. and Ozima M. (1987) Temporal variation of $^{3}He/^{4}He$ ratio recorded in deep-sea sediment cores. *J. Geophys. Res.* **92**, 12531-12538.

Valbracht P. J., Staudigel H., Honda M., McDougall I., and Davies G. R. (1996) Isotopic tracing of volcanic source regions from Hawaii: decoupling of gaseous from lithophile magma components. *Earth Planet. Sci. Lett.* **144**, 185-198.

Weissman P. R. (1985) Terrestrial impactors at geological boundary events: comets or asteroids? *Nature* **314**, 517-518.

Yabushita S. (1992) Periodicity and decay of craters of the past 600 Myr. *Earth, Moon, and Planets* **5**8, 57-63.

Chapter 1: A 35 Myr Record of Helium in Pelagic Limestones from Italy: Implications for Interplanetary Dust Accretion from the Early Maastrichtian to the Middle Eocene

S. Mukhopadhyay
K. A. Farley
A. Montanari

(This chapter was reprinted from Geochimica et Cosmochimica Acta (2001), 65, 653-669; references have been updated)

Abstract – We have determined the helium concentration and isotopic composition of a suite of early Maastrichtian through middle Eocene pelagic limestones in the Italian Apennines. The results provide a 35 Myr record of the implied flux of extraterrestrial ^{3}He, which is a proxy for the accretion rate of interplanetary dust particles (IDPs).

Our measurements show that the ^{3}He flux was fairly constant in the Maastrichtian, except for possible minor increases (factor of two or less) from ~70.5 Ma to 68 Ma and at ~66 Ma, which probably reflect transient increases in the accretion rate of asteroidal and/or cometary IDPs. We find no evidence for an increase in IDP accretion at or immediately prior to the K/T boundary, implying that the K/T impact was not associated with enhanced solar system dustiness. This observation precludes the possibility that the K/T impactor was a member of a major comet shower, and is more consistent with impact of a lone comet or asteroid. Our data suggest a 2-4 fold increase in IDP accretion between 57 and 54 Ma, followed by a factor of three decrease over an ~4 Myr period in the early to middle Eocene. The duration and magnitude of this variability is inconsistent

with previous observations attributed to a shower of long period comets, and is more likely the result of collisions in the asteroid belt/and or Kuiper belt. In the entire 35 Myr record we find no evidence for major enhancements of the IDP accretion rate of the type expected from comet showers. Our results, in combination with earlier ^{3}He measurements, do not support models that predict recurrent comet showers with periods of <38 Myrs. If there is a periodicity in the cratering record that is caused by periodic modulation of the Oort cloud, it is not evident in the Apennine sediment data.

Along with the ^{3}He measurements we also obtained ^{4}He concentrations, which record temporal changes in the flux or composition of terrigenous matter. The most significant change in ^{4}He occurs in the last 4 Myrs of the Cretaceous, over which the concentration of ^{4}He in the detrital component rises by 300%. This rise tracks a strong increase in the seawater $^{87}Sr/^{86}Sr$ ratio, suggesting a globally significant change in the composition of continental detritus delivered to the oceans, possibly arising from increased continental weathering.

1. Introduction

Accumulation of interplanetary dust particles (IDPs) enriched in implanted solar wind, solar flare and solar energetic particles (Merrihue, 1964; Ozima et al., 1984; Nier and Schlutter, 1990; Farley, 1995) imparts high helium concentrations and $^{3}He/^{4}He$ ratios to many deep-sea sediments. Extraterrestrial He is preserved in the sedimentary record for geologically significant periods (Hiyagon, 1994; Farley, 1995) and at least in one instance for 480 Myrs (Patterson et al., 1998). The long-term retention of extraterrestrial He in the sedimentary record provides the potential to characterize the delivery history of

IDPs over geologic time (Takayanagi and Ozima, 1987), and several recent studies have investigated this application (Farley, 1995; Farley et al., 1998; Patterson et al., 1998).

IDPs are derived from the asteroid belt, active comets and the Kuiper belt (Nier and Schlutter, 1990; Liou et al., 1996; Flynn, 1999), and presently accrete to the Earth at a rate of about 40×10^6 kg/yr (Love and Brownlee, 1993). These particles range in size from a few μm to a few hundred μm in diameter (Love and Brownlee, 1993), but most IDPs >35 μm in diameter suffer severe atmospheric heating and He loss (Farley et al., 1997). While occasional large IDPs (50 μm or even larger) collected from the Earth's surface retain some He (Stuart et al., 1999), these particles likely arise from statistically rare conditions such as low entry velocity or angle. Quantitative modeling of entry-heating coupled with observations of seafloor sediments indicates that ^{3}He is predominantly delivered as a surface-correlated component in particles between ~3 and 35 μm diameter (Farley et al., 1997). Like large IDPs, large bodies (>few meters in diameter) are intensely heated and probably vaporized, so they do not contribute substantial amounts of He to the seafloor either. ^{3}He is, therefore, a tracer of only the IDP accretion rate, in contrast to other common extraterrestrial indicators, such as Ir and Os (e.g., Peucker-Ehrenbrink, 1996), which trace the total extraterrestrial mass flux.

Importantly, He accumulating in sediments does not derive from asteroidal, Kuiper-belt, and cometary sources in direct proportion to their abundance in the zodiacal cloud. There is a strong bias toward terrestrial accretion of asteroidal and Kuiper-belt particles over cometary particles, owing to their lower geocentric encounter velocity (Dermott et al., 1996; Kortenkamp and Dermott 1998a; Flynn 1989). Dermott et al. (1996) and Kortenkamp and Dermott (1998a) have argued that a large fraction of IDPs

presently accreting to Earth are asteroidal in origin. However, it is likely that the relative proportions of asteroidal and cometary IDPs have varied in presently unknown ways over geologic time due to the transient nature of dust sources. The terrestrial accretion rate of IDPs responds rapidly to changing dustiness in the inner solar system because Poynting-Robertson (P-R) drag causes IDPs to be swept into the sun in ~10^4 to 10^5 years. There are no known mechanisms to buffer the temporal changes in dust production over million year timescales. Therefore, passage of comets or showers of comets into the inner solar system, or major collisions in the asteroid belt or Kuiper belt, are likely to change the total mass accretion and the relative proportions of the IDP components.

^{3}He accumulation in sediments is a sensitive indicator of these phenomena. For example, Farley et al. (1998) reported a long-lived increase in ^{3}He flux in late Eocene sediments containing Ir, shocked quartz, and Ni-rich spinels (Montanari et al., 1993; Clymer et al., 1996; Pierrard et al., 1998), and proposed the occurrence of a shower of long-period comets. Although previously suggested on the basis of orbital dynamics and statistical analysis of the ages of impact craters (Hut et al., 1987), ^{3}He provides the only known record of the enhanced solar system dustiness characteristic of a large comet shower. The geologic history of IDP accretion can therefore provide insights to major events in the solar system and to possible identification of some terrestrial impactors.

To further document variations of solar system dustiness over geologic time and to better characterize the relationship between IDP accretion rate and major terrestrial impacts, especially at the Cretaceous/Tertiary boundary, we undertook a high resolution study (few hundred kyr sampling interval) of the He content and isotopic composition of pelagic limestones ranging from Maastrichtian to middle Eocene in age (74-39 Ma). This

study complements the late Eocene record of Farley et al. (1998), and a low resolution ^{3}He study of the entire Cenozoic (Farley, 1995).

2. Sample And Techniques

Our samples are part of the Cretaceous to middle Eocene Scaglia Rossa and the middle to late Eocene Scaglia Variegata Formations from the Bottaccione Gorge and Contessa Highway sections at Gubbio, in the Umbrian Apennines of central Italy. The two sections are ~2.5 km apart and have been tightly correlated based on magnetostratigraphy and biostratigraphy (Alvarez et al., 1977; Lowrie and Alvarez, 1977; Roggenthen and Napoleone, 1977; Arthur and Fischer, 1977; Premoli-Silva, 1977; Lowrie et al., 1982; Napoleone et al., 1983; Monechi and Tierstein, 1985; Montanari and Koeberl, 2000). Based on the correlation between the two sections we have constructed a composite stratigraphic section from the early Maastrichtian to the middle Eocene (Fig. 1).

Samples were collected at 1-2 meter intervals except near the K/T boundary, where they were collected every 0.5 m. The Contessa Highway section was sampled from 73 m below the K/T boundary (early Maastrichtian) to 3 m above the boundary (early Paleocene) and from 79 m to 150 m above the boundary (early to middle Eocene). The Bottaccione Gorge section was sampled from 7 m below the K/T boundary to 90 m above the boundary (the earliest middle Eocene).

Samples were either pulverized with a masonry power drill at the outcrop site, or powdered by hand with a ceramic mortar and pestle in the laboratory. To maximize

Figure 1. Composite stratigraphic section based on the correlation between the Contessa and Bottaccione sections (after Alvarez et al., 1977; Napoleone et al., 1983; Chauris et al., 1998). Ages are after Cande and Kent (1995).

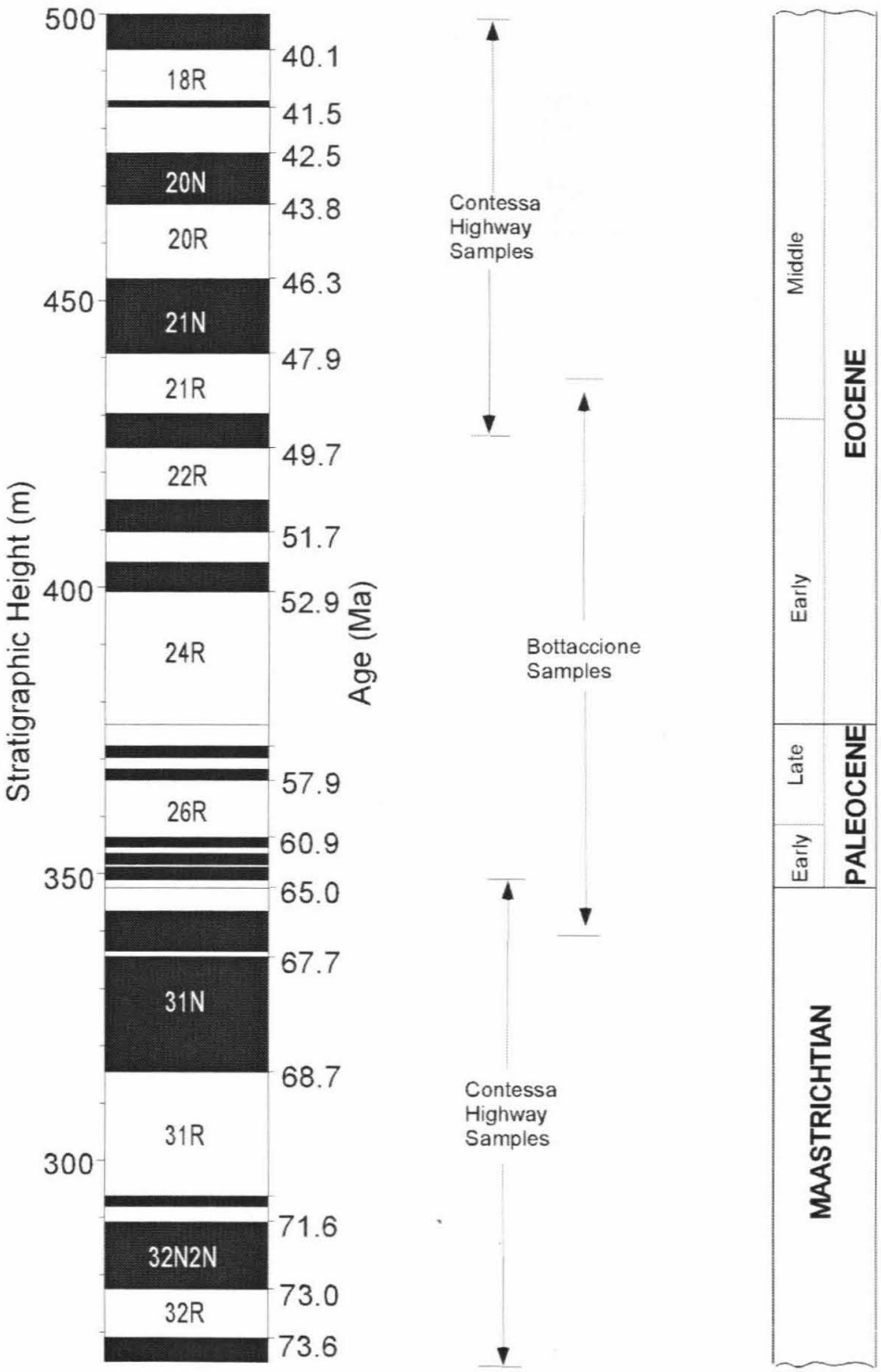
Stratigraphic Height (m)
500
450
400
350
300
18R
20N
20R
21N
21R
22R
24R
26R
31N
31R
32N2N
32R
40.1
41.5
42.5
43.8
46.3
47.9
49.7
51.7
52.9
57.9
60.9
65.0
67.7
68.7
71.6
73.0
73.6
Age (Ma)
Contessa Highway Samples
Bottaccione Samples
Contessa Highway Samples
Middle
Early
EOCENE
Late
Early
PALEOCENE
MAASTRICHTIAN

Table 1: Helium concentration in leached and bulk carbonates.

Sample	Type of Analyses	No of Analyses	[^{3}He] 10^{-15} cc STP g^{-1} of bulk	[^{4}He] 10^{-9} cc STP g^{-1} of bulk	^{3}He/^{4}He R_A
CON304	unleached	7	77±28	18.9±4.7	2.91±1.3
CON304	leached	5	105±9	23.0±0.8	3.68±0.36
CON312	unleached	20	72±34	41.1±3.9	1.24±0.6
CON312	leached	4	102±1	30.2±1.1	2.4±0.26

CON refers to samples from the Contessa highway section; errors are 1-σ. Note that sample 312 has a higher ^{4}He content in the unleached samples; this could be the result of some ^{4}He in the carbonate material. R_A is the ^{3}He/^{4}He ratio normalized to the atmospheric ratio of 1.39×10^{-6}.

sample size, aliquots of 2 to 3 g were leached in 10% acetic acid to remove carbonate (Patterson and Farley, 1998), leaving a residue of ~3.3 to 30% of the original samples. Comparison between 2 to 3 g of leached sample and 0.45 g of bulk sediment (Table 1) shows that ^{3}He is not affected by acetic acid leaching, consistent with earlier observations (Patterson and Farley, 1998). Sample preparation, gas extraction, and mass spectrometric techniques are described by Patterson and Farley (1998).

Typical ^{4}He hot blanks were $<0.2 \times 10^{-9}$ cm^{3} at standard temperature and pressure (cc STP), and averaged <1% of the ^{4}He in the samples. ^{3}He hot blanks were always $<1 \times 10^{-15}$ cc STP, in all cases <1% of the sample. The 1σ variation on ~300 standards of similar size to the samples analyzed during this project was 0.5% for ^{4}He and 3.0% for ^{3}He. Note that the natural variability in ^{3}He concentration of a sample (1σ of ~20%) is a much greater source of uncertainty in estimating the extraterrestrial ^{3}He flux than is the analytical precision. We routinely performed repeat extractions and in all cases the amounts of He were at blank levels, indicating complete extraction of He during the initial heating.

Several experiments were undertaken to evaluate possible sources of ^{3}He in addition to that hosted in IDPs. The presence of air-derived ^{3}He was estimated from neon abundance and isotopic ratios from four samples that have He isotopic compositions close to the atmospheric ratio. Gas extraction and purification procedures for Ne were similar to those used for He. Ne was separated from argon in a cryogenic trap held at 78 K and then inlet to the mass spectrometer. All three Ne isotopes were measured on a channeltron multiplier. Ne abundance and isotope ratios were calibrated by comparison to an air standard. The 1 σ variation of 4 air standards of similar size to the samples was ~5

% for ^{20}Ne, ~5% for $^{20}Ne/^{22}Ne$ and ~3% for $^{21}Ne/^{22}Ne$ ratios. Ne measurements were corrected for isobaric interference; the $^{40}Ar^{2+}/^{40}Ar^{+}$ ratio was 0.2 and the CO_2^{2+}/CO_2^{+} ratio was 0.004. The correction to ^{20}Ne from $^{40}Ar^{2+}$ was <1%, whereas the correction to ^{22}Ne from CO_2^{2+} was negligible.

To determine the contribution of nucleogenic ^{3}He from the $^{6}Li(n,\alpha)$ reaction we measured the lithium, thorium and uranium concentrations in six samples by inductively coupled plasma mass spectrometry. Aliquots of 2 mg of bulk sediment were taken from the same samples on which He measurements were made. Samples were dissolved in concentrated HF-HNO_3 and spiked with ^{230}Th and ^{235}U for precise determination of U and Th concentrations. Lithium concentrations in the samples were calculated from the $Li/^{235}U$ ratio and by calibrating to a Li standard solution.

3. Results

Helium results for the leached samples are summarized in Table 2. He isotope ratios range from 0.2 to 3.7 times the air ratio (R_A, $1.4x10^{-6}$), with a mean of 1.2 R_A. These ratios are elevated with respect to typical crustal values of 0.015 R_A (Tolsthikin 1978; Andrews, 1985), requiring the presence of a high $^{3}He/^{4}He$ component in the sediments. The likely candidates are cosmogenic, nucleogenic, atmospheric and extraterrestrial He.

3.1. Cosmogenic and Nucleogenic Contributions to ^{3}He

Cosmic ray interactions occurring in the uppermost ~1 m of the Earth's surface produce He with an extremely high $^{3}He/^{4}He$ ratio (Lal, 1987). Because the limestones we

Table 2: Average He concentration, ratios, ages, and mass accumulation rates in Gubbio carbonates.

Stratigraphic Height (m)	^3He 10^{-15} cc STP g^{-1}	± 2σ	^4He 10^{-9} cc STP g^{-1}	± 2σ	$^3He/^4He$ R_A	NCF	Age (Ma)	Chron MAR
264.85	40	16	26.0	4.5	1.1	0.06	73.92	3.78
266.00	49	14	24.4	3.0	1.4	0.07	73.83	3.78
267.00	67	27	23.5	4.1	2.0	0.06	73.76	3.78
268.00	38	11	20.8	2.6	1.3	0.05	73.69	3.78
269.00	68	27	20.8	3.6	2.3	0.06	73.62	3.78
270.00	119	33	33.2	4.0	2.7	0.07	73.55	3.78
271.00	23	6	21.7	2.7	0.8	0.06	73.48	3.78
272.00	44	12	30.4	3.7	1.0	0.07	73.40	3.78
273.10	51	14	28.4	3.5	1.3	0.07	73.33	3.78
274.00	49	14	22.3	2.7	1.6	0.06	73.26	3.78
276.00	55	15	19.7	2.4	2.0	0.06	73.12	3.78
277.00	52	14	35.3	4.3	1.1	0.06	73.05	3.78
278.00	76	21	35.6	4.4	1.5	0.09	72.95	2.19
279.00	43	12	27.4	3.4	1.1	0.07	72.83	2.19
280.00	53	9	30.0	2.3	1.3	0.07	72.71	2.19
281.00	49	14	29.9	3.7	1.2	0.07	72.59	2.19
282.00	57	11	27.9	2.2	1.7	0.06	72.46	2.19
283.00	45	13	24.7	3.0	1.3	0.05	72.34	2.19
284.00	67	13	29.3	2.3	1.6	0.06	72.22	2.19
285.00	56	16	25.7	3.1	1.5	0.06	72.09	2.19
286.00	38	9	28.6	2.9	0.9	0.08	71.97	2.19
288.00	25	6	22.8	2.3	0.8	0.06	71.72	2.19
290.00	42	10	21.5	2.2	1.5	0.05	71.51	3.14
291.00	42	10	17.7	1.8	1.7	0.05	71.42	3.14
294.00	45	10	16.2	1.6	2.0	0.04	71.05	2.51
295.35	39	9	20.6	2.1	1.4	0.05	70.90	2.51
298.00	60	24	23.6	2.9	1.9	0.05	70.62	2.51
299.00	42	8	18.1	1.6	1.6	0.03	70.51	2.51
300.00	103	29	27.0	3.3	2.7	0.06	70.40	2.51
301.00	59	16	13.7	1.7	3.1	0.04	70.30	2.51
302.00	51	20	19.4	3.4	1.9	0.06	70.19	2.51
303.00	46	13	20.6	2.5	1.6	0.06	70.08	2.51
304.00	105	19	23.0	1.8	3.7	0.05	69.97	2.51
305.00	49	14	27.0	3.3	1.3	0.05	69.87	2.51
306.00	48	8	22.5	1.5	1.6	0.05	69.76	2.51
307.00	43	12	18.0	2.2	1.7	0.05	69.65	2.51
308.00	53	11	23.3	1.8	1.6	0.05	69.54	2.51
309.00	55	15	19.0	2.3	2.1	0.04	69.44	2.51
310.00	82	23	26.1	3.2	2.2	0.07	69.33	2.51
311.00	46	13	24.2	3.0	1.3	0.05	69.22	2.51
312.00	102	20	30.2	2.1	2.4	0.05	69.11	2.51
313.00	36	10	12.2	1.5	2.1	0.05	69.01	2.51
314.00	44	12	25.8	3.2	1.2	0.06	68.90	2.51
315.00	42	10	20.7	2.1	1.6	0.05	68.79	2.51
316.00	69	19	14.9	1.8	3.3	0.05	68.71	5.39
317.00	77	18	21.6	2.1	2.6	0.06	68.66	5.39
320.00	50	12	17.2	1.7	2.1	0.04	68.51	5.39

Table 2 (continued)

Stratigraphic Height (m)	^{3}He 10^{-15} cc STP g^{-1}	± 2σ	^{4}He 10^{-9} cc STP g^{-1}	± 2σ	^{3}He/^{4}He R_A	NCF	Age (Ma)	Chron MAR
323.90	26	6	23.5	2.0	0.8	0.04	68.32	5.39
326.00	45	10	27.7	2.8	1.2	0.06	68.21	5.39
328.00	42	10	26.0	2.6	1.2	0.05	68.11	5.39
330.15	62	12	32.7	2.5	1.4	0.06	68.00	5.39
332.00	29	6	34.0	3.4	0.6	0.05	67.91	5.39
334.00	40	9	61.2	4.8	0.5	0.08	67.81	5.39
336.00	34	8	41.2	4.1	0.6	0.06	67.67	2.16
338.00	29	7	41.4	4.2	0.5	0.06	67.27	0.93
340.00	55	12	41.1	4.1	0.9	0.05	66.69	0.93
340.60	110	44	51.7	8.9	1.5	0.06	66.52	0.93
341.50	99	39	114.4	19.9	0.6	0.09	66.26	0.93
342.00	69	16	62.1	6.2	0.8	0.07	66.11	0.93
342.60	21	8	66.3	11.5	0.2	0.07	65.94	0.93
343.70	159	63	49.5	8.5	2.3	0.05	65.55	1.75
344.00	23	5	43.8	4.4	0.4	0.05	65.50	1.75
344.50	33	13	41.3	7.2	0.6	0.05	65.42	1.75
345.40	43	17	59.4	10.3	0.5	0.07	65.28	1.75
346.00	54	15	46.2	5.7	0.8	0.07	65.19	1.75
346.40	79	31	60.1	10.4	0.9	0.06	65.13	1.75
347.00	39	15	65.1	8.0	0.5	0.07	65.04	1.75
347.40	23	9	51.8	9.0	0.3	0.05	65.0	1.75
347.80	72	28	37.3	6.5	1.4	0.04	64.91	1.75
348.50	128	50	109.3	19.0	0.8	0.10	64.81	1.75
349.00	114	45	67.7	11.7	1.2	0.10	64.71	0.81
349.50	75	30	49.5	8.6	1.1	0.06	64.54	0.81
349.90	60	24	26.1	4.5	1.6	0.05	64.41	0.81
350.00	72	28	36.9	6.4	1.4	0.07	64.38	0.81
350.50	81	32	55.8	9.7	1.0	0.09	64.21	0.81
351.06	114	45	67.2	11.6	1.2	0.11	64.02	0.81
352.06	160	63	101.7	17.6	1.1	0.12	63.37	0.48
352.71	100	23	60.5	6.1	1.2	0.11	63.00	0.48
353.05	219	50	119.8	12.0	1.3	0.15	62.81	0.48
354.00	148	34	65.0	6.5	1.6	0.10	62.01	0.22
355.00	169	39	88.9	8.9	1.4	0.14	61.20	1.37
356.00	161	64	66.2	11.5	1.7	0.11	61.00	1.37
357.00	167	38	83.9	8.4	1.4	0.12	60.74	0.89
358.00	79	31	37.2	6.4	1.5	0.06	60.43	0.89
359.00	95	22	45.5	4.5	1.5	0.07	60.13	0.89
360.00	109	25	110.7	11.1	0.7	0.10	59.83	0.89
361.00	72	20	52.6	6.5	1.0	0.07	59.52	0.89
362.00	41	9	34.4	3.4	0.9	0.05	59.22	0.89
363.00	58	13	60.2	6.0	0.7	0.08	58.91	0.89
364.00	29	8	35.0	4.3	0.6	0.07	58.61	0.89
365.00	93	26	61.6	7.6	1.1	0.10	58.31	0.89
366.00	53	21	51.6	9.0	0.7	0.09	58.00	0.89
367.00	54	15	58.0	7.1	0.7	0.08	57.79	1.51
368.00	68	19	34.7	4.3	1.3	0.08	57.61	1.51

Table 2 (continued)

Stratigraphic Height (m)	^3He 10^{-15} cc STP g^{-1}	± 2σ	^4He 10^{-9} cc STP g^{-1}	± 2σ	$^3He/^4He$ R_A	NCF	Age (Ma)	Chron MAR
369.00	120	34	43.9	5.4	2.0	0.09	57.14	0.45
370.00	48	19	34.4	6.0	1.0	0.08	56.54	0.45
371.00	123	34	114.6	14.1	0.8	0.15	56.21	1.10
372.00	102	28	148.8	18.3	0.5	0.22	55.97	1.10
373.00	91	25	104.1	12.8	0.6	0.17	55.82	2.43
375.00	83	23	111.5	13.7	0.5	0.13	55.60	2.43
377.00	110	44	49.9	8.6	1.6	0.08	55.38	2.43
379.00	43	17	19.6	3.4	1.6	0.06	55.15	2.43
381.00	53	21	24.2	4.2	1.6	0.05	54.93	2.43
383.00	59	23	38.0	6.6	1.1	0.08	54.71	2.43
385.00	123	49	62.2	10.8	1.4	0.10	54.49	2.43
387.00	72	28	63.7	11.1	0.8	0.11	54.27	2.43
389.00	51	14	67.5	8.3	0.6	0.12	54.04	2.43
391.00	68	16	37.3	3.7	1.5	0.06	53.82	2.43
393.00	68	15	28.5	2.8	1.7	0.07	53.60	2.43
397.00	89	20	32.2	3.2	2.0	0.06	53.15	2.43
399.00	62	14	27.7	2.8	1.6	0.05	52.93	2.43
401.00	54	15	31.0	3.8	1.3	0.06	52.71	2.50
403.00	56	13	37.9	3.8	1.1	0.08	52.50	2.50
404.90	68	15	60.4	6.1	0.8	0.11	52.29	2.39
405.10	61	14	40.5	4.1	1.0	0.07	52.27	2.39
407.00	51	14	29.1	3.6	1.3	0.06	52.05	2.39
409.00	76	30	68.4	11.9	0.8	0.12	51.83	2.39
411.00	48	19	43.4	7.5	0.8	0.09	51.52	1.54
415.00	100	39	64.2	11.1	1.1	0.11	50.82	1.54
417.00	33	9	41.6	5.1	0.6	0.16	50.57	2.28
419.00	18	5	23.2	2.9	0.6	0.05	50.33	2.28
421.00	29	11	38.9	6.8	0.5	0.06	50.10	2.28
423.00	53	21	32.9	5.7	1.1	0.06	49.86	2.28
425.00	27	11	26.8	4.7	0.7	0.07	49.63	2.39
426.95	51	14	29.9	3.7	1.2	0.07	49.41	2.39
428.54	12	3	21.2	2.6	0.4	0.06	49.23	2.39
429.00	21	8	27.4	4.8	0.6	0.06	49.18	2.39
430.12	32	9	41.5	5.1	0.3	0.09	49.05	2.39
431.00	24	9	37.5	6.5	0.5	0.06	48.96	2.51
432.25	20	5	37.2	4.6	0.4	0.10	48.82	2.51
433.00	46	18	89.5	15.5	0.4	0.07	48.74	2.51
434.98	49	13	61.1	7.5	0.6	0.17	48.53	2.51
435.00	10	4	20.3	3.5	0.4	0.06	48.53	2.51
436.55	33	9	44.3	5.4	0.5	0.08	48.36	2.51
437.00	28	11	34.3	6.0	0.6	0.06	48.31	2.51
438.65	37	10	35.1	4.3	0.8	0.07	48.13	2.51
440.75	20	5	32.2	4.0	0.4	0.07	47.91	2.51
442.75	35	10	45.8	5.6	0.6	0.12	47.65	2.14
444.75	40	11	39.2	4.8	0.7	0.06	47.40	2.14
446.75	36	10	58.8	7.2	0.4	0.09	47.15	2.14
450.45	41	11	71.6	8.8	0.4	0.11	46.68	2.14

Table 2 (continued)

Stratigraphic Height (m)	^{3}He 10^{-15} cc STP g^{-1}	± 2σ	^{4}He 10^{-9} cc STP g^{-1}	± 2σ	^{3}He/^{4}He R_A	NCF	Age (Ma)	Chron MAR
452.75	136	38	132.4	16.3	0.7	0.18	46.39	2.14
454.75	31	8	49.5	6.1	0.5	0.09	46.07	1.42
458.75	46	12	76.0	9.3	0.4	0.11	45.31	1.42
462.60	90	25	95.3	11.7	0.7	0.17	44.58	1.42
464.65	76	21	112.9	13.9	0.5	0.18	44.19	1.42
466.85	30	8	63.0	7.7	0.3	0.13	43.78	1.94
468.95	39	11	77.9	9.6	0.4	0.15	43.48	1.94
473.75	25	7	44.3	5.4	0.4	0.10	42.81	1.94
475.85	41	11	70.0	8.6	0.4	0.12	42.52	2.13
477.75	41	11	65.4	8.0	0.5	0.10	42.28	2.13
479.75	41	11	76.4	9.4	0.4	0.12	42.03	2.13
481.75	41	11	76.3	9.4	0.4	0.13	41.77	2.13
483.75	30	8	47.4	5.8	0.4	0.10	41.52	2.13
486.75	28	11	47.8	5.9	0.4	0.10	41.01	2.16
488.65	23	6	45.3	5.6	0.4	0.11	40.77	2.16
490.75	77	21	103.1	12.7	0.5	0.17	40.51	2.16
492.75	49	13	55.1	6.8	0.6	0.12	40.26	2.16
494.75	170	66	205.2	25.2	0.6	0.31	39.96	1.58
496.75	151	42	138.9	17.0	0.8	0.20	39.62	1.58
497.50	65	18	108.0	13.3	0.4	0.17	39.49	1.58

^{3}He, ^{4}He and ^{3}He/^{4}He represent averages of leached replicates. He concentrations are per gram of bulk sdeiment. NCF is the non-carbonate fraction in the sediments as measured by our mass loss data. The age for each sample was calculated from individual chron boundaries assuming a constant sedimentation rate. MAR is the mass accumulation rate in gm/cm^2/kyr calculated from ages of chron boundaries; bulk density of carbonate used = 2.7 gm/cm^3. The position of the K/T boundary is at 347.63 m.

analyzed were deposited in a marine environment, had a long burial history, and were sampled from recently exposed quarry faces or road cuts, post-depositional production of cosmogenic ^{3}He is negligible. While it is possible that the detrital fraction of the sediment was exposed to cosmic rays prior to deposition, exposure ages of >200 kyrs would be required to account for all of the ^{3}He in our samples using the accepted production rate at sea level and high latitude (Cerling and Craig, 1993). These exposure ages seem unreasonably high, particularly given the fact that detrital minerals have very low He retentivity (Farley, 1995). Low ^{3}He concentrations in loess suggest wind-blown dust contributes negligible amounts of cosmogenic ^{3}He to deep sea sediments (Farley and Patterson, 1995; Farley, 2001). We therefore conclude that the limestone samples are unlikely to have significant cosmogenic ^{3}He.

The reaction $^6\mathrm{Li}(n,\alpha) \longrightarrow {}^3\mathrm{H} \xrightarrow{\beta} {}^3\mathrm{He}$, is another potential source of ^{3}He in sediments. This reaction yields a correlated production of both He isotopes, with ^{3}He/^{4}He ratios between 0.016 R_A and 0.0016 R_A in typical lithologies (Andrews, 1985). The Li content of the six analyzed Gubbio samples is very low (< 7 ppm, Table 3), yielding a calculated ^{3}He/^{4}He production ratio of 0.0014 R_A based on the model of Andrews (1985). This ratio is two to three orders of magnitude lower than the ^{3}He/^{4}He ratios we measure, arguing against significant nucleogenic ^{3}He in our samples. Loosli et al. (1995) and Tolstikhin et al. (1996) called on preferential retention of ^{3}H compared to the α particle to explain their observation of ^{3}He/^{4}He ratios higher than that of nuclear production in some chemical sediments. However, these authors did not consider the presence of an IDP-hosted component, which is almost certainly present, and which we feel is a more likely explanation for their observation.

Table 3: $^{3}He/^{4}He$ production ratios.

Stratigraphic Height (m)	U ppm	Th ppm	Calculated $^{3}He/^{4}He$ production ratio (R_A)
279	0.16	0.70	0.0014
299	0.17	0.51	0.0014
314	0.18	0.70	0.0014
326	0.17	0.69	0.0014
334	0.18	0.88	0.0013
341.5	0.19	1.19	0.0013

$^{3}He/^{4}He$ production ratios are calculated using the formulation in Andrews (1985). Neutron capture probabilities used in this calculation are from Andrews and Kay (1982). [Li] in our samples were at blank levels of our acids (6.8 ppm). We have, therefore, used this value as an upper limit of the [Li] in our samples.

Table 4: He/Ne ratios in selected limestone samples.

Sample	$^{3}He/^{4}He$ R_A	^{4}He conc 10^{-9} cc STP g^{-1}	^{20}Ne conc 10^{-9}cc STP g^{-1}	$^{4}He/^{20}Ne$
CON279	1.13	26.4±1.68	0.14±.007	195
CON286	1.2	25.8±1.5	0.14±.007	181
CON314	0.94	28.6±1.6	0.11±.006	256
CON326	1.16	27.7±1.4	0.10±.005	284

Limestones were selected with $^{3}He/^{4}He$ ratios close to the atmospheric ration of 1 R_A. The He/Ne ratio in air is 0.3 and >200 for extraterrestrial matter (Ozima and Podosek, 1983).

3.2. Deconvolution of Extraterrestrial and Crustal Helium

In the absence of nucleogenic and cosmogenic components, He in sediments is a mixture of extraterrestrial, crustal, and air-derived He. The relative proportions of these components can be evaluated using He-Ne systematics. Because the He/Ne ratio of the atmosphere is far lower than in extraterrestrial matter (0.3 vs. ≥200; Ozima and Pododsek, 1983), the He/Ne ratio of a sediment can be used to identify the presence of atmospheric He (Farley and Patterson, 1995). In 4 limestone samples with $^3He/^4He$ ratios close to the atmospheric value, we found He/Ne ratios of >180 (Table 4), implying that less than 1% of the He is air-derived. Therefore, we model the He in our samples as a two-component mixture of extraterrestrial and crustal He. For deconvolution of these two components we assumed that the extraterrestrial endmember has a $^3He/^4He$ ratio of 290 R_A, similar to that observed in solar wind and in bulk lunar fines (Geiss et al., 1972; Nier and Schlutter, 1990). For the crustal component we assumed a $^3He/^4He$ ratio of 0.03 R_A, similar to that observed in Chinese loess (Farley and Patterson, 1995; Farley, 2001). Using these values, the calculated fraction of extraterrestrial ^3He in our samples, with the exception of a single sample, is >90%. Even if the $^3He/^4He$ ratio of the crustal component were assumed to be 0.15 R_A, well in excess of typical crustal ratios (Andrews, 1985; Farley, 2001), the fraction of extraterrestrial ^3He would still be dominantly >90% and only in two instances <70%. This difference is much smaller than the inherent variations between samples. Extraterrestrial ^3He fluxes computed below are based on this deconvolution, using a crustal $^3He/^4He$ ratio of 0.03 R_A.

Deconvolution of the total ^{4}He content yields crustal contributions >99%, using the same end-members as the previous calculation; no reasonable variations in endmember ratios change the conclusion that ^{4}He is exclusively terrestrial.

3.3. Reproducibility of Replicate Analyses

^{3}He in sediments is carried by a relatively small number of IDP grains that are generally not representatively sampled in 2 to 3 g aliquots (Farley et al., 1997; Patterson and Farley, 1998). This leads to an underestimation of the global mean extraterrestrial ^{3}He flux because rare large particles are under-sampled, and more importantly to a lack of reproducibility in replicate ^{3}He analyses (Farley et al., 1997; Patterson and Farley 1998). The degree of statistical undersampling depends on the area-time product of the sample, and is 0.125 m^2a for our samples, which should undersample the global flux by only ~20% (Farley et al., 1997). Because all of our samples represent approximately the same area-time product (within a factor of a few) this effect can be ignored when considering apparent changes in ^{3}He flux. To reduce the effects of irreproducibility we have replicated measurements on most samples, and on occasions measured a single sample many times.

The reproducibility of these replicate analyses is plotted in Figure 2. The reproducibility distribution is in good agreement with the model prediction of Farley et al. (1997) for sediments with an area-time product of 0.25 m^2a, and with the observed distribution from ODP Site 806 (Patterson and Farley, 1998). Note that while our samples have an area-time product of ~0.125 m^2a, a factor of two lower than that used in the model, an order of magnitude difference is required to significantly alter the

Figure 2. Observed fractional difference for multiple replicates from the Gubbio sections. Fractional difference is defined as abs[(a1–a2)/(a1+a2)/2], where a1 and a2 represent the replicate analyses of the same sample. For samples that were run more than twice, the fractional difference of the first two analyses is plotted. The solid curve is the distribution modeled for a surface-correlated He component in IDPs subjected to atmospheric entry heating (also see Patterson and Farley, 1998). There is good agreement between the observed and theoretical distributions, and the observed distribution can be approximated by a gaussian with 1σ of ~20%.

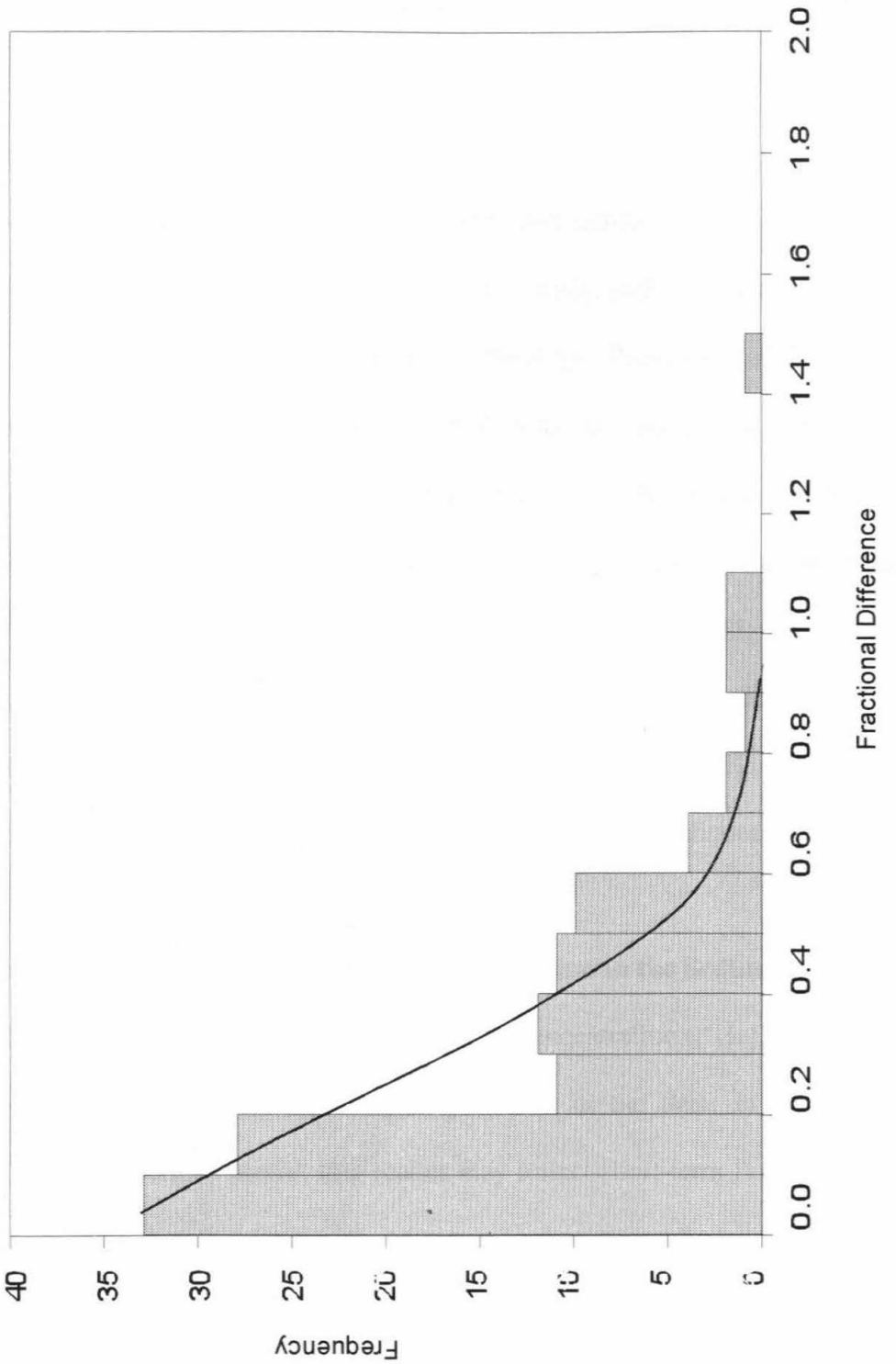
Frequency
40
35
30
25
20
15
10
5
0
0.0
0.2
0.4
0.6
0.8
1.0
1.2
1.4
1.6
1.8
2.0
Fractional Difference

reproducibility distribution (Farley et al., 1997). The observed distribution can be approximated by a Gaussian with 1σ of ~20% (see also Patterson and Farley, 1998). The 2σ uncertainty in our samples, therefore, scales as $40\%/\sqrt{N}$, where N is the number of measurements of a given sample.

In rare cases an individual aliquot of a particular sample may be wildly discrepant compared to replicates. This has been observed previously, and attributed to the presence of rare IDPs with a volume-correlated ^{3}He component (Patterson and Farley. 1998). Using Chauvenet's criterion for elimination of aberrant data points, we have eliminated replicate analyses that plot further than 3σ from the mean of the sample. Fourteen out of 160 replicate analyses were eliminated using this method. Note that the elimination of these points reduces scatter but does not change the overall pattern in Figure 3a.

In contrast to the ^{3}He concentration, the ^{4}He abundances replicate well, with a population standard deviation of 8.7%. This reflects the fact that ^{4}He is derived from terrestrial radiogenic ^{4}He and is sampled fairly representatively in aliquots of 2-3 g.

3.4. Helium Concentration and Non-carbonate Fraction in the Sediments

Figure 3a is a plot of the extraterrestrial ^{3}He concentration ([^{3}He]) as a function of stratigraphic height. There is high frequency scatter in the data; in addition to the statistical effects described above, this scatter may reflect short-term fluctuations in ^{3}He flux or sedimentation rates. Following previous workers (e.g., Farley et al., 1998), to prevent the high frequency variability from obscuring long-term trends, we consider only a five-point running mean through the data. The major features of the smoothed data are:

- [^{3}He] is constant to within a factor of two throughout the Maastrichtian.

- [^{3}He] is low and invariant across the K/T boundary, i.e., from 344.5 (~65.5 Ma) to 348.5 m (~64.8 Ma). This is also seen in a high-resolution study (~20 cm sampling interval) of the K/T boundary from the Bottaccione Gorge section (Mukhopadhyay et al., 2001).
- Starting approximately 2 m above the K/T boundary (349.5 m), [^{3}He] increases and reaches a clear maximum of about four times the Maastrichtian average at 7.5 m above the boundary. This is the most prominent feature in the entire 35 Myr record.
- Following a dip in the middle Paleocene, [^{3}He] increases by a factor of two in the late Paleocene, and then steadily declines by a factor of four in the Eocene. The end of the middle Eocene is marked by an increase in [^{3}He].

Figures 3c and 3d show the crustal ^{4}He concentration ([^{4}He]) and the non-carbonate fraction in the sediments as a function of stratigraphic height. Both of these tracers provide insight to relative sedimentation rates: changes in carbonate sedimentation rate will inversely affect the non-carbonate and ^{4}He contents of the sediment (e.g., Herbert and D'Hondt, 1990; Ten Kate and Sprenger, 1993; Patterson et al., 1999). The major features of these profiles are:

- [^{4}He] and the non-carbonate fraction in the sediments are low and constant through the early Maastrichtian.
- Starting ~27 m below the K/T boundary (320 m), [^{4}He] increases rapidly and monotonically, reaching a maximum of four times early Maastrichtian values at 6 m below the K/T boundary (341.5 m). The non-carbonate fraction in the sediments is, however, approximately constant through this interval.

Figure 3. [^{3}He] (a), ^{3}He/^{4}He ratio (b), [^{4}He] (c), and non-carbonate fraction (d) in the Gubbio sediments. Points are individual values representing the averages of the leached replicates. Arrows represent data points that plot off scale. The shaded envelopes represent the 2σ uncertainty of the five-point running mean calculated from the uncertainties of individual data points. The non-carbonate fraction is operationally defined as the fraction of mass remaining after leaching with acetic acid. The age for each sample was calculated from individual chron boundaries assuming a constant sedimentation rate (solid line in Fig. 4a).

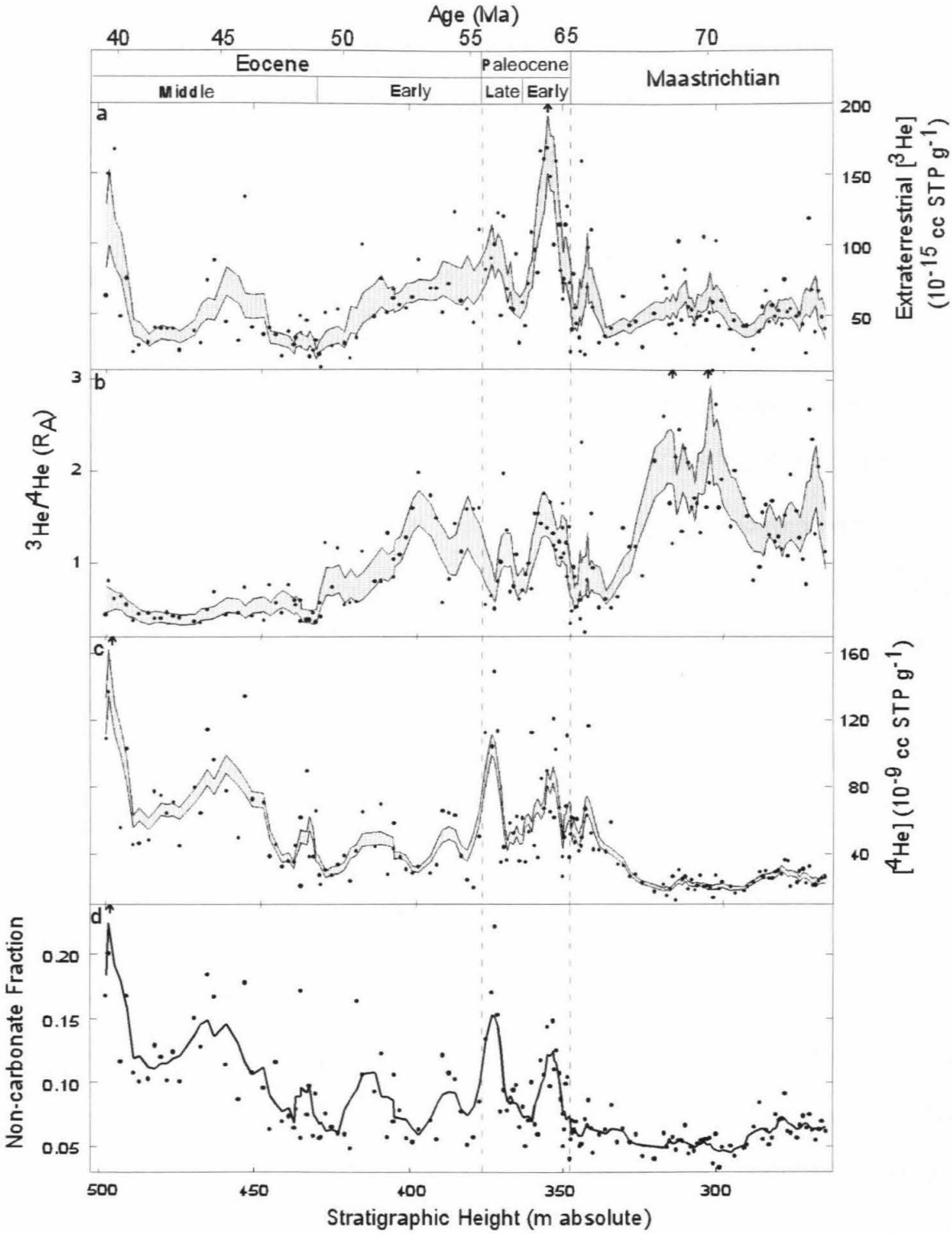
Age (Ma)
40
45
50
55
65
70
Eocene
Paleocene
Middle
Early
Late
Early
Maastrichtian
a
b
c
d
Extraterrestrial [3He] (10-15 cc STP g-1)
3He/4He (RA)
[4He] (10-9 cc STP g-1)
Non-carbonate Fraction
Stratigraphic Height (m absolute)

- Both [^{4}He] and the non-carbonate fraction of the sediments are higher and show more fluctuations in the Eocene when compared to early Maastrichtian values, indicating a higher and variable detrital component during the Eocene (Lowrie et al., 1982).

4. Helium Flux

The extraterrestrial ^{3}He concentration in sediments is controlled by both the ^{3}He flux from space and the sediment mass accumulation rate (MAR) through the relationship $[^3He]=fR/\alpha$, where [^{3}He] is the concentration in sediments, f is the flux of ^{3}He from space, R is the fractional He retentivity (Farley, 1995) and α is the sediment MAR. If the sediment MAR can be determined independently, fR can be calculated. To the extent that R is relatively constant over the interval of interest, the product fR is a proxy for the relative flux of ^{3}He to the seafloor. Because ^{3}He is retained in sediments for hundreds of millions of years (Patterson et al., 1998), assumption of an invariant R over the 35 Myrs of interest here seems appropriate. Here we use the term "implied ^{3}He flux" for the quantity fR derived from a particular sedimentation rate model.

In the absence of absolute and instantaneous sedimentation rates, we have taken two approaches to determining the implied ^{3}He flux. The first is to calculate the average flux for an epoch based on the average sedimentation rate over the epoch. This is a conservative approach because the ages of the epoch boundaries are relatively well known (see Cande and Kent, 1992 and 1995, and references therein; Gradstein et al., 1994, and references therein), but provides little temporal resolution. The second approach is to calculate the average implied ^{3}He flux over individual magnetochrons

based on the average sedimentation rate for the chron. This approach provides about 5x higher temporal resolution but is more uncertain, because the ages of the chron boundaries are often poorly constrained (see Cande and Kent, 1992, and references therein).

The epoch and chron averaged MARs are plotted in Figure 4a. The paleomagnetic data suggest that the MAR in chron 31N (315.5-335.5 m; 68.74-67.74 Ma) was more than twice that in chron 31R (293.8-315.5 m; 71.07-68.74 Ma). Such a big change in MAR is likely to be controlled by the flux of carbonate, which would change the relative proportions of non-carbonate and carbonate material. However, there is no change in the non-carbonate fraction of the sediments between these chrons (Fig. 3d). Therefore, we speculate that the increase in MAR in chron 31N is not real, but arises from errors in the Cande and Kent (1995) timescale. Below we test this hypothesis using the extraterrestrial [^{3}He] record.

It is also possible that the stratigraphic section was affected by synsedimentary slumps and/or faulting. This leads to uncertainty in the actual stratigraphic thickness of the chron. Evidence for minor synsedimentary slumping and faulting in the Contessa and Bottaccione sections have been presented (Lowrie et al., 1982; Napoleone et al., 1983). The MARs computed for the individual magnetochrons are, therefore, subject to uncertainties that cannot be directly quantified. However, based on our non-carbonate data, the uncertainties in sedimentation rates are unlikely to be greater than a factor of 2-3. To identify major extraterrestrial events, we look for large variations in the implied ^{3}He flux that are not correlated with changes in MAR, and which exceed reasonable uncertainties in the MARs. An alternate and independent approach to determining if

Figure 4. (a). Sediment mass accumulation rate (MAR) as a function of stratigraphic height. The dashed line is the average MAR in each epoch, while the solid line represents average MAR in individual magnetochrons. (b). Epoch-averaged implied ^{3}He flux. The shaded envelope is the 2σ uncertainty in the implied flux calculated from the 2σ uncertainty in the epoch averaged [^{3}He]. Possible errors in MAR have not been taken into account for calculating the error envelope. (c) Chron-averaged implied ^{3}He flux. Because of incomplete sampling of chrons 32R and 18N, the fluxes for these chrons were not computed. Error envelope calculated as in (B). (d). Non-carbonate normalized [^{3}He]. Points are individual values, and arrows represent data that are off scale. The shaded region is the 2σ uncertainty on the five-point running mean. The age for each sample was calculated as in Figure 3.

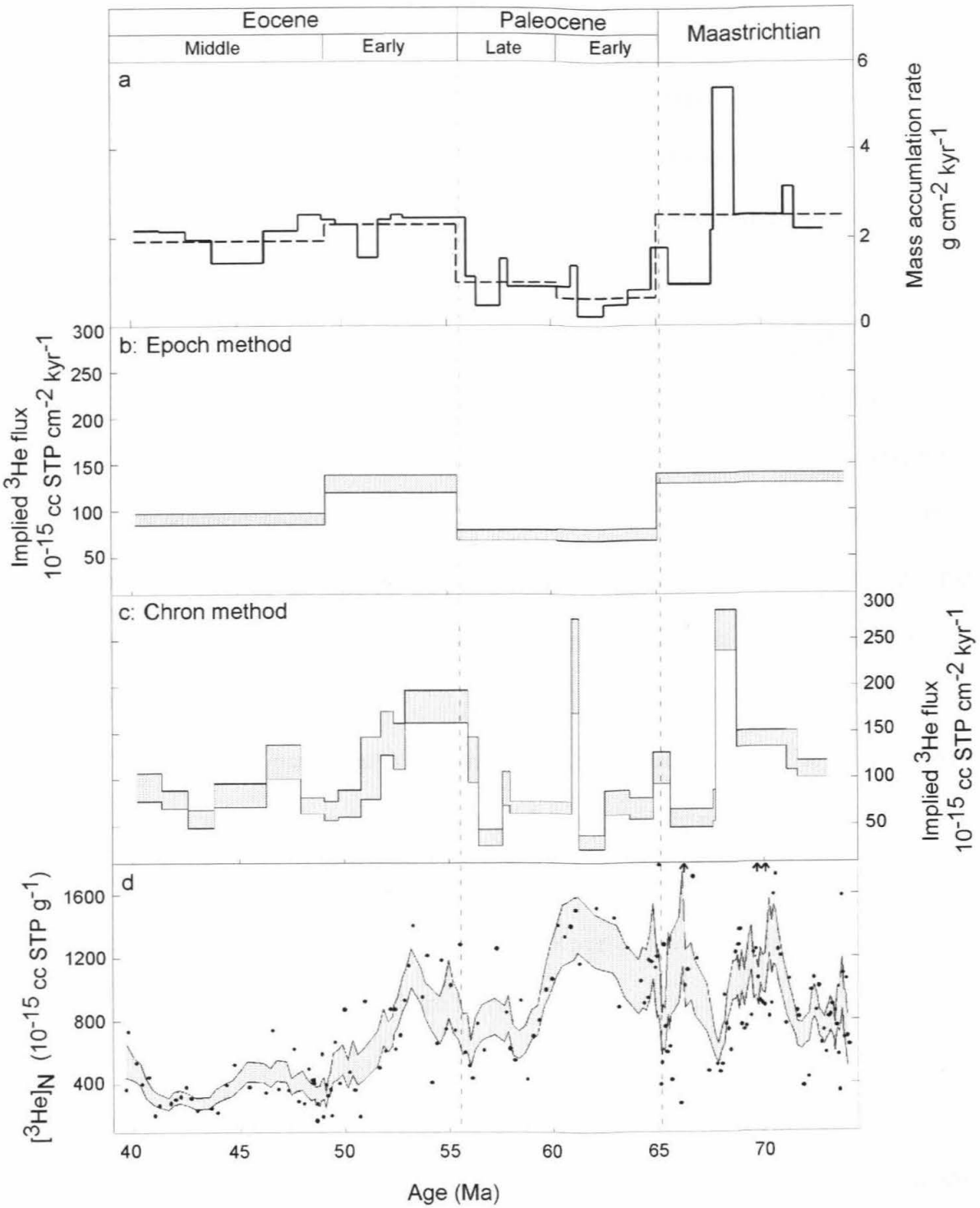
Eocene
Middle
Early
Paleocene
Late
Early
Maastrichtian
a
Mass accumulation rate
g cm-2 kyr-1
b: Epoch method
Implied 3He flux
10-15 cc STP cm-2 kyr-1
c: Chron method
Implied 3He flux
10-15 cc STP cm-2 kyr-1
d
[3He]N (10-15 cc STP g-1)
Age (Ma)

variations in [^{3}He] are the result of variations in the ^{3}He accretion rate or are instead the product of sedimentation rate changes is to normalize the [^{3}He] to the non-carbonate fraction ([^{3}He]$_N$) and also to the [^{4}He] in the sediments. As discussed earlier, the non-carbonate fraction and [^{4}He] are crude proxies for the relative sedimentation rate. Therefore, conclusions about changes in ^{3}He accretion rate are most robust when changes in implied ^{3}He flux based on sedimentation rate models are accompanied by changes in [^{3}He]$_N$ and the ^{3}He/^{4}He ratio.

Sedimentary phenomena, such as winnowing or focusing, may cause the computed ^{3}He flux for a given site to differ from the true global flux (Farley and Patterson, 1995; Marcantonio et al., 1996). Extensive discussions on this issue have been presented by Marcantonio et al. (1996), Patterson and Farley (1998), and Farley (2001). In interpreting our results we consider the possibility that focusing might be an issue, and thus have also relied on the [^{3}He] data in conjunction with ^{3}He/^{4}He and [^{3}He]$_N$, neither of which are affected by bulk focusing.

The epoch- and magnetochron-averaged implied ^{3}He flux, and [^{3}He]$_N$, are plotted as a function of age in Figures 4b-4d. Our goal is to identify robust features in the He record, and, in the following part of this section, we discuss whether the observed fluctuations in the implied ^{3}He flux are the result of variations in the ^{3}He accretion rate or arise from uncertainties in the calculated MAR.

4.1. Epoch-averaged Implied ^{3}He Flux

It is evident from Figure 4b that there are no large, long-lived fluctuations in the implied ^{3}He flux. The average implied ^{3}He flux in the Maastrichtian is $135 \pm 5 \times 10^{-15}$ cc

STP cm^{-2} kyr^{-1} and is indistinguishable from values in the Oligocene (Farley et al., 1998). The implied ^3He flux in the Maastrichtian and in the early Eocene is almost a factor of two higher than in the entire Paleocene. We note that part of the stratigraphic section is missing in the early Eocene (Napoleone et al., 1983), so the true ^3He accretion rate is likely to be higher than our calculated values. These data suggest a factor of two higher extraterrestrial ^3He accretion rate during the Maastrichtian and early Eocene when compared to the Paleocene.

4.2. Chron-averaged Implied ^3He Flux

4.2.1. Maastrichtian

The most prominent feature in the Maastrichtian record is the factor of ~2.5 enhancement occurring between 68.7 Ma and 67.7 Ma, in chron 31N. However, this peak does not arise from higher [^3He] but from a short-term increase in MAR (Fig. 4a). In addition, [^3He], $^3He/^4He$ ratio, and $[^3He]_N$ actually decrease between 68.7 and 67.7 Ma (Fig. 3a-3b and 4d). These observations are inconsistent with a rise in the ^3He accretion rate. Instead, as noted earlier, we believe that there is an error in the calculated MAR resulting from an error in the Cande and Kent (1995) timescale. Assuming that the average implied ^3He flux in the Maastrichtian holds for this chron, we calculate a duration of 2 Myr for chron 31N, instead of the1 Myr interval suggested by Cande and Kent (1995). This increase would bring the sediment MAR in to good agreement with the surrounding section (Fig. 4a).

In contrast to the chron 31N peak, there are minor synchronous elevations (factor of two) in $[^3He]_N$, $^3He/^4He$ ratio and [^3He] at ~70.5 Ma and ~66 Ma. These observations

suggest minor increases (~ factor of two) in the extraterrestrial ^{3}He accretion rate between 70.5 and 68 Ma and at ~66 Ma.

4.2.2. K/T Boundary

The implied ^{3}He flux across the K/T boundary, between 65.5 Ma and 64.8 Ma, is ~120 × 10^{-15} cc STP cm^{-2} kyr^{-1}, slightly lower that the Maastrichtian average (Fig. 4b & 4c). Along with [^{3}He], ^{3}He/^{4}He ratio, and $[^3He]_N$, the implied flux suggests a low and near constant extraterrestrial ^{3}He accretion rate at the K/T boundary. This result is corroborated by a high-resolution study of the boundary interval (Mukhopadhyay et al., 2001). There is a 4-fold increase in the [^{3}He] concentration 2 m above the K/T boundary, but the implied ^{3}He flux remains nearly constant at 75 × 10^{-15} cc STP cm^{-2} kyr^{-1} in the early Paleocene. The increase in [^{3}He], therefore, reflects a decrease in the sedimentation rate (further considered by Mukhopadhyay et al., 2001).

4.2.3. Paleocene

The implied ^{3}He flux is nearly constant in the Paleocene, except for a spike at ~61 Ma (Fig. 4c), in chron 27N. However, this increase correlates with a short-lived, 6-fold increase in the MAR, and is not associated with a sharp increase in [^{3}He], ^{3}He/^{4}He ratio, or $[^3He]_N$. We conclude that the increase in implied ^{3}He flux at ~61 Ma is due to an error in the MAR. Taking the average implied ^{3}He flux of ~75 × 10^{-15} cc STP cm^{-2} kyr^{-1} for the Paleocene implies a duration of ~1 Myr for chron 27 N instead of the 356 kyr suggested by the Cande and Kent (1995) timescale. We conclude that the extraterrestrial ^{3}He accretion rate in the Paleocene was essentially invariant.

4.2.4. Paleocene/Eocene

Between ~57 Ma and 54 Ma the chron averaged implied ^{3}He flux increases by a factor of 4.5 over the late Paleocene values (Fig. 4c), an increase which is correlated with a 2.5-fold enhancement in [^{3}He] between 57 and 56 Ma (Fig. 3a). The ^{3}He/^{4}He ratio and $[^3He]_N$ are approximately constant between 57 and 56 Ma, but increase by a factor of two in the interval from 56 to 54 Ma (Fig. 3b and 4d). Unfortunately, there are several factors that complicate interpretation of the peak in implied flux. First, marly layers in the late Paleocene/early Eocene sediments imply rapid but poorly constrained variations in MAR. These variations in MAR could reflect either primary biogenic productivity (R. Coccioni, private communication) or short-term fluctuations in the terrigenous flux. Note that an enhancement in the terrigenous flux, between 57 and 56 Ma, would suppress a rise in the ^{3}He/^{4}He ratio and $[^3He]_N$, and may explain the difference in timing of the increases in extraterrestrial [^{3}He], ^{3}He/^{4}He ratio and $[^3He]_N$. Second, Napoleone et al. (1983) report tectonic disturbances, such as faulting and synsedimentary slumping, in this part of the stratigraphic section, and suggest that part of chron 24R is missing at Bottaccione.

Despite these factors, the data suggest a 2-4 fold enhancement in extraterrestrial ^{3}He accretion between ~56 Ma and 54 Ma, the exact timing and magnitude of which are equivocal. We suggest that this increase should be verified from a stratigraphic section free of tectonic disturbance and/or facies changes. Note that if part of the stratigraphic section is missing (as implied by the work of Napoleone et al., 1983), the calculated MAR is less than the true value. Therefore, the suggested increase is a *lower limit* to the true magnitude of the increase in extraterrestrial ^{3}He accretion.

4.2.5. Eocene

While the magnitude and timing of the increase in extraterrestrial ^{3}He accretion at the P/E boundary or in the early Eocene is debatable, the data strongly suggest that the extraterrestrial ^{3}He accretion rate decreased by a factor of three between 54 and ~50 Ma (Fig. 4c). The decrease in implied ^{3}He flux is mirrored by similar decreases in [^{3}He], ^{3}He/^{4}He ratio, and [^{3}He]$_N$, so it is not likely to be a sedimentation phenomenon. The alternative possibility of a three-fold decrease in the MAR is inconsistent with the paleomagnetic data, and our non-carbonate and ^{4}He data (Fig. 3c-3d and 4a; see also Lowrie et al., 1982; Napoleone et al., 1983). Therefore, it seems necessary to conclude that the extraterrestrial ^{3}He accretion rate decreased by a factor of three in the early Eocene over a period of 4–5 Myrs.

Although there is an increase in [^{3}He] at the end of the middle Eocene in chron 18N, we cannot evaluate this part of the record since the magnetochron continues beyond the currently accessible part of the stratigraphic section.

5. Discussion

Helium analyses in the Gubbio limestones provide information on the flux of ^{3}He and ^{4}He to the seafloor over a 35 Myr period from the Maastrichtian to the middle Eocene. These two isotopes are almost completely independent of each other, with ^{3}He overwhelmingly derived from interplanetary dust, and ^{4}He from terrigenous matter. Here we discuss the implications of the record of these two tracers.

5.1. IDP Accretion

Based on the arguments in the previous section, our best estimate of the ^{3}He accretion rate from the Apennine sections is presented in Figure 5. The shape of the ^{3}He profile is generally similar to the low temporal resolution record from a pelagic clay core in the central Pacific (LL44-GPC3; Farley, 1995), but the implied fluxes at Gubbio are on average a factor of four lower. The origin of this discrepancy is not yet known. The area-time products of the samples composing these two records are similar, so differential undersampling is unlikely to be the cause. However, it is possible that diagenetic effects are involved. For example, Patterson et al. (1998) found that the magnetic fraction in subaerially exposed 480 Myr old marine limestone carried no measurable ^{3}He, in contrast to pelagic clays from the GPC3 core, where the magnetic fraction carries >50% of the total ^{3}He (Farley 1995, 2001). It is possible that extended subaerial exposure leads to decomposition of ^{3}He-bearing magnetic grains, leaving only a second, more resistant carrier. More work is required to address the issue, e.g., by determining the carrier phase(s) responsible for long term retention of ^{3}He. Regardless of this discrepancy, the similarity of pattern between the high-resolution Gubbio record and that from GPC3 gives us confidence that our record provides a global, but relative, history of the terrestrial ^{3}He accretion rate.

The ^{3}He record from Gubbio is most simply interpreted in terms of variations in the terrestrial accretion rate of IDPs arising from various solar system processes, a hypothesis supported by the correlation of terrestrial impacts with a several Myr period of enhanced ^{3}He accretion in the late Eocene (Farley et al., 1998). Although other processes may affect the ^{3}He accretion rate (e.g., changes in solar wind output), we believe these

Figure 5. Extraterrestrial ^{3}He accretion rate. The solid line represents our best estimate of the extraterrestrial ^{3}He accretion rate from 74 to 39 Ma, based on the arguments presented in the text. The late Eocene data is from Farley et al. (1998). The dotted line is an interpolation of the extraterrestrial ^{3}He flux between 39 and 36 Ma. The shaded envelope is the same as in Figure 4c.

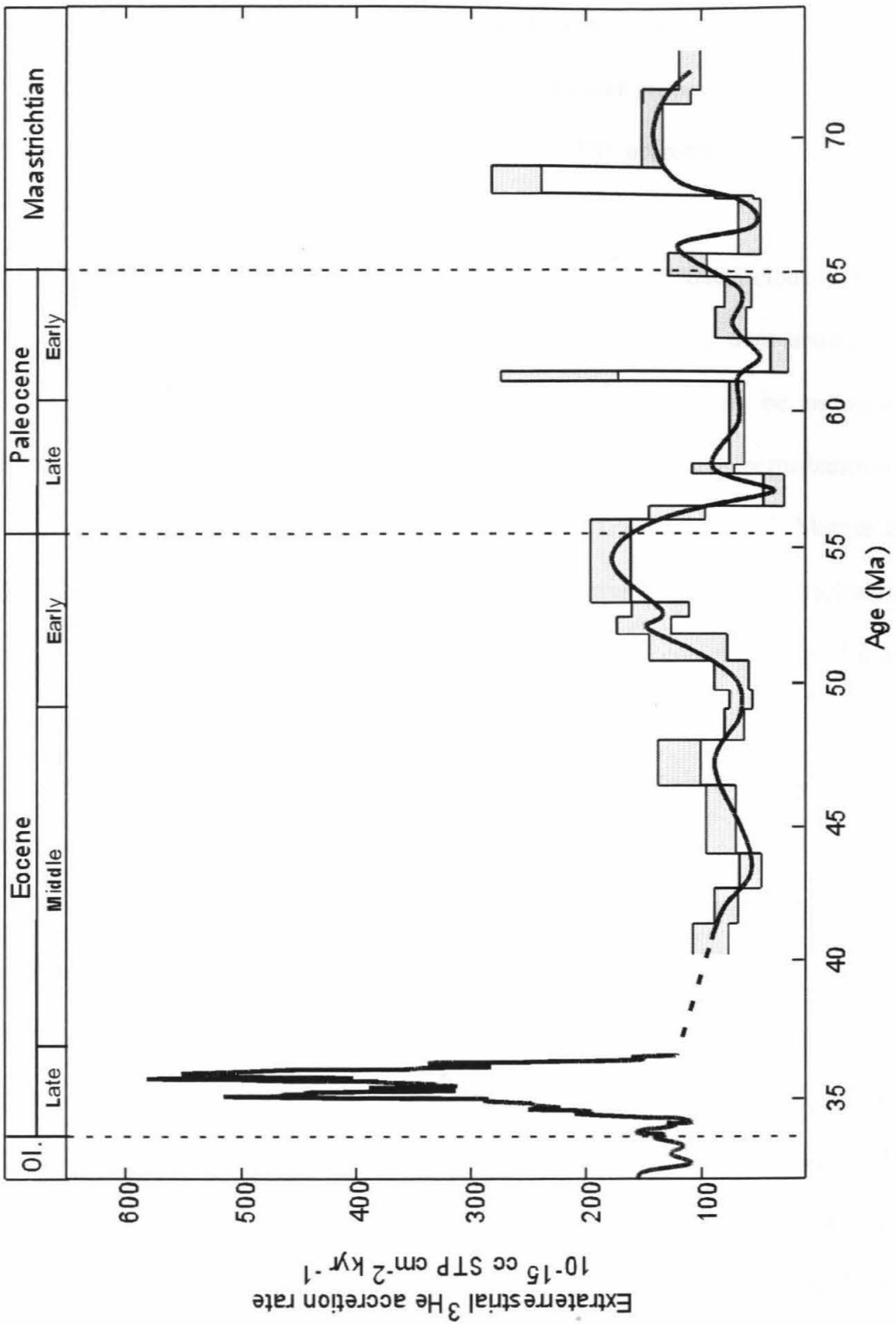
Olig.
Eocene
Late
Middle
Early
Paleocene
Late
Early
Maastrichtian
600
500
400
300
200
100
35
40
45
50
55
60
65
70
Age (Ma)
Extraterrestrial 3He accretion rate
10-15 cc STP cm-2 kyr-1

processes are less significant than those that directly modulate the abundance of IDPs in the zodiacal cloud (also see Farley, 2001). Here we consider processes responsible for the pattern shown in Figure 5, and how variations in IDP accretion may be related to terrestrial impact events.

Cometary particles are an important component of the zodiacal cloud (Liou et al., 1995). While a single comet is unlikely to substantially modify dust abundances or terrestrial impact probability, the abundance of active comets can be tremendously enhanced over a two to several million-year period by gravitational perturbation of the Oort cloud (e.g., Hills, 1981; Byl, 1983; Heisler and Tremaine, 1986; Matese et al., 1995). Such an event is expected to increase the IDP accretion rate and the probability of terrestrial impacts over the duration of the shower. Although comet showers have been invoked to explain various aspects of the terrestrial cratering record, beside the late Eocene event (Farley et al., 1998) little observational evidence exists regarding the timing and recurrence interval of these important events.

Major collisions in the asteroid belt are also expected to increase the abundance of IDPs in the zodiacal cloud. Depending on grain size, dust from the asteroid belt becomes earth crossing in ~10^4 to 10^5 years after collision due to P-R drag. Larger bodies ejected from the asteroid belt by the collision can become Earth-crossing on time scales in excess of 1 Myr and possibly as long as 100 Myr, if they do so at all (Gladman, 1997). Therefore, a close (~10^6 years) temporal correlation between IDP accretion rates and impacts following a major collision in the asteroid belt is not expected *a priori* (also see Kortenkamp and Dermott 1998b; Farley 2001). This distinction provides one approach by

which to distinguish enhanced IDP accretion from a comet shower vs. that from an asteroidal collision.

A third possible mechanism for increasing the IDP accretion is associated with major collisions in the Kuiper belt. Dust production in the Kuiper belt may significantly exceed that in the asteroid belt (Flynn, 1999). Liou et al. (1996) suggested that ~20% of the dust produced by the Kuiper belt enters the inner solar system, but dust grains bigger than 9 μm will probably be destroyed by collisions with interstellar grains. However, particles <9 μm may be recorded by ^{3}He in sediments. Further work is needed to establish the timescale of enhanced dustiness and its relationship to terrestrial impact following a collision between Kuiper belt objects.

Our data preclude large, long-lived variations in ^{3}He accretion rate (Fig. 4b). However, factor of 2-4 variations in the ^{3}He accretion rate are suggested. Below we discuss possible origins of these fluctuations; the relation, if any, between this record and known terrestrial impacts; and the implications of our data for models predicting periodic showers of long-period comets.

Minor increases (< factor of 2) in the extraterrestrial ^{3}He accretion rate are suggested between 70.5 and 68 Ma and at ~66 Ma, 1 Myr prior to the K/T boundary. These peaks are at the margin of detection, far smaller and of shorter duration than the late Eocene peak (Fig. 5). Two moderately large impact craters of Maastrichtian age are known: Manson (37 km diameter, 74.1 ± 0.1 Ma, Izett et al., 1998) and Kara Ust-Kara (70.3 ± 2.2 Ma, Trieloff et al., 1998). Kara Ust-Kara is either a single crater or two different craters, and diameter estimates are between 70 and 120 km for the two structures (Koeberl et al., 1990, Nazarov et al., 1991). While Manson is older than the

increase in ^{3}He accretion, the age of Kara Ust-Kara overlaps with the peak at 70.5 Ma. A high-resolution iridium (Ir) profile down to 305 m in the Bottaccione section, corresponding to ~71 Ma, failed to reveal any anomalies in the Ir abundance (Alvarez et al., 1990). Therefore, the minor peaks in ^{3}He accretion rate seen in the Maastrichtian are not in any clear way correlated with impact indicators. If these peaks are real, they probably reflect minor fluctuations in the dustiness of the inner solar system associated with random events in the asteroid and/or Kuiper belt.

The nature of the K/T impactor is a matter of debate upon which our observations have bearing. Suggested candidates include member(s) of a comet shower (e.g., Hut et al., 1987) or an asteroid/comet with a carbonaceous chondritic composition (e.g., Shukolyukov and Lugmair, 1998; Kyte, 1998). Based on data from the GPC3 core, Farley (1995) argued against substantial enhancement in the ^{3}He accretion rate at the K/T boundary. Similarly, our Gubbio analyses reveal a low and constant extraterrestrial ^{3}He accretion rate between 66 Ma and ~57 Ma, implying a low and invariant solar system IDP abundance through this time interval. This observation argues strongly against the possibility that the K/T bolide was associated with a comet shower. Instead our results support the hypothesis that a single earth-crossing asteroid or comet was responsible for the K/T impact. Further consideration of the K/T impact is presented elsewhere (Mukhopadhyay et al., 2001).

Our data suggest a 2-4 fold increase in ^{3}He accretion rate near the P/E boundary (~55 Ma), followed by a decrease over an ~4-5 Myr period. A ^{3}He peak at about this time was also found in the GPC3 core (Farley, 1995). The GPC3 peak appears to be of longer duration, but may be smeared by bioturbation. The P/E peak at Gubbio is similar in shape

to the far larger ^{3}He peak observed in the late Eocene, previously attributed to a shower of long-period comets (Fig. 5 and Farley et al., 1998). Like the late Eocene peak, the P/E peak is asymmetric, with the rise occurring faster than the decline, but is of substantially longer duration than found in the late Eocene. Modeling suggests that comet showers generated by close stellar encounters decay with a period of only 1-2 Myr (Hut et al., 1987; Weissman 1982). The decrease in IDP accretion from 54 to 50 Ma occurs over a longer period, arguing against a comet shower produced by an impulsive perturbation of the Oort cloud. Alternatively, it has been proposed that perturbation of the Oort cloud by Galactic tidal forces may cause a broad maximum in the comet flux over a several million year period with a peak-to-trough comet flux variation of 4:1 (Matese et al., 1995). However, the flux of these long-period comets is predicted to rise and fall symmetrically. This contrasts with the strongly asymmetric P/E peak we have identified. Thus we are aware of no cometary mechanism which predicts a peak of the type we observe.

There are three moderately large impact craters in the Paleocene/early Eocene: Montagnais (D = 45 km; age = 50.5 ± 0.8 Ma; Bottomley and York, 1988), Kamensk (D = 25 km; Age = 49.2 ± 0.2 Ma; Izett et al., 1994) and Marquez Dome (D = 13 km; Age = 58.3 ± 3.1; Sharpton and Gibson, 1990; McHone and Sorkhabi, 1994). With the possible exception of Marquez Dome, these impacts are not temporally correlated with the P/E peak. No correlated PGE anomalies were reported from pelagic clay cores in the Pacific, despite measurements covering this period (Kyte and Wasson, 1986; Peucker-Ehrenbrink, 1996). Although Schmitz et al. (1997) reported a small Ir anomaly in the latest Paleocene, no shocked quartz was found, leaving the origin of the Ir enrichment

uncertain. Thus, we find no clear evidence for impact features that correlate with the P/E peak, further distinguishing it from the late Eocene peak.

A collision in the asteroid belt provides a reasonable alternative explanation. Although the temporal variation of dust production following a collision in the asteroid belt has not been modeled in detail, Durda et al. (1992) suggested variations in the dust production rates of asteroid families. In general their model shows large stochastic asymmetric variations in dust production over timescales of millions to tens of millions of years. Thus, the IDP accretion pattern we infer for the late Paleocene to the middle Eocene is consistent with an increase in the dustiness of the inner solar system following a major collision in the asteroid belt. It may also be possible for collisions in the Kuiper belt to produce this increase in IDP accretion. However, this is speculative since the temporal evolution of dust production in the Kuiper belt is even more poorly constrained than in the asteroid belt.

5.1.1. Implications for Comet Shower Periodicity

Several investigators have suggested that showers of long-period comets may recur with a fixed period and may be responsible for mass extinction events (e.g., Alvarez and Muller, 1984; Davis et al., 1984; Rampino and Stothers, 1984a,b). While arguments against periodic cometary impacts have been presented (e.g., Weissman, 1985; Montanari et al., 1998), modulation of the Oort cloud resulting from the vertical oscillation of the solar system about the Galactic mid-plane (e.g., Matese et al., 1995) apparently remains a viable mechanism for generating cyclical comet showers. The period of this motion is

uncertain; Matese et al. (1995) favored a value between 30-44 Myr while Stothers (1998) suggested a period of 37±4 Myr.

If showers of long-period comets are periodic, the most probable impact crater candidates in the past 75 Myrs are the Popigai and Chesapeake Bay in the late Eocene, the Chicxulub impact at the K/T boundary or the Manson and Kara impact structures in the Maastrichtian. While the increase in IDP accretion rate during the late Eocene may be the result of a shower of long-period comets, Farley et al. (1998) argued against Galactic tidal forcing as a mechanism for its generation. Similarly, we have presented evidence against comet showers associated with the K/T or the Manson and Kara impacts. Indeed, our data preclude major comet showers in the interval from 74 to 39 Ma. If comet showers are periodic, it is not evident from our proxy record of the IDP accretion rate, and comet showers are not associated with any known impact craters in our time window.

5.2. Implications of Terrestrial [^{4}He]

Along with providing insight to relative sedimentation rates, [^{4}He] in sediments is a useful tracer in its own right (Marcantonio et al., 1998; Patterson et al., 1999). In contrast to ^{3}He, ^{4}He in many deep-sea sediments, including those from the Gubbio section, is completely terrestrial in origin. We believe that most of the ^{4}He is transported to the deep sea in a small, He-retentive fraction of the detrital component, possibly zircon (also see Patterson et al., 1999). As shown in Figure 3, there is a strong correlation between ^{4}He and the non-carbonate fraction of the sediment. This is further emphasized in Figure 6, where [^{4}He] is plotted per unit mass of non-carbonate material, ([^{4}He]$_N$). Were [^{4}He]$_N$ constant throughout the record shown in Figure 6, ^{4}He would convey no

Figure 6. $[^4He]_N$ in the Gubbio sediments as a function of age. Points are individual values representing the averages of each sample. Arrows indicate data points that are off scale. The shaded band is the 2σ uncertainty on the five-point running mean. $[^4He]_N$ is approximately constant, except between 66 Ma and 68 Ma, where there is a ~3-fold increase. See text for discussion. Ages have been computed as in Figure 3.

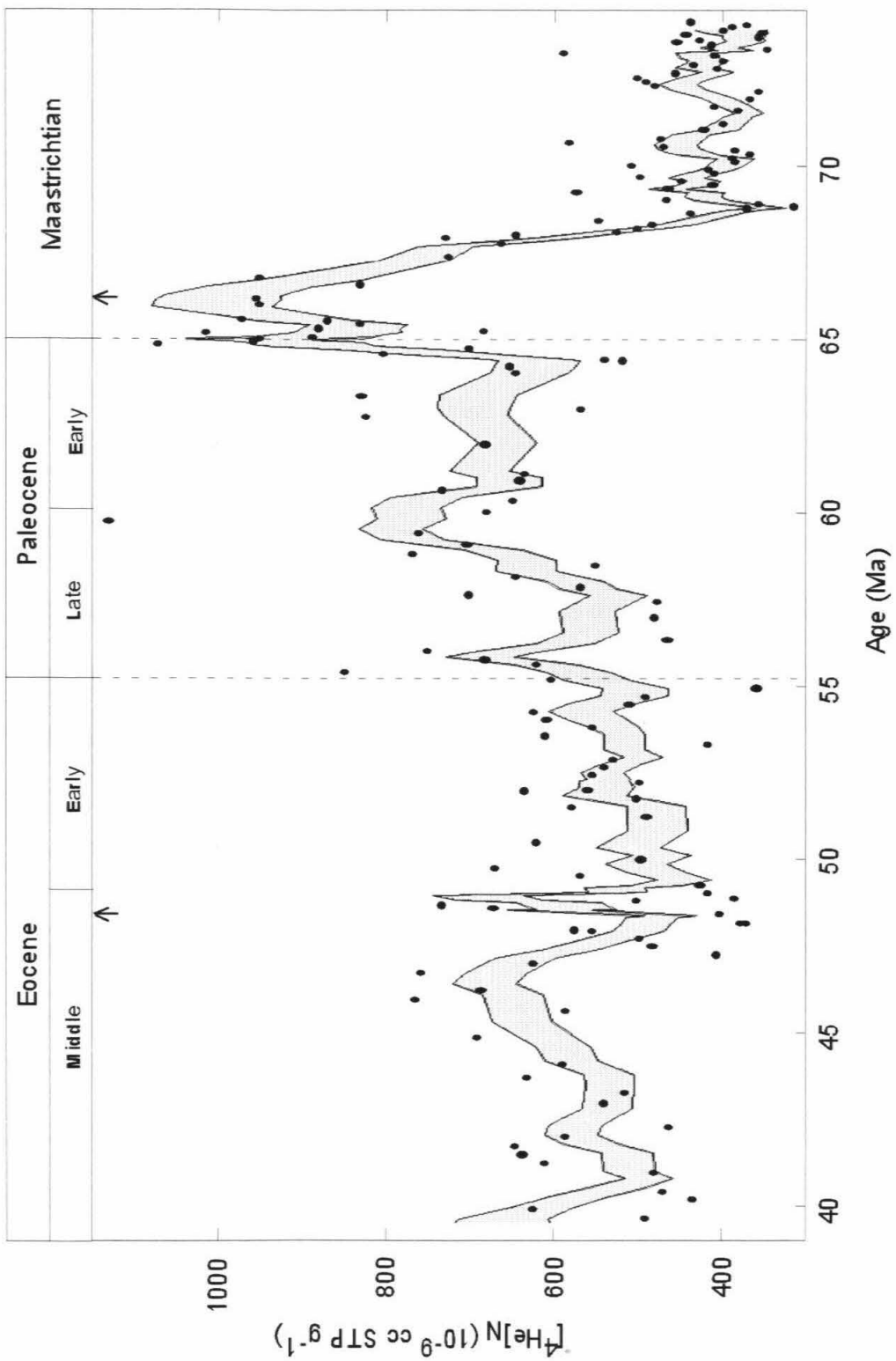
Eocene
Middle
Early
Paleocene
Late
Early
Maastrichtian
40
45
50
55
60
65
70
Age (Ma)
400
600
800
1000
[4He]N (10-9 cc STP g-1)

Figure 7. Seawater Sr-isotopic composition and [^{4}He] as a function of age. Solid circles are [^{4}He] in the Gubbio sediments. Open squares are Sr-isotopic data from Nelson et al. (1991) and open triangles from McArthur et al. (1998).

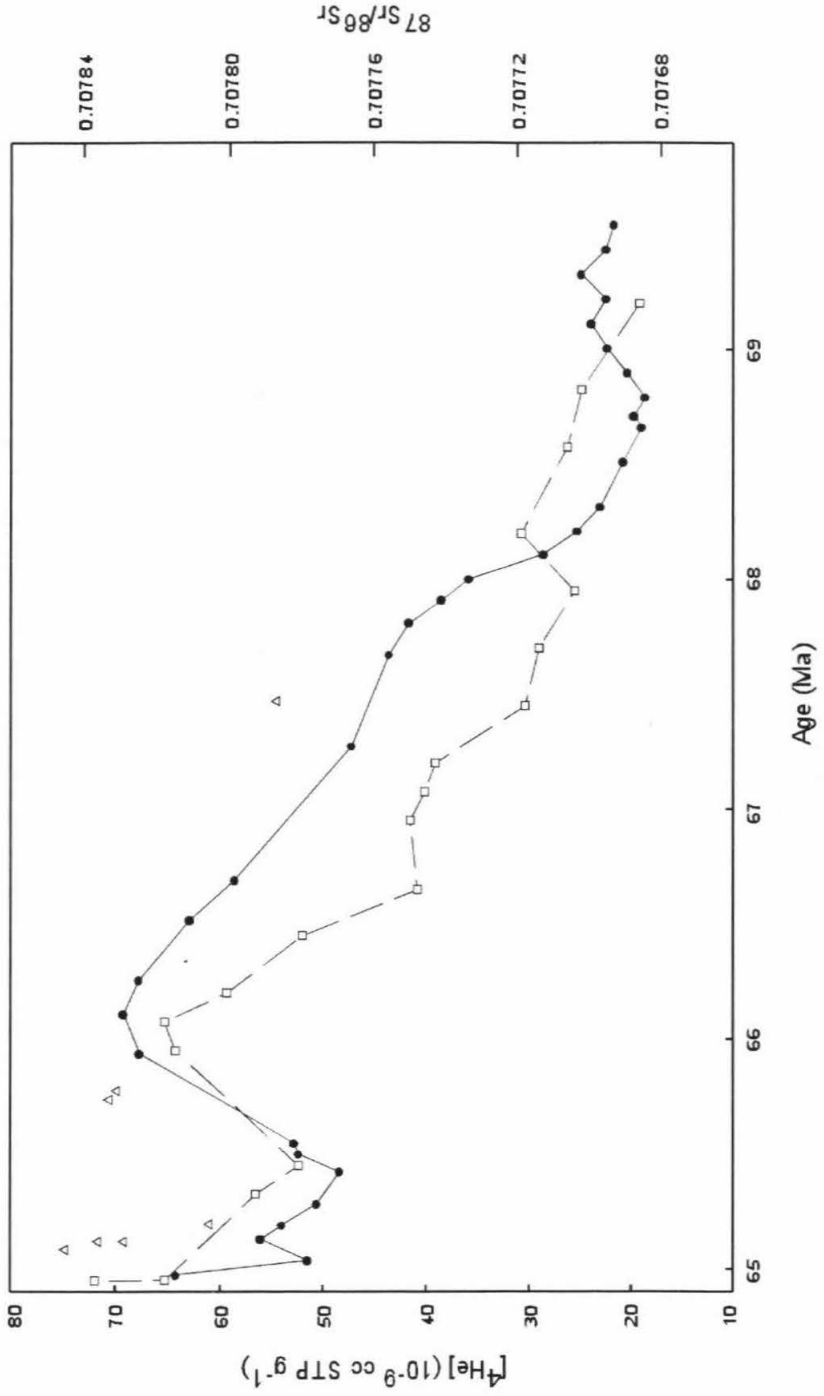
$^{87}Sr/^{86}Sr$
0.70784
0.70780
0.70776
0.70772
0.70768
$[^4He]$ (10^{-9} cc STP g^{-1})
80
70
60
50
40
30
20
10
65
66
67
68
69
Age (Ma)

new information beyond what is available from measurements of the non-carbonate fraction. However, there is a very large increase in $[^4He]_N$ in the Maastrichtian (Fig. 6). Prior to 69 Ma $[^4He]_N$ is invariant, but between 69 and 67 Ma it increases 3-fold, then falls to the nearly constant Cenozoic values. The increase in $[^4He]_N$ most likely documents a change in the composition of the terrigenous input, such that starting at approximately 69 Ma there was an influx of geologically older or more U and Th rich crustal material with higher $[^4He]$, reaching a maximum just prior to the K/T boundary.

Figure 7 shows that the increase in $[^4He]_N$ correlates well with the Sr-isotope composition of seawater between 68 and 65 Ma, including the maximum at 66 Ma and the rise preceding the K/T boundary. This unexpected correlation provides insights to the mechanism driving the change in seawater strontium and terrigenous He in this interval. The strontium isotope composition of seawater, as recorded by marine carbonates, reflects a globally-averaged balance between radiogenic strontium derived from continental weathering and input of non-radiogenic strontium from mid-ocean ridge hydrothermal activity (e.g., Richter et al., 1992; Jones et al., 1994).

The Late Cretaceous seawater $^{87}Sr/^{86}Sr$ record was attributed by Jones et al., (1994) to variations in hydrothermal strontium flux. Since $[^4He]$ in the terrigenous fraction is not directly affected by hydrothermal activity, changes in hydrothermal activity are not likely to account for the correlation in Figure 7. However it is reasonable to expect that changes in continental weathering modify $[^4He]_N$ and $^{87}Sr/^{86}Sr$ together, for example by shifting the composition of weathered continental material towards more radiogenic Sr and $[^4He]$ compositions. Thus our data favor a change in weathering regime or source rocks as an explanation for the $[^4He]_N$ and $^{87}Sr/^{86}Sr$ changes in the last few

Myrs of the Cretaceous, and supports the idea of Nelson et al. (1991) of an increased continental strontium flux. It is important to note that the increase in seawater Sr isotopic composition is a global signal, whereas the Gubbio [^{4}He] is a local signal, recording only the detrital components delivered to the Umbria-Marche Basin. If the increased $[^4He]_N$ signal is restricted to sediments from this general region, it would imply that climatic/tectonic changes in Southern Europe were the dominant control on the global Sr budget of the oceans in the late Maastrichtian. We are aware of no data with which to evaluate this possibility.

6. Summary And Conclusions

We measured the He abundance and isotopic composition of a suite of pelagic limestones exposed in the Italian Apennines that were deposited from ~74 to ~39 Ma. Our data indicate:

- The IDP accretion rate in the Maastrichtian was fairly constant, except for probable but minor increases between ~70.5 Ma and 68 Ma, and at ~66 Ma. These increases are not likely to be related to showers of long-period comets, but may reflect random events in the asteroid or Kuiper belt.
- The IDP accretion rate through the K/T boundary is low and invariant, indicating that the K/T impactor was not a member of a comet shower. Instead, the K/T impactor is more likely to have been a single earth-crossing asteroid or comet.
- We observe a 2-4 fold increase in the IDP accretion rate close to the P/E boundary followed by a factor of three decay over a ~4-5 Myr period. This increase does not exhibit the temporal pattern expected from a comet shower arising from a

gravitational perturbation of the Oort cloud. Instead, our data are more consistent with an increase in IDP accretion resulting from a major collision in the asteroid belt. Collisions in the Kuiper belt may provide an alternate explanation.

- The absence of appropriate peaks in ^{3}He accretion provide strong evidence against long-period comet showers through the 74 to 39 Ma interval. If comet shower periodicity exists, it is either of period longer than 38 Myrs, or the showers do not substantially perturb the ^{3}He accretion rate. The latter seems unlikely given the ^{3}He-based observations for a late Eocene comet shower (Farley et al., 1998).
- The strong correlation between ^{4}He flux and seawater $^{87}Sr/^{86}Sr$ suggests that the rapid rise in strontium isotopic composition in the three million years prior to the K/T boundary was, at least in part, driven by a change in the source of continental material delivered to the sea.

Acknowledegments. We thank Kim Robinson, Elizabeth Navarro, and Selene Eltgroth for sample preparation and P. Clayes, B. Peucker-Ehrenbrink and B. Schmitz for thorough and helpful reviews. This was work was supported by NASA.

References

Alvarez W. and Muller R. A. (1984) Evidence from crater ages for periodic impacts on the earth. *Nature* **308**, 718-720.

Alvarez W., Asaro F., and Montanari A. (1990) Iridium profile for 10 million years across the Cretaceous-Tertiary boundary at Gubbio (Italy). *Science* **250**, 1700-1702.

Alvarez W., Arthur M., Fischer A., Lowrie W., Napoleone G., Premoli Silva I., and Roggenthen W. (1977) Upper Cretaceous-Paleocene magnetic stratigraphy at Gubbio, Italy V.: type section for the Late Cretaceous-Paleocene geomagnetic reversal time scale. *Geol. Soc. Am. Bull.* **88**, 367-389.

Andrews J. N. (1985) The isotopic composition of radiogenic helium and its use to study groundwater movement in confined aquifers. *Chem. Geol.* **49**, 339-351.

Andrews J. N. and Kay R. L. F. (1982) Natural production of tritium in permeable rocks. *Nature* **298**, 361-363.

Arthur M. A. and Fischer A. G. (1977) Upper Cretaceous-Paleocene magnetic stratigraphy at Gubbio, Italy, I. Lithostratigraphy and sedimentology. *Geol Soc. Am. Bull.* **88**, 67-371.

Bottomley R. and York D. (1988) Age measurement of the submarine Montagnais impact crater. *Geophys. Res. Lett.* **15**, 1409-1412.

Byl J. (1983) Galactic perturbations on nearly cometary orbits. *Moon and Planets* **29**, 121-137.

Cande S. C. and Kent D. V. (1992) A new geomagnetic polarity time scale for the Late Cretaceous and Cenozoic. *J. Geophys. Res.* **97**, 13917-13951.

Cande S. C. and Kent D. V. (1995) Revised calibration of the geomagnetic polarity timescale for the Late Cretaceous and Cenozoic. *J. Geophy. Res.* **100**, 6093-6095.

Cerling T. and Craig H. (1993) Geomorphology and in-situ cosmogenic isotopes. *Ann. Rev. Earth Planet. Sci.* **22**, 273-317.

Chauris H., LeRousseau J., Beaudoin B., Propson S., and Montanari A. (1998) Inoceramid extinction in the Gubbio basin (northeastern Apennines of Italy) and relations with mid-Maastrichtian environmental change. *Paleogeogr. Paleoclimatol. Paleoecol.* **139**, 177-193.

Clymer A. K., Bice D. M., and Montanari A. (1996) Shocked quartz from the late Eocene: Impact evidence from Massignano, Italy. *Geology* **24**, 483-486.

Davis M., Hut P., and Muller R. (1984) Extinction of species and periodic comet showers. *Nature* **308**, 715-717.

Dermott S. F., Gorgan K., Gustafson B. A. S., Jayaraman S., Kortenkamp S. J., and Xu Y. L. (1996) Sources in interplanetary dust. In *Physics, Chemistry and dynamics of interplanetary dust* (eds. B. A. S. Gustafson and M. S. Hanner) pp. 143-153. Astronom. Soc. Pac. Conf. Ser. Vol. 104.

Durda D. D., Dermott S. F., and Gustafson B. A. S. (1992) Modeling of asteroidal dust production rates. *Asteroids, Comets, Meteors 1991* (eds. A.W. Harris and E. Bowell), pp. 161-164. Lunar and Planetary Institute, Houston, Texas.

Farley K. A. (1995) Cenozoic variations in the flux of interplanetary dust recorded by ^{3}He in a deep-sea sediment. *Nature* **376**, 153-156.

Farley K. A. (2001) Extraterrestrial helium in seafloor sediments: Identification, characteristics, and accretion rate over geologic time. In *Accretion of*

Extraterrestrial matter throughout Earth's History (eds. B. Peucker-Ehrenbrink and B. Schmitz). In press.

Farley K. A. and Patterson D. B. (1995) A 100-kyr periodicity in the flux of extraterrestrial ^{3}He to the sea floor. *Nature* **378**, 600-603.

Farley K. A., Love S. G., and Patterson D. B. (1997) Atmospheric entry heating and helium retentivity of interplanetary dust particles. *Geochim. Cosmochim. Acta* **61**, 2309-2316.

Farley K. A., Montanari A., Shoemaker E. M., and Shoemaker C. S. (1998) Geochemical evidence for a comet shower in the Late Eocene. *Science* **280**, 1250-1252.

Flynn G. J. (1989) Atmospheric entry heating: A criterion to distinguish between asteroidal and cometary sources of interplanetary dust. *Icarus* **77**, 287-310.

Flynn G. J. (1999) Dust from the Kuiper belt: Modelling the production rate, orbital evolution, and criteria for identification among particles collected at earth. In *Asteroids Comets Meteors 1999*, Cornell University, p30. (abstr.).

Geiss J., Buehler F., Cerutti H., Eberhardt P., and Filleaux C. H. (1972) Solar wind composition experiments. *Apollo 16 Preliminary Sci. Rep.* NASA SP-315, 14.1-14.10.

Gladman B. J. (1997) Dynamical lifetimes of objects injected into asteroid belt resonances. *Science* **277**, 197-201.

Gradstein F. M., Agterberg F. P., Ogg J. G., Hardenbol J., Van Veen P., Thierry J., and Huang Z. (1994) A Mesozoic time scale. *J. Geophys. Res.* **99**, 24051-24074.

Heisler J. and Tremaine S. (1986) The influence of the galactic tidal field on the Oort comet cloud. *Icarus* **65**, 13-26.

Herbert T. D. and D'Hondt S. L. (1990) Precessional climate cyclicity in Late Cretaceous-Tertiary marine sediments: a high resolution chronometer of Cretaceous-Tertiary boundary events. *Earth Planet. Sci. Lett.* **99**, 263-275

Hills J. G. (1981) Comet showers and the steady-state infall of comets from the Oort cloud. *Astron. J.* **86**, 1730-1740.

Hiyagon H. (1994) Retention of solar helium and neon in IDPs in deep sea sediments. *Science* **263**, 1257-1259.

Hut P., Alvarez W., Elder W. P., Hansen T., Kauffman E. G., Keller G., Shoemaker E. M., and Weissman P. R. (1987) Comet showers as a cause of mass extinctions. *Nature* **329**, 118-126.

Izett G. A., Cobban W. A., Dalrymple G. B., and Obradovich J. D. (1998) $^{40}Ar/^{39}Ar$ age of the Manson impact structure, Iowa, and correlative impact ejecta in the Crow Creek Member of the Pierre Shale (Upper Cretaceous), South Dakota and Nebraska. *Geol. Soc. Am. Bull.* **110**, 361-376.

Izett G. A., Masaitis V. L., Shoemaker E. M., Dalrymple G. B., and Steiner M. B. (1994) Eocene age of the Kamensk buried crater of Russia. In *New developments regarding the KT event and other catastrophes in Earth history*. LPI Contrib. **825**, 55-56 (abstr.).

Jones C. E., Jenkyns C. H., Coe A. L., and Hesselbo S. P. (1994) Strontium isotopic variations in Jurassic and Cretaceous seawater. *Geochim. Cosmochim. Acta* **58**, 3061-3074.

Koeberl C., Sharpton V. L., Murali A. V., and Burke K. (1990) Kara and Ust-Kara impact structures (USSR) and their relevance to the K/T boundary event. *Geology* **18**, 50-53.

Kortenkamp S. J. and Dermott S. F. (1998a) Accretion of interplanetary dust particles by the Earth. *Icarus* **135**, 469-495.

Kortenkamp S. J. and Dermott S. F. (1998b) A 100,000-year periodicity in the accretion rate of interplanetary dust. *Science* **280**, 874-876.

Kyte F. T. (1998) A meteorite from the Cretaceous/Tertiary boundary. *Nature* **396**, 237-239.

Kyte F. T. and Wasson J. T. (1986) Accretion rate of extraterrestrial matter: Iridium deposited 33 to 67 million years ago. *Science* **232**, 1225-1229.

Lal D. (1987) Production of ^{3}He in terrestrial rocks. *Chem. Geol.* **66**, 89-98.

Liou J. C., Dermott S. F., and Xu Y. L. (1995) The contribution of cometary dust to the zodiacal cloud. *Planet. Space Sci.* **43**, 717-722.

Liou J. C., Zook H. A., and Dermott S. F. (1996) Kuiper belt dust grains as a source of interplanetary dust particles. *Icarus* **124**, 429-440.

Loosli H. H., Lehmann B. E., Gautschi A., and Tolstikhin I. N. (1995) Helium isotopes in rocks, minerals and related groundwaters. In *Water-Rock Interaction* (eds. Y.K. Kharara and O. Chudaev), pp. 31-34. Proc. 8th International Symp. Water-Rock-Interaction, Vladivostok.

Love S. G. and Brownlee D. E. (1993) A direct measurement of the terrestrial mass accretion rate of cosmic dust. *Science* **262**, 550-553.

Lowrie W. and Alvarez W. (1977) Upper Cretaceous-Paleocene magnetic stratigraphy at Gubbio, Italy, III. Upper Cretaceous magnetic stratigraphy. *Geol. Soc. Am. Bull,* **88**, 374-377.

Lowrie W., Alvarez W., Napoleone G., Perch-Nielsen K., Premoli Silva I., and Toumarkine M. (1982) Paleogene magnetic stratigraphy in Umbrian pelagic carbonate rocks: the Contessa sections, Gubbio. *Geol. Soc. Am. Bull.* **93**, 414-432.

Marcantonio F., Anderson R. F., Stute M., Kumar N., Schlosser P., and Mix A. (1996) Extraterrestrial ^{3}He as a tracer of marine sediment transport. *Nature* **383**, 705-707.

Marcantonio F., Higgins S., Anderson R. F., Stute M. Schlosser P., and Rasbury E. T. (1998) Terrigenous helium in deep-sea sediments. *Geochim. Cosmochim. Acta* **62**, 1535-1543.

Matese J. J., Whitman P. G., Innanen K. A., and Valtonen M. J. (1995) Periodic modulation of the Oort Cloud comet flux by the adiabatically changing galactic tide. *Icarus* **116**, 255-268.

Merrihue C. (1964) Rare gas evidence for cosmic dust in modern Pacific red clay. *Ann. N.Y. Acad. Sci.* **119**, 403-411.

McArthur J. M., Thirlwall M. F., Engkilde M., Zinsmeister W. J., and Howarth R. J. (1998) Strontium isotope profile across the K/T boundary sequences in Denmark and Antartica. *Earth Planet. Sci. Lett.* **160**, 179-192.

McHone J. F. and Sorkhabi R. S. (1994) Apatite fission-track age of Marquez Dome impact structure. *Lunar Planet. Sci.* **XXV**, 881-882. (abstr.).

Monechi S. and Thierstein H. R. (1985) Late Cretaceous-Eocene nannofosil and magnetostratigraphic correlations near Gubbio, Italy. *Mar. Micropaleontology* **9**, 419-440.

Montanari A. and Koeberl C. (2000) *Impact Stratigraphy: The Italian record.* Springer-Verlag, 364 pp.

Montanari A., Bagatin A. C., and Farinella P. (1998) Earth cratering record and impact energy flux in the last 150 Ma. *Planet Space. Sci.* **46**, 271-281.

Montanari A., Asaro F., Michel H. V., and Kennett J. P. (1993) Iridium anomalies of late Eocene age at Massignano (Italy), and ODP site 689B (Maud Rise, Antarctic). *Palaios* **8**, 420-437.

Mukhopadhyay S., Farley K. A., and Montanari A. (2001) A short duration of the Cretaceous-Tertiary boundary event: Evidence from extraterrestrial Helium-3. *Science* **291**, 1952-1955.

Napoleone G., Premoli Silva I., Heller F., Cheli P., Corezzi S and Fischer A. G. (1983) Eocene magnetic stratigraphy at Gubbio, Italy, and its implications for Paleogene geochronology. *Geol. Soc. Am. Bull.* **94**, 181-191.

Nazarov M. A., Badjukov D. D., Barsukova L. D., and Alekseev A. S. (1991) Reconstruction of original morphology of the Kara impact structure and its relevance to the K/T boundary event. *Lunar Planet. Sci.* **XXII**, 959-960 (abstr.).

Nelson B. K., Macleod G. K., and Ward P. K. (1991) Rapid change in strontium isotopic composition of sea-water before the Cretaceous Tertiary boundary. *Nature* **351**, 644-647.

Nier A. O. and Schlutter D. J. (1990) Helium and neon isotopes in stratospheric particles. *Meteoritics* **25**, 263-267.

Ozima M. and Podosek F. A. (1983) *Noble gas geochemistry*. Cambridge University Press, 367 pp.

Ozima M., Takayanagi M., Zashu S., and Amari S. (1984) High $^{3}He/^{4}He$ in ocean sediments. *Nature* **311**, 449-451.

Patterson D. B. and Farley K. A. (1998) Extraterrestrial ^{3}He in seafloor sediments: Evidence for correlated 100 kyr periodicity in the accretion rate of interplanetary dust, orbital parameters, and Quaternary climate. *Geochim. Cosmochim. Acta* **62**, 3669-3692.

Patterson D. B., Farley K. A., and Schmitz B. (1998) Preservation of extraterrestrial 3He in 480-Ma-old marine limestones. *Earth Planet. Sci. Lett.* **163**, 315-325.

Patterson D. B., Farley K. A., and Norman M. D. (1999) ^{4}He as a tracer of continental dust: a 1.9 million year record of aeolian flux to the west equatorial Pacific Ocean. *Geochim. Cosmochim. Acta* **63**, 615-625.

Pierrard O., Robin E., Rocchia R., and Montanari A. (1998) Extraterrestrial Ni-rich spinel in upper Eocene sediments from Massignano, Italy. *Geology* **26**, 307-310.

Peucker-Ehrenbrink B. (1996) Accretion of extraterrestrial matter during the last 80 million years and its effect on the marine osmium isotope record. *Geochim. Cosmochim. Acta* **60**, 3187-3196.

Premoli Silva I. (1977) Upper Cretaceous-Paleocene magnetic stratigraphy at Gubbio, Italy, II. Biostratigraphy. *Geol. Soc. Am. Bull.* **88**, 371-374.

Rampino M. R. and Stothers R. B. (1984a) Terrestrial mass extinctions, cometary impacts and the Sun's motion perpendicular to the galactic plane. *Nature* **308**, 709-712.

Rampino M. R. and Stothers R. B. (1984b) Geological rhythms and cometary impacts. *Science* **226**, 1427-1431.

Richter F. M., Rowley D. B., and DePaolo D. J. (1992) Sr isotope evolution of seawater: the role of tectonics. *Earth Planet. Sci. Lett.* **109**, 11-23.

Roggenthen W. M. and Napoleone G. (1977) Upper Cretaceous-Paleocene magnetic stratigraphy at Gubbio, Italy, IV. Upper Maastrichtian-Paleocene magnetic stratigraphy. *Geol. Soc. Am. Bull.* **88**, 378-382.

Schmitz B., Asaro F., Molina E., Monechi S., Salis K. V., and Speijer R. P. (1997) High-resolution iridium $\delta^{13}C$, $\delta^{18}O$, foraminifera and nannofossil profiles across the latest Paleocene benthic extinction event at Zumaya, Spain. *Paleogeogr. Paleoclimatol. Paleoecol.* **133**, 49-68.

Sharpton V. L. and Gibson J. W. Jr. (1990) The Marquez Dome impact structure, Leon County, Texas. *Lunar Planet. Sci.* **XXI**, 1136-1137 (abstr.).

Shukolyukov A. and Lugmair G. W. (1998) Isotopic evidence for the Cretaceous-Tertiary impactor and its type. *Science* **282**, 927-929.

Stothers R. B. (1998) Galactic disk dark matter; terrestrial impact cratering and the law of large numbers. *Mon. Not. R. Astron. Soc.* **300**, 1098-1104.

Stuart F. M., Harrop P. J., Knott S., and Turner G. (1999) Laser extraction of helium isotopes from Antarctic micrometeorites: Source of He and implications for the

flux of extraterrestrial ^{3}He flux to earth. *Geochim. Cosmochim. Acta* **63**, 2653-2665.

Takayanagi M. and Ozima M. (1987) Temporal variation of $^{3}He/^{4}He$ ratio recorded in deep-sea sediment cores. *J. Geophys. Res.* **92**, 12531-12538.

Ten Kate W. G. and Sprenger A. (1993) Orbital cyclicities above and below the Cretaceous/Paleogene boundary at Zumaya (N Spain), Agost and Relleu (SE Spain). *Sed. Geol.* **87**, 69-101.

Tolstikhin I. N. (1978) Some recent advances in isotope geochemistry of light rare gases. In: *Advances in Earth and Planetary Sciences, 3.* (eds E. C. Alexander, Jr. and M. Ozima), Japan Scientific Societies Press, Tokyo, 33-62.

Tolstikhin I. N., Lehmann B. E., Loosli H. H., and Gautschi A. (1996) Helium and argon isotopes in rocks, minerals and related groundwaters: A case study in Northern Switzerland. *Geochim. Cosmochim. Acta* **60**, 1497-1514.

Trieloff M., Deutsch A., and Jessberger E. K. (1998) The age of the Kara impact structure, Russia. *Meteoritics Planet. Sci.* **33**, 361-372.

Weissman P. R. (1982) Dynamical history of the Oort cloud. In *Comets* (eds. L. L. Wilkening). Univ. Arizona Press, 637 pp.

Weissman P. R. (1985) Terrestrial impactors at geological boundary events: comets or asteroids? *Nature* **314**, 517-518.

Chapter 2: A Short Duration of the Cretaceous/Tertiary Boundary Event: Evidence from Extraterrestrial ^{3}He

S. Mukhopadhyay

K.A. Farley

A. Montanari

(This chapter was reprinted from Science (2001), 291, 1952-1955; Figures have been resized and subheadings added)

Abstract - Analyses of marine carbonates through the interval 63.9 to 65.4 Ma indicate a near-constant flux of extraterrestrial ^{3}He, a tracer of the accretion rate of interplanetary dust to Earth. This observation indicates that the bolide associated with the Cretaceous/Tertiary (K/T) extinction event was not accompanied by enhanced solar system dustiness and so could not have been a member of a comet shower. Using ^{3}He as a constant-flux proxy of sedimentation rate implies deposition of the K/T boundary clay in 10 ± 2 kyr, precluding the possibility of a long hiatus at the boundary and requiring extremely rapid faunal turnover.

1. Introduction

The Cretaceous/Tertiary (K/T) boundary at 65 Ma records a major mass extinction event and though the occurrence of an extraterrestrial impact (*1, 2*) is widely accepted, the nature of the impactor and its role in the K/T mass extinction is debated.

Possible candidates for the impactor are a single asteroid or comet (*1-3*) or a member of a comet shower (*4*). An extraterrestrial impact would have severely perturbed Earth's ecosystems and climate by injecting large quantities of dust (*1*) and climatically active gases (*5*) into the atmosphere. An alternative hypothesis to explain the biotic calamity invokes voluminous volcanism (*6*). Recent work (*7*) suggests that most of the Deccan Traps flood basalts were erupted in a <1 Myr interval coincident with the K/T boundary. The global environmental effects from extensive volcanism could be similar to a large impact (*6*), but the time scale of the two processes would be different. The perturbation on climate and ecosystems from an impact would be geologically instantaneous, but the effects from volcanism would be spread over at least a few hundred thousand years.

The K/T boundary clay is a distinctive, typically few cm thick bed that separates sedimentary rocks of the Cretaceous from those of the Tertiary. Knowledge of the deposition interval of the clay would provide important insights to the cause(s) and rates of mass-extinction and climate change at the boundary, but most geochronologic tools are inadequate for this purpose. Estimates of this time interval are based on the assumption that the K/T clay was deposited at the same rate as the clay fraction in the surrounding paleomagnetically-dated limestones (e.g., *8*); this assumption is questionable during such a turbulent period. Cyclostratigraphy constrains the sedimentation rate before and after the K/T boundary (*9*), but cannot be applied to the clay itself. The duration of the K/T boundary is thus uncertain, with estimates ranging from a few thousand to hundreds of thousands of years (*8-11*). Here we use extraterrestrial He to better characterize the K/T impactor and the depositional interval of the associated clay.

Accumulation of interplanetary dust particles (IDPs) imparts high ^{3}He concentrations ([^{3}He]) and high ^{3}He/^{4}He ratios to many deep-sea sediments (*12*). Extraterrestrial materials have higher ^{3}He/^{4}He ratios than terrestrial matter (>100 R_A versus <0.03 R_A, where R_A is the ^{3}He/^{4}He ratio normalized to the atmospheric value of 1.39×10^{-6}), and this distinction can be used to establish the concentration of extraterrestrial ^{3}He ($[^3He]_{Et}$) in sedimentary rocks. $[^3He]_{Et}$ is most sensitive to the accretion of IDPs smaller than ~35 μm because larger IDPs undergo frictional heating and He loss during atmospheric entry (*13*). Like large IDPs, large bolides (km sized) should not contribute ^{3}He-bearing particles to sediments because they are vaporized upon impact; we verify this expectation below. Therefore, unlike platinum group elements (e.g., Ir and Os), ^{3}He does not directly record the accretion of single large impactors.

$[^3He]_{Et}$ is controlled by the relation $[^3He]_{Et}=f_{3He}r/\alpha$, where f_{3He} is the extraterrestrial ^{3}He accretion rate, α is the sediment mass-accumulation rate (MAR), and r is a retentivity parameter that accommodates diagenetic and/or diffusional He losses, varying between unity and zero. Because $[^3He]_{Et}$ is retained in the sedimentary record for at least 480 Myr (*14*), we assume a constant r over the few million years of interest for the present problem. Measurements of $[^3He]_{Et}$ in a sedimentary sequence thus constrain the ratio f_{3He}/α through time. If f_{3He} is constant, this ratio is inversely proportional to the MAR and permits estimation of the instantaneous sedimentation rate without knowledge of absolute age.

Figure 1. (A) $[^3He]_{Et}$, (B) $[^4He]$ and non-carbonate fraction (solid black line) in the Gubbio sediments. Points are individual values and are averages of leached replicates (if replicated). ◆ indicates the K/T boundary clay. He concentrations are per gram of bulk sediment. The shaded envelope represents the 1σ uncertainty of the three-point running mean calculated from the uncertainties of individual data points (*17*). The K/T boundary sample was not included in the running mean. C29N and C29R refer to magnetic polarity chrons and the chron boundary ages are from (*25*).

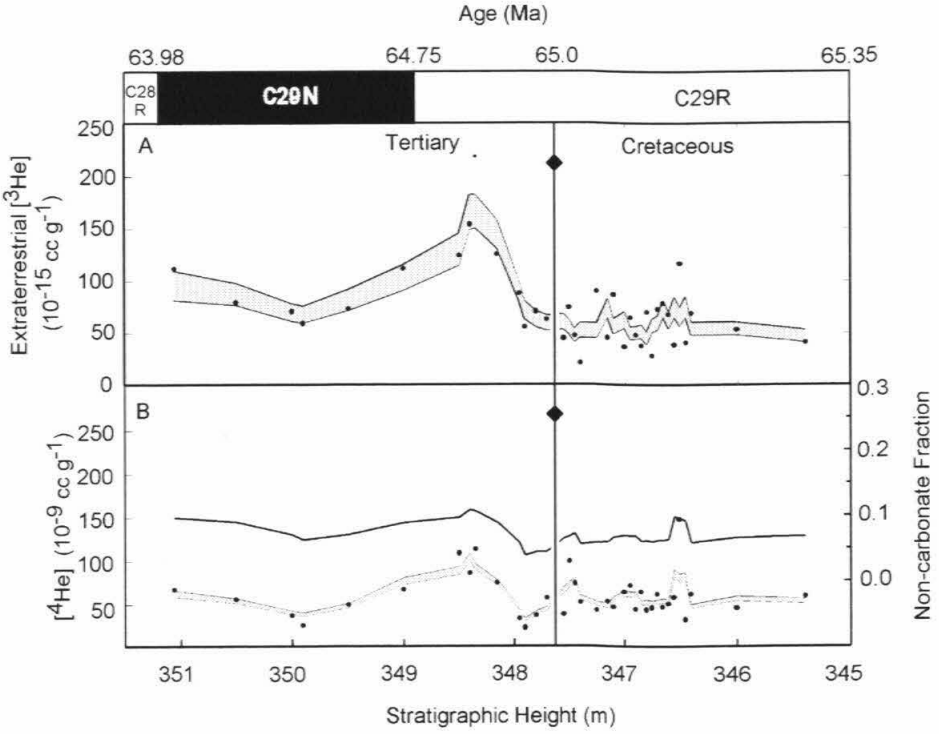
Age (Ma)
63.98
64.75
65.0
65.35
C28 R
C29N
C29R
A
Tertiary
Cretaceous
Extraterrestrial [3He] (10-15 cc g-1)
250
200
150
100
50
0
B
[4He] (10-9 cc g-1)
250
200
150
100
50
0.3
0.2
0.1
0.0
Non-carbonate Fraction
351
350
349
348
347
346
345
Stratigraphic Height (m)

Table 1: ^{3}He, ^{4}He, and ^{3}He/^{4}He ratios in K/T boundary clays.

Site	[^{3}He] 10^{-15} cc STP g^{-1}	± 1σ	[^{4}He] 10^{-9} cc STP g^{-1}	± 1σ	^{3}He/^{4}He R_A
Gubbio	219	25.3	265.7	13.4	0.6
Monte Conero	309	43.7	477.2	67.5	0.5
STW 0	15	3.0	251.8	50.4	0.04
20	19.9	3.9	551.0	110.0	0.03
80	25.9	5.2	458.5	91.7	0.04

He concentrations are per gram of bulk sediment. For the Gubbio and Monte Conero K/T clay, an entire strip of the clay was sampled and homogenized prior to He measurements (supplemental information). The reported values therefore represent an average value for the K/T clay. The numbers (in mm) next to the STW site represent the stratigraphic height from the base of the 0.5 m thick K/T clay layer (*15*, *16*).

Table 2: Duration of K/T Boundary event.

Site	Thickness of K/T clay (mm)	Sedimentation Rate (mm kyr^{-1})	$\pm 1\sigma$	Duration (kyr)	$\pm 1\sigma$
Gubbio	20	2.5	0.3	7.9	1.0
Monte Conero	20	1.8	0.3	10.9	1.6
STW	500	44	9	11.3	2.3
STW Ir-rich layer	3	53	11	<0.06	0.01

Sedimentation rate was computed using an average ^{3}He accretion rate of $106 \pm 4.6 \times 10^{-15}$ cc cm^{-2} kyr^{-1} and a density of 2 g cm^{-3} for the boundary clay. The 1σ uncertainty in the duration of the boundary event is the propagated uncertainty of the ^{3}He accretion rate and measured $[^3He]_{Et}$ (*13*, *17*).

2. Samples and Results

We measured helium concentration and isotopic ratio on samples from the Gubbio and Monte Conero sections in the Umbrian Apennines of Italy (supplemental information), and at three stratigraphic levels in the 0.5 m thick K/T clay from the Ain Settara section (STW) near El Kef, Tunisia (Table 1; *15, 16*). $^3He/^4He$ ratios in the Gubbio sediments vary from 1.9 to 0.3 R_A (supplemental information) and can be modeled as a two-component mixture of crustal and extraterrestrial He (*17*). Assuming reasonable end-member $^3He/^4He$ ratios of 0.03 R_A and 290 R_A (*18, 19*) for the crustal and extraterrestrial components, the calculated $[^3He]_{Et}$ is >86% of the total ^3He. Helium-4 ($[^4He]$) is >99% terrestrial and may therefore be used as a tracer of the relative terrigenous flux (*20*).

High frequency scatter in $[^3He]_{Et}$ (Fig. 1A) is probably a statistical artifact of the small number of IDPs hosted in the sediments (e.g., *13*). A 3-point running mean through the data reduces this scatter; the smoothed $[^3He]_{Et}$ is constant to within ±20% from 345 m to the K/T boundary at 347.63 m, increases in the K/T clay, and returns to pre-K/T values within the first limestones of the Tertiary. About 0.5 m above the K/T boundary $[^3He]_{Et}$ increases briefly, then decreases (Fig. 1).

3. Discussion and Implications

$[^3He]_{Et}$ is correlated with proxies of relative sedimentation rate (*17, 20, 21*) such as sediment non-carbonate fraction (NCF) and $[^4He]$ (Fig. 1). This correlation implies that between 63.9 Ma and 65.4 Ma, the ^3He accretion rate was constant and $[^3He]_{Et}$ in the sediments was controlled predominantly by changes in carbonate MAR. Hence the K/T

impact was not preceded nor immediately followed by a change in ^{3}He accretion greater than ±20%. ^{3}He/^{4}He ratio is constant across the K/T boundary (supplemental information, Table 1), and because ^{4}He and NCF increase when sediment MAR decreases (*17, 20, 21*), the higher $[^3He]_{Et}$ in the K/T clay is attributable solely to a decrease in sedimentation rate.

Possible candidates for the K/T impactor include an asteroid or comet (*1-3*), or a member of a shower of long-period comets (*4*). Showers of long-period comets are produced by gravitational perturbations of the Oort cloud that enhance the cometary flux over a 1-2 Myr period (*4*). Cometary activity increases the interplanetary dust abundance in the inner solar system (*22*), and because this dust is swept into the sun on a lifetime that is shorter than the mean life of a long-period comet (600 kyr; *23*), terrestrial impacts produced by members of a comet shower should be associated with enhanced IDP (and $^3He_{Et}$) accretion (*21*). The near-constant ^{3}He accretion rate observed from 65.4 to 63.9 Ma rules out such an event at the K/T boundary. Instead our data are more consistent with an impact of an asteroid or a lone comet, since a single comet would not significantly increase the total IDP flux. Major collisions in the asteroid belt also enhance the terrestrial accretion rate of IDPs over a 10^4 to 10^6 year period (*18, 24*). Such collisions might lead to new Earth-crossing asteroids in 10^6 years (*24*), so an increase in inner solar system dustiness may be associated with an enhanced probability of terrestrial impact. Our $[^3He]_{Et}$ data argue against this scenario for the K/T impactor.

The near-constant ^{3}He accretion rate across the K/T boundary allows the $[^3He]_{Et}$ record to be inverted for instantaneous sedimentation rate within the K/T clay. In calculating the time associated with the K/T boundary event we must assume that no part

Figure 2. $[^3He]_{Et}$ based sedimentation rate. Points are values of the instantaneous sedimentation rate; ◆ indicates the K/T boundary. The line is a three-point running mean. A ^3He accretion rate of 106×10^{-15} cc cm^{-2} kyr^{-1} and a density of 2.7 g cm^{-3} for the limestones as measured by (*17*) were used to compute sedimentation rates. The arrow indicates an off-scale point. The K/T sample along with the off scale point were not included in the running mean. Time relative to the K/T boundary was calculated from the ^3He-based sedimentation rate.

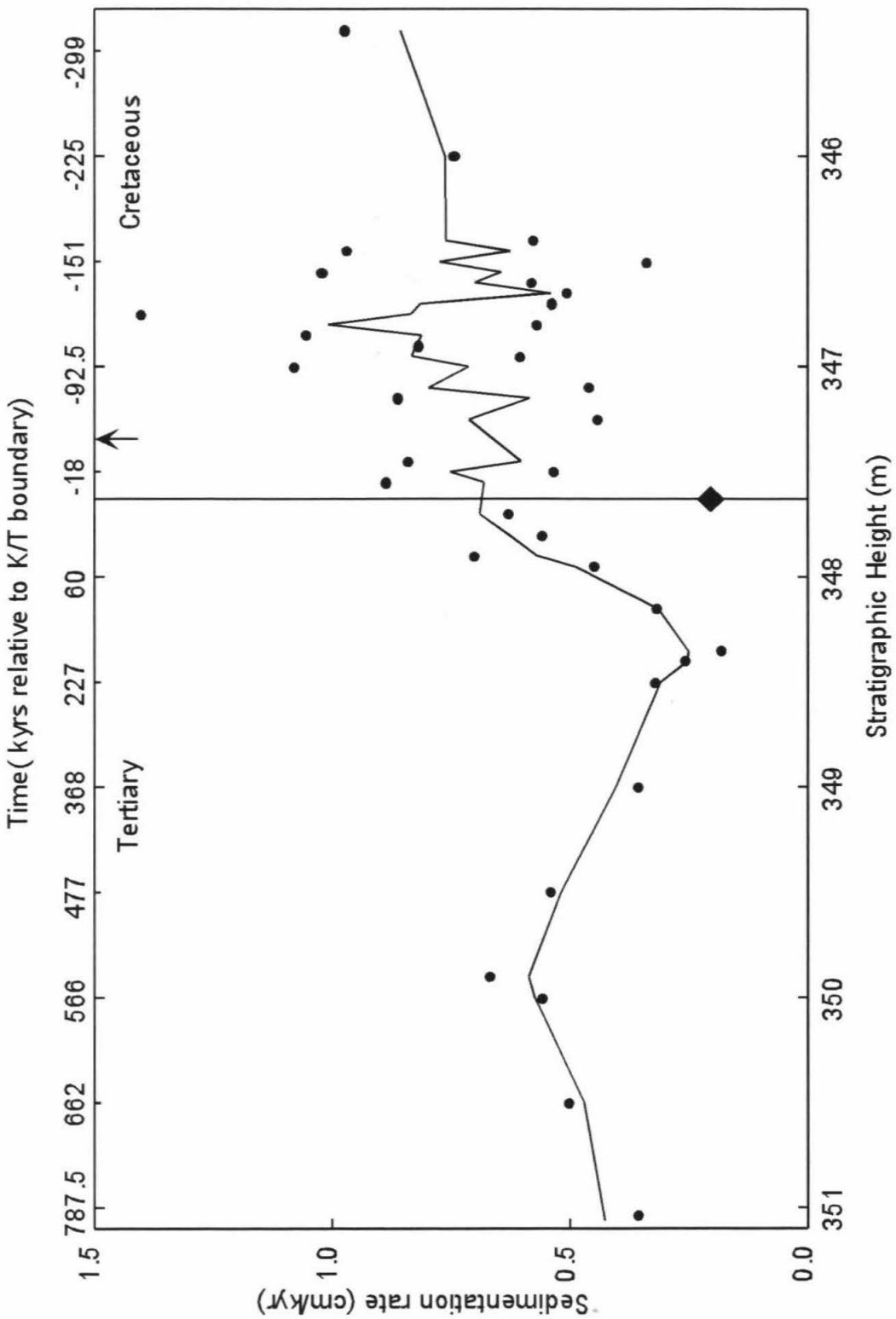
Time (kyrs relative to K/T boundary)
787.5
662
566
477
368
227
60
-18
-92.5
-151
-225
-299
Tertiary
Cretaceous
1.5
1.0
0.5
0.0
Sedimentation rate (cm/kyr)
351
350
349
348
347
346
Stratigraphic Height (m)

of the K/T clay has been lost by erosion or slumping. To test this assumption we analyzed K/T boundary clays from multiple locations.

Calculated sedimentation rates of the K/T clay vary from 2.5 mm kyr^{-1} at Gubbio to 53 mm kyr^{-1} at STW (Table 2, supplemental information). The original thickness and density of the K/T boundary clay at Gubbio are uncertain owing to the presence of secondary calcite (*10*). The thickness (20 mm) and dry bulk density (2 g cm^{-3}) of the clay are better known and more representative at Monte Conero (9). Using these values for the Italian sites, the depositional intervals for the K/T clay are 7.9 ± 1.0 kyr and 10.9 ± 1.6 kyr at Gubbio and Monte Conero respectively (Table 2). The deposition interval of the 0.5 m thick boundary clay at STW is 11.3 ± 2 kyr (Table 2, *26*), consistent with the results from the Italian sections. At STW an ~3 mm thick layer near the base of the K/T clay has been identified as the fallout lamina (*16*, *27*). Based on $[^3He]_{Et}$, an upper limit for the depositional interval of this layer is 60 ± 12 years (Table 2).

The recent discovery of fullerene-hosted extraterrestrial ^3He in K/T boundary clays (*28*) provides a potential complication for our calculation. However, the total ^3He contribution from the bolide cannot exceed 8% of the $[^3He]_{Et}$ in the K/T clay from Gubbio (*29*). Note that if part of the $[^3He]_{Et}$ *is* from the bolide, the fraction from IDPs is lowered, so our computed durations of the boundary event are firm upper limits.

Some investigators (e.g., *11*) have proposed that the mass extinction at the K/T boundary was not catastrophic, but only appears so because of long-duration (100 kyr) hiatus(es) at the K/T boundary in many deep-sea sections. A long hiatus in the Gubbio and Monte Conero sites would have resulted in high concentrations of IDPs and consequently low $[^3He]_{Et}$-based sedimentation rate. Because our samples from these sites

are homogenized strips covering the entire length of the K/T boundary clay, any hiatus present would have been sampled. The computed depositional time of ~10 kyr for the boundary clay, coupled with the agreement from the three different K/T sites, leads us to conclude that there was no long duration hiatus. The mass-extinction at the K/T boundary was an extremely rapid catastrophe and the time span is too short to be explained by Deccan volcanism, which was erupted over a period >500 kyr (*6, 7*). We conclude that the impact of an asteroid or a single comet at the K/T boundary was the main driving force of the biotic calamity.

Following the K/T impact, oceanic productivity was drastically reduced (*30*). Global darkness would have lasted at most a few years, and once surface irradiance returned it would have been difficult to maintain low-productivity oceans (*31*). Our data indicate that, in the deep-ocean, carbonate sedimentation remained low for the ~10 kyr of K/T clay deposition and, surprisingly, imply that sedimentation rates after the K/T boundary event returned to and remained constant at pre-K/T values for the next ~20 kyr (Fig. 2). We hypothesize that 10 kyr was the time required to restore food chains and repair ecosystems. Subsequently, life rebounded, and the oceans were re-populated with planktonic species characterized by high turnover rates. The initial fauna was then replaced by a more stable fauna with lower turnover rates (*32*), possibly explaining the drop in sedimentation rate in the early Tertiary. Our reconstruction of the sedimentation history at Gubbio in the Late Cretaceous suggests rapid variations in sedimentation rates on time scales of 10-20 kyr (Fig. 2), similar to inferences drawn from other sites based on cyclostratigraphy (*9*). These variations may reflect sedimentation responses to orbital forcing (*9*) or fluctuations in primary productivity.

4. References and notes

1. L. W. Alvarez, W. Alvarez, F. Asaro, H. V. Michel, *Science* **208**, 1097, (1980).

2. A. Shukolyukov, G. W. Lugmair, *Science* **282**, 927, (1998).

3. F. T. Kyte, *Nature* **396**, 237, (1998).

4. P. Hut et al., *Nature* **329**, 118, (1987).

5. D. A. Kring, *GSA Today* **8**, 2, (2000).

6. C. B. Officer, A. Hallam, C. L. Drake, J. D. Devine, *Nature* **326**, 143, (1987).

7. C. Hofmann, G. Feraud, V. Courtillot, *Earth Planet. Sci. Lett.* **180**, 13, (2000).

8. J. Smit, A. J. T. Romein, *Earth Planet. Sci. Lett.* **74**, 155, (1985).

9. T. D. Herbert, S. D'Hondt, *Earth Planet. Sci. Lett.* **99**, 263, (1990).

10. A. Montanari, *J. Sed. Petrol.* **61**, 315, (1991).

11. G. Keller, B. Barrera, B. Schmitz, E. Mattson, *Geol. Soc. Am. Bull.* **105**, 979, (1993).

12. M. Ozima, M. Takayanagi, S. Zashu, S. Amari, *Nature* **311**, 449, (1984).

13. K. A. Farley, S. G. Love, D. B. Patterson, *Geochem. Cosmochim. Acta* **61**, 2309, (1997).

14. D. B. Patterson, K. A. Farley, B. Schmitz, *Earth Planet. Sci. Lett.* **163**, 315, (1998).

15. The Ain Settara section (STW) is ~50 km south of the El Kef section. The thickness of the K/T clay in the two sections is approximately equal, and the STW section has been correlated to the El Kef stratotype (J. Kirschvink, personal communication and 16).

16. C. Dupuis, E. Steurbaut, M. F. Matmati, Abstracts presented at the *International workshop on Cretaceous-Tertiary Transition*, Tunis, Tunisia, May 1998.

17. S. Mukhopadhyay, K. A. Farley, A. Montanari, *Geochim. Cosmochim. Acta*. **65**, 653, (2001).

18. K. A. Farley in *Accretion of Extraterrestrial matter throughout Earth's History*: (eds. B. Peucker-Ehrenbrink and B. Schmitz). (2001) In press.

19. A. O. Nier, D. J. Schlutter, *Meteoritics* **25**, 263, (1990).

20. D. B. Patterson, K. A. Farley, M. D. Norman, *Geochem. Cosmochim. Acta* **63**, 615, (1999).

21. K. A. Farley, A. Montanari,E. M. Shoemaker C. S. Shoemaker, *Science* **280**, 1250, (1998).

22. M. V. Sykes, A. A. Lebofsky, D. M. Hunter, F. Low, *Science* **232**, 1115, (1986).

23. P. R. Weissman, *Ann. NY. Acad. Sci.*, **822**, 67, (1997).

24. S. J. Kortenkamp, S. F. Dermott, *Science* **280**, 874, (1998).

25. S. C. Cande, D. V. Kent, *J. Geophys. Res.*, **100**, 6093, (1995).

26. At STW, He measurements were made from the Ir-rich layer (*16*), and 20 and 80 mm above this layer (Table 1). Based on the three measurements we assign an average [^{3}He] of 20×10^{-15} cc STP g^{-1} for the boundary clay. ^{3}He/^{4}He ratios at STW (Table 2) are close to typical crustal ratios of 0.03 R_A (*18*), suggesting that 20% or less of [^{3}He] is extraterrestrial. A reasonable lower limit of the crustal end-member is 0.015 R_A (*18*) and we adopted this value for calculating $[^3He]_{Et}$. Hence, the computed duration of the boundary event from STW is an upper limit.

27. J. Smit, *Annu. Rev. Earth Planet. Sci.* **27**, 75, (1999).

28. L. Becker, R. J. Poreda, T. E. Bunch, *Proc. Natl. Acad. Sci.* **97**, 2979, (2000).

29. The total ^{3}He contribution from the bolide in the Italian K/T clay cannot exceed the ^{3}He concentration of 15×10^{-15} cc STP g^{-1} in the fallout lamina at STW, which is < 8% of the measured ^{3}He in the Italian K/T clays.

30. K. J. Hsu, J. A. McKenzie, Q. X. He, *Geol. Soc. Am. Spec. Pap.* **190**, 317, (1982).

31. S. D'Hondt, P. Donaghay, J.C. Zachos, D. Luttenberg, M. Lindinger, *Science* **282**, 276, (1998).

32. J. Smit, *Geol. Mijnbouw* **69**, 187, (1990).

Acknowledgements: We thank Joe Kirschvink and Tim Raub for providing the STW samples (sample collection funded by NSF EAR9807741) and F. Robaszynski for discussion on the STW section. This work was funded by NASA and the David and Lucille Packard Foundation.

Supplemental Information

Table 3: ^{3}He and ^{4}He concentrations, $^{3}He/^{4}He$ ratios, and non-carbonate fraction in Gubbio limestones. He concentrations are per gram of bulk sediment and [^{3}He], [^{4}He], $^{3}He/^{4}He$ represent averages of leached replicates. R_A is the $^{3}He/^{4}He$ ratio normalized to the atmospheric value of 1.39×10^{-6}. NCF = non-carbonate fraction in the sediments as measured by our mass loss data. The 1σ uncertainty is based on reproducibility of replicate analyses (*1, 2*).

Stratigraphic Height (m)	[^{3}He] 10^{-15} cc STP g^{-1}	± 1σ	[^{4}He] 10^{-9} cc STP g^{-1}	± 1σ	$^{3}He/^{4}He$ R_A	NCF
346.45	41.9	8.1	33.1	2.9	0.9	0.05
346.50	122.8	23.3	148.1	12.9	0.6	0.17
346.55	41.3	7.8	58.3	5.1	0.5	0.07
346.60	70.2	13.6	51.0	4.4	1.0	0.06
346.65	80.1	15.6	46.9	4.1	1.2	0.06
346.70	75.9	10.3	62.5	3.8	0.8	0.06
346.75	29.9	5.6	46.7	4.1	0.5	0.06
346.80	71.4	13.9	44.1	3.8	1.2	0.06
346.85	40.0	7.5	64.4	5.6	0.4	0.07
346.90	49.6	9.5	44.4	3.9	0.8	0.06
346.95	67.9	13.0	72.7	6.3	0.7	0.08
347.00	39.0	7.3	65.1	5.7	0.5	0.07
347.10	88.2	17.2	47.5	4.1	1.3	0.06
347.15	47.8	9.1	53.2	4.6	0.6	0.07
347.25	91.1	17.9	43.6	3.8	1.5	0.05
347.40	23.0	4.2	51.8	4.5	0.3	0.05
347.45	49.9	9.4	74.1	6.4	0.5	0.06
347.50	77.9	14.8	99.8	8.7	0.6	0.10
347.55	46.1	8.9	39.0	3.4	0.8	0.04
347.63			K/T boundary			
347.70	64.9	12.5	57.1	5.0	0.8	0.05
347.80	72.0	14.1	37.3	3.2	1.4	0.04
347.90	56.5	11.1	23.2	2.0	1.7	0.11
347.95	89.2	17.6	33.4	2.9	1.9	0.04
348.15	128.0	17.7	74.9	4.6	1.3	0.15
348.35	222.7	30.8	113.4	6.9	1.4	0.17
348.40	157.0	30.7	86.6	7.5	1.3	0.09
348.50	128.0	24.7	109.3	9.5	0.8	0.10
349.00	114.0	22.2	67.7	5.9	1.2	0.10
349.50	75.0	14.6	49.5	4.3	1.1	0.06
349.90	60.0	11.8	26.1	2.3	1.6	0.05
350.00	72.0	14.1	36.9	3.2	1.4	0.07
350.50	81.0	15.7	55.8	4.8	1.0	0.09
351.06	114.0	22.2	67.2	5.8	1.2	0.11

Notes: Magnetostratigraphic, lithostratigaphic and biostratigraphic data from Gubbio have been reported previously (*3, 4*). The sampling interval was every ~ 0.05-0.10 m within ±1 m of the Cretaceous/Tertiary (K/T) boundary and every 0.50 m further away. Samples were pulverized with a masonry power drill at the outcrop site or powdered with a mortar and pestle in the laboratory. An entire strip of K/T clay was sampled from both Gubbio and Monte Conero. The clay was gently powdered with a mortar and pestle and the powder was thoroughly mixed. For all samples aliquots of 1 to 3 g were leached in 10% acetic acid to remove carbonate. The residue was termed non-carbonate fraction. The leaching does not remove either ^{3}He or ^{4}He (*1*). The decarbonated residue was transferred to tin foil cups. The samples were fused under vacuum at temperatures in excess of 1300°C. Repeat extraction on the samples were performed frequently and in all cases were at blank levels of $<0.2 \times 10^{-9}$ cc STP for ^{4}He and $<1 \times 10^{-15}$ cc STP for ^{3}He. Gas handling and mass spectrometric techniques are described in (*5*), The 1σ variation on ~300 standards of similar size to the samples analyzed during this project was 0.5% for ^{4}He and 3.0% for ^{3}He.

The mean extraterrestrial ^{3}He concentration ($[^{3}He]_{Et}$) in the interval from the base of magnetochron 29R to the K/T boundary is $55 \pm 2.4 \times 10^{-15}$ cc STP g^{-1}. Data from (*1*) have been included for calculating the mean ^{3}He concentration. The uncertainty in the mean $[^{3}He]_{Et}$ was calculated from

$$\sigma_{mean} = \sqrt{\frac{\sum_{i=1}^{n} \sigma_i^2}{n^2}}$$

where σ_i is the 1σ uncertainty in $[^3He]_{Et}$ in an individual sample and n is the total number of samples. The 1σ uncertainty on an individual sample is $20\%/\sqrt{N}$, where N is the number of measurements of the sample (*1, 2*).

The base of magnetochron 29R is at 65.58 Ma (*7*) and the age of the K/T boundary is ~ 65.0 Ma (*8*). Using a density of 2.7 g cm^{-3} for the Gubbio limestones (*1*), the average mass accumulation rate (MAR) in this interval is 1.9 g cm^{-2} kyr^{-1} and the average ^3He accretion rate (the product of $[^3He]_{Et}$ and MAR; *1, 6*) is $106 \pm 4.6 \times 10^{-15}$ cc cm^{-2} kyr^{-1}. The uncertainty in the ^3He accretion rate is given by, $\sigma_{flux} = \sigma_{mean} \times MAR$.

The $[^3He]_{Et}$-based sedimentation rate in mm kyr^{-1}, *s*, was computed using the following relation:

$$s = \frac{f_{3He} r}{[^3He]_{Et} \times \rho}$$

The product $f_{3He}r$ is the average ^3He accretion rate (*1, 6*), where f_{3He} is the extraterrestrial ^3He accretion rate, *r* is a retentivity parameter that accommodates diagenetic and/or diffusional He losses, varying between unity and zero. $[^3He]_{Et}$ is the extraterrestrial ^3He concentration in the sediment, and ρ is the sediment density of 2.7 g cm^{-3} (*1*).

References

1. S. Mukhopadhyay, K. A. Farley, A. Montanari A, *Geochim. Cosmochim. Acta* **65**, 653 (2001).

2. K. A. Farley, S. G. Love, D. B. Patterson., *Geochem. Cosmochim. Acta* **61**, 2309, (1997).

3. W. Alvarez et al., *Geol. Soc. Am. Bull.* **88**, 367, (1977).

4. W. M. Roggenthen, G. Napoleone, *Geol. Soc. Am. Bull.* **88**, 378, (1977).

5. D. B. Patterson, K. A. Farley, *Geochim. Cosmochim. Acta* **62**, 3669, (1998).

6. K. A. Farley, *Nature* **376**, 153, (1995).

7. S. C. Cande, D. V. Kent, *J. Geophys. Res.* **100**, 6093, (1995).

8. C. C. Swisher et al., *Science* **257**, 954, (1992).

Chapter 3: The Carrier Phase(s) of Extraterrestrial ^{3}He in Geologically Old Sediments

S. Mukhopadhyay

Abstract - To better understand the composition, characteristics of helium diffusion, and size distribution of interplanetary dust particles (IDPs) responsible for the long-term retention of extraterrestrial ^{3}He, we carried out leaching, stepped heating, and sieving experiments on pelagic clays that varied in age from 0.5 Ma to ~90 Ma. The leaching experiments suggest that the host phase(s) of ^{3}He in geologically old sediments are neither organic matter nor refractory phases, such as diamond, graphite, Al_2O_3, and SiC, but are consistent with extraterrestrial silicates, Fe-Ni sulfides, and possibly magnetite. Stepped heating experiments demonstrate that the ^{3}He release profiles from the magnetic and non-magnetic components of the pelagic clays are remarkably similar. Because helium diffusion is likely to be controlled by mineral chemistry and structure, the stepped heating results suggest a single carrier that may be magnetite, or more probably a phase associated with magnetite. Furthermore, the stepped outgassing experiments indicate that about 20% of the ^{3}He will be lost through diffusion at seafloor temperatures after 50 Myrs, while sedimentary rocks exposed on the Earth's surface for the same amount of time would lose up to 60%. The absolute magnitude of the ^{3}He loss is, however, likely to depend upon the ^{3}He concentration profile within the IDPs, which is not well known.

Contrary to previous suggestions that micrometeorites in the size range of 50-100 μm in diameter are responsible for the extraterrestrial ^{3}He in geologically old sediments

(Stuart et al., 1999), our sieving experiment demonstrates that at most 20% of the ^{3}He is carried by particles greater than 50 μm in diameter. The size-distribution of the ^{3}He-bearing particles implies that extraterrestrial ^{3}He in sediments record the IDP flux rather than the micrometeorite flux. Further, unlike micrometeorites, ^{3}He-bearing IDPs will be less prone to concentration or depletion relative to bulk sediments by sedimentary processes such as winnowing.

1. Introduction

High ^{3}He/^{4}He ratios in many deep-sea sediments result from accumulation of extraterrestrial material (Merrihue, 1964). From the observation that ^{3}He/^{4}He ratios in sediments are inversely correlated to sedimentation rates, Ozima et al. (1984) concluded that interplanetary dust particles (IDPs) were the carriers of extraterrestrial ^{3}He (^{3}He$_{ET}$). However, modeling indicates that ^{3}He$_{ET}$ is sensitive to the accretion of IDPs less than ~35 μm in size because larger particles are intensely heated during atmospheric entry and lose helium (Farley et al., 1997). ^{3}He-bearing IDPs in oceanic sediments are preserved for geologically long periods (Farley, 1995) and at least in one instance for 480 Myrs (Patterson et al., 1998). The long-term retention of ^{3}He$_{ET}$, therefore, provides an opportunity to characterize the delivery history of IDPs over geologic time. The carrier phase(s) responsible for the long-term retention of ^{3}He, however, remains unclear. Identification of the ^{3}He carrier phase is important for understanding He-retentivity as a function of environmental variables such as redox condition and temperature. Furthermore, the size distribution of ^{3}He$_{ET}$-bearing particles in geologically old sediments is controversial. Stuart et al. (1999) suggested that instead of IDPs, micrometeorites

might be responsible for the long-term retention of ^{3}He, where micrometeorites are defined as dust particles greater than 50 μm in diameter (e.g., Klock and Stadermann, 1994). Knowledge of the size distribution of ^{3}He-bearing particles is important for understanding how sedimentary phenomena such as resuspension and transport by ocean bottom currents may redistribute these particles on the seafloor (e.g., Farley and Patterson, 1995; Marcantonio et al., 1996).

Based on magnetic separations and chemical dissolution experiments performed on Quaternary sediments, previous studies have suggested magnetite and an unknown silicate phase as the carriers of $^3He_{ET}$ (Fukumoto et al., 1986; Amari and Ozima, 1988; Matsuda et al., 1990). The suggestion of magnetite as one of the carriers is, however, problematic. Magnetite in IDPs is not primary but formed during atmospheric entry heating through oxidation of Fe-Ni sulfides, olivine, pyroxene, and poorly ordered silicates (Fraundorf et al., 1982; Brownlee, 1985; Bradley et al., 1988). Because magnetite formation during entry heating will involve breaking chemical bonds and diffusion of oxygen, pervasive loss of ^{3}He from the material undergoing the chemical transformation might be expected.

Fukumoto et al. (1986) noted that in Quaternary sediments approximately 50% of the ^{3}He was in the non-magnetic fraction, probably associated with extraterrestrial silicates. While extraterrestrial silicates may be responsible for the long-term retention of ^{3}He, the diffusivity of ^{3}He in the non-magnetic fraction is not well characterized. Furthermore, olivine and pyroxene, the dominant silicate phases in IDPs would be susceptible to diagenetic alteration on the seafloor. Although chemical leaching on recent sediments suggests that refractory phases such as diamond, graphite, SiC, and Al_2O_3 do

not account for more than 10% of the $^3He_{ET}$, refractory phases may or may not be the major carriers in older sediments. Therefore, to understand the nature of the phase(s) responsible for the long-term retention of ^3He and the size distribution of He-bearing particles, we carried out chemical leaching, stepped heating, and sieving experiments on geologically old sediments.

2. Samples and Experimental Techniques

2.1. Samples

The sediments used in this study are from the LL-44-GPC-3 core (Corliss and Holister, 1982; Kyte et al., 1993), Deep Sea Drilling Project (DSDP) Site 596B, and the 1.85 Ga Onaping Breccia in the Sudbury impact crater (Becker et al., 1986). The GPC-3 and DSDP 596B samples were selected on the basis of high ^3He concentrations, available mass from the curators, and to cover a wide range in ages. Samples from the GPC-3 core are between 32 and 51 Ma, while the sample from DSDP 596B (1-6 80-83) has an age between 75 and 90 Ma (Montgomery and Johnson, 1983) (Table 1). The Onaping Breccia was selected to confirm the preservation of extraterrestrial ^3He in fullerenes (Becker et al., 1996) in 1.85 Ga old sediment. Prof. Tom Ahrens at Caltech provided the Onaping Breccia sample.

To determine if magnetic and non-magentic carrier(s) exist, some of the samples were separated into magnetic and non-magnetic fractions. The sediment was suspended in water in a beaker, and a test tube containing a rare earth magnet (Nd-B magnet) was immersed in the beaker. Magnetic particles were found to stick to the walls of the test

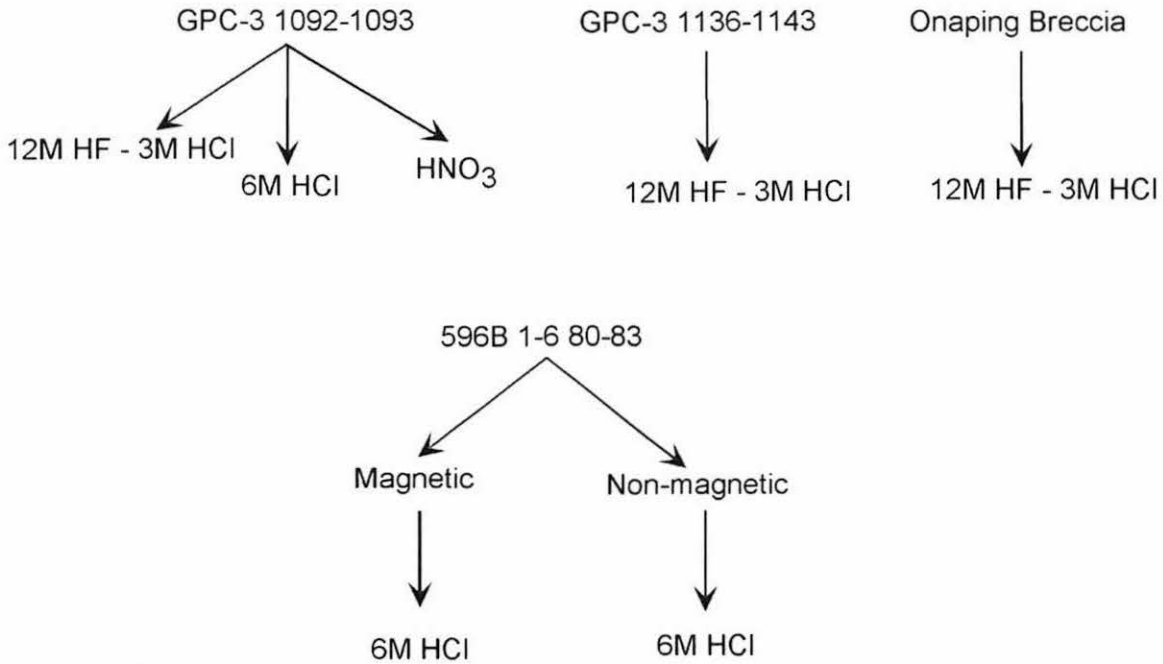

Figure 1: Sample dissolution scheme.

tube adjacent to the magnet. The test tube was then taken out of the beaker and the particles washed off into a separate beaker (the magnetic fraction). The above step was repeated multiple times until no more particles were found to stick to the test tube when it was immersed in the beaker.

2.2. Chemical Leaching

The acid dissolution procedure is shown in Figure 1. Aliquots of the bulk sediment samples were treated with either 12 M HF – 3M HCl, 6M HCl, or concentrated HNO_3 solutions for 2 days at room temperature. The leaching time and temperature are similar to those used by previous researchers (e.g., Fukumoto et al., 1986; Matsuda et al., 1990). In addition, magnetic and a non-magnetic fraction of 596B 1-6 80-83 were treated with 6M HCl solution for 2 days at room temperature. Following the dissolution, samples were rinsed in distilled water and centrifuged to isolate the residue. The residues were transferred onto tin foil and dried in an oven at approximately 60°C and then loaded into the Caltech Noble Gas Laboratory's automated gas extraction system. Helium was extracted at temperatures of 1400°C in a radiatively heated double-walled vacuum furnace.

2.3. Stepped Heating

Stepped heating experiments were conducted on bulk clay as well as on the magnetic and non-magnetic fractions from the GPC-3 (Kyte et al., 1993) and DSDP 596B samples. Prior to the experiments, samples were dried in an oven for 0.5-1 hr at 75°C and then loaded into copper envelopes. The apparatus used (Fig. 2) for the diffusion

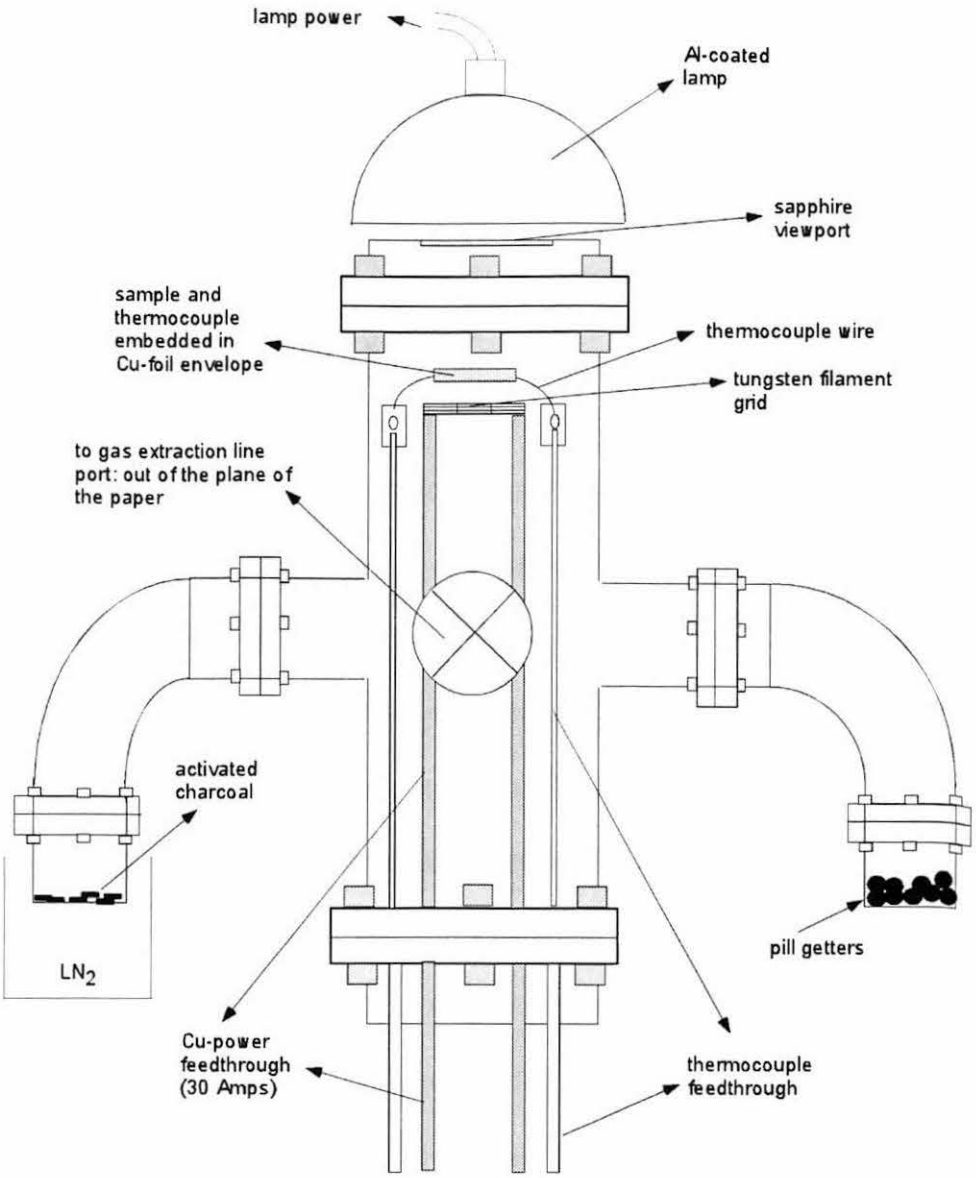

Figure 2: Schematic diagram of the diffusion cell used in the stepped heating experiments (modified after Farley et al., 1999).

experiments is a modification of that described by Farley et al. (1999). In their design the only heat source is a halogen lamp, whose inside reflector is coated with aluminum to increase the forward transmission of radiation through the sapphire window. Because the thermocouple is directly embedded into the Cu-foil housing the sample, the sample temperature is known accurately (± 3°C). However, using the lamp as the only heat source, we could not reach temperatures greater than about 550°C for 150 mg of pelagic clay. To achieve higher temperatures, we added a second heat source in the form of a tungsten filament grid located inside the vacuum chamber about 3-5 mm below the Cu-envelope (Fig. 2). Because we can achieve good temperature control, thermal stability and rapid heating with the lamp, at low-temperatures (< 500°C), heating is accomplished exclusively by the lamp. At higher temperatures, the tungsten filament grid is activated to reach temperatures about 20°C below the desired set point. The final temperature is reached by heating with the lamp, and temperature set points were reached in less than 4 minutes and with under 3°C overshoot. The pill getters (Fig. 2) were used for adsorbing H_2 while activated charcoal at liquid nitrogen temperature was used to freeze down CO_2 and H_2O. The schematic shown in Figure 2 was used for temperatures ≤ 850°C, following which samples were transferred to a resistively-heated furnace and the temperature was monitored using a dual wavelength optical pyrometer. Estimated temperature accuracy for furnace runs is ±10°C. Stepwise heating began as low as 150°C and step intervals were usually 50-100°C. The duration of each step was 30-60 minutes.

2.4. Size Distribution

To determine the size distribution of ^{3}He-bearing IDPs, we studied a 33 Ma old pelagic clay (1092-1093) from the GPC-3 core, selected based on the available mass. The sample was immersed in a beaker of water and swirled with a non-magnetic rod to disaggregate the clay. We then used mesh sizes of 53 μm, 37 μm, and 13 μm to sort the sediment into four size bins of >53 μm, 37-53 μm, 13-37 μm, and <13 μm. The sample was sieved under ethanol and then dried in an oven for 1 hr at 100°C following which it was transferred onto tin foil and loaded into the gas extraction system. Like the other samples, helium was extracted at temperatures of 1400°C in a radiatively-heated furnace.

2.5. Helium Measurements

Gas cleanup and mass spectrometric techniques have been described by Patterson and Farley (1998). Typical ^{4}He blanks for both the resistance furnace and the diffusion cell were less than 0.1×10^{-9} cc STP, and averaged less than 1% of the ^{4}He from the samples. ^{3}He hot blanks were always less than 1×10^{-15} cc STP, in all cases constituting <1% of the sample. The 1-σ variation on standards of similar sizes to the samples analyzed was 0.5% for ^{4}He and ~3.5% for ^{3}He.

3. Results and Discussion

3.1. Chemical Leaching

The results of our acid leaching experiments on the pelagic clays are summarized in Table 1 and Figure 1. The chemical leaches removed 71% to 94% of the

Table 1: Helium concentration in bulk and leached pelagic clays from the GPC3 core and DSDP 596B.

Sample	Age (Ma)	Procedure	Residue (%)	$^3He/^4He$ R_A	$[^3He]$ 10^{-12} cc STP g^{-1}	$[^4He]$ 10^{-9} cc STP g^{-1}
GPC3 1092 – 1093	33	Bulk pelagic clay	-	47.7	16.0	240.7
		Pelagic clay i) 12 M HF – 3M HCl	7.8	44	1.0	15.7
		leached ii) 6M HCl	58	57.9	4.7	56.7
		with iii) 98% HNO3	67	28.2	2.1	51.0
Dried acid waste		12 M HF – 3M HCl	-	3.8	0.02	3.3
		6M HCl	-	4	0.04	6.5
		98% HNO3	-	3.8	0.02	3.2
GPC3 1136-1144	35.14	Bulk pelagic clay	-	176.3	129.7	529.0
		Pelagic clay + 12 M HF – 3M HCl	13	60.3	13.6	160.1
DSDP 596B 1-6 80-83	~75 -90	Magnetic Fraction (MF)	-	60.9	75.2	875.2
		MF leached w/6M HCl	78	15.7	2.3	106.5
		Non-magnetic (NMF)	-	33.5	29.2	630.1
		NMF leached w/6M HCl	82	23	3.8	114.4
Onaping Breccia	1850	Bulk rock	-	0.01	0.4	30992.0
		Bulk rock + 12M HF – 3M HCl	29	0.04	0.00	362.0

The total volume of acids used in all cases were 50 ml. Helium concentrations have been reported per gram of starting material and *not* to the amount of residue left following the leach. R_A is the $^3He/^4He$ ratio normalized to the air ratio of 1.39×10^{-6}. Age assignments for GPC3 samples are from Kyte et al. (1993). Age for the DSDP sample is from Montgomery and Johnson (1983).

^{3}He. To verify that ^{3}He-bearing IDPs were not lost during centrifuging and subsequent decanting procedures, the acid waste from some of the leaches were collected, dried, and analyzed for ^{3}He content. The dried acid waste has negligible amounts of ^{3}He (Table 1), and hence, we conclude that ^{3}He was lost because the acids chemically destroyed the carrier phase(s).

Treatment of bulk pelagic clays with a mixture of 12M HF – 3M HCl removed 90-94% of the ^{3}He, consistent with previous observations (Fukumoto et al., 1986). Refractory phases found in meteorites, such as chromite, diamond, SiC, graphite, amorphous carbon, Al_2O_3, and organic material, are chemically resistant to HF - HCl (Huss and Lewis, 1995). If these phases, residing in IDPs on the ocean floor for tens of millions of years, behave chemically in an analogous fashion to those in meteorites, our observations preclude them as the primary carriers of ^{3}He in geologically old sediments. However, silicates, magnetite, ilmenite, Fe-Ni sulfides, and Fe-Ni metal are dissolved or etched by HF – HCl (Fukumoto et al., 1986; Wieler et al., 1986) and, thus, may be responsible for the long-term retention of $^3He_{ET}$.

Leaching bulk pelagic clay with 6M HCl removes about 70% of the ^{3}He. Because magnetite is attacked by 6M HCl (Scott et al., 1981), the HCl step is consistent with magnetite being a carrier of $[^3He]_{ET}$ (Amari and Ozima, 1984; Fukumoto et al., 1986; Matsuda et al., 1990). Matsuda et al. (1990) observed that 75% of the ^{3}He in the magnetic fraction of the sediments is lost by treatment with 3M HCl in two days at room temperature. Since the magnetic fraction usually accounts for ≤50% of the total ^{3}He (Fukumoto et al., 1986; Amari and Ozima, 1988), our HCl leaching results suggest that, if other carriers of ^{3}He exist, they are not resistant to 6M HCl either. To verify this

assertion, we separated the 90 Myr old pelagic clay from DSDP Site 596B into a magnetic and non-magnetic fraction. Approximately 50% of the ^{3}He was in the magnetic fraction (Table 1). Both magnetic and non-magnetic components were leached with 6M HCl. While 97% of $[^3He]_{ET}$ was lost from the magnetic fraction, 87% was lost from the non-magnetic fraction (Table 1). The result implies either (1) magnetic and non-magnetic carriers exist and both are strongly attacked by 6M HCl or (2) the carrier is magnetic, or associated with a magnetic phase, and the magnetic separation only removed 50% of magnetic grains from the sediment. We discuss this possibility later.

Fukumoto et al. (1996) observed that $[^3He]_{Et}$ in the magnetic fraction in quaternary sediments is resistant to 98% HNO_3 and, therefore, suggested magnetite as a carrier. If so, we argue against magnetite as the dominant carrier of $[^3He]_{ET}$ in geologically old sediments because following our HNO_3 leach on bulk pelagic clay, 87.5% of $[^3He]_{ET}$ is lost (Table 1). However, we cannot rule out the possibility that residence on the ocean floor for tens of millions of years makes magnetite more susceptible to attack by HNO_3 acid.

Becker et al. (1996) suggested that fullerenes are a carrier phase of extraterrestrial ^{3}He in the 1.85 Ga ejecta layer that is associated with the Onaping Breccia in the Sudbury impact crater. Because fullerenes are resistant to HF and HCl, our leaching experiments do not support fullerenes as the host of ^{3}He in oceanic sediments. To test for the presence of extraterrestrial ^{3}He in the 1.85 Ga sediments associated with the Sudbury impact structure, we analyzed the supposed fullerene-bearing impact breccia. The samples were colleted from the same locality (Dowling township) as Becker et al. (1996), although not from the same outcrop (Tom Ahrens, personal communication). To avoid the potentially

problematic extraction of fullerene, we simply analyzed the bulk rock. Fusion at 1400°C yielded a ^{3}He concentration of 0.4×10^{-12} cc STP g^{-1}, comparable with the ^{3}He concentration implied by the fullerene data (Becker et al., 1986). However, the $^3He/^4He$ ratio of the bulk rock is 10^{-8}, similar to the value expected from the reaction $^6Li(n,\alpha) \longrightarrow {}^3H \xrightarrow{\beta} {}^3He$ (Andrews, 1985) and provides no evidence for an extraterrestrial component. Furthermore, we treated 0.5 g of bulk rock with HF-HCl, which removed more than 99% of the ^{3}He and ^{4}He (Table 1 and Fig. 1). Therefore, we find no evidence of fullerene-hosted ^{3}He in the Sudbury impact breccia.

In summary, our chemical leaching experiments are consistent with extraterrestrial silicates, ilmenite, Fe-Ni sulfides and possibly magnetite, but not with organic matter (including fullerenes), SiC, graphite, amorphous carbon, Al_2O_3, or diamond as the primary phase(s) responsible for the long-term retention of ^{3}He in the sedimentary record. The dominant silicates in IDPs are olivines and pyroxenes. Layer silicates such as serpentine and smectite, may be abundant in a few IDPs (up to 40% modal abundance; Germani et al., 1990). While terrestrial layer silicates are stable on the seafloor for millions of years, olivine and pyroxene crystals, such as those found in Mid Ocean Ridge Basalts, undergo alteration within a few million years. Extraterrestrial olivine and pyroxene are likely to behave similarly. For example, in 50 Myr old silicate cosmic spherules recovered from the seafloor, the silicate minerals are completely altered and only magnetite grains are preserved (Brownlee, 1985). In IDPs olivine and pyroxene grains are often rimmed by magnetite, a few to few tens of nm thick, that forms during atmospheric entry-heating (Bradley et al., 1988; Germani et al., 1990). Because magnetite is stable on the ocean floor for tens of millions of years (Brownlee 1985), the magnetite

rims may protect the silicate phases against chemical alteration and may also explain the association of the ^{3}He carrier(s) with magnetite. If Fe-Ni sulfides and/or magnetite are the carriers of extraterrestrial ^{3}He, the long-term retention of ^{3}He in the sedimentary record may be affected by redox conditions, such as Eh and pH of pore waters in sediments. Compared to magnetite, Fe-sulfides, such as troilite and pyrrhotite, are stable in more reducing environments and over a narrower range of Eh and pH conditions (e.g., Brookins, 1988). Thus, Fe-sulfides may be more susceptible to variations in redox conditions on the seafloor than magnetite. However, it is possible that the mineral transformation reactions are controlled by kinetics, and minerals out of equilibrium with the environment may survive over geologically long periods. More work is required to identify the carrier of ^{3}He in sediments and understand the stability of the phase(s) to variations in redox conditions.

Finally, we note that following the chemical leaches about 5-30% of the total ^{3}He remains in the residue, implying either multiple carriers of ^{3}He, or incomplete dissolution of the carrier phase. We favor the latter interpretation because the HCl step on DSDP 596B, which had a higher acid volume to sample mass ratio compared to the HCl step on GPC3 1092-1093, lost significantly more ^{3}He.

3.2. Stepped Heating

Results of the stepwise degassing experiments are listed in Table 2. All seven samples, display remarkably similar ^{3}He release patterns, characterized by a small peak between 350-400°C and a larger but broader peak between 600-750°C (Figs. 3-4). Approximately 15% of the ^{3}He is released at temperatures between 350-400°C,

Figure 3: Fraction of ^{3}He released from pelagic clays as a function of temperature. Note the small peak at 350°C and a larger but broader peak between 600 and 750°C. $^{3}He/^{4}He$ ratios >20 R_A indicate that the low temperature peak is from the release of extraterrestrial ^{3}He. Sample ages are listed in Table 2. The errors in the fraction of ^{3}He released are based on the uncertainty in ^{3}He measurements, which is ~3.5%. Uncertainty on temperature measurements is ±3°C at steps < 850°C. At higher temperatures the uncertainty is ±5-10°C.

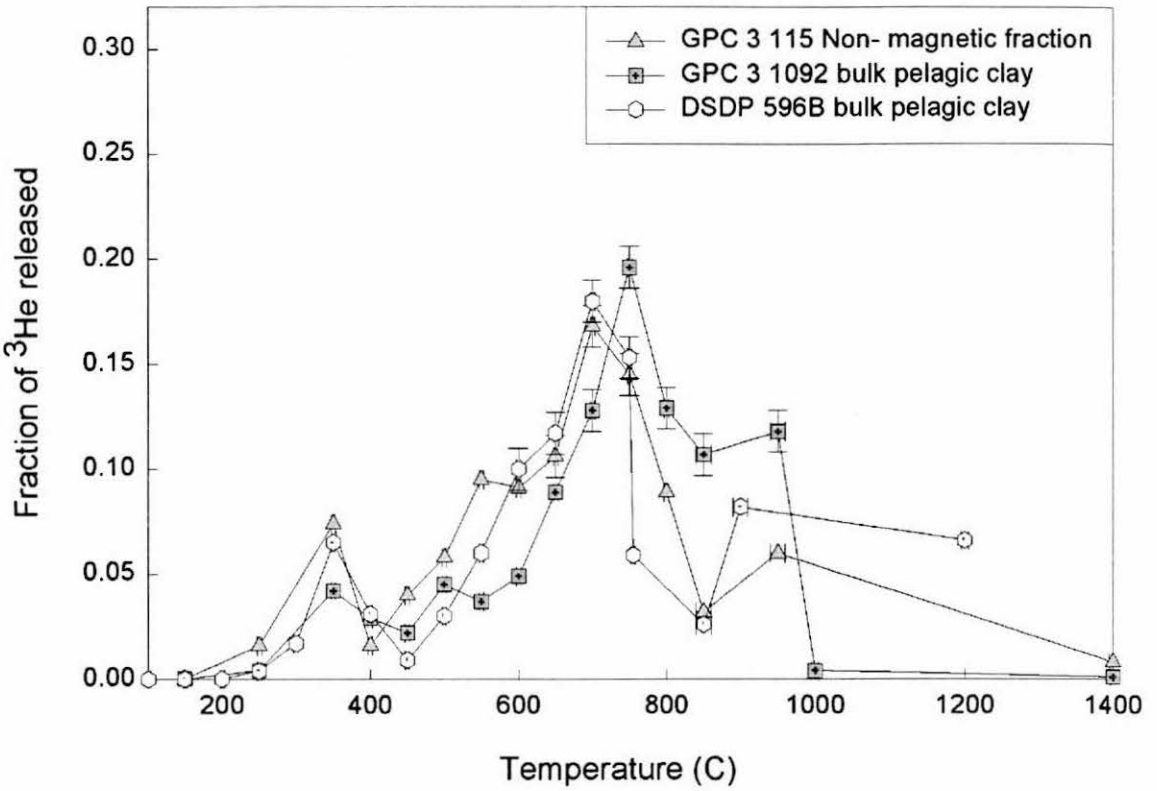
GPC 3 115 Non- magnetic fraction
GPC 3 1092 bulk pelagic clay
DSDP 596B bulk pelagic clay
Fraction of 3He released
0.30
0.25
0.20
0.15
0.10
0.05
0.00
200
400
600
800
1000
1200
1400
Temperature (C)

Figure 4: ^{3}He release profile as a function of temperature in magnetic and non-magnetic fraction of pelagic clays from the GPC3 core. Sample ages are listed in Table 2. Note the similarity in release profiles in the magnetic and non- magnetic components of the two samples. Symbols and colors have been chosen to be consistent with Figure 5. Error bars as in Figure 3.

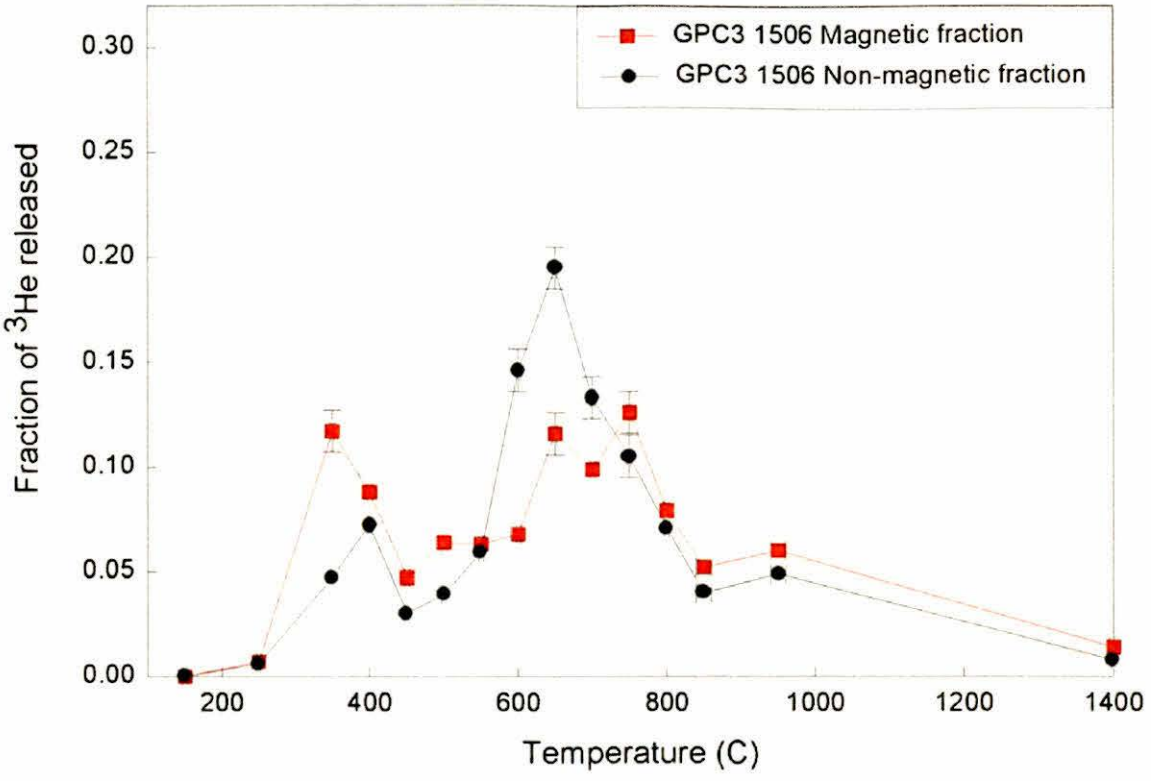
GPC3 1506 Magnetic fraction
GPC3 1506 Non-magnetic fraction
Fraction of ^{3}He released
0.30
0.25
0.20
0.15
0.10
0.05
0.00
200
400
600
800
1000
1200
1400
Temperature (C)

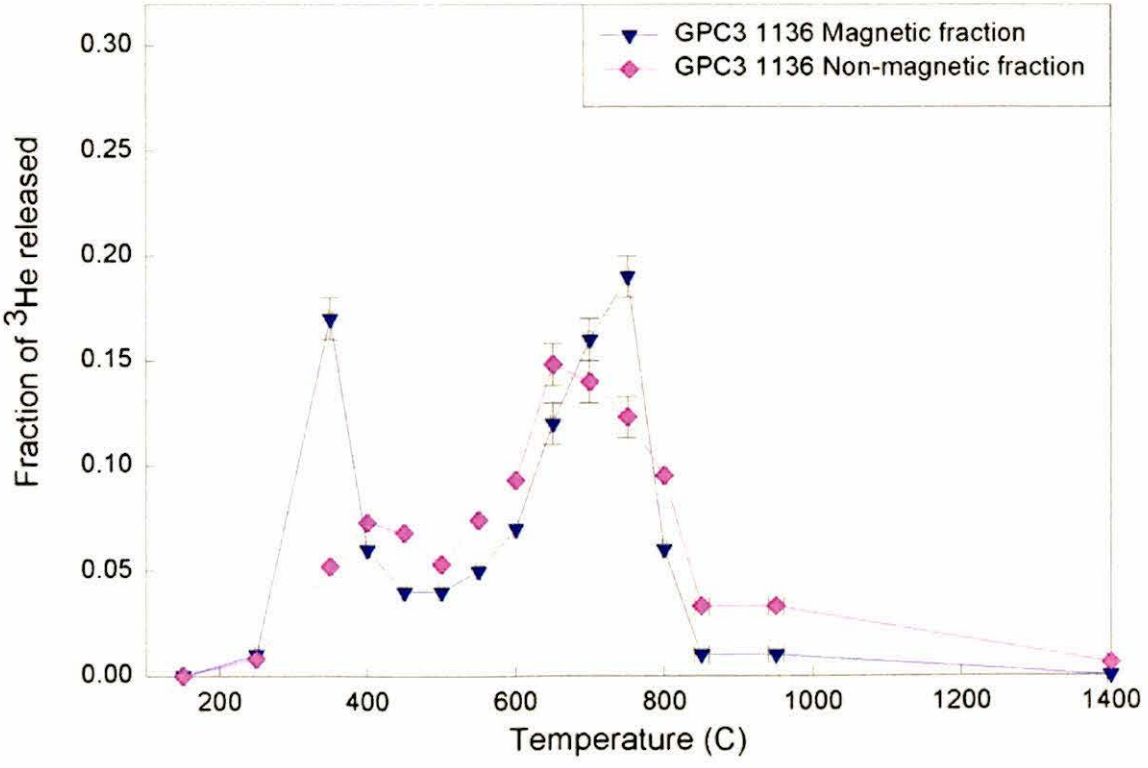
GPC3 1136 Magnetic fraction
GPC3 1136 Non-magnetic fraction
Fraction of ^{3}He released
0.30
0.25
0.20
0.15
0.10
0.05
0.00
200
400
600
800
1000
1200
1400
Temperature (C)

Table 2: Results of diffusion runs on pelagic clays.

Temperature (°C)	^3He 10^{-12} cc STP	$^3He/^4He$ R_A	Log D/a^2 s^{-1}
Sample: GPC3 115 Non-magnetic fraction; Age = 0.54 Ma; mass = 100 mg			
150	0.00	0.0	-
250	0.06	0.4	-8.2
350	0.29	0.5	-6.7
400	0.06	0.2	-7.1
450	0.16	0.5	-6.6
500	0.23	1.0	-6.2
550	0.37	2.4	-5.8
600	0.36	3.3	-5.7
650	0.42	6.7	-5.4
700	0.66	14.4	-5.0
750	0.57	21.5	-4.8
800	0.35	23.9	-4.7
850	0.13	5.7	-5.0
950	0.24	20.1	-4.2
1400	0.03	4.4	
Sample: GPC3 1092-1093 bulk pelagic clay; Age = 33 Ma; mass = 100 mg			
150	0.01	1.0	-11.6
250	0.11	1.8	-9.3
350	1.18	21.9	-7.3
400	0.83	30.5	-7.1
450	0.62	47.0	-7.0
500	1.29	44.4	-6.5
550	1.04	60.2	-6.5
600	1.38	99.5	-6.2
650	2.51	151.1	-5.8
700	3.61	165.3	-5.5
750	5.55	166.8	-5.0
800	3.66	172.1	-4.9
850	3.03	158.2	-4.8
950	3.32	171.2	-4.0
1000	0.13	64.8	-4.2
1400	0.02	11.8	
DSDP 596B 1-6 80-83 bulk pelagic clay; Age = between 75 and 90 Ma; mass = 150 mg			
100	0.00	3.2	-12.8
150	0.01	2.2	-12.0
200	0.02	1.7	-11.0
250	0.17	4.2	-9.2
300	0.62	9.3	-8.0

Table 2 (continued)

Temperature (°C)	^3He 10^{-12} cc STP	$^3He/^4He$ R_A	Log D/a^2 s^{-1}
400	1.16	8.7	-6.8
450	0.35	3.0	-7.2
500	1.11	11.4	-6.6
550	2.21	33.0	-6.2
600	3.68	66.9	-5.8
650	4.34	70.1	-5.5
700	6.64	58.5	-5.1
750	5.65	86.1	-4.9
755	2.19	65.4	-5.1
850	0.95	134.8	-5.4
900	3.04	163.2	-4.6
1400	2.44	162.7	
Sample: GPC3 1136-1143 magnetic fraction; Age = 35.1 Ma; mass = 14 mg			
150	0.00	9.9	-
250	0.06	76.2	-8.5
350	0.89	153.0	-6.1
400	0.31	128.5	-6.2
450	0.23	112.2	-6.2
500	0.21	114.0	-6.1
550	0.26	95.3	-5.9
600	0.38	163.2	-5.7
650	0.64	145.0	-5.5
700	0.85	197.0	-5.2
750	1.00	162.2	-4.4
800	0.34	170.5	-4.4
850	0.04	114.0	-4.8
950	0.05	104.2	-4.3
1400	0.00		
Sample: GPC3 1136-1143 Non-magnetic fraction; Age = 35.1 Ma; mass = 82 mg			
150	0.00	6.0	-11.5
250	0.05	12.6	-8.7
350	0.29	29.1	-7.1
400	0.41	38.9	-6.4
450	0.38	45.9	-6.2
500	0.30	54.9	-6.1
550	0.41	86.1	-5.9
600	0.52	110.9	-5.6
650	0.83	139.1	-5.2
700	0.79	141.8	-5.0
750	0.69	136.2	-4.8
800	0.53	135.2	-4.6

Table 2 (continued)

Temperature (°C)	^3He 10^{-12} cc STP	$^3He/^4He$ R_A	Log D/a^2 s^{-1}
850	0.19	154.2	-4.8
950	0.19	126.0	-4.3
1400	0.03	122.0	
Sample: GPC3 1506-1514 magnetic fraction; Age = 50.6 Ma; mass = 16 mg			
150	0.00	1.3	-
250	0.95	27.7	-9.0
350	16.48	121.0	-6.4
400	12.39	110.6	-6.1
450	6.63	88.2	-6.2
500	9.08	122.2	-5.9
550	8.83	98.2	-5.8
600	9.64	105.2	-5.7
650	16.29	138.9	-5.3
700	14.00	167.6	-5.2
750	17.75	207.2	-4.9
800	11.20	222.0	-4.9
850	7.30	44.9	-4.8
950	8.40	239.5	-4.3
1400	1.99	7704.0	
Sample: GPC3 1506-1514 Non-magnetic fraction; Age = 50.6 Ma; mass = 130 mg			
150	0.00	6.0	-12.3
250	0.17	6.0	-9.0
350	1.31	24.6	-7.2
400	2.02	35.5	-6.5
450	0.83	16.6	-6.6
500	1.10	32.0	-6.4
550	1.65	61.6	-6.1
600	4.07	101.0	-5.5
650	5.46	121.6	-5.1
700	3.72	110.8	-5.0
750	2.93	117.6	-4.9
800	2.00	157.4	-4.8
850	1.11	143.7	-4.8
950	1.37	141.1	-4.3
1400	0.24	160.8	

For all samples duration of each step was 60 minutes. Age assignments for GPC3 samples are from Kyte et al. (1993). Age for the DSDP sample is from Montgomery and Johnson (1983).

while about 70% of the total ^{3}He is released between 600-750°C. The bimodal release has been previously observed in one sample from DSDP Site 607 (Farley, 2001) although the low temperature peak was associated with a ^{3}He/^{4}He ratio of 0.1 R_A and, thus, attributed to release of crustal helium. However, ^{3}He/^{4}He ratios in excess of 20 R_A (Table 2) in our experiments strongly suggest that the ^{3}He released in the lower temperature steps is either extraterrestrial or cosmogenic in origin. If we assume that ^{3}He released at temperatures ≤450°C is cosmogenic helium, exposure ages of ≥5 Myrs are required to account for all the ^{3}He in the samples using the production rate at sea level and high latitude (Cerling and Craig, 1993). Such long exposure ages are improbable, especially since detrital minerals have low ^{3}He retentivity (Farley, 1995). Hence, we conclude that ^{3}He released at low temperatures (<450°C) is extraterrestrial. Previous workers may have failed to identify the low-temperature peak because their experiments started at temperatures in excess of 500°C (e.g., Amari and Ozima, 1985; Amari and Ozima, 1988; Hiyagon, 1994). The high temperature peak observed in our experiments (600-750°C) is also different from previous studies, occurring at temperatures significantly lower than the peak release temperature of 900°C in seafloor magnetic fines (e.g., Hiyagon, 1994). This difference is probably related to the larger number of steps in our experiments (discussed later).

Our stepped heating experiments provide additional insights into whether the carrier phase(s) in the magnetic and non-magnetic fraction of sediments are different. Because helium diffusivities in IDPs must be controlled by mineral structure and chemistry (e.g., Trull et al., 1991; Wolf et al., 1996; Reiners and Farley, 1998), if the ^{3}He is carried in both a magnetite and a non-magnetic phase, for identical laboratory heating schedules, the ^{3}He release pattern in the magnetic and non-magnetic components would

in general be expected to be distinct. It is clear that the ^{3}He release profiles, shown in Figure 4, in the magnetic and non-magnetic separates from two GPC3 samples are remarkably similar suggesting a single non-magnetic carrier. Alternatively the carrier is magnetic or associated with a magnetic phase, and the magnetic separation was not effective in removing all the magnetic grains from the sediment. To test this possibility we measured the magnetic properties of a pelagic clay (GPC3 1136-1144) in the Superconducting Rock Magnetometer in Prof. Joe Kirschvink laboratory at Caltech. The anhysteric remanent magnetization (ARM) and isothermal remanent magnetization (IRM) acquisitions characterize the magnetism as dominated by single domain (< 70 nm sized) magnetite crystals (Fig. 5). The total magnetic moment of the pelagic clay was 2.37×10^{-2} emu, implying ~500 ppm by weight of magnetite (Joe Kirschvink personal communication). The pelagic clay was then separated into magnetic and non-magnetic components by procedures described earlier. The non-magnetic component had a magnetic moment of 1.36×10^{-2} emu, suggesting that 57% by weight of the magnetite remained in the non-magnetic component. Thus, although the magnetic separation technique concentrates the magnetic particles in the "magnetic fraction" of the sediment, it removes only ~50% of all the magnetic particles. As a result, we conclude from our step heating results that ^{3}He is probably carried by a single phase, that is either magnetic (e.g., magnetite, pyrrhotite) or a phase associated with magnetite. We favor the latter since extensive loss of ^{3}He might be expected in the material that transforms into magnetite during atmospheric entry heating.

3.2.1. Comparison with Seafloor Magnetic Fines

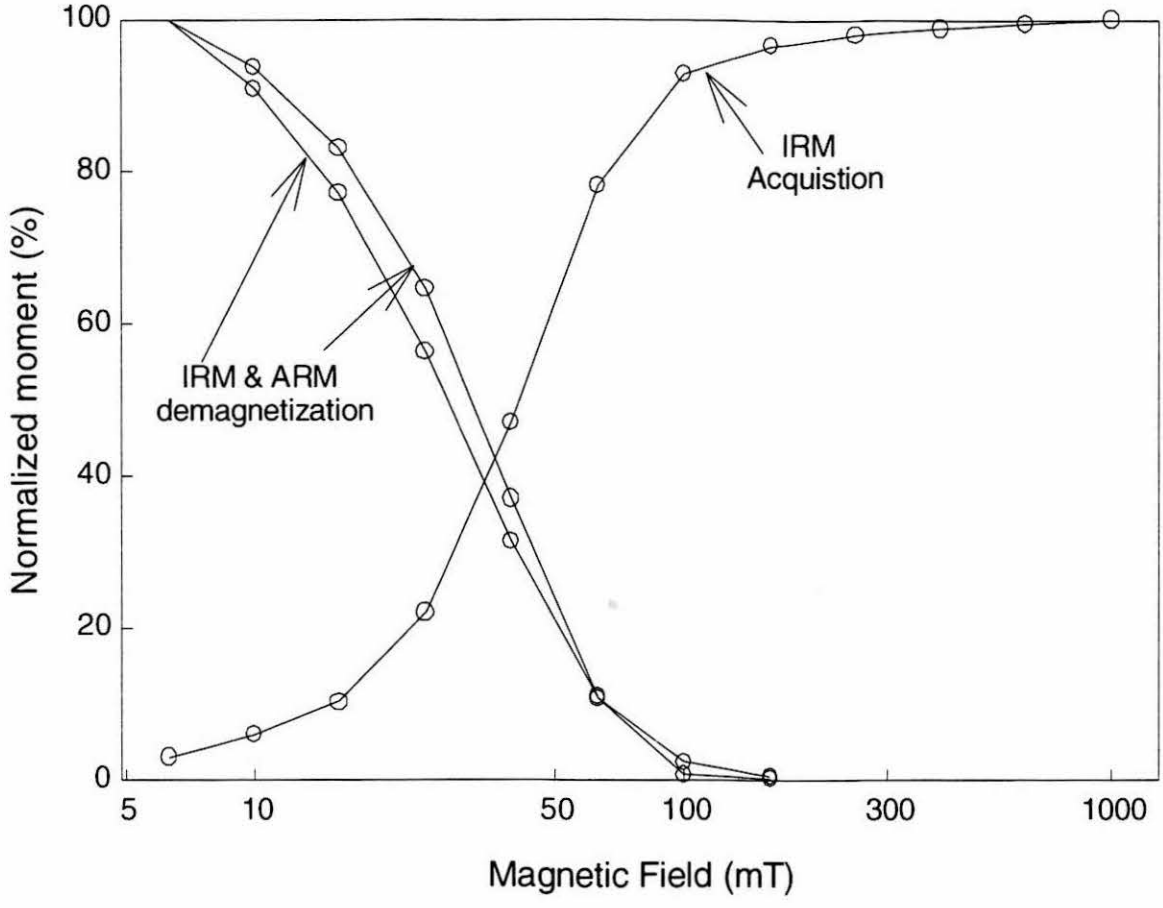

Figure 5: Magnetic properties of a 35 Myr old pelagic clay from the GPC3 core (1136-1144). The IRM acquisition and IRM and ARM demagnetization indicates single domain magnetite as the primary carrier of the magnetization in the sediment (see Kirschvink et al., 1997).

Stepped heating experiments on seafloor sediments have typically used different step-heat schedules to study the ^{3}He release profile (e.g., Amari and Ozima, 1985; Amari and Ozima 1988; Hiyagon, 1994; Farley 2001). Therefore, we cannot directly compare the ^{3}He release profiles from the stepped heating experiments. To facilitate the comparison, we computed apparent ^{3}He diffusivities at each temperature step from the fraction of gas released at that temperature, using the solution to the spherical diffusion equation given by Fechtig and Kalbitzer (1966). We use the term "apparent diffusivity" because implicit in this calculation are the assumptions that volume diffusion through a sphere adequately describes He diffusion in IDPs, the carrier phase does not undergo thermal decomposition or reactions with other minerals present, and the ^{3}He concentration in the carrier phase(s) prior to the stepped heating experiments was homogeneous. The last two assumptions are difficult to verify and are unlikely to be strictly valid. For example, the implantation depth of solar wind ions, the probable ^{3}He source, is only about 30 nm. Hence, a near-surface step-function may be a better description of the initial ^{3}He concentration profile (e.g., Harris-Kuhlman, 1998), but it is not clear how atmospheric entry heating and residence on the seafloor for tens of millions of years perturbs this profile.

The diffusivity profiles from our experiments are shown on an Arrhenius plot in Figure 6. The diffusion profiles are characterized by linear segments from about 250°C to 400°C and above 550°C, and are not consistent with simple volume diffusion from a single diffusion domain (e.g., Lovera et al., 1991; Reiners and Farley, 1998). The shape of the diffusion profile is qualitatively similar to the profile for Ar diffusion through K-feldspar, attributed to a range of diffusion domain sizes (e.g., Lovera et al., 1997).

Figure 6: Arrhenius plot of ^{3}He diffusion in IDPs. Diffusivity at each step was calculated using the formulation for diffusion through a sphere (Fechtig and Kalbitzer, 1966). The bottom panel is our new experimental data. The top panel is a comparison of two of our samples with previous studies. P 97 is Patterson et al., 1997; H 94 is Hiyagon 94; A & O 85 is Amari and Ozima, 1985; A & O 85 is Amari and Ozima, 1988; F 01 is Farley, 2001.

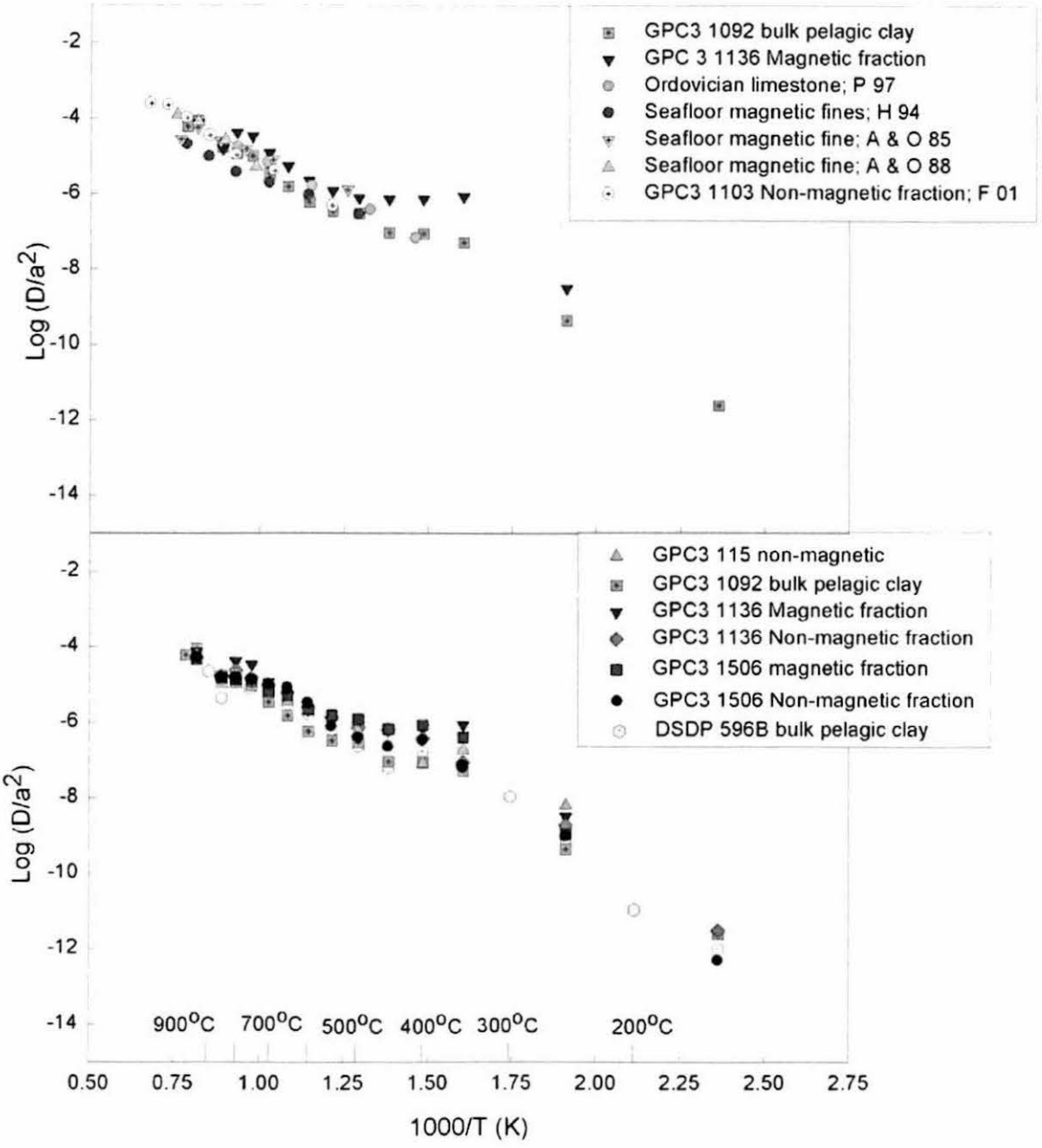
GPC3 1092 bulk pelagic clay
GPC 3 1136 Magnetic fraction
Ordovician limestone; P 97
Seafloor magnetic fines; H 94
Seafloor magnetic fine; A & O 85
Seafloor magnetic fine; A & O 88
GPC3 1103 Non-magnetic fraction; F 01
GPC3 115 non-magnetic
GPC3 1092 bulk pelagic clay
GPC3 1136 Magnetic fraction
GPC3 1136 Non-magnetic fraction
GPC3 1506 magnetic fraction
GPC3 1506 Non-magnetic fraction
DSDP 596B bulk pelagic clay
Log (D/a2)
-2
-4
-6
-8
-10
-12
-14
900°C
700°C
500°C
400°C
300°C
200°C
0.50
0.75
1.00
1.25
1.50
1.75
2.00
2.25
2.50
2.75
1000/T (K)

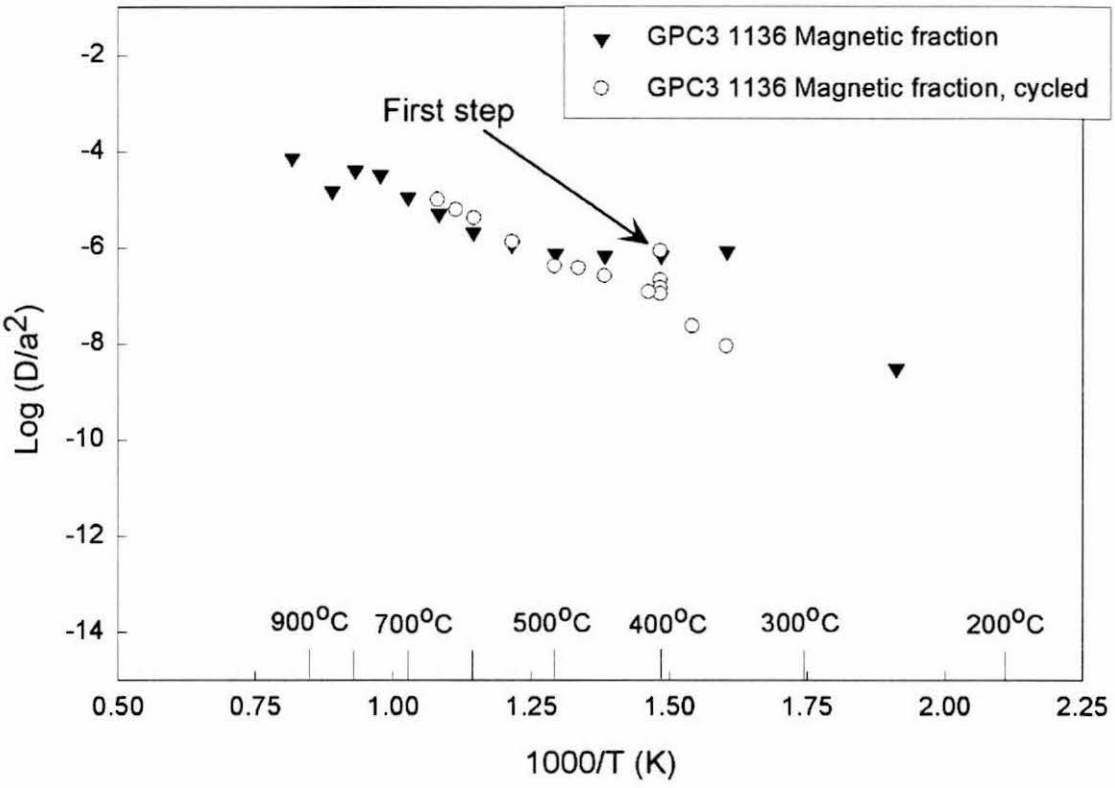

Figure 7: Arrhenius plot of the thermally cycled run of GPC3 1136-1143. For comparison, data from the monotonic run have been plotted.

Table 3: Results of cycled diffusion run on the magnetic fraction of GPC3 1136.

Temperature (°C)	Duration (min)	^3He 10^{-12} cc STP	$^3He/^4He$ R_A	Log D/a^2 s^{-1}
400	30	2.01	134.8	-6.2
400	30	0.30	161.1	-6.7
400	30	0.17	218.6	-6.8
400	30	0.12	193.0	-7.0
300	30	0.001	5.8	-
325	30	0.002	28.9	-
350	30	0.01	85.8	-8.0
375	30	0.02	138.6	-7.6
410	30	0.12	176.3	-6.9
450	30	0.25	168.8	-6.6
475	30	0.32	178.6	-6.4
500	30	0.32	230.1	-6.4
550	30	0.83	170.2	-5.9
600	30	1.80	195.9	-5.4
625	30	1.73	196.7	-5.2
650	30	1.97	198.5	-5.0
1400	30	7.58	179.4	

Log D/a^2 was not computed for the 300 and 325 °C steps because of the low gas yields and high associated uncertainties. Mass of sample was 31 mg.

Figure 8: Extent of deviation from linearity of the diffusion profile vs. cumulative fraction of ^{3}He released in the cycled diffusion experiment from the magnetic fraction of GPC3 1136-1143. The parameter Log (D/a^2) - Log $(D/a^2)_o$, (Reiners and Farley, 1998), is similar to Ln (R/R_o) of Lovera et al. (1991), and is the extent of deviation from linearity, where the linear segment is defined by the high temperature steps (>500°C). Log $(D/a^2)_o$ is Log (D/a^2) for a perfectly linear correlation. Compared to the high temperature segment (>500°C), diffusivities in the first two steps at 400°C are anomalously high, followed by transient low diffusivities.

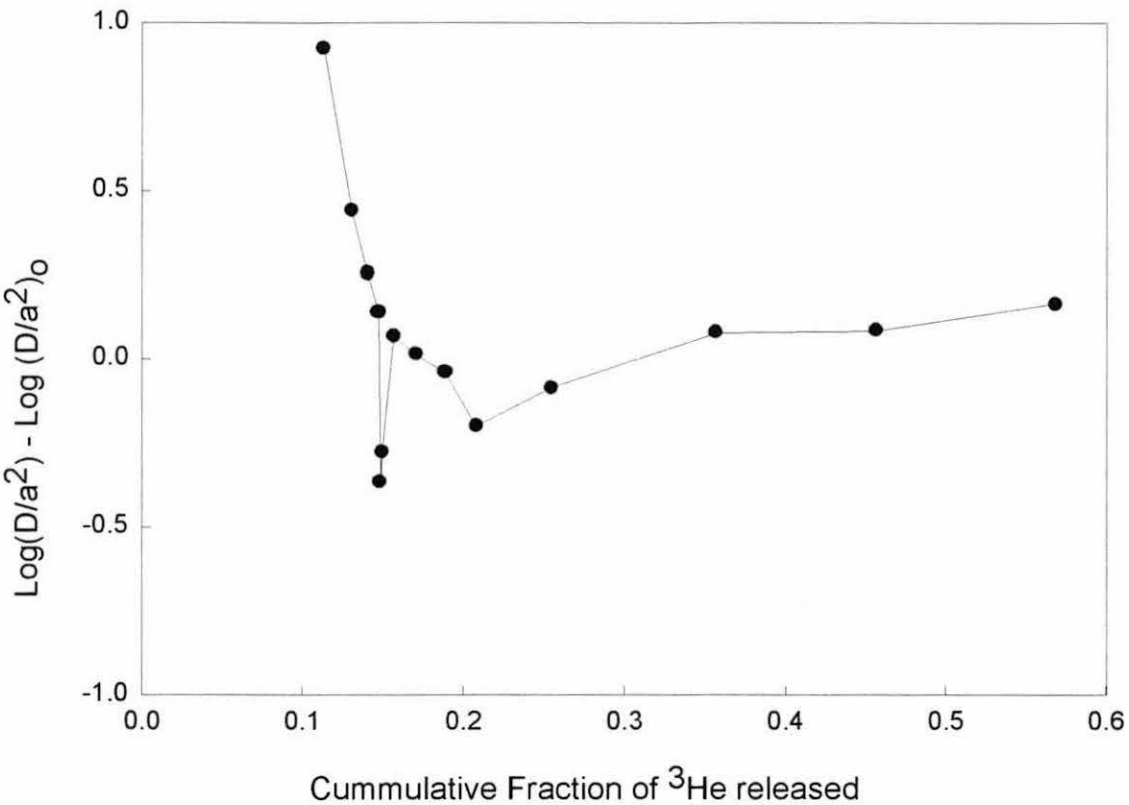
1.0
0.5
0.0
-0.5
-1.0
0.0
0.1
0.2
0.3
0.4
0.5
0.6
Log(D/a2) - Log (D/a2)o
Cummulative Fraction of 3He released

To better understand the diffusion profile in our stepwise outgassing experiments, we analyzed a separate aliquot of the magnetic fraction of GPC-3 1136-1143. Four steps, each of 30 minute duration, were initially performed at 400°C, following which the sample was cooled to a lower temperature (300°C). The outgassing then followed a monotonic schedule with temperature increments of 25-50°C. The results from this cycled experiment are listed in Table 3. The diffusivity of the first step at 400°C is identical to the original outgassing experiment but drops to lower diffusivities in the next few steps (Figs. 7 & 8). Similar profiles have been observed for Ar diffusion through K-feldspar (Lovera et al., 1991) and He diffusion through titanite (Reiners and Farley, 1999). The ^{3}He diffusion profile can be reasonably attributed to rapid depletion of a weakly bound gas- fraction that is nearly exhausted at 400°C, significantly prior to depletion of a high temperature ^{3}He reservoir.

The amount of ^{3}He released in the lower temperature steps (corresponds to the first peak on the step heat profile) accounts for about 15% of the total ^{3}He. At least two distinct physical processes may account for the weakly bound ^{3}He in IDPs. Irradiation of IDPs by solar wind and solar flare ions may damage the crystal lattice and produce an outer amorphous layer that is on the order of a few to few tens of nm thick (e.g., Ducati et al., 1973; Ziegler et al., 1985). Solar wind implanted He (SW-He) residing in this amorphous layer would be lost by diffusion more readily than SW-He residing deeper in the relatively undamaged crystal lattice at depths of >30 nm (Ducati et al., 1973). Recently, Koscheev et al. (2001) demonstrated that ion implantation of a single energy and isotopic composition into diamonds can produce both low and high-temperature release peaks from the same grains. Although these authors did not give a physical

explanation of their results we suggest that creation of an amorphous layer by radiation damage may explain the bimodal release pattern that they observed in diamonds, and that we see in our stepped heating experiments.

Alternatively, 15% of the ^{3}He released at low temperatures in our stepped heating experiments may be SW-He, with the high temperature gas-fraction representing He from solar energetic particles (SEP). SEPs typically have energies on the order of 100 KeV/amu (Wieler et al., 1986), and the stopping distance for such particles would be a few tenths of a micron to few microns (Ziegler et al., 1985). Thus, compared to SW-He, SEP-He would be implanted significantly deeper into minerals. An implication of this hypothesis is that >99% of the SW-He has been lost from IDPs now residing on the ocean floor, because the ratio of solar particles with energies of ~1 KeV/amu to particles with ~100 KeV/amu is about 10,000 (Wieler et al., 1986; Geiss and Bochsler, 1991). The loss of SW-He may result from atmospheric entry heating, or diffusional loss on the seafloor, or both.

The high temperature diffusivities calculated from our experiments are in good agreement with previous studies (Fig. 6; e.g., Hiyagon et al., 1994; Farley, 2001). Hence, the shift in peak release temperature from 900°C to between 600-750°C in our experiments is a result of the heating schedule we used. The mean activation energy for the high temperature portion of the profile is 20.1 kcal/mole (range = 14.5 to 24.2 kcal/mole), higher than previous estimates of 17 kcal/mole (e.g., Amari and Ozima, 1988; Hiyagon, 1994). To investigate the ^{3}He-retentivity at seafloor temperatures, we extrapolated the high temperature part of the diffusion profile (corresponding to >80% of the total ^{3}He) to 2°C. Using the mean activation energy (20.1 kcal/mole) and the

measured mean value of the frequency factor (log D_o/a^2 = –0.65), our experiments suggest a diffusivity of 2×10^{-17} cm^2 s^{-1} at 2°C. This estimate is two orders of magnitude lower than previous estimates (e.g., Amari and Ozima, 1985; Hiyagon, 1994) and indicates that at ambient temperatures of the ocean floor, 19% of the ^{3}He would be lost from the IDPs in 50 Myrs, about 25% in 100 Myrs, and 53% in 500 Myrs.

Mukhopadhyay et al. (2001) noted that although the ^{3}He flux pattern obtained from Cretaceous and Cenozoic limestones exposed in the Italian Apennines is similar to the pelagic clay core (GPC3), the absolute values at Gubbio are a factor of four lower. Our diffusivity calculations suggest that sediments deposited on the seafloor 50 Myrs ago and exposed on the Earth's surface at 25°C for the past 20 Myrs would lose ~60% of its ^{3}He, a factor of three higher than sediments that have resided on the seafloor at 2°C for 50 Myrs. This provides a possible explanation for the discrepancy between the Gubbio and GPC3 results. Geothermal gradients in sedimentary basins vary from 10 to 35°C/km (Choquette and James, 1987).

Assuming a geothermal gradient of 25°C/km, sediments that are buried to depths of 2 km for 1 and 5 Myrs would lose 40 and 75% of their ^{3}He, respectively (Fig. 9). Because we are extrapolating diffusivities over many orders of magnitude, the retentivity calculations are extremely sensitive to the slope (activation energy) of the diffusion profile and the absolute values should be treated with some caution. Furthermore, the absolute magnitude of the ^{3}He loss must depend upon the ^{3}He concentration profile within the IDPs, which we have assumed to be uniform and, thus, unlikely to be strictly valid. Nonetheless, the retentivity computations qualitatively suggest that sedimentary rocks exposed on continents or sediments that have undergone diagenesis to low

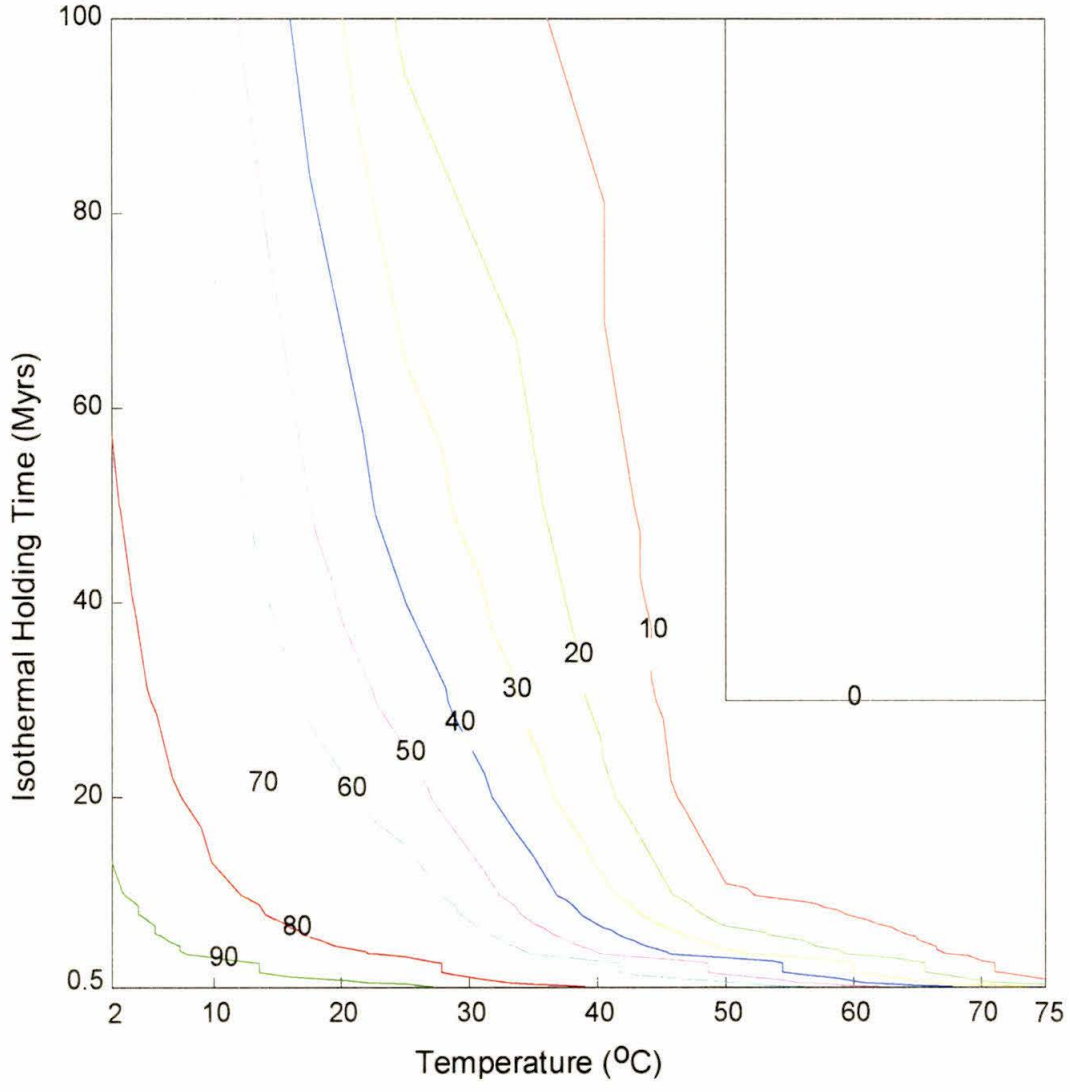

Figure 9: ^{3}He retentivity in IDPs contoured as a function of temperature and holding time. The number on the contours is the percent of ^{3}He still remaining in the IDPs.

temperatures (50°C) would have lost significantly more ^{3}He than sediment cores recovered from the ocean floor. Further, because each sedimentary basin may have different thermal histories and geothermal gradients (Choquette and James, 1987), the magnitude of the ^{3}He loss in different stratigraphic sections might be distinct. Further detailed work is required to better characterize He diffusivities, particularly at temperature relevant to sediment diagenesis (< 350°C).

3.3. Size Distribution

The results from our sieving experiment on the 33 Ma pelagic clay are summarized in Table 4 and Figure 10. ^{3}He concentration and ^{3}He/^{4}He ratios increase as the particle size decrease, suggesting that ^{3}He is preferentially incorporated in the smaller particles. About 60% of the $[^3He]_{ET}$ resides in particles <37 μm in diameter and only about 20% in particles with diameters greater than 53 μm (if the particles are not spheres then 37 μm and 53 μm refer to the intermediate axis of the grains). Note that immersing the sample in water may not have disaggregated all the particles. Furthermore, sieving is biased against smaller particles because such particles can stick or 'clump' together and, therefore, the 20% must be considered an upper limit to the amount of $[^3He]_{ET}$ in particles >53 μm in size. Hence, contrary to the suggestion of Stuart et al. (1999), we demonstrate that ^{3}He in geological old sediments residing predominantly in 50-100 μm micrometeorites. While ^{3}He-bearing particles >50 μm in diameter do exist (Stuart et al., 1999), such particles are probably rare, having experienced lower than average heating upon atmospheric entry, possibly from unusually low entry velocities or angles (Farley et al., 1997).

Table 4: ^{3}He concentration in pelagic clay as a function of particle size.

Sample: GPC3 1092-1093; Age 33 Ma

Size (μm)	Weight (mg)	Fraction of total ^{3}He	$[^{3}He]$ 10^{-12} cc STP	$^{3}He/^{4}He$ (R_A)
<13	42	0.28	0.76	47.3
13-37	43	0.28	0.75	47.0
37-53	46	0.22	0.60	34.4
>53	53	0.21	0.55	28.1
Bulk sediment	50		0.8	47.7

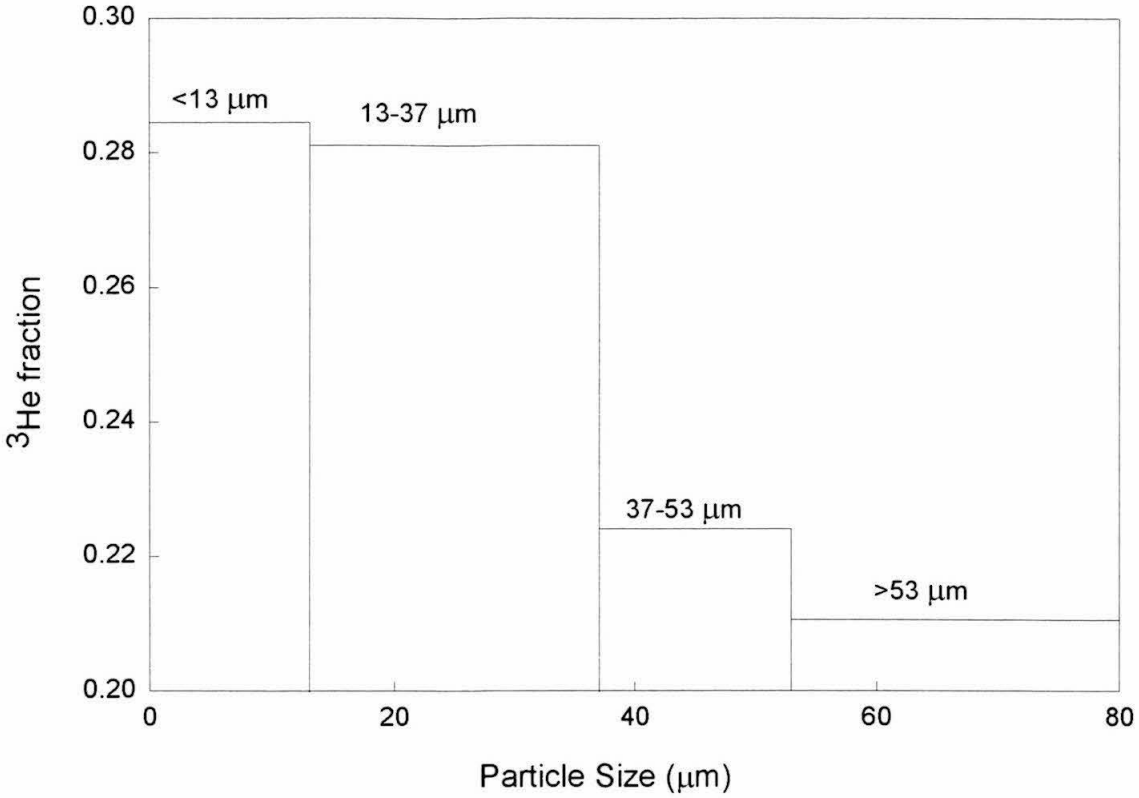

Figure 10: ^{3}He as a function of particle size in a 33 Ma old pelagic clay from the GPC3 core.

The size distribution of ^{3}He-bearing IDPs has implications for the use of ^{3}He as a tracer of extraterrestrial matter. If ^{3}He in seafloor sediments predominantly reflects contribution from micrometeorites, then ^{3}He will record events, such as meteor showers, passage of a single short-period comet through the inner solar system or breakup of a meteorite in the upper atmosphere (Stuart et al., 1999), rather than the time-averaged flux of asteroidal or cometary particles. Farley et al., (1997) numerically modeled the frictional heating of cosmic dust particles during atmospheric entry and concluded that about 70% of the ^{3}He is carried by particles 3 μm to 35 μm in size. Our observation that at least 60% of the ^{3}He is in particles < 37 μm in size is, therefore, in remarkable agreement with the model results of Farley et al. (1997). Hence, we conclude that ^{3}He in seafloor sediment does not reflect the micrometeorite flux but predominantly represents the accretion of IDPs less than 35 μm in diameter.

Micrometeorites are significantly larger than typical carbonate sediments (~25 μm) and pelagic clays (~1 μm). As a result, during sediment resuspension and transport by bottom currents, micrometeorites would be preferentially left behind. Therefore, sediment focusing or redistribution would lead to apparent changes in extraterrestrial ^{3}He flux (e.g., Marcantonio et al., 1996) even when the delivery rate from space remains constant. The observed size distribution of ^{3}He-bearing IDPs indicates that they will be less prone to concentration or depletion relative to bulk sediments than micrometeorites and, hence, a better recorder of the delivery rate of extraterrestrial matter (also see Farley et al., 1997).

4. Conclusion

We performed chemical leaching, stepped heating, and sieving experiments to better characterize the ^{3}He carrier(s) responsible for the long-term retention of ^{3}He in sediments. Our data indicate:

- Organic matter, diamond, spinel, SiC, graphite, and amorphous carbon are not the primary carrier phase(s) of ^{3}He although they may account for up to ~10% of the total ^{3}He. Our data, however, are consistent with extraterrestrial silicates, ilmenite, Fe-Ni sulfides, and possibly magnetite as the principal carrier phase(s) of extraterrestrial ^{3}He.
- ^{3}He release profiles as a function of temperature in both the magnetic and non-magnetic fractions in sediments are similar, suggesting a single carrier phase that may be magnetite or more probably a phase associated with magnetite. The association may be in the form of composite grains, inclusions, or few nm thick rims around the grains.
- In contrast to previous suggestions that extraterrestrial ^{3}He would be quantitatively lost from the magnetic fraction in a few million years (e.g., Amari and Ozima, 1985), our stepped heating experiments indicate that 80% of the ^{3}He might be retained after 50 Myrs and about 75% after 100 Myrs, although the absolute values will likely depend upon the ^{3}He concentration profile within the IDPs.
- Contrary to previous suggestions (Stuart et al., 1999), the size distribution of ^{3}He-bearing IDPs in geologically old sediments has not been shifted to larger grain sizes. Greater than 60% of the ^{3}He resides in particles less than 37 μm in diameter in 33 Ma sediments. Hence, ^{3}He in sediments and sedimentary rocks records the IDP flux and not the micrometeorite flux.

References

Amari S. and Ozima M. (1985) Search for the origin of exotic helium in deep-sea sediments. *Nature* **317**, 520-522.

Amari S. and Ozima. (1988) Extra-terrestrial noble gases in deep sea sediments. *Geochim. Cosmochim. Acta* **52**, 1087-1095.

Andrews J. N., 1985. The isotopic composition of radiogenic helium and its use to study groundwater movement in confined aquifers. *Chem. Geol.* **49**, 339-351.

Becker L., Poreda R. J., and Bada J. L. (1996) Extraterrestrial helium trapped in fullerenes in the Sudbury impact structure. *Science* **272**, 249-252.

Bradley J. P., Sandford S. A., and Walker R. M. (1988) Interplanetary dust particles. In *Meteorites and the Early Solar System* (eds. J. Kerridge and M. S. Mathews), Univ. Arizona Press, Tucson, pp 861-895.

Brookins D. G. (1988) Eh-pH diagrams fro geochemistry. Springer-Verlag, 176 pp.

Brownlee D. E. (1985) Cosmic dust: Collection and research. *Ann. Rev. Earth Planet. Sci.* **13**, 147-173.

Cerling T. and Craig H. (1993) Geomorphology and in-situ cosmogenic isotopes. *Ann. Rev. Earth Planet. Sci.* **22**, 273-317.

Choquette P. W. and James N. P. (1987) Diagenesis #12: Diagenesis in limestones –3. The deep burial environement. *Geosci. Can.* **14**, 3-35.

Corliss B. H. and Hollister C. D. (1982) A paleoenvironmental model for Cenozoic sedimentation in the central North Pacific. In *The Ocean Floor* (eds. R. A. Scrutton and M. Talwani). J. Wiley & Sons, pp 277-304.

Ducati H., Kalbitzer S., Kiko J., Kirsten T., and Muller H. W. (1973) Rare gas diffusion studies in individual lunar soil particles and in artificial implanted glasses. *The Moon* **8**, 210-227.

Farley K. A. (1995) Cenozoic variations in the flux of interplanetary dust recorded by ^{3}He in a deep-sea sediment. *Nature* **376**, 153-156.

Farley K.A. (2001) Extraterrestrial helium in seafloor sediments: Identification, characteristics, and accretion rate over geologic time. In *Accretion of Extraterrestrial matter throughout Earth's History*: (eds. B. Peucker-Ehrenbrink and B. Schmitz). In press.

Farley K.A. and Patterson D.B. (1995). A 100-kyr periodicity in the flux of extraterrestrial ^{3}He to the sea floor. *Nature* **378**, 600-603.

Farley K. A., Love S. G. and Patterson D. B. (1997) Atmospheric entry heating and helium retentivity of interplanetary dust particles. *Geochem. Cosmochim. Acta* **61**, 2309-2316.

Farley K.A., House M. A., and Kohn B. P. (1998) Laboratory and natural diffusivity calibrations for apatite (U-Th)/He thermochronometry. *Mineral. Mag.* **62A**, 426-427.

Farley K. A., Reiners P. W., and Nenow V. (1999) An apparatus for measurement of noble gas diffusivities from minerals in vacuum. *Analyt. Chem.* **71**, 2059-2061.

Fraundorf P., Brownlee D. E., and Walker R. M. (1982) Laboratory studies of interplanetary dust, In *Comets*, (eds. L. L. Wiikening), University Arizona Press, Tucson, pp 383-409.

Fukumoto H., Nagao K., and Matsuda J., (1986) Noble gas studies on the host phase of high $^{3}He/^{4}He$ ratios in deep-sea sediments. *Geochim. Cosmochim. Acta* **50**, 2245-2253.

Futagami T., Ozima M., Nagai S., and Aoki Y. (1993) Experiments on thermal release of implanted noble gases from minerals and their implications for noble gases in lunar soil grains. *Geochim. Cosmochim. Acta* **57**, 3177-3194.

Geiss J. and Bochsler P. (1991) Long term variations in solar wind properties: Possible causes versus observations. In *The Sun in Time* (eds. C. P. Sonett, M. S. Giampapa and M. S. Matthews), Univ. Arizona Press, Tucson, pp 98-117.

Germani M. S., Bradley J. P., and Brownlee D. E. (1990) Automated thin-film analyses of hydrated interplanetary dust particles in the analytical electron microscope. *Earth Planet. Sci. Lett.* **101**, 162-179.

Harris-Kuhlman K. R. (1998) Trapping and diffusion of helium in lunar minerals. PhD thesis, University of Wisconsin – Madison.

Hiyagon H. (1994) Retention of solar helium and neon in IDPs in deep sea sediments. *Science* **263**, 1257-1259.

Huss G. R. and Lewis R. S. (1995) Presolar diamond, SiC, and graphite in primitive chondrites: abundances as a function of meteorite classand petrologic type. *Gecohim. Cosmochim. Acta* **59**, 115-160.

Klock W. and Stadermann F. J. (1994) Mineralogical and chemical relationships of interplanetary dust particles, micrometeorites and meteorites. In *Analysis of Interplanetary Dust* (eds. M. E. Zolensky, T. L. Wilson, F. J. M. Rietmeijer, and G. J. Flynn) AIP Press, pp 51-87.

Koscheev A. P., Gromov M. D., Mohapatra R. K., and Ott U. (2001) History of trace gases in presolar diamonds inferred from ion-implantaion experiments. *Nature* **412**, 615-617.

Kirschvink J. L., Maine A. T., and Hojatollah V. (1997) Paleomagnetic evidence of a low-temperature origin of carbonate in the Martial meteorite ALH84001. *Science* **275**, 1629-1933.

Kyte F. T., Leinen M., Heath G. R. and Zhou, L. (1993) Cenozoic sedimentation history of the central North Pacific: inferences from the elemental geochemistry of core LL44-GPC3. *Geochim. Cosmochim. Acta* **57**, 1719-1740.

Lovera O. M., Richter F. M., and Harrison T. M. (1991) Diffusion domains determined by ^{39}Ar released during step heating. *J. Geophys. Res.* **96**, 2057-2069.

Lovera O. M., Grove M. G., Harrision T. M., and Maho K. I. (1997) Systematic analysis of K-feldspar ^{40}Ar/^{39}Ar step heating results. I. Significance of activation energy determinations. *Geochim. Cosmochim. Acta* **61**, 3171-3192.

Marcantonio F., Anderson R.F., Stute M., Kumar N., Schlosser P., and Mix A. (1996) Extraterrestrial ^{3}He as a tracer of marine sediment transport. *Nature* **383**, 705-707.

Matsuda J. and Murota M. (1990) He and Ne isotopic studies om the extraterrestrial material in deep-sea sediments. *J.Geophys. Res.* **95**, 7111-7117.

Merrihue C. (1964) Rare gas evidence for cosmic dust in modern Pacific red clay. *Ann. N.Y. Acad. Sci.* **119**, 403-411.

Montgomery A.F. and Johnson H. P. (1983) Paleomagnetic studies of Leg 91 basalts and sediments. *Proc. Ocean Drill. Prog. Sci. Res.* **88**, 475-482.

Mukhopadhyay S., Farley K. A., and Montanari A. (2001a) A 35 Myr record of helium in pelagic limestones from Italy: Implications from interplanetary dust accretion from the early Maastrichtian to the middle Eocene. *Geochem. Cosmochim. Acta* **65**, 653-669.

Ozima, M., Takayanagi, M., Zashu, S. and Amari, S. (1984). High $^{3}He/^{4}He$ ratios in ocean sediments. *Nature* **311**, 449-451.

Patterson D. B. and Farley K. A., (1998). Extraterrestrial ^{3}He in seafloor sediments: Evidence for correlated 100 kyr periodicity in the accretion rate of interplanetary dust, orbital parameters, and Quaternary climate. *Geochem. Cosmochim. Acta* **62**, 3669-3692.

Patterson D. B., Farley K. A., and Schmitz B. (1998) Preservation of extraterrestrial 3He in 480-Ma-old marine limestones. *Earth Planet. Sci. Lett.* **163**, 315-325.

Reiners P. W. and Farley K. A. (1999) Helium diffusion and (U-Th)/He thermochronometry of titanite. *Geochim. Cosmochim. Acta* **63**, 3845-3859.

Scott E. R. D., Taylor G.J., Rubin A. E., Okada A., and Keil K. (1981) Graphite-magnetite aggregates in ordinary chondritic meteorites. *Nature* **291**, 544-546.

Stuart F.M., Harrop P.J., Knott S., and Turner G., (1999). Laser extraction of helium isotopes from Antarctic micrometeorites: Source of He and implications for the flux of extraterrestrial ^{3}He flux to earth. *Geochim. Cosmochim. Acta* **63**, 2653-2665.

Trull T. W., Kurz M. D., and Jenkins W. J. (1991) Diffusion of cosmogenic ^{3}He in olivine and quartz: implications for surface exposure dating. *Earth Planet. Sci. Lett.* **103**, 241-256.

Wieler R., Anders E., Baur H., Lewis S. R., and Signer P. (1986) Noble gases from solar energetic particles revealed by closed system stepwise etching of lunar soil minerals. *Geochim. Cosmochim. Acta* **50**, 1997-2017.

Wolf R. A., Farley K.A., and Silver L. T. (1996) Helium diffusion and low temperature thermochronometry of Apatite. *Geochim. Cosmochim. Acta* **60**, 4231-4240.

Ziegler J. F., Biersack J. P., and Littmark U. (1985) The stopping and range of ions in solids. Pergamon Press, New York, 321 pp.

Chapter 4: Geochemistry of Kauai Shield-Stage Lavas: Implications for the Chemical Evolution of the Hawaiian Plume

S. Mukhopadhyay

K. A. Farley

J. C. Lassiter

S. W. Bogue

Abstract - We measured He, Sr, Nd, Pb, and Os isotope ratios and major and trace element concentrations in stratigraphically and paleomagnetically controlled shield-stage lavas from Kauai, Hawaii. The range in $^{3}He/^{4}He$ ratios (17-28 R_A) from Kauai is similar to that reported from Loihi Seamount and, thus, challenges the prevailing notion that high $^{3}He/^{4}He$ ratios are restricted to the pre-shield stage of Hawaiian magmatism. $^{3}He/^{4}He$ ratios vary erratically with stratigraphic position and chronostratigraphic control from paleomagnetic data indicate very rapid changes in the $^{3}He/^{4}He$ ratios (up to 8 R_A in ~100 years). These variations in helium isotopic ratios are correlated with variations in radiogenic isotope ratios, suggesting rapid changes in melt composition supplying the magma reservoir.

A three-component mixing model, previously proposed for Hawaiian shield lavas, does not adequately explain the isotopic data in Kauai shield lavas. The presence of a depleted-mantle component with the isotopic characteristics of post-shield and post-erosional basalts can explain the isotopic variability. The depleted mantle component is

most apparent in lavas from the Kauai shield but may also be present in varying proportion in other Hawaiian shield volcanoes.

Shield lavas from Kauai sample a high $^{3}He/^{4}He$ end-member (Loihi component), but while lavas from western Kauai have a larger contribution from the Kea component (high $^{206}Pb/^{204}Pb$, anomalously low $^{207}Pb/^{204}Pb$ relative to $^{206}Pb/^{204}Pb$), lavas from eastern Kauai have a larger proportion of an enriched (Koolau) component. The systematic isotopic differences between eastern and western Kauai either reflect a gradual migration of the locus of volcanism from west to east, or alternatively east and west Kauai are two distinct shield volcanoes (Holcomb et al., 1997). In the latter case the two shield volcanoes have maintained distinct magma supply sources and plumbing systems.

Our new geochemical data from Kauai support the existence of a single high $^{3}He/^{4}He$ reservoir in the mantle and suggest that the proportion of the different mantle components in the Hawaiian plume have changed significantly in the past 5 Myrs. The long-term evolution of the Hawaiian plume and the temporal variability recorded in Kauai lavas require more complex geochemical heterogeneities than suggested by radially zoned plume models. These complexities may arise from heterogeneities in the thermal boundary layer, and through variable entrainment of ambient mantle by the upwelling plume.

1. Introduction

The geochemistry of ocean island basalts (OIBs), such as those from Hawaii, provides information on the composition of the mantle, and the processes and dynamics of mantle melting. The Hawaiian-Emperor chain of volcanoes represents one of the best

examples of hotspot volcanism (Wilson, 1963; Morgan, 1971) commonly explained by thermal upwelling of deep mantle material. Individual Hawaiian volcanoes are thought to evolve systematically through different stages that are indicated by differences in magma production rates and chemistry of the lavas (Clague and Dalrymple, 1989). Temporal geochemical variability within a single volcano and differences in geochemistry between the different shield volcanoes provide information about the nature of the Hawaiian plume. Here we present new geochemical data from the shield-building stage of Kauai, the oldest of the main Hawaiian islands, that offer new insights into the mantle sources of Hawaiian magmatism and into the chemical evolution of the plume.

Isotopic variability in Hawaiian shield lavas is usually interpreted as mixing between at least three distinct mantle components present in the Hawaiian plume (Stille et al., 1986; West et al., 1987; Kurz et al., 1995; Eiler et al., 1996; Hauri, 1996). To explain the temporal evolution of individual volcanoes and the difference in chemistry of Loa and Kea trend volcanoes (Fig. 1), recent models of the Hawaiian plume favor a cylindrically zoned structure (e.g., Kurz et al., 1995; Hauri et al., 1996; Kurz et al., 1996; Lassiter et al., 1996). The spatial distribution of these components within the plume and their location in the mantle, however, are subject to debate (e.g., Hofmann et al., 1986; Kurz et al., 1995; Hauri et al., 1996; Kurz et al., 1996). Hauri (1996) suggested that the core of the plume is composed of recycled material (referred to as the Koolau component) rising from either the core-mantle boundary or from the lower mantle. The buoyant, upwelling plume entrains lower mantle material (Loihi component), and surrounding the entrained material is passively upwelling asthenosphere (Kea component) (Hauri, 1996; Lassiter et al., 1996). Kurz et al. (1995 and 1996), however,

argued that the relatively undegassed lower mantle (Loihi component) is the plume core rather than the entrained material.

Helium is a useful tracer of the different mantle source components of OIBs and, in combination with other radiogenic isotope tracers, can potentially constrain the spatial and temporal geochemical variability within the Hawaiian plume and the origin of chemical heterogeneities in the mantle (e.g., Kurz et al., 1995; Hauri and Kurz, 1997; Farley and Neroda, 1998). Previous studies have shown that Hawaiian lavas have high $^{3}He/^{4}He$ ratios (6 – 32 RA; with Loihi Seamount having the highest ratios of ~20 – 32 R_A Kurz et al., 1982; Kurz et al., 1983, Kurz et al., 1995, Rison and Craig, 1983) compared to Mid-Ocean-Ridge Basalt (MORB) glasses that are removed from influences of hotspot volcanism (8-10 R_A; e.g., Kurz et al., 1982; Graham et al., 1992; Graham et al., 1996). Such high ratios are usually attributed to sampling of a relatively undegassed mantle source with high time-integrated $^{3}He/(U+Th)$ ratio. In particular, correlations between lithophile isotope ratios and $^{3}He/^{4}He$ ratios suggest to some investigators (e.g., Kurz et al., 1983; Farley et al., 1992) that high $^{3}He/^{4}He$ ratios provide the best if not the only evidence of relatively undifferentiated mantle material. Some studies have suggested that helium is decoupled from the lithophile tracers and, hence, does not provide information about the mantle sources of magmas (e.g., Condomines et al., 1983; Zindler and Hart, 1986; Hilton et al., 1995; Valbracht et al., 1996). These studies have interpreted helium isotopic variations as reflecting shallow level magmatic degassing, contamination, and radiogenic ingrowth of ^{4}He in magma chambers. However, He-Sr-Nd-Pb isotopic data obtained over the last 10 years are generally inconsistent with such interpretations (e.g., Farley et al., 1992; Kurz et al., 1995).

Combined He, Sr, Nd, Pb isotopic data from older Hawaiian islands, like Kauai, are useful for understanding the long-term geochemical evolution of the Hawaiian plume. Kauai, the northernmost and oldest of the main Hawaiian islands (Fig. 1), has generally been interpreted as a single large shield volcano (Macdonald et al., 1960) although field relations between shield lavas exposed in different parts of the island are often obscured by post-erosional lava flows (Fig 1) and heavy forest cover. The shield building stage lasted from 5.1 to 4.3 Ma (K-Ar ages; McDougall, 1979; Clague and Dalrymple, 1988). Recent geochemical data suggest a more complicated structure for Kauai including the presence of two different shield volcanoes on the island (Holcomb et al., 1997; Reiners et al., 1998). To our knowledge, only two published helium isotopic analysis from the Kauai shield exist (Rison and Craig, 1983; Scarsi, 2000). The reported $^{3}He/^{4}He$ ratios of 24 R_A (Rison and Craig, 1983) and 25 R_A (Scarsi, 2000) are surprisingly high compared to other Hawaiian shield volcanoes, which dominantly have $^{3}He/^{4}He$ ratios <20 R_A. The following study was undertaken to identify temporal and spatial variations in helium isotopic compositions on Kauai, gain insights into the mantle sources of Kauai lavas, and understand the origin of chemical heterogeneities in the mantle through a combined study of helium isotopic ratios, lithophile isotope tracers (e.g., Sr, Nd, Pb) and major and trace elements.

2. Samples and Analytical Techniques

Our samples are paleomagnetic cores (diameter = 1.5 cm; length = 6-10 cm) from subaerial shield stage lava flows, which were previously studied for paleomagnetic intensity and direction (Bogue and Coe, 1984). The shield stage lavas belong to the

Figure 1: Generalized geological map of Kauai (after Macdonald et al., 1960). Anahola (East Kauai), Kahililoa (Central Kauai), Ohaiula and Polihale (West Kauai) are the sampling sites (also see Bogue and Coe, 1984).

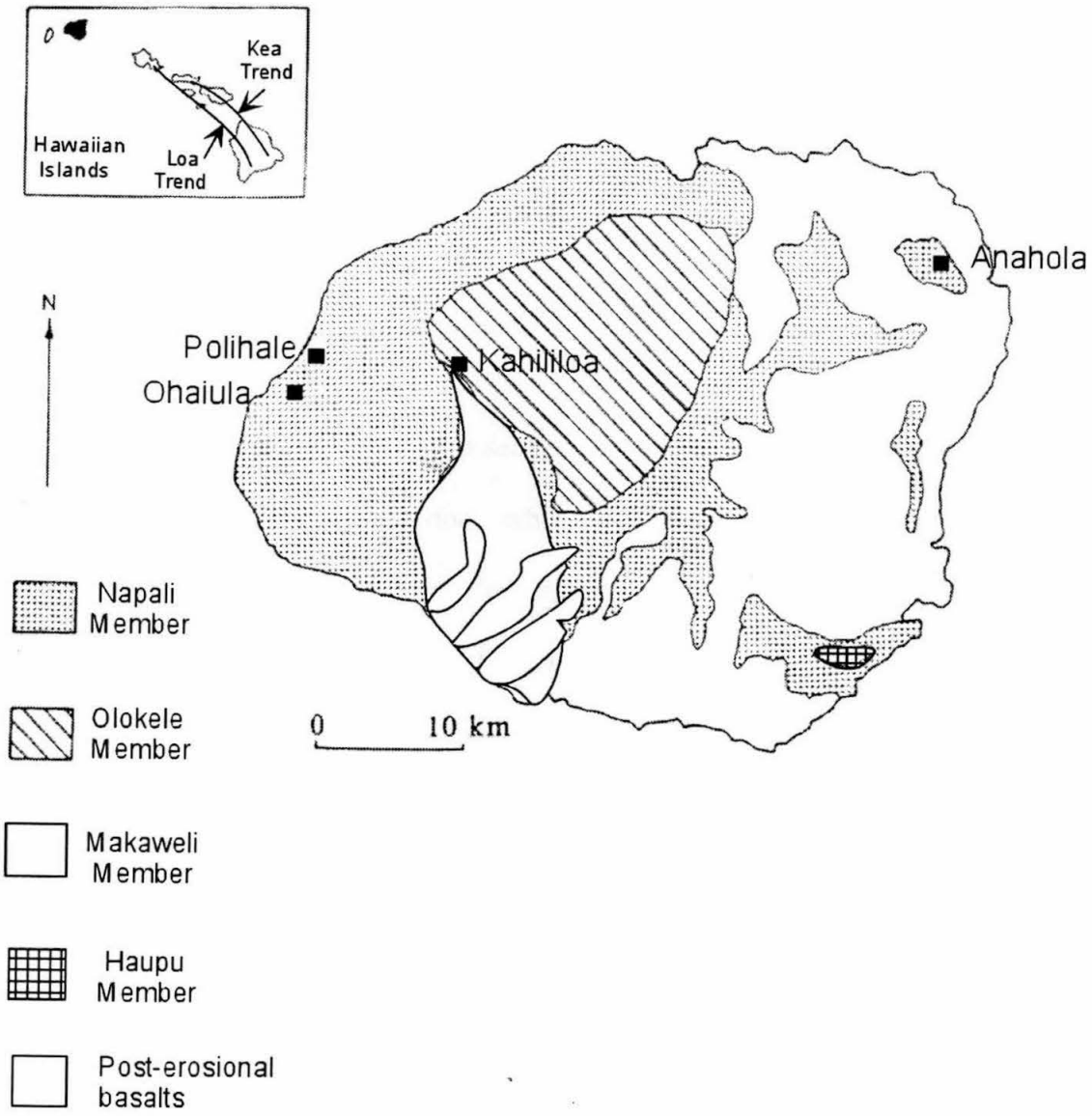
Kea
Trend
Hawaiian
Islands
Loa
Trend
N
Polihale
Ohaiula
Kahililoa
Anahola
0
10 km
Napali
Member
Olokele
Member
Makaweli
Member
Haupu
Member
Post-erosional
basalts

Waimea Canyon Basalt Group (Macdonald et al., 1960). The Waimea Canyon Basalt is subdivided into four members, the oldest and most widespread of which is the Napali Member (Macdonald et al., 1960; Fig. 1). Next in surface area is the Olokele Member exposed in the central part of Kauai. Lavas of the Olokele Member are younger than the Napali Member and are comprised of thick, flat lying flows (Macdonald et al., 1960). The Makaweli and Haupu Members are the two other constituents of the Waimea Canyon Basalt Group, but were not sampled for this study.

Samples from stratigraphic sections at Polihale, Ohaiula, Kahililoa, and Anahola were analyzed during this study (Fig. 1). The Polihale, Ohaiula and Anahola sections belong to the Napali Member, while the Kahililoa section belongs to the Olokele Member. The Polihale and Ohaiula ridge sections have been superimposed to construct a single composite stratigraphic section, which we term the West Kauai section. Correlation of these two sections comes from tracing a Reverse – Normal (R-N) polarity transition that appears at the top of the Polihale ridge section and near the base of the Ohaiula ridge section (Bogue and Coe, 1984; Bogue 2001). The Kahililoa section in the Olokele Member records a Normal-Reverse (N-R) polarity transition and field relations indicate that this section is younger than the West Kauai section. We designate the Kahililoa section as the Central Kauai section. The Anahola section in the eastern part of the island, which also records a R-N polarity transition, is termed the East Kauai section. The total number of flows in the West, Central, and East Kauai sections are 48, 25 and 19 (see Bogue and Coe, 1984; Bogue 2001), although we sampled only the olivine rich flows. Using the mean recurrence interval of 0.5 kyr/flow unit estimated from the pilot hole of the Hawaii Scientific Drilling Project (HSDP) at Mauna Kea (Sharp et al., 1996),

the total time represented by the West, Central, and East Kauai sections are likely to be ~ 25, 13, and 10 kyr respectively.

Based on the similarity in virtual geomagnetic pole (VGP) sequence across the R-N polarity transition in the East and West Kauai section, previous workers had correlated the two sections (e.g., Bogue and Coe, 1984). Recently, based on observed differences in the isotopic composition of the lavas across the R-N transition in the eastern and western parts of Kauai, Holcomb et al. (1997) suggested while the R-N transition might be temporally correlated, East and West Kauai are two different shield volcanoes. Field relations alone are not sufficient to evaluate this hypothesis and there are no absolute ages of the R-N transition in the West and East Kauai sections. Thus, the relationship in space and time between the East and West Kauai sections is not clear.

2.1. Methods

The paleomagnetic cores were crushed and olivine phenocrysts 1-3 mm in diameter were hand picked. The olivine crystals were inspected under a binocular microscope to ensure that they were free from alteration products and adhering matrix. The crystals were ultrasonically cleaned in distilled water and then in acetone and dried in an oven at 100°C for 1-2 hours. Gases from fluid inclusions were liberated by crushing in vacuum ~0.2 g to 0.9 g of olivine crystals for 3-4 minutes with an electromagnetic crusher (see Patterson et al., 1997 for details). Following crushing, some of the powders were fused to check for the presence of cosmogenic or radiogenic helium. Gas purification and mass spectrometric techniques were described by Patterson et al. (1997). Typical ^{4}He crusher blanks were $< 3 \times 10^{-11}$ cc STP and averaged 1% of the sample

Table 1: Major and trace element data from Kauai shield lavas.

	West Kauai											
	PB1	**PB10**	**PB12**	**PB16**	**PB17**	**PB18**	**PB19**	**PB20**	**PB21**	**OR1**	**OR3**	**OR5**
SiO_2	48.2	46.3	46.2	49.6	49.5	45.6	46.1	48.6	50.0	49.1	47.5	46.2
Al_2O_3	10.0	8.1	8.1	13.1	12.6	7.4	8.6	11.1	13.0	11.7	9.9	7.9
TiO_2	1.9	1.5	1.5	2.6	2.5	1.4	1.7	1.9	2.3	2.1	1.8	1.5
FeO*	11.7	11.9	12.4	11.8	12.0	12.0	12.1	11.7	11.5	11.9	11.7	12.4
MnO	0.2	0.2	0.2	0.2	0.2	0.2	0.2	0.2	0.2	0.2	0.2	0.2
CaO	8.3	6.8	6.8	10.9	10.6	6.1	7.2	9.1	10.8	9.7	8.1	6.7
MgO	17.8	23.6	23.1	9.2	9.9	25.7	22.1	15.3	9.7	13.2	18.9	23.7
K_2O	0.2	0.2	0.1	0.2	0.3	0.1	0.2	0.2	0.2	0.2	0.2	0.2
Na_2O	1.6	1.4	1.4	2.2	2.2	1.4	1.6	1.9	2.1	1.8	1.6	1.3
P_2O_5	0.19	0.15	0.15	0.26	0.26	0.16	0.20	0.17	0.22	0.20	0.17	0.15
Ni	821	1137	1163	253	278	1280	1039	645	243	476	915	1181
Cr	902	1400	1374	522	559	1365	1232	848	525	726	1058	1186
Sc	23	15	25	32	27	24	26	25	30	30	28	20
V	224	193	203	305	275	172	211	244	281	272	225	188
Ba	44	36	54	54	74	57	79	46	44	39	42	44
Sr	235	184	185	319	310	189	245	235	291	261	216	176
Zr	104	80	79	141	137	78	99	100	125	113	98	80
Y	22	17	21	30	27	17	19	23	27	24	24	17
Nb	12	8	9	16	15	10	13	11	13	13	11	10
Ga	14	14	10	17	18	13	13	15	20	21	14	13
Cu	101	66	86	117	114	55	60	105	111	76	77	47
Zn	102	98	97	101	102	97	99	99	102	101	96	98
Ce	11	17	12	42	41	11	21	26	26	25	21	6

Table 1 (continued)

	Central Kauai					East Kauai							
	OK9	**OK19**	**OK20**	**OK22**	**OK25**	**A2**	**A3**	**A9**	**A11**	**A14**	**A16**	**A17**	**A19**
SiO_2	44.9	52.0	46.2	46.5	48.3	50.1	51.5	48.7	48.5	44.5	47.1	45.0	48.1
Al_2O_3	5.8	13.1	7.6	8.7	9.9	13.7	13.9	12.0	11.9	6.3	10.9	6.6	12.7
TiO_2	1.1	2.3	1.3	1.6	1.7	2.2	2.6	2.2	2.1	0.9	2.2	1.2	2.3
FeO*	12.9	9.5	12.1	11.8	11.4	10.4	10.3	11.6	12.3	12.5	12.4	12.0	12.2
MnO	0.2	0.2	0.2	0.2	0.2	0.2	0.2	0.2	0.2	0.2	0.2	0.2	0.2
CaO	4.8	9.9	5.9	6.8	7.9	10.9	10.8	9.5	8.9	4.8	8.6	5.1	9.6
MgO	29.3	10.1	25.2	22.7	18.3	10.0	7.7	13.6	13.8	29.7	16.5	28.7	12.4
K_2O	0.1	0.3	0.2	0.1	0.3	0.1	0.4	0.2	0.1	0.1	0.1	0.1	0.1
Na_2O	0.9	2.3	1.3	1.4	1.7	2.1	2.5	1.9	1.8	1.0	1.8	1.1	2.1
P_2O_5	0.12	0.23	0.14	0.15	0.19	0.23	0.26	0.22	0.25	0.10	0.22	0.11	0.21
Ni	1721	313	1419	1183	904	245	157	480	593	1592	697	1676	493
Cr	1704	620	1294	1332	1173	578	385	813	862	1249	798	1283	540
Sc	11	25	18	22	25	25	28	24	24	15	29	15	20
V	154	274	171	199	219	268	292	274	258	132	251	154	264
Ba	50	62	35	40	63	100	82	45	58	29	39	34	45
Sr	137	292	161	185	235	307	332	275	251	128	274	144	280
Zr	57	128	73	85	97	121	138	120	112	48	114	61	123
Y	13	25	19	19	20	26	27	25	25	15	23	18	29
Nb	8	12	6	8	10	13	14	10	10	5	11	6	12
Ga	8	19	13	13	14	18	18	19	18	7	19	10	20
Cu	53	77	46	79	90	105	108	91	91	51	86	56	119
Zn	98	82	102	102	101	96	97	107	104	103	107	99	109
Ce	9	35	14	21	8	33	27	28	18	17	16	20	30

* Denotes total iron; major oxides are in weight % and trace element concentrations are in ppm.

Table 2: Isotopic composition of Kauai shield lavas.

	Flow Name	Stratigraphic Height (ft)	Crush $^{3}He/^{4}He$ R_A	[He] (10^{-9} cc STP g^{-1})	$\frac{^{87}Sr}{^{86}Sr}$	$\frac{^{143}Nd}{^{144}Nd}$	$\frac{^{206}Pb}{^{204}Pb}$	$\frac{^{207}Pb}{^{204}Pb}$	$\frac{^{208}Pb}{^{204}Pb}$	$\frac{^{187}Os}{^{188}Os}$
West	PB1	5	22.9	9.4						
Kauai	PB10	260	20.2	1.0	0.70361		18.322	15.45	37.989	
	PB11	280	26.7	1.9						
	PB12	300	27.3	10.0	0.70365	0.51297	18.320	15.45	37.998	0.1334
	PB16	380	26.8	1.6	0.70356		18.324	15.45	37.947	
	PB17	390	19.5	0.8						
	PB18	420	19.7	3.6	0.70351	0.51302	18.292	15.44	37.884	
	PB19	430	17.9	1.7	0.70345	0.51302	18.257	15.45	37.854	
	PB20	450	24.9	1.5	0.70368	0.51303	18.369	15.46	38.020	0.1345
	PB21	470	22.3	1.4	0.70364	0.51299	18.299	15.45	37.955	
	OR1	475	28.3	5.0	0.70365					
	OR2	485	24.1	1.1						
	OR3	495	24.6	1.8	0.70364		18.299	15.43	37.925	
	OR4	500	22.9	5.0						
	OR5	508	23.9	5.9						
	OR18	690	23.9	3.1	0.70364	0.51299	18.377	15.45	38.011	
	OR19	700	24.7	3.3						
	OR27	895	26.8	12.7	0.70363	0.51300	18.366	15.44	37.958	
Central	OK9	100	25.7	5.6	0.70367	0.51298	18.25	15.44	37.9	0.1364
Kauai	OK19	233.33	23.3	0.9						
	OK20	266.67	22.9	1.0	0.70370	0.51294	18.2	15.44	37.89	0.1379
	OK22	300	28.3	5.8						
	OK23	306.67	24.1	0.5						
	OK25	336.67	21.4	0.6	0.70369	0.51297	18.22	15.44	37.92	0.1352
East	A2	27.3	19.9	3.4	0.70371	0.51296	18.157	15.44	37.871	
Kauai	A3	54.6	21.4	1.3	0.70379	0.51296	18.22	15.45	37.91	0.1389

Table 2 (continued)

	Flow Name	Stratigraphic Height (ft)	Crush $^{3}He/^{4}He$ R_A	[He] (10^{-9} cc STP g^{-1})	$\frac{^{87}Sr}{^{86}Sr}$	$\frac{^{143}Nd}{^{144}Nd}$	$\frac{^{206}Pb}{^{204}Pb}$	$\frac{^{207}Pb}{^{204}Pb}$	$\frac{^{208}Pb}{^{204}Pb}$	$\frac{^{187}Os}{^{188}Os}$
	A9	218.4	27.7	27.1	0.70381		18.186	15.45	37.9	
	A11	273	24.5	34.3	0.70378		18.102	15.42	37.813	
	A12	300.3	24.9	4.0						
	A13	327.6	26.6	3.3						
	A14	354.9	25.4	5.5						
	A16	409.5	22.1	1.2	0.70369		18.198	15.45	37.879	
	A17	436.8	26.8	6.6	0.70373	0.51296	18.14	15.43	37.84	0.1378
	A19	491.4	23.7	19.7	0.70375	0.51295				0.1376
Post shield alkalic cap, Central Kauai	Olokele Member	3120	7.0	0.5						

Stratigraphic height is with respect to the base of the section. Uncertainties in $^{3}He/^{4}He$ ratios are ~3.3%, based on reproducibility of standards of similar size to the samples. $^{87}Sr/^{86}Sr$ reported relative to NBS 987 = 0.71025. $^{143}Nd/^{144}Nd$ values are reported relative to La Jolla 143Nd/144Nd = .511860. External precisions for Sr, Nd isotopes are 0.00002 (2σ). Pb-isotopes were corrected for mass fractionation using NBS 981 values of Todt et al. (1996) and reproducibility of measured ratios is better than 0.05% a.m.u $^{-1}$. Analytical uncertainties for Os isotopes are 3 $^{o}/_{oo}$ (2σ).

Table 3: Comparison of crush and fused $^{3}He/^{4}He$ ratios from olivine phenocrysts in Kauai shield lavas.

Sample	$^{3}He/^{4}He$ Crush (R_A)	$^{3}He/^{4}He$ Fusion (R_A)	Cosmogenic [^{3}He] (10^{-15} cc STP g-1)	^{3}He cosmogenic / ^{3}He crush	Apparent Exposure Age (kyr)
PB12	27.3	97.0	117	0.3	80.3
PB17	19.5	37.5	70.2	3.2	75.5
PB19	17.9	33.3	56	1.4	45.6
PB20	24.9	41.1	35.9	0.7	37.1
OR1	28.3	45.4	88.1	0.5	65.8
OR18	23.9	32.9	57.1	0.5	38.4
OR27	26.8	30.5	9.37	0.0	6.14
A2	19.9	38.9	126	1.4	103
A11	24.5	18.3	0	0.0	0
A17	26.8	48.0	40.5	0.2	32.1

The exposure ages have been calculated using a ^{3}He production rate of 50 atoms/g/year in olivine crystals.

measurements. ^{3}He crush blanks were always less than 1×10^{-15} cc STP, in all cases <1% of the sample. The uncertainty in the computed $^{3}He/^{4}He$ ratio is dominated by the blank correction of ^{4}He but is typically $\leq \pm 1$ R_A.

Major and minor elements were measured by X-ray fluorescence at the GeoAnalytical Laboratories, Washington State University (Pullman). In addition, a subset of the samples was analyzed for Sr, Nd, Pb, and Os. Analytical methods for the measurements of these isotopic ratios have been presented previously (Lassiter et al., 2000 and references therein). Note that olivine was not extracted from the splits analyzed for major and trace elements.

3. Results

Major and trace element data are listed in Table 1 and isotopic ratios are summarized in Table 2.

3.1. Major and Trace Element Composition

The Kauai lavas investigated in this study are tholeiites (Fig. 2). Hawaiian tholeiites with K_2O/P_2O_5 <1 are considered to have undergone post-eruptive alteration (Lipman et al., 1990; Frey et al., 1994). Most of the samples we analyzed have K_2O/P_2O_5 <1, suggesting that they have undergone some alteration. In general, K_2O/P_2O_5 in East Kauai tholeiites are lower than those from West Kauai, which is not surprising since East Kauai is on the windward side of the island.

The MgO content of the Kauai lavas varies from 29.7 wt % to 7.7 wt % Abundances of MgO are inversely correlated with other major element oxides (e.g., SiO_2,

CaO, Al_2O_3; Fig. 3) and the linear trends seen in Figure 3 are consistent with olivine addition or subtraction (e.g., Frey and Rhodes, 1993; Frey et al., 1994; Yang et al., 1996). Concentrations of Ni (157 to 1721 ppm) and Cr (385 to 1704 ppm), elements compatible in olivine and Cr-spinel, are positively correlated with the MgO contents. In comparison, Sc (an element compatible in clinopyroxene) is inversely correlated with MgO (Fig 3), indicating that fractionation of clinopyroxene was not a dominant factor in controlling the major element composition. Abundances of incompatible trace elements such as Nb, Zr, P_2O_5 and Sr positively correlated with each other (Fig 4). Such correlations have been observed in other Hawaiian shield volcanoes and have been interpreted to reflect magmatic processes (e.g., Frey et al., 1994). In contrast, Rb concentrations are not correlated with other incompatible elements (Fig. 4) suggesting Rb loss during post-magmatic weathering processes (e.g., Frey et al., 1994).

3.2. Helium Isotopic Ratios

Before interpreting the helium isotopic data from Kauai as a mantle signature, we first discuss the potential effect of post-eruptive cosmogenic or radiogenic helium on the measured $^3He/^4He$ ratios. The helium concentration in the Kauai lavas varies from 0.5 to 34×10^{-9} cc STP g^{-1} (Table 2), which is within the normal range of helium concentration in olivine phenocrysts from Hawaii (e.g., Kurz et al., 1987; Kurz et al., 1996). There is no correlation between the measured $^3He/^4He$ ratios and the helium concentration of the phenocrysts (Fig. 5a), suggesting that the helium isotopic ratios are not strongly influenced by post-eruptive He production.

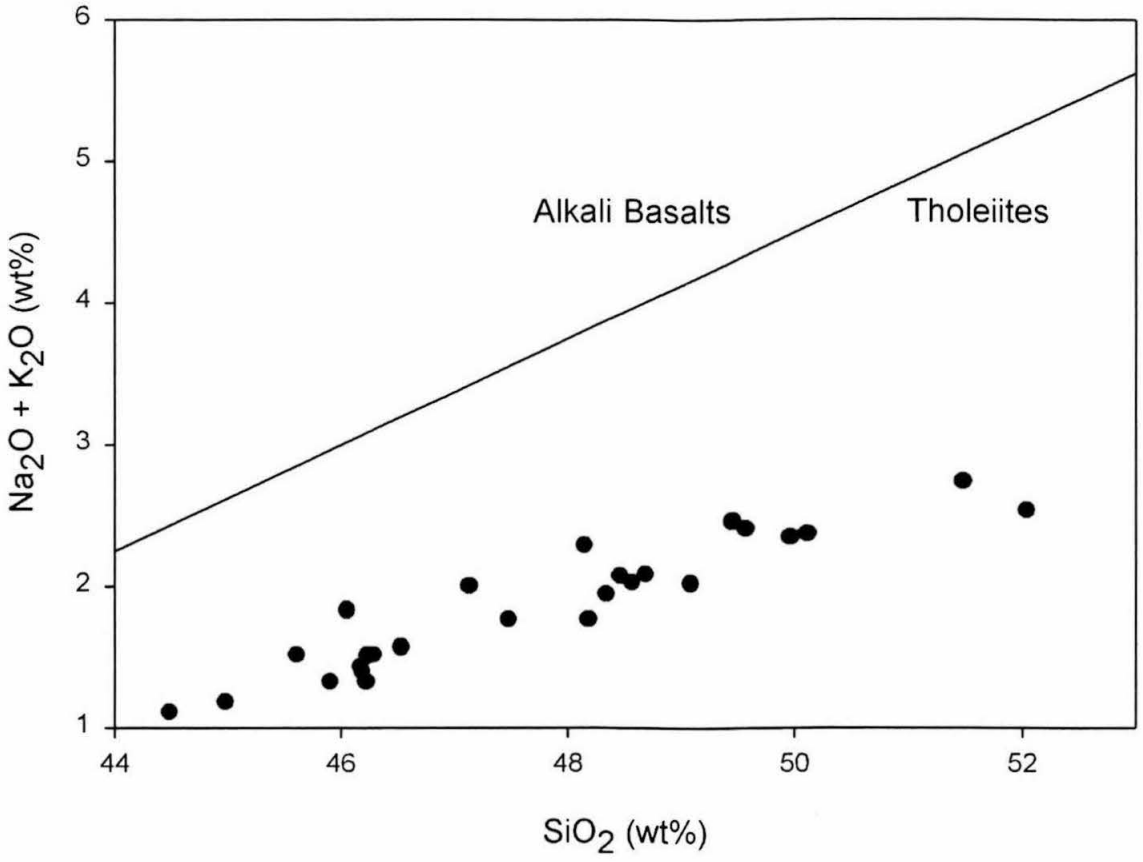

Figure 2: SiO_2 versus alkalis in Kauai shield lavas. Note that all the Kauai samples plot in the tholeiite field.

Figure 3: (a) Major oxide abundance and (b) concentration of transition metals trace elements versus MgO content of Kauai lavas. The linear trends reflect the olivine control line.

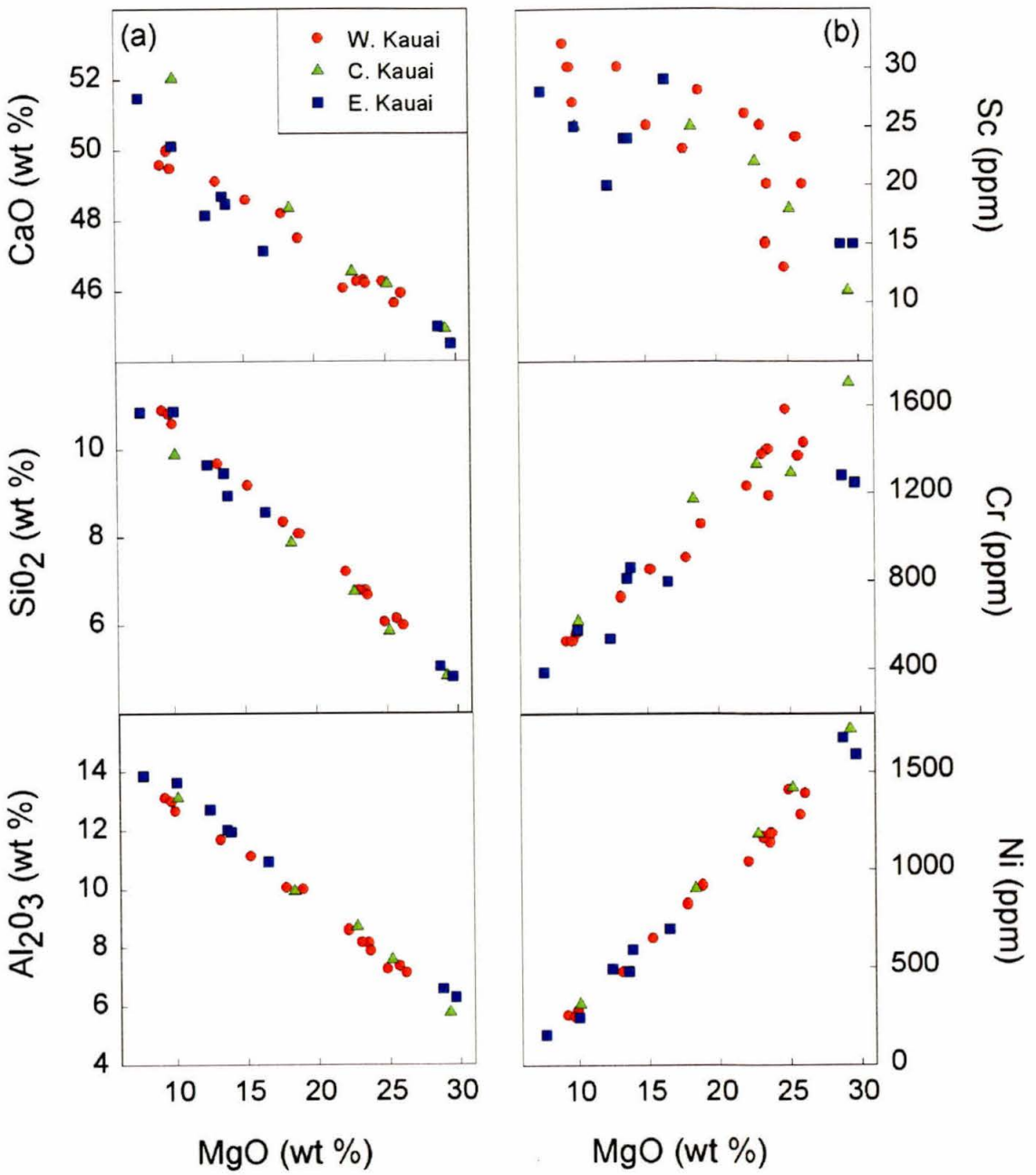
(a)
W. Kauai
C. Kauai
E. Kauai
CaO (wt %)
52
50
48
46
SiO_2 (wt %)
10
8
6
Al_2O_3 (wt %)
14
12
10
8
6
4
10
15
20
25
30
MgO (wt %)
(b)
Sc (ppm)
30
25
20
15
10
Cr (ppm)
1600
1200
800
400
Ni (ppm)
1500
1000
500
0
10
15
20
25
30
MgO (wt %)

Figure 4: Concentrations of incompatible trace elements and minor oxides (P_2O_5) in Kauai shield lavas. While Nb, Sr, Zr, and P_2O_5 abundances correlate well with each other, Rb contents are not correlated with abundances of other incompatible trace elements.

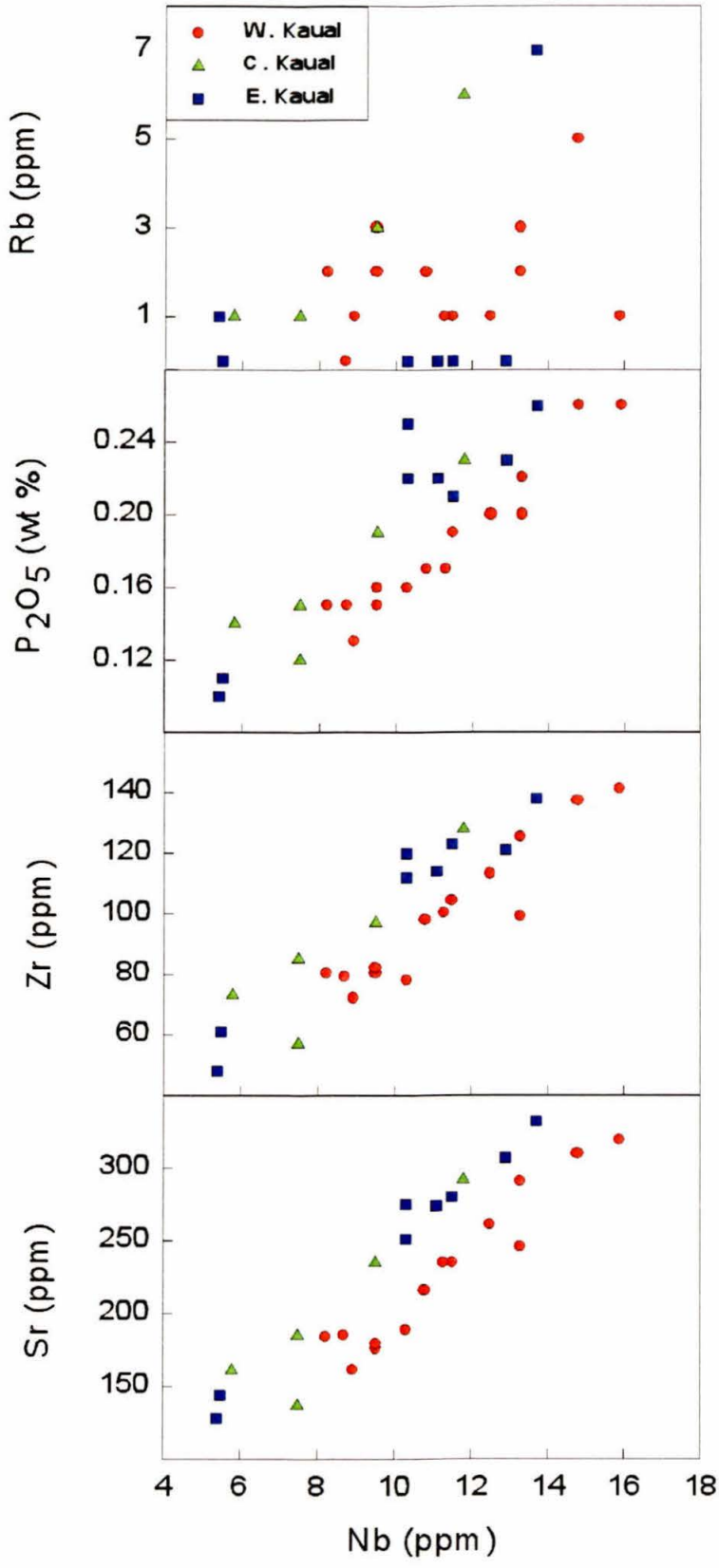
W. Kauai
C. Kauai
E. Kauai
Rb (ppm)
7
5
3
1
P2O5 (Wt %)
0.24
0.20
0.16
0.12
Zr (ppm)
140
120
100
80
60
Sr (ppm)
300
250
200
150
4
6
8
10
12
14
16
18
Nb (ppm)

Figure 5: (a) $^{3}He/^{4}He$ ratios versus $1/[^{4}He]$ in olivine phenocrysts from Kauai. The lack of a correlation suggests that $^{3}He/^{4}He$ ratios are not a simple mixture between mantle sources and post-eruptive components. Note that samples with high He concentration plot on the left-hand side of the figure. (b) Step-crushing experiment on PB12, the sample with the highest $^{3}He/^{4}He$ ratio in the fusion. For comparison, data from the original 4 minute crush is shown and has been offset to the right for clarity. Note that the $^{3}He/^{4}He$ ratios are identical in the first two steps.

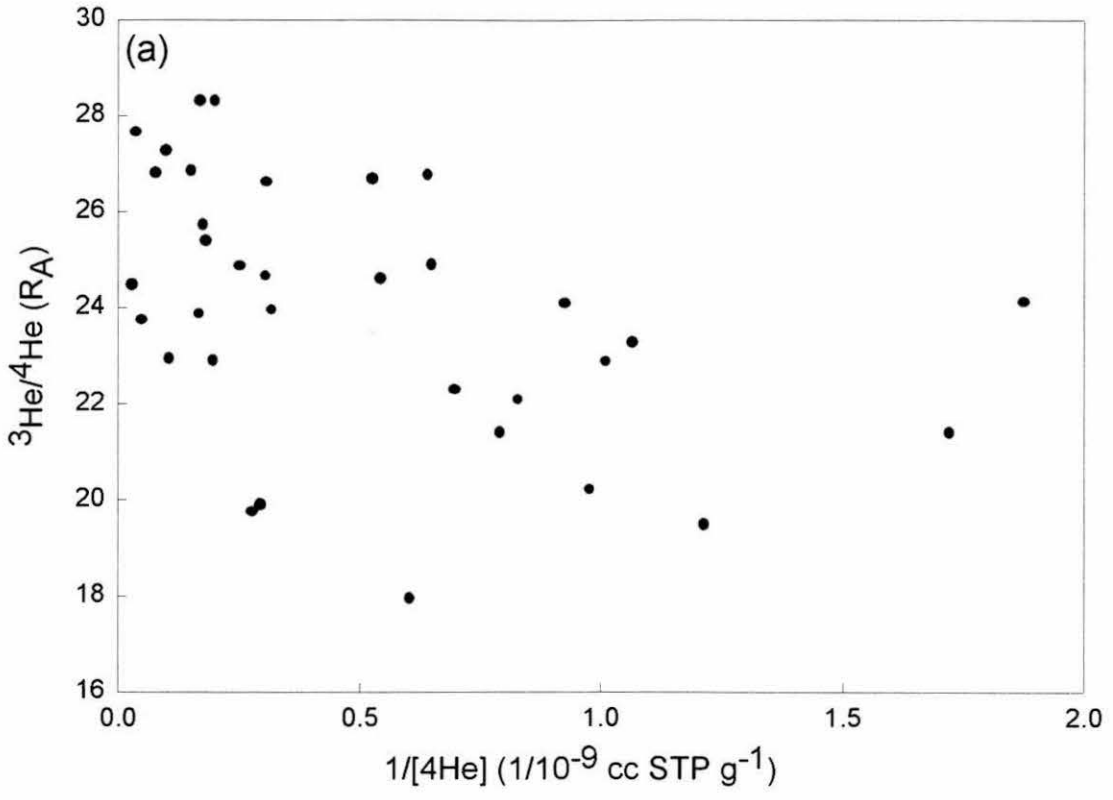
(a)
30
28
26
24
22
20
18
16
0.0
0.5
1.0
1.5
2.0
3He/4He (RA)
1/[4He] (1/10-9 cc STP g-1)

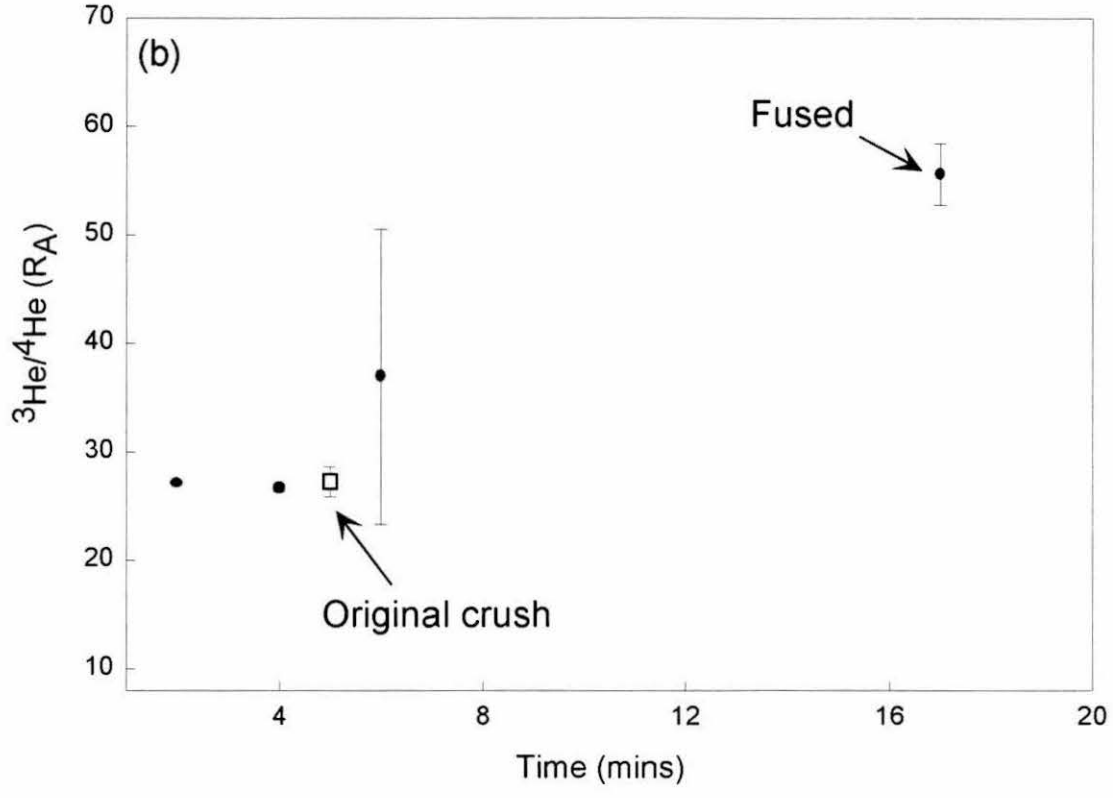
(b)
70
60
50
40
30
20
10
4
8
12
16
20
3He/4He (RA)
Time (mins)
Fused
Original crush

Kurz (1986) demonstrated that crushing under vacuum effectively separates magmatic helium trapped in fluid inclusions from post-eruptive components that reside in the matrix of the mineral. However, intense pulverization of the sample may lead to some cosmogenic/radiogenic helium being released (Hilton et al., 1993). Our crushing time of 3-4 minutes is shorter or comparable to those normally used by other workers (e.g., Kurz, 1986; Patterson et al., 1997) and therefore should not have released cosmogenic or radiogenic helium (also see Scarsi, 2000). To verify this assertion we fused a set of crushed powders. Cosmogenic helium was detected in most of the fused powders and radiogenic ^{4}He was detected in one sample (Table 3). Cosmogenic ^{3}He concentrations varied from 1.3×10^{-13} cc STP g^{-1} to 9.4×10^{-15} cc STP g^{-1} and $^3He_{cosmogenic}/^3He_{crush}$ ratios varied from 0.002 to 3.15. These values are similar to those found in Haleakala basalts (Kurz 1986b, 1987). Based on these cosmogenic ^{3}He concentrations, apparent exposure ages of the Kauai lavas vary from 8 kyr to 100 kyr (Table 3). These imply erosion rates of 1-10 m/Myr, consistent with rates obtained from Haleakala near sea level (Kurz, 1986). More detailed interpretation of the exposure ages is beyond the scope of this work.

Step crushing experiments are a potential way of verifying if ^{3}He/^{4}He ratios in the original crush have been affected by the presence of cosmogenic ^{3}He (Hilton et al., 1993). Because sample PB12 had the highest ^{3}He/^{4}He ratio of the fusion analyses (Table 3), we took a second aliquot of the sample and subjected it to step crushing. The results are shown in Figure 5b. The ^{3}He/^{4}He ratio in the two and four minute steps was 26 R_A, identical to the original crush ratio. Although the six-minute step suggests an increase in the ^{3}He/^{4}He ratio, there is a large uncertainty associated with the analysis. The large error bar reflects the very low gas content in the step (99% of the helium was extracted in the

first two crushing steps). A step crushing experiment on olivine phenocrysts from Kauai by Scarsi (2000) also documents no variation in the $^3He/^4He$ ratio after thirty minutes of crushing. The crusher design used by Scarsi (2000) is similar to that used at Caltech. Thus, we conclude that the range of $^3He/^4He$ values obtained from Kauai is indicative of the composition of the mantle sources of these lavas.

3.2.1. Temporal Variability in Helium Isotopic Ratios

Helium isotopic ratios from Kauai vary from 17.9 R_A to 28.3 R_A and the average for 34 samples is 24 R_A (Table 2). Although differences in radiogenic isotope ratios between West and East Kauai have been suggested (Holcombe et al., 1997), there is no distinction in the range of $^3He/^4He$ ratios from the different geographical localities.

Absolute ages of post-shield alkalic lavas at the top of the Olokele Formation (Figs. 1 and 6) provide a minimum estimate of the total time over which the high $^3He/^4He$ ratios were sampled at Kauai. Alkalic lavas in the Olokele Formation yield an Ar-Ar age of 3.92 ± 0.03 Ma (Clauge and Dalrymple, 1988) and, hence, were erupted during reversed polarity chron 2r. There is no evidence of a missing normal polarity zone between the alkalic lavas (chron 2r) and the N-R transition in our Central Kauai section. Therefore, it is simplest to hypothesize that the reversed polarity chron in the Central Kauai section is 2r and the normal polarity chron is 3n.1.n (Fig. 6). Since field relations suggest that no magnetic chrons are missing between the West Kauai and Central Kauai sections (Bogue and Coe, 1984), the normal polarity chron in West Kauai (Fig. 6) is also 3n.1.n. Based on the Cande and Kent (1995) timescale the total duration of chron 3n.1.n

Figure 6: Stratigraphic variations in He and Sr isotope ratios from (a) West (b) Central and (c) East Kauai. West Kauai represents a composite stratigraphic section, constructed by superposing the Polihale (reverse polarity) and Ohaiula sections (normal polarity). Note the rapid variations in $^{3}He/^{4}He$ ratios particularly from West Kauai and the correlation in He and Sr isotope ratios. Stratigraphic height is relative to the base of the section (and not with respect to elevation above sea-level).

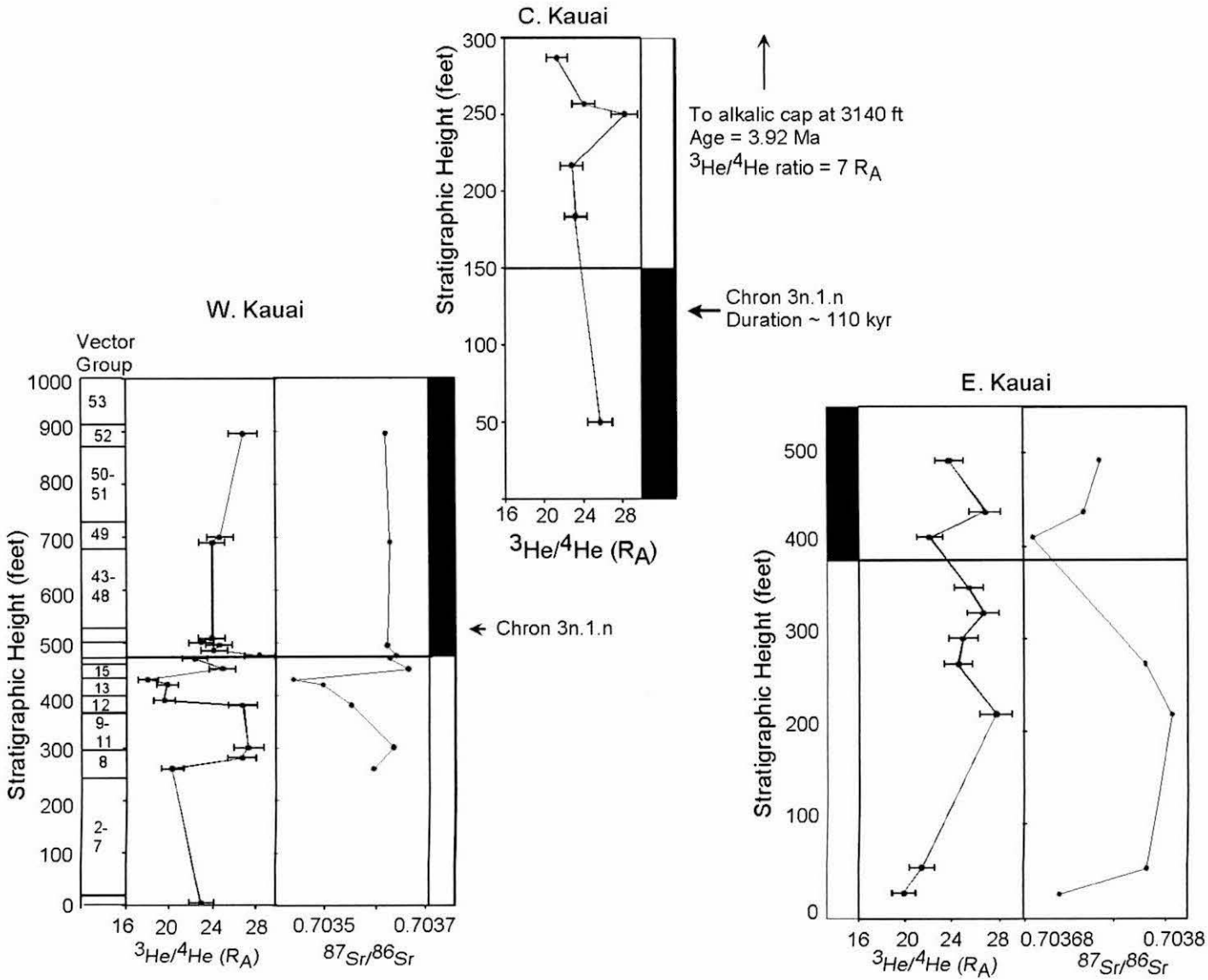
C. Kauai
Stratigraphic Height (feet)
300
250
200
150
100
50
16 20 24 28
3He/4He (RA)
To alkalic cap at 3140 ft
Age = 3.92 Ma
3He/4He ratio = 7 RA
Chron 3n.1.n
Duration ~ 110 kyr
W. Kauai
Vector Group
1000
900
800
700
600
500
400
300
200
100
0
53
52
50-51
49
43-48
15
13
12
9-11
8
2-7
Chron 3n.1.n
16 20 24 28
3He/4He (RA)
0.7035 0.7037
87Sr/86Sr
E. Kauai
500
400
300
200
100
0
16 20 24 28
3He/4He (RA)
0.70368 0.7038
87Sr/86Sr

is 110 kyr. Therefore, the He isotope ratios documented from Kauai represent tapping of a high $^3He/^4He$ component, at least episodically, for >110 kyr.

$^3He/^4He$ ratios in shield lavas from all three Kauai sections vary erratically with stratigraphic position (Figs. 6a-c; Table 2). For example in West Kauai, the $^3He/^4He$ ratio decreases from 26.8 R_A in flow PB16 to 19.5 R_A in PB17 and then increases from 17.9 R_A in PB19 to 24.9 R_A in PB20 (Table 2). Paleointensity and paleodirection measurements on the Kauai samples (Bogue and Coe, 1984; Bogue 2001) provide us with a time constraint on these variations. Bogue (2001) grouped individual flows from West Kauai that differ by no more 10% in paleointensity and 5% in paleodirection into vector groups (Fig. 6a). Based on historical records of the geomagnetic field a vector group represents on <100 years (Holcomb et al., 1986; Bogue, 2001). Within the time interval represented by a single vector group the $^3He/^4He$ ratio varies by 7 R_A (Fig. 6a). In addition, many of the documented variations in $^3He/^4He$ ratio are close to a reversal boundary and during a reversal both inclination and intensity may change more rapidly. Therefore, we conclude that the variations in $^3He/^4He$ ratios in West Kauai lavas between 275 feet and 475 feet (Fig. 6a) occur on timescales of ≤ 100 years.

A post-shield alkalic basalt in the Olokele Formation yielded a $^3He/^4He$ ratio of 7 R_A (Table 2), similar to ratios obtained from alkalic lavas at Haleakala and Mauna Kea (Kurz et al., 1987; Kurz et al., 1996) and from MORBs tholeiites (e.g., Graham et al., 1992, 1996). The alkalic basalts in the Olòkele Formation are from an elevation of ~ 3140 ft above sea-level. The stratigraphically highest flow from which we have a helium measurement (OK25; Table 2) in the Central Kauai section has an elevation of ~ 2250 ft (Bogue and Coe, 1984). Since lavas in the Olokele Formation are near horizontal, the

$^{3}He/^{4}He$ ratio decreased by 14 R_A over ~ 900 ft (270 m). If we assume that magma production rates near the end of the main shield building stage on Kauai were comparable to that of Mauna Kea (Sharp et al., 1996), the decrease in $^{3}He/^{4}He$ ratios from plume like values of 21 R_A to MORB values of 7 R_A occurs over a timescale of ~75 kyr. Because of the lack of olivine-rich flows near the top of the Olokele section, we could not determine whether the drop occurred gradually or rapidly. For comparison, in the last 75 kyr of the shield building stage of Mauna Kea the $^{3}He/^{4}He$ ratio decreases by only 1-2 R_A units (Kurz et al., 1996) while at Mauna Loa the $^{3}He/^{4}He$ ratio decreased from 18 R_A to 8 R_A in ~ 20 kyr (Kurz et al., 1987).

3.3. Radiogenic Isotope Ratios

Our new isotopic data extend the Kauai field in Sr, Nd, and Pb space and provide the first Os-isotopic measurements from the shield building stage of Kauai (Fig 7-10). The erratic variations in $^{3}He/^{4}He$ ratios with stratigraphic position are also seen in Sr, Nd, and Pb isotope ratios (Fig 6; Table 2). For example, the decrease in $^{3}He/^{4}He$ ratios from ~25 R_A to 17 R_A and the subsequent recovery to 25 R_A between 375 and 475 feet in West Kauai are correlated with variations in Sr isotope ratios (Fig 6a). Similar variations in $^{3}He/^{4}He$ ratios and $^{87}Sr/^{86}Sr$ ratios are also seen in East Kauai lavas (Fig. 6c).

The Sr, Nd and Os isotopic composition of West Kauai lavas are similar to those from Loihi (Figs. 7 and 8a). In addition, our new data suggest that Sr isotope ratios in some West Kauai rocks are amongst the most unradiogenic (0.70345) from Hawaiian shield building lavas (Figs. 8-9). East Kauai lavas have more enriched $^{87}Sr/^{86}Sr$ and $^{143}Nd/^{144}Nd$ ratios compared to West Kauai lavas (Fig 8b). In general, East Kauai lavas

Figure 7: Sr versus Os isotopic ratios in Kauai lavas. Loihi and Mauna Loa fields are from literature sources, available from the author on request. The correlation between Sr and Os argues against significant melt-mantle reaction. Data for the Loihi and Mauna Loa fields where retrieved from the GEOROC database (http://georoc.mpch-mainz.gwde.de).

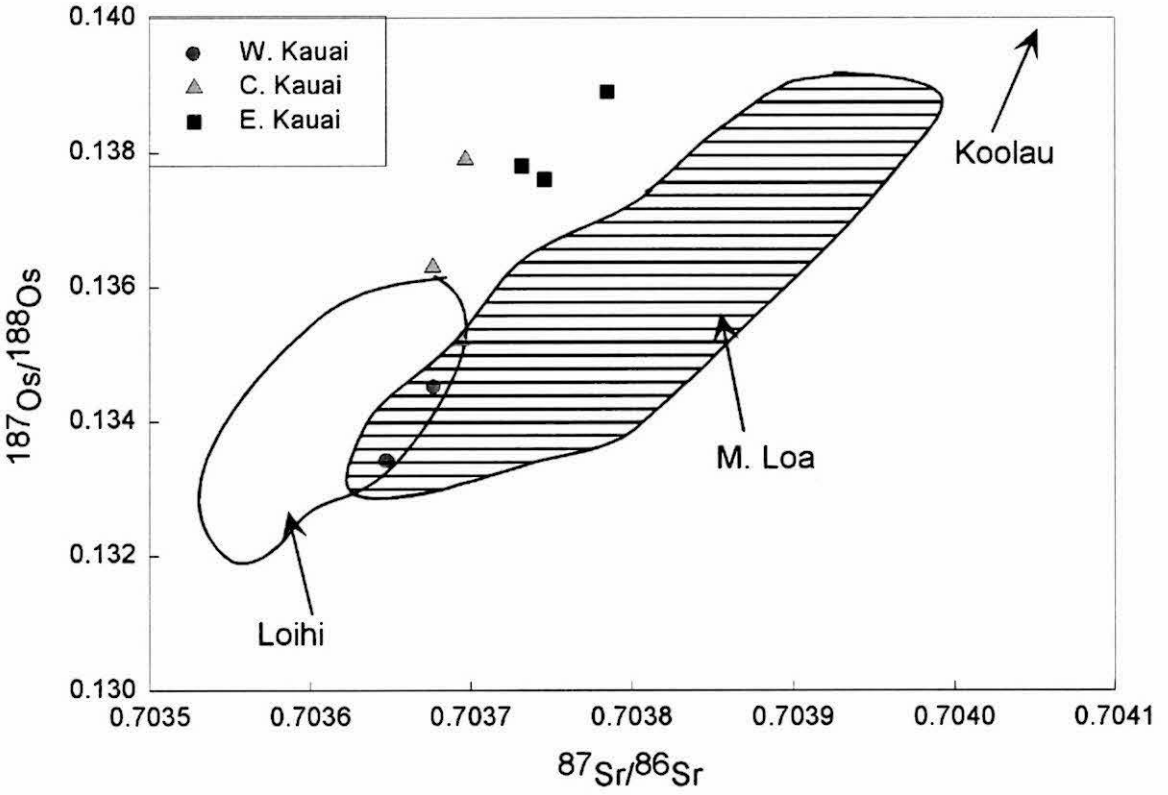
W. Kauai
C. Kauai
E. Kauai
Koolau
M. Loa
Loihi
0.140
0.138
0.136
0.134
0.132
0.130
0.7035
0.7036
0.7037
0.7038
0.7039
0.7040
0.7041
$^{187}Os/^{188}Os$
$^{87}Sr/^{86}Sr$

Figure 8: (a) $^{87}Sr/^{86}Sr$ vs. $^{206}Pb/^{204}Pb$ and (b) $^{87}Sr/^{86}Sr$ vs. $^{143}Nd/^{144}Nd$ from Kauai. Individual points represent our new data while the fields, including the East and West Kauai fields, are from literature sources available from the GEOROC database (http://georoc.mpch-mainz.gwde.de). For clarity only the fields for Loihi, Mauna Kea, Koolau, Kauai, and Mauna Loa are shown. K, L, and MK are the composition of the Koolau, Loihi, and Mauna Kea end-members as defined by Eiler et al. (1996, 1998). The West Kauai data significantly overlap with the Loihi field, while East Kauai is similar to Mauna Loa. Note that the West Kauai data appear to trend towards EPR MORB.

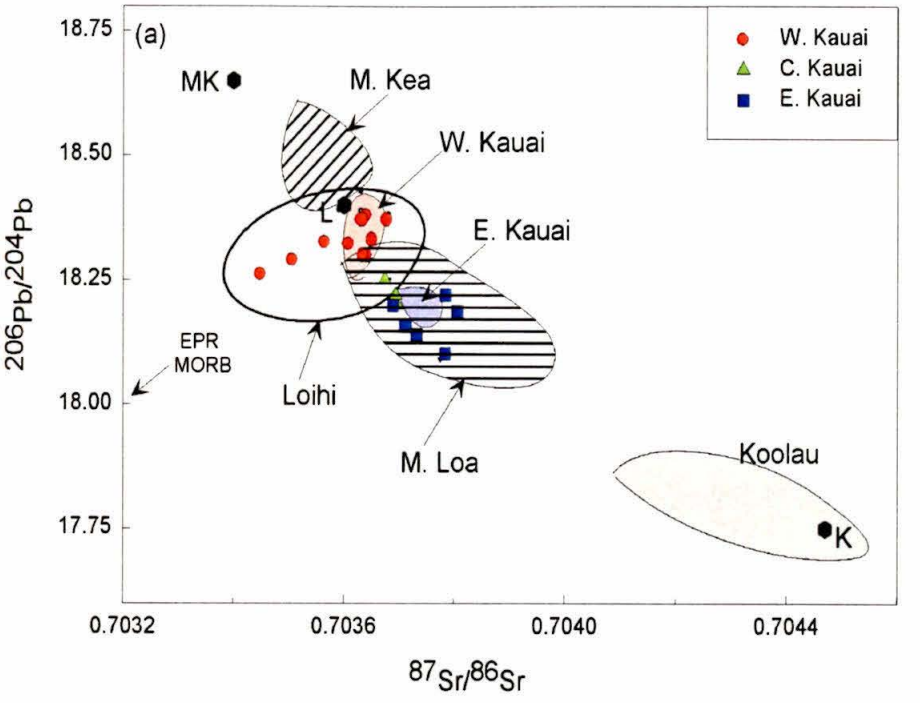
(a)
W. Kauai
C. Kauai
E. Kauai
MK
M. Kea
W. Kauai
L
E. Kauai
EPR
MORB
Loihi
M. Loa
Koolau
K
18.75
18.50
18.25
18.00
17.75
0.7032
0.7036
0.7040
0.7044
$^{206}Pb/^{204}Pb$
$^{87}Sr/^{86}Sr$

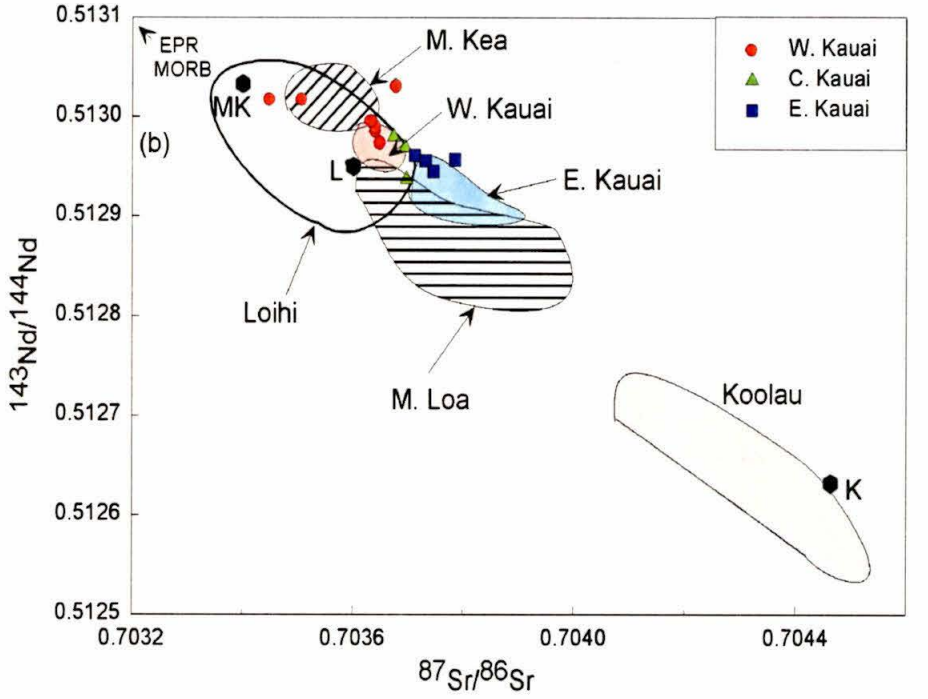
(b)
W. Kauai
C. Kauai
E. Kauai
EPR
MORB
M. Kea
MK
W. Kauai
L
E. Kauai
Loihi
M. Loa
Koolau
K
0.5131
0.5130
0.5129
0.5128
0.5127
0.5126
0.5125
0.7032
0.7036
0.7040
0.7044
$^{143}Nd/^{144}Nd$
$^{87}Sr/^{86}Sr$

Figure 9: $^{206}Pb/^{204}Pb$ vs. $^{3}He/^{4}He$ and $^{87}Sr/^{86}Sr$ vs. $^{206}Pb/^{204}Pb$. Symbols and fields as in Figure 8. The West Kauai data once again significantly overlap with the Loihi field. Note that in the He-Sr plot West Kauai trends towards a depleted component that is commonly sampled in post-shield and post-erosional lavas, like those from Haleakala.

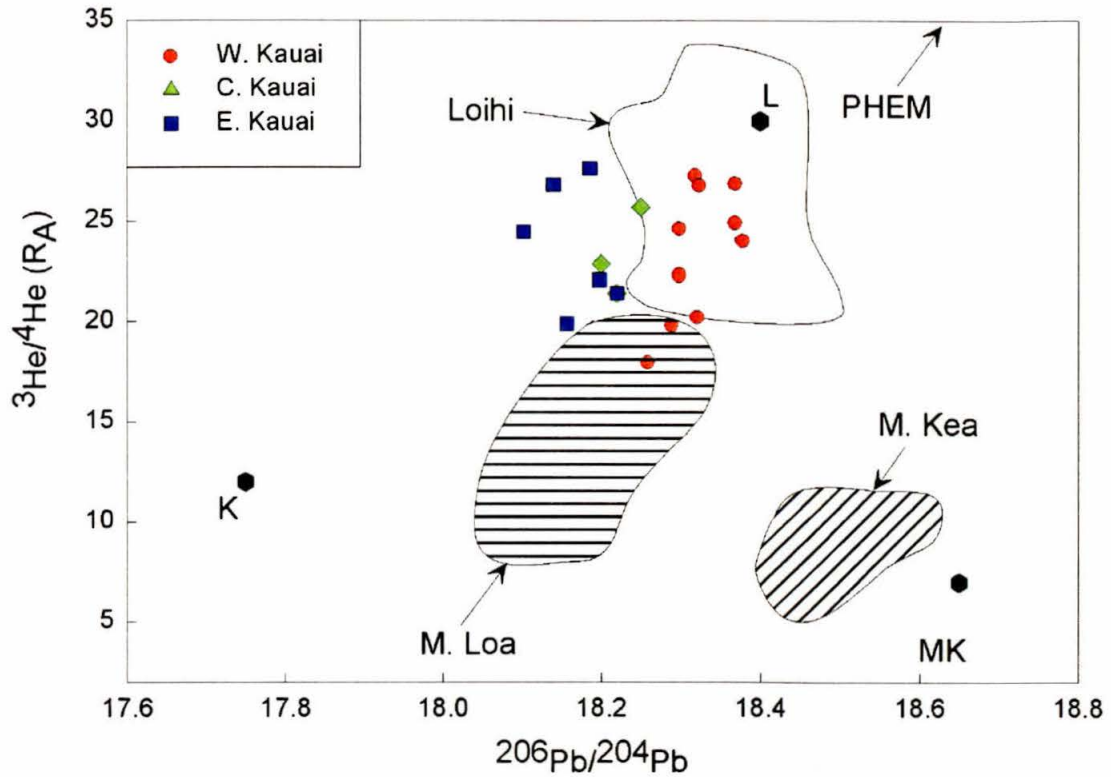
W. Kauai
C. Kauai
E. Kauai
Loihi
L
PHEM
M. Kea
K
M. Loa
MK
35
30
25
20
15
10
5
17.6
17.8
18.0
18.2
18.4
18.6
18.8
$^{3}He/^{4}He$ (R_A)
$^{206}Pb/^{204}Pb$

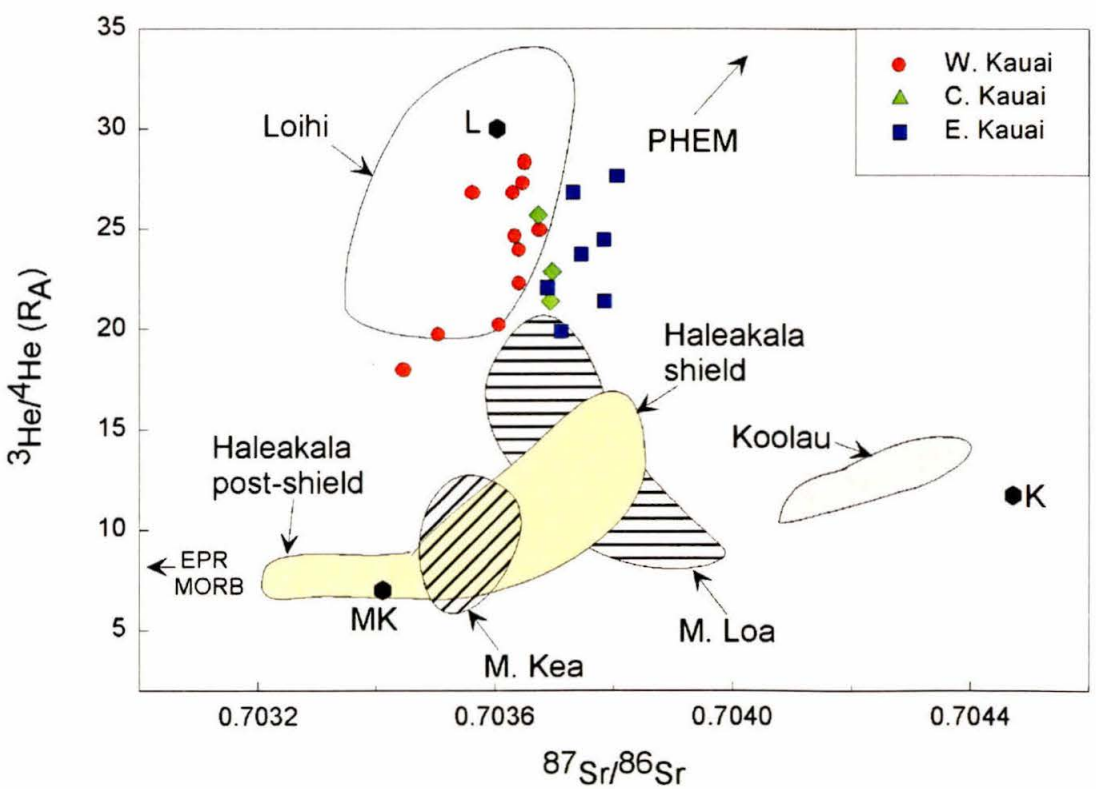
W. Kauai
C. Kauai
E. Kauai
Loihi
L
PHEM
Haleakala
shield
Koolau
K
Haleakala
post-shield
EPR
MORB
MK
M. Kea
M. Loa
35
30
25
20
15
10
5
0.7032
0.7036
0.7040
0.7044
$^{3}He/^{4}He$ (R_A)
$^{87}Sr/^{86}Sr$

Figure 10: Pb-Pb correlations in Hawaiian shield basalts. In $^{208}Pb/^{204}Pb$-$^{206}Pb/^{204}Pb$ space, Kauai defines an elongated field between the Mauna Loa and Mauna Kea fields. Although the West Kauai and Loihi fields overlap in $^{206}Pb/^{204}Pb$-$^{207}Pb/^{204}Pb$ space there is almost no overlap in $^{208}Pb/^{204}Pb$-$^{206}Pb/^{204}Pb$ space. Symbols and fields are as in Figure 8.

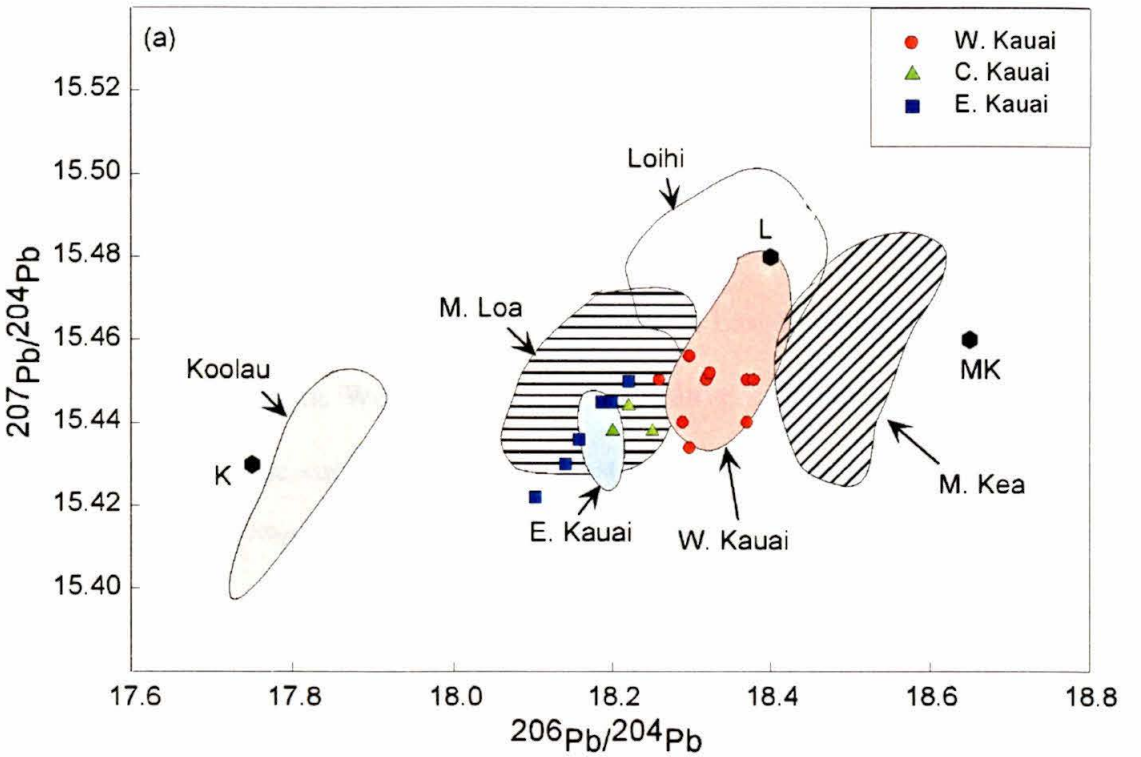
(a)
W. Kauai
C. Kauai
E. Kauai
Loihi
L
M. Loa
MK
Koolau
K
M. Kea
E. Kauai
W. Kauai
15.52
15.50
15.48
15.46
15.44
15.42
15.40
17.6
17.8
18.0
18.2
18.4
18.6
18.8
207Pb/204Pb
206Pb/204Pb

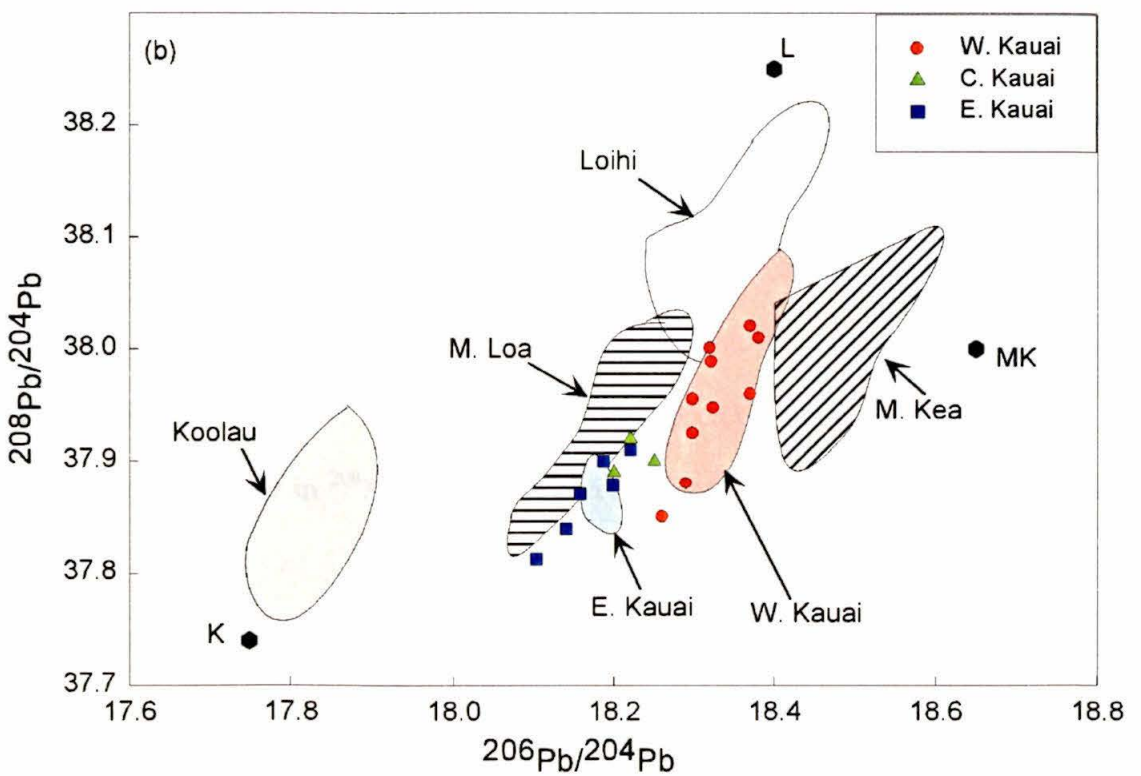
(b)
W. Kauai
C. Kauai
E. Kauai
L
Loihi
M. Loa
MK
M. Kea
Koolau
K
E. Kauai
W. Kauai
38.2
38.1
38.0
37.9
37.8
37.7
17.6
17.8
18.0
18.2
18.4
18.6
18.8
208Pb/204Pb
206Pb/204Pb

are similar in Sr and Nd isotopic composition to those from Mauna Loa although for a given Sr-isotopic composition East Kauai lavas have higher $^{187}Os/^{188}Os$ and $^{143}Nd/^{144}Nd$ ratios than those from Mauna Loa (Figs. 7 and 8b).

Hawaiian shield lavas in general show a negative correlation between Sr and Pb isotopic ratios (Figs. 8a). Although shield lavas from East Kauai display a broad negative correlation, those from West Kauai show a positive correlation and appear to trend towards MORB. The similarity between West Kauai and Loihi lavas is further borne out in He-Sr and He-$^{206}Pb/^{204}Pb$ space (Fig. 9). Note that both Loihi and West Kauai lavas appear to trend towards the MORB field with decreasing $^{3}He/^{4}He$ ratios. While lavas from East Kauai have similar $^{3}He/^{4}He$ ratios as those from West Kauai, the East Kauai field is shifted towards higher $^{87}Sr/^{86}Sr$ and lower $^{206}Pb/^{204}Pb$ ratios (Fig. 9).

In $^{207}Pb/^{204}Pb$-$^{206}Pb/^{204}Pb$ space East and West Kauai lavas form distinct fields and Central Kauai is the 'bridge' between the two (Fig. 10a). West Kauai overlaps with the Loihi field while East Kauai overlaps with the Mauna Loa field, consistent with observations from Figure 8. In $^{208}Pb/^{204}Pb$-$^{206}Pb/^{204}Pb$ space, East and West Kauai display steep sub-parallel arrays. Unlike in all other isotope spaces, West Kauai and Loihi lavas are distinct in $^{208}Pb/^{204}Pb$-$^{206}Pb/^{204}Pb$ space, with lavas from West Kauai systematically lower in $^{208}Pb/^{204}Pb$ for a given $^{206}Pb/^{204}Pb$ ratio, compared to lavas from Loihi.

4. Discussion

A striking feature of our Kauai data is the very high $^{3}He/^{4}He$ ratios (17-28 R_A), similar to those from Loihi (Loihi range ≅ 18-32 R_A). In the following section, we discuss

(a) the different mantle components required to explain the geochemical data in Kauai shield lavas, (b) the temporal and spatial geochemical variability in Kauai shield lavas, and (c) the implications of our data for models of the Hawaiian plume.

4.1. Isotopic Composition of Kauai Lavas: Three or Four Mantle Components?

The isotopic variability in Kauai lavas might be generated by mixing between distinct mantle sources (e.g., Staudigel et al., 1984; Stille et al., 1986; West et al., 1987; Kurz et al., 1995; Eiler et al., 1996; Hauri, 1996) or through magma-mantle reaction during melt transport to the surface (McKenzie and O'Nions, 1991; DePaolo, 1996). The correlation between Sr and Os in Kauai lavas (Fig. 7), however, strongly argues against the latter, since melt-mantle reaction would produce horizontal or vertical arrays in Sr-Os space (Hauri et al., 1996). Hence, following previous interpretations from other Hawaiian shield volcanoes (Staudigel et al., 1984; Kurz et al., 1995; Eiler et al., 1996; Hauri et al., 1996), we explain the isotopic variability and the correlations among the isotopic ratios of Sr, Nd, Pb, and Os in Kauai shield lavas by mixing between distinct mantle sources.

At least three distinct mantle components are required to explain the isotopic variability in Hawaiian shield lavas (e.g., Staudigel et al., 1984; Stille et al., 1986; West et al., 1987; Kurz et al., 1995; Eiler et al., 1996; Hauri, 1996). The three components are referred to as Loihi, Koolau, and Kea, for the volcanoes where the geochemical signatures of these components are most strongly manifested. The compositions of these three end-members (Eiler et al., 1996) have been plotted in Figures 8-10. To investigate if the most recent three-component model (Eiler et al., 1996, 1998) can successfully explain isotopic variability of Kauai lavas, we fit the isotopic composition of

Figure 11: (a) The Kauai data plotted in $^{87}Sr/^{86}Sr$-$^{206}Pb/^{204}Pb$-$^{208}Pb/^{204}Pb$ space. Also shown are the Loihi (Lo), Kea, and Koolau (Koo) components as defined by Eiler et al. (1996, 1998). The figure is then rotated (b) to view the plane through the three end-members edge on (i.e., the plane through the three components runs vertical out of the plane of the paper). The Kauai data lie outside the plane containing the Loihi, Kea, and Koolau components, requiring an additional component.

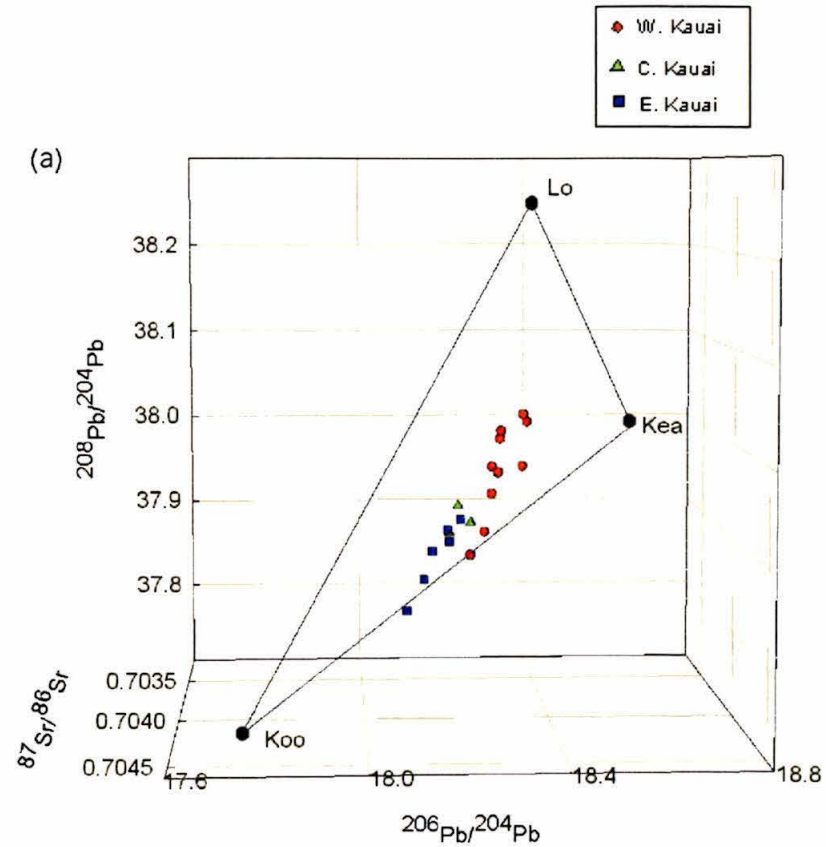
W. Kauai
C. Kauai
E. Kauai
(a)
Lo
Kea
Koo
38.2
38.1
38.0
37.9
37.8
208Pb/204Pb
0.7035
0.7040
0.7045
87Sr/86Sr
17.6
18.0
18.4
18.8
206Pb/204Pb

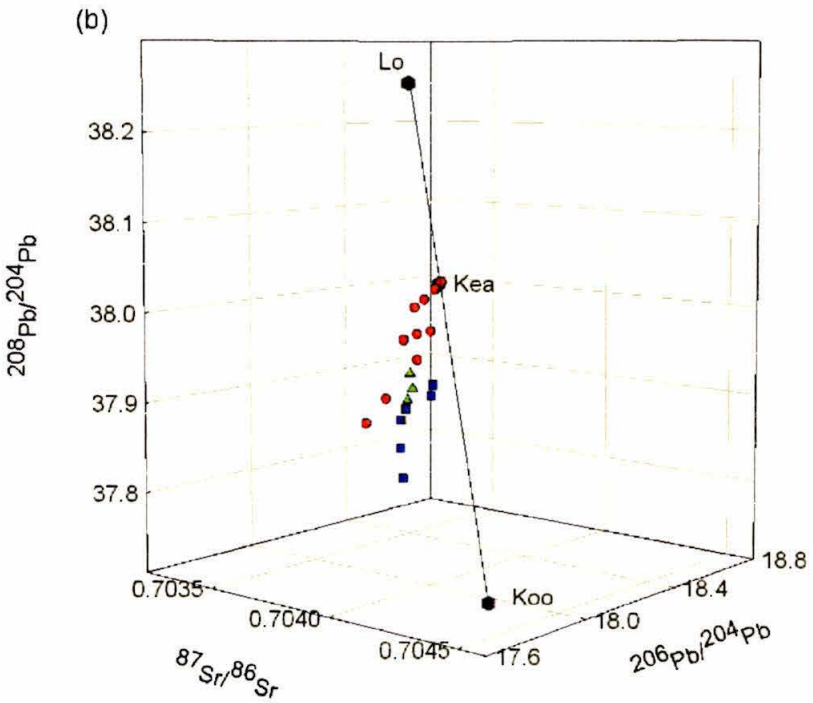
(b)
Lo
Kea
Koo
38.2
38.1
38.0
37.9
37.8
208Pb/204Pb
0.7035
0.7040
0.7045
87Sr/86Sr
17.6
18.0
18.4
18.8
206Pb/204Pb

He, Sr, Nd, and Pb simultaneously in Kauai lavas by a least squares mixture of the three defined components (see Eiler et al., 1996, for details). However, in the calculations, the sums of the three components in the different Kauai samples are frequently negative, which is a result of the Kauai samples lying outside the plane defined by the three components (Fig. 11).

Based on Pb-isotopic ratios from Mauna Loa and Mauna Kea lavas, Abouchami et al. (2000) suggested the presence of four components in Hawaiian shield lavas. To quantitatively test this idea, we conducted a principal component analysis based on literature data and our new He, Sr, Nd and Pb data (see Appendix). Only samples with combined He-Sr-Nd-Pb data were selected and we did not include Os in the analysis, as this would considerably decrease the size of the database. To weight the different isotope systems equally, isotopic ratios were normalized following the procedure of Eiler et al. (1996). The principal component analysis indicates that the first three eigenvectors account for 51%, 25% and 15% of the variance respectively and a total of 91% of the variance in the data set (the next eigenvector accounts for 6% of the variance). We note that the principal component analysis conducted by Eiler et al. (1996), which did not include the Kauai data, had 89% of the variance in the first two eigenvectors but only 4% in the third. Hence, addition of the Kauai data increases the variance associated with the third eigenvector and we conclude that four components are required to explain the full spectrum of isotopic variability in Hawaiian shield lavas.

While the mantle end-members are not precisely defined by the principal component analysis, the eigenvectors indicate that the previously defined Loihi, Koolau and Kea components (e.g., Eiler et al., 1996; Hauri 1996; Eiler et al., 1998), and a

Table 4: End member compositions for the four-component mixing model.

Endmember	$^{87}Sr/^{86}Sr$	εNd	$^{206}Pb/^{204}Pb$	$^{207}Pb/^{204}Pb$	$^{208}Pb/^{204}Pb$	$^{3}He/^{4}He$
Koolau	0.70447	0.0	17.75	15.43	37.74	12
Loihi	0.7036	6.1	18.4	15.48	38.25	32
Kea	0.7035	7.7	18.64	15.46	38	7
DM	0.7029	11	18.12	15.42	37.73	8

Modified after Eiler et al. (1996, 1998)

Figure 12: Comparison between measured Nd, Sr, Pb, and He isotopic ratios that are consistent with a best fit of the samples to a mixture of the four components (n=55). All isotope ratios have been fit simultaneously. ± indicates average difference between measured and fit values. Our four-component model can explain the isotopic data from Kauai and also improves the fit to other Hawaiian shield lavas. (compare with Figure 4 of Eiler et al., 1996).

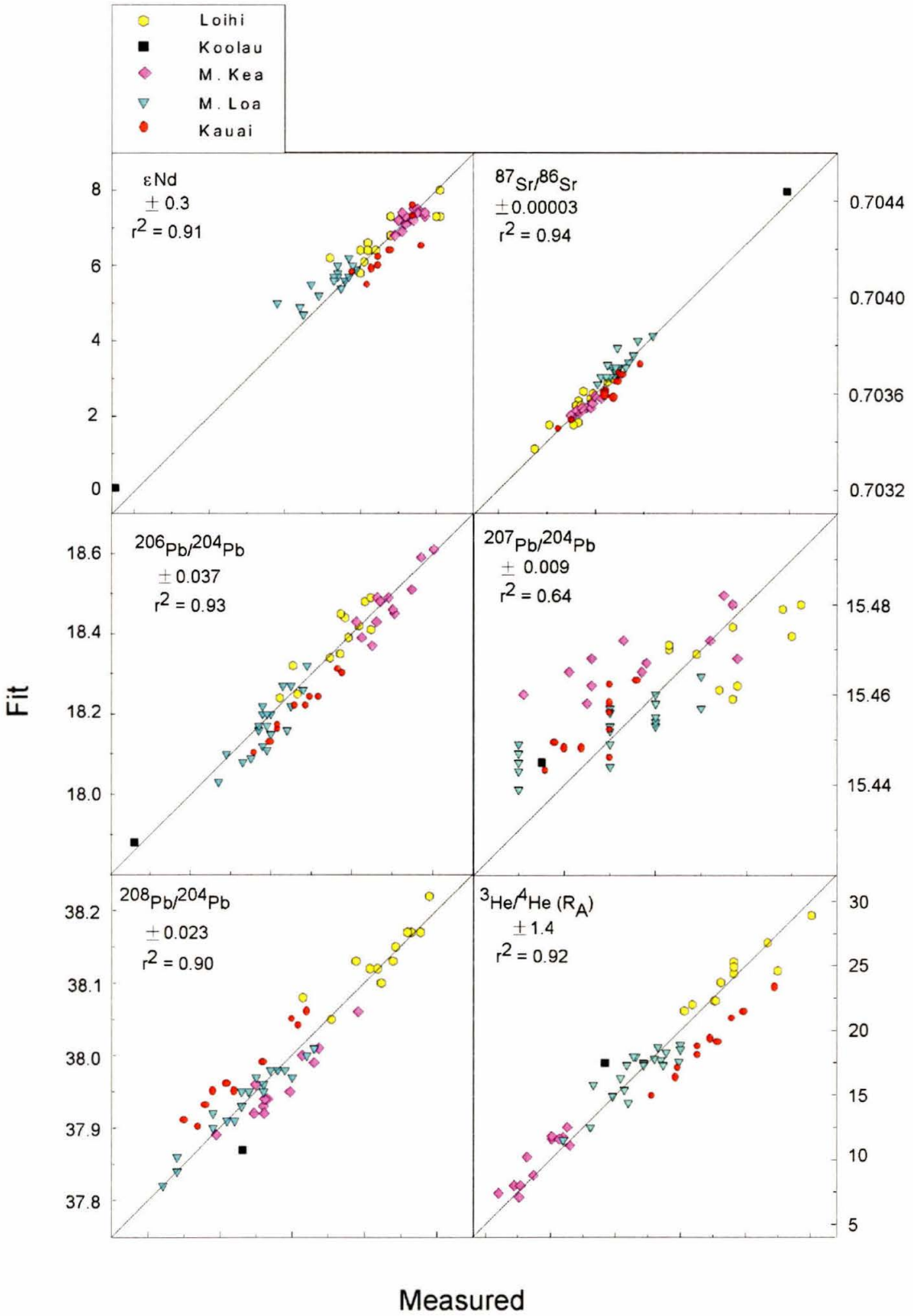
Loihi
Koolau
M. Kea
M. Loa
Kauai
εNd
± 0.3
r2 = 0.91
87Sr/86Sr
±0.00003
r2 = 0.94
206Pb/204Pb
± 0.037
r2 = 0.93
207Pb/204Pb
± 0.009
r2 = 0.64
208Pb/204Pb
± 0.023
r2 = 0.90
3He/4He (RA)
± 1.4
r2 = 0.92
Fit
Measured

Figure 13: Comparison between the model results of Eiler et al. (1996) and our four-component model. εNd and $^{206}Pb/^{204}Pb$ ratios are fit significantly better using our four component model. Symbols for this work as in Figure 13.

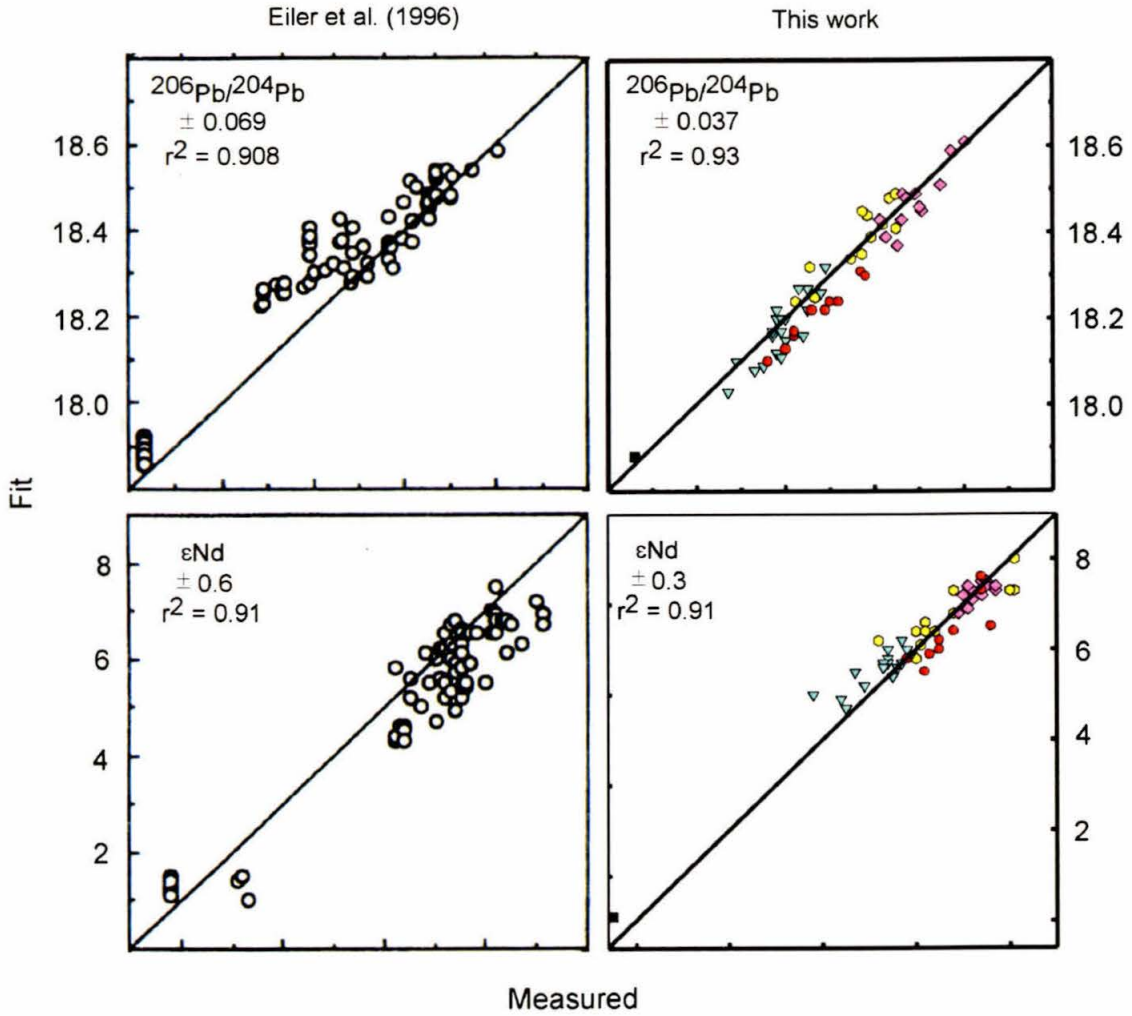
Eiler et al. (1996)
This work
$^{206}Pb/^{204}Pb$
± 0.069
r^2 = 0.908
$^{206}Pb/^{204}Pb$
± 0.037
r^2 = 0.93
18.6
18.4
18.2
18.0
εNd
± 0.6
r^2 = 0.91
εNd
± 0.3
r^2 = 0.91
8
6
4
2
Fit
Measured

Figure 14: Average proportion of the Loihi, Koolau, Kea and DM components in shield lavas from different volcanoes. The proportions of the four-components were calculated in each sample by simultaneously fitting the Nd, Sr, Pb, and He isotopic data using least squares regression. Combined He, Sr, Nd, and Pb data are available for only a single sample from Koolau and are not available from Haleakala and Kilauea (not shown).

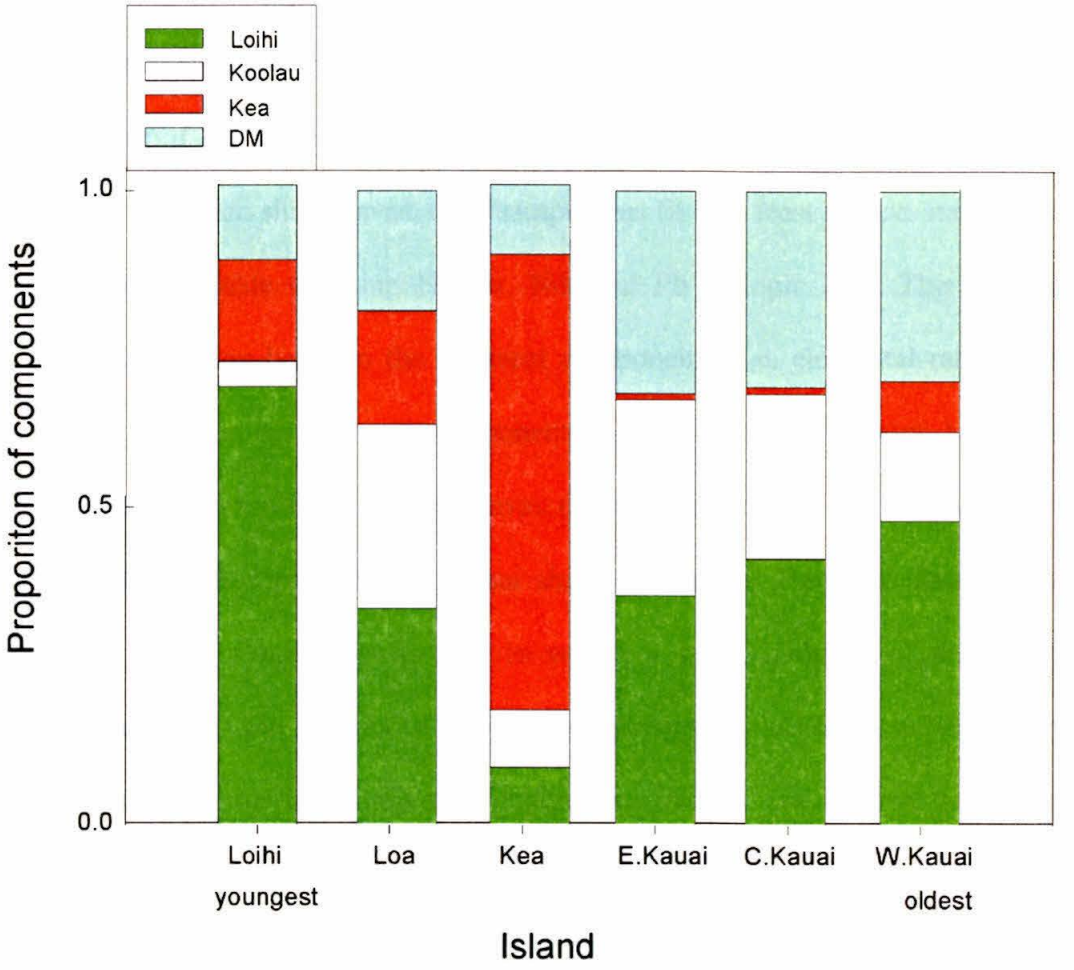
Loihi
Koolau
Kea
DM
1.0
0.5
0.0
Proporiton of components
Loihi
youngest
Loa
Kea
E.Kauai
C.Kauai
W.Kauai
oldest
Island

depleted mantle component (DM) with MORB-like Sr, Nd, Pb, and He would be appropriate end-members (Table 4). The isotopic composition of the DM component is similar to the post-erosional end-member sampled during post-shield and post-erosional stages of Hawaiian volcanism (Stille et al., 1986; Kurz et al., 1987; West et al., 1987; Reiners and Nelson, 1998). However, because this study focuses on shield lavas, our principal component analysis was conducted only on Hawaiian *shield-stage* lavas. The DM component is discussed later in this section.

To test if the four-component model can successfully describe the isotopic variability in Hawaiian shield lavas, each sample was fit by a least squares mixture of the four-components (Table 4) using He, Sr, Nd, and Pb isotopic data. This calculation assumes linear mixing between the different components (i.e. elemental ratios such as Pb/Sr are the same in the different components), a reasonable assumption based on the linearity of isotope arrays in Hawaiian lavas (also see Eiler et al., 1996). As shown in Figure 12, all the isotope ratios in Kauai shield lavas, and Hawaiian shield lavas in general, can be fit simultaneously and to within a small multiple of the analytical precision, illustrating the success of the four-component model. Thus, unlike the three-component model, our four-component model can explain the isotopic variability in Kauai lavas and, furthermore, significantly improves the fit to the isotopic data from other Hawaiian shield lavas (Fig. 13). For example, the three-component mixing model by Eiler et al. (1996) systematically underestimates εNd and overestimates $^{206}Pb/^{204}Pb$ ratios (Fig. 13). We note that $^{3}He/^{4}He$ ratios in Kauai lavas calculated from the least squares fit are lower than the measured value by ~3.5 R_A. A possible explanation for this may be distinctive He/Sr or He/Pb ratios in the different mantle reservoirs (e.g., Kurz et

al., 1995). Subsequently, linear mixing calculations would not perfectly fit the measured $^{3}He/^{4}He$ ratios.

Based on the least squares fit to each sample, we computed the average proportion of the four components in different Hawaiian shield volcanoes (Fig. 14). While four components are required to explain the isotopic data from all Hawaiian shield stage lavas, only three components can reasonably explain the isotopic composition of Kauai shield stage lavas (Fig. 14). However, a *different set* of 3-components is required to explain the Kauai data (Loihi, Koolau and DM) than the previously proposed Loihi, Koolau and Kea components (e.g., Eiler et al., 1996). Further, our Kauai data data indicate that the proportion of the different components in the Hawaiian plume have changed over time (Fig. 14).

4.1.1 The DM Component

The DM component in principle could be assimilated Pacific crust, Pacific lithospheric mantle, or asthenosphere entrained by the upwelling plume. Correlations between Os and Sr (Fig. 7) and Os and O in Hawaiian lavas argue against crustal assimilation (Lassiter and Hauri, 1998; Lassiter et al., 2000). Although our isotopic data cannot distinguish between Pacific lithospheric mantle and entrained asthenosphere, as noted earlier, the DM component is isotopically similar to the component sampled in Hawaiian post-shield and post-erosional basalts (Chen and Frey, 1985; Stille et al., 1986; Kurz et al., 1987; West et al., 1987; Reiners and Nelson, 1998). Both asthenospheric and lithospheric origin is permissible for post-shield and post-erosional basalts (e.g., Chen and Frey, 1985; Reiners and Nelson, 1998; Lassiter et al., 2000). Irrespective of the

precise origin of post-erosional basalts, our principal component analysis indicates that melts from this source(s) are present during the shield building stage of Kauai and also present in other Hawaiian shield volcanoes, albeit varyingly, and may normally be overwhelmed by the plume melts (Fig. 14). Future $\delta^{18}O$ and Os isotopic studies in Kauai lavas may more positively identify the character of the DM component. For example, shallow Pacific lithosphere might have low $\delta^{18}O$ (<5 $^{o}/_{oo}$) due to high temperature hydrothermal alteration (Eiler et al., 1996) while asthenospheric material would have normal upper mantle $\delta^{18}O$ values of 5.5 ± 0.1 $^{o}/_{oo}$ (Ito et al., 1987; Eiler et al., 1996).

4.1.2 The High $^{3}He/^{4}He$ Component

The existence of a primitive mantle as the source of many OIBs was proposed nearly 30 years ago (Schilling, 1973). Based on He, Sr, Nd, and Pb from Samoa (Farley et al., 1992), Iceland (Kurz et al., 1985), Loihi (Staudigel et al., 1984; Kurz et al., 1983; Rison and Craig, 1983), and MORBs (Hanan and Graham, 1996) the occurrence of a single high $^{3}He/^{4}He$ reservoir in the Earth's mantle has been suggested. This reservoir has been termed PHEM (Farley et al., 1992), FOZO (Hart et al., 1992) or C (Hanan and Graham, 1996). For the following discussion we use the term PHEM to imply PHEM/FOZO/C. While the exact composition of PHEM is debated, it is probably slightly depleted relative to bulk Earth estimates (Farley et al., 1992; Hart et al., 1992; Hanan and Graham, 1996). If PHEM is the high $^{3}He/^{4}He$ reservoir in the mantle, Farley et al. (1992) noted that high $^{3}He/^{4}He$ islands should trend towards PHEM in Sr, Nd, and Pb isotope space. There is a significant overlap between West Kauai lavas and Loihi lavas in He, Sr, Nd, $^{206}Pb/^{204}Pb$, and Os isotopic composition (Figs. 4-7). Further, in He-Sr space and He-

$^{206}Pb/^{204}Pb$ space, with increasing $^{3}He/^{4}He$ ratios, West Kauai tholeiites trend towards PHEM (Fig. 6). Therefore, the high $^{3}He/^{4}He$ Kauai lavas further support the existence of a distinct lithophile reservoir in the Earth that is less degassed than the MORB source.

What is the location of the PHEM reservoir? Anderson (1993) suggested that high $^{3}He/^{4}He$ ratios in the mantle were produced by subduction of ^{3}He-rich interplanetary dust particles in seafloor sediments. However, Allegre et al. (1993) noted that the flux of ^{3}He out of the mantle far exceeds the current ^{3}He flux from space, and that He/Ne systematics of mantle rocks are not consistent with derivation from subducted extraterrestrial material. Further, diffusion measurements suggest that He in IDPs is completely removed within subduction zones (<200 km; Hiyagon, 1994). Thus subducted ^{3}He-rich IDPs are unlikely to be the source of high $^{3}He/^{4}He$ ratios in mantle rocks. An alternative hypothesis presented by Anderson (1998) suggested that ^{3}He is selectively stored in the shallow mantle (perisphere) although Kurz and Geist (1998) have presented isotopic evidence refuting the hypothesis.

There is some evidence that the Iceland and Hawaiian plumes originate in the lower mantle (Shen et al., 1998; Fouch et al., 2001), which could, therefore, be the location of the PHEM reservoir. Tomographic evidence for whole mantle convection (e.g., Van der Hilst et al., 1997), however, poses a problem for the lower mantle being the PHEM reservoir. Previous studies of whole-mantle convection had suggested that if the viscosity of the lower mantle was a factor of ~100 higher than that of the upper mantle, a primitive composition of the lower mantle could be preserved over Earth's history (Gurnis and Davies, 1986). However, recent numerical simulations suggest that regardless of higher viscosity or a phase transition across the 660 km boundary, the lower

mantle will become well mixed and outgassed over 1 Ga (e.g., Van Keken and Ballentine, 1998; Van Keken and Zhong, 1999). Hence, the PHEM reservoir would have to be isolated from whole mantle convection.

D'', a 200-300 km thick layer near the base of the mantle which displays seismic heterogeneities and anisotropy (Lay et al., 1998; Fouch et al., 2001), is a possible location of the PHEM reservoir. A chemical origin for D'' is possible though not certain (Sidorin et al., 1999). Alternatively the PHEM reservoir may occur as a discontinuous layer near the base of the lower mantle consisting of two piles (corresponding to the Pacific and African megaplumes; e.g., Tackley, 1998) or as a globally undulating layer with an average thickness of ~1300 km (Kellogg et al., 1999). However, in the first case the volumes of the piles may be too small to satisfy geochemical mass balance arguments (e.g., Hofmann, 1997), and in the second case, it is not clear why a globally undulating layer is not visible seismically (Tackley, 2000). Therefore, the precise location and size of the PHEM reservoir remains uncertain.

4.1.2. Major Element Chemistry of Kauai Tholeiites: Source Heterogeneity or Melting Effects?

While the isotopic variability in Kauai and other Hawaiian shield volcanoes demonstrates the presence of mantle components with distinct isotopic signatures in the Hawaiian plume, an important question is whether these components are also characterized by distinctive major element chemistry. Previous studies on Hawaiian volcanoes noted systematic inter-volcano differences in major element chemistry (e.g., Frey and Rhodes, 1993; Frey et al., 1994; Yang et al., 1996). Based on correlations

Table 5: Major element data corrected for olivine fractionation

	West Kauai					Central Kauai			East Kauai	
	PB10	PB17	PB19	OR5	OR18	OK19	OK20	OK25	A3	PB10
SiO_2	47.5	47.4	46.7	47.2	47.5	50.5	47.8	48.4	49.0	47.5
Al_2O_3	9.7	9.7	9.5	9.2	8.8	11.3	9.6	9.9	10.7	9.7
TiO_2	1.8	1.9	1.9	1.7	1.8	2.0	1.7	1.7	2.0	1.8
FeO*	11.8	11.8	12.1	12.4	12.5	9.6	12.0	11.4	10.5	11.8
MnO	0.2	0.1	0.2	0.2	0.2	0.1	0.2	0.2	0.1	0.2
CaO	8.1	8.1	8.0	7.8	7.4	8.5	7.4	7.9	8.4	8.1
MgO	18.9	18.8	19.3	19.7	20.0	15.4	19.3	18.3	16.8	18.9
Na_2O	1.6	1.7	1.8	1.5	1.4	2.0	1.6	1.8	1.9	1.6
K_2O	0.2	0.2	0.2	0.2	0.2	0.3	0.2	0.3	0.3	0.2
P_2O_5	0.2	0.2	0.2	0.2	0.2	0.2	0.2	0.2	0.2	0.2

* Denotes total iron; major element oxides are in weight %.

Figure 15: Fractionation corrected SiO_2 versus (a) Sr isotopic ratios (b) CaO/Al_2O_3 and, (c) FeO. Note that the SiO_2 vs. CaO/Al_2O_3 trend is opposite to that expected from differences in extent of melting. In addition the correlation between isotopes and major elements indicates that differences in major element chemistry are (at least) partly due to variations in mineralogy and/or bulk chemistry of the source.

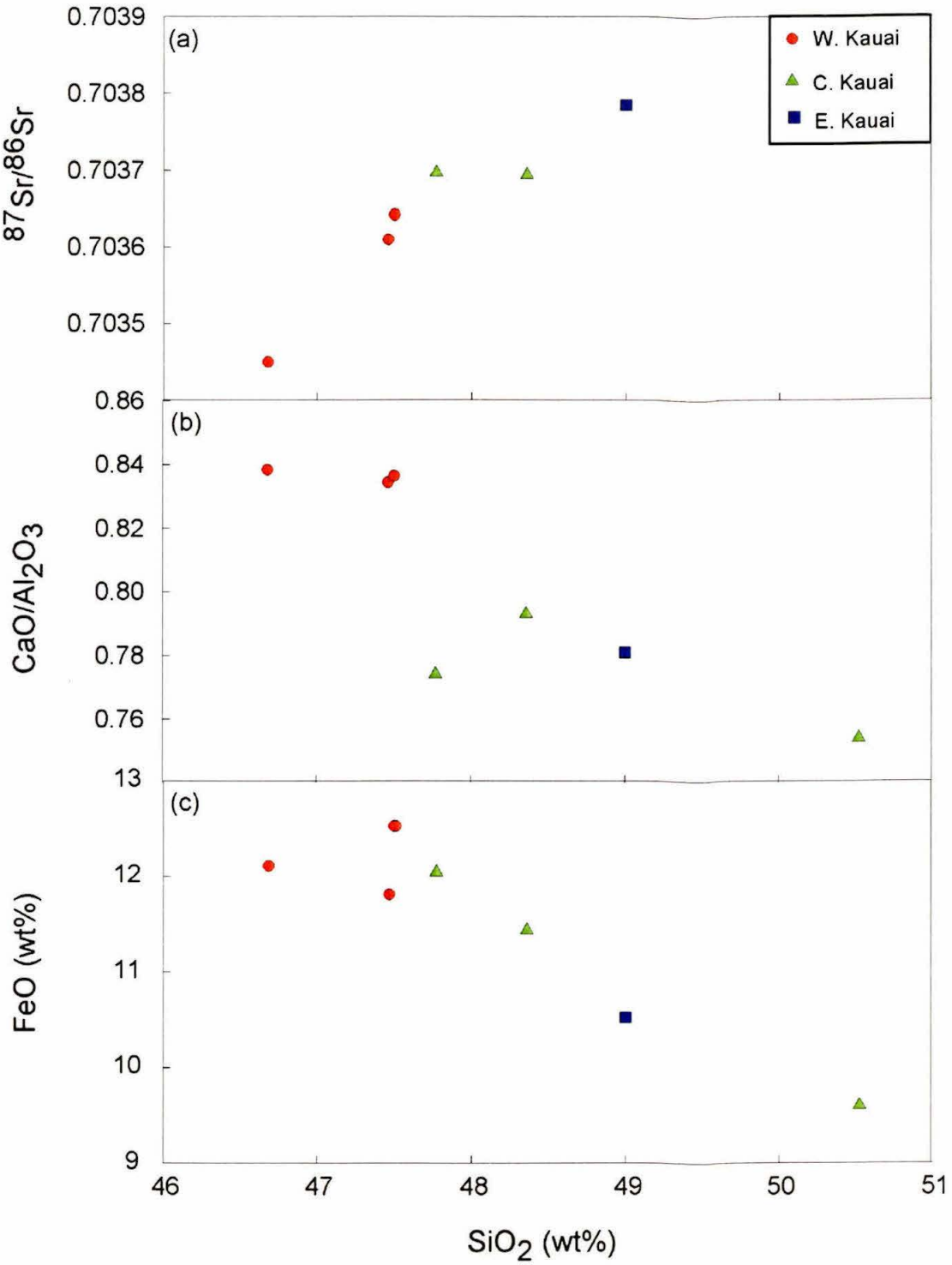
(a)
(b)
(c)
W. Kauai
C. Kauai
E. Kauai
$^{87}Sr/^{86}Sr$
CaO/Al_2O_3
FeO (wt%)
SiO_2 (wt%)
0.7039
0.7038
0.7037
0.7036
0.7035
0.86
0.84
0.82
0.80
0.78
0.76
13
12
11
10
9
46
47
48
49
50
51

Figure 16: Correlation between CaO/Al_2O_3 and (a) $^{206}Pb/^{204}Pb$, (b) $^{87}Sr/^{86}Sr$ and (c) Zr/Nb. The correlations suggest that the lower Ca/Al ratios in East Kauai lavas are not an artifact of post-eruptive alteration processes. Note that the correlation between Zr/Nb and CaO/Al_2O_3 cannot be explained by variable degrees of melting of a homogeneous source.

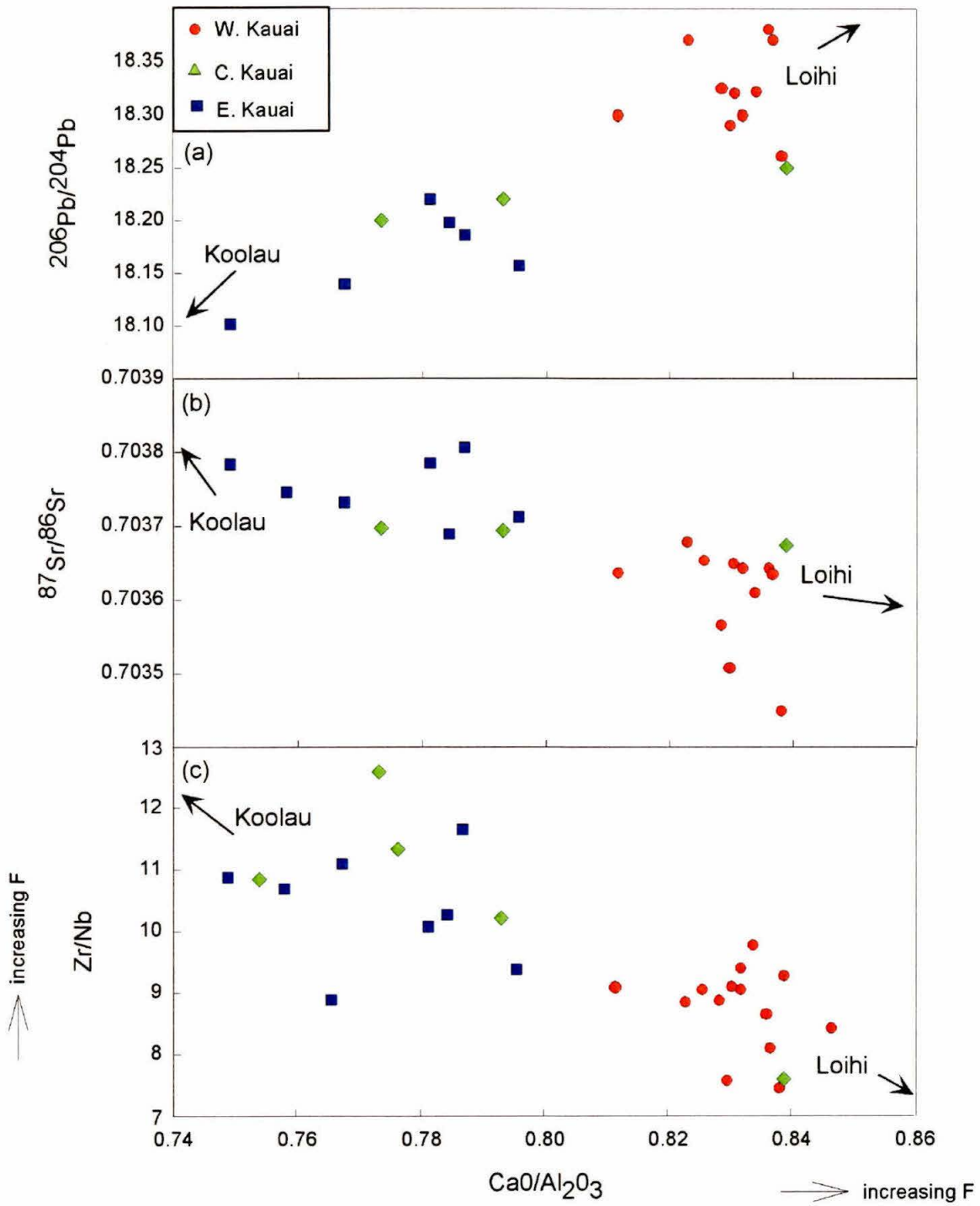
W. Kauai
C. Kauai
E. Kauai
(a)
(b)
(c)
Koolau
Loihi
$^{206}Pb/^{204}Pb$
$^{87}Sr/^{86}Sr$
Zr/Nb
CaO/Al_2O_3
increasing F
increasing F
18.35
18.30
18.25
18.20
18.15
18.10
0.7039
0.7038
0.7037
0.7036
0.7035
13
12
11
10
9
8
7
0.74
0.76
0.78
0.80
0.82
0.84
0.86

between isotopic ratios and major element composition of shield lavas, Hauri (1996) suggested that major element variability might be related to source heterogeneity within the Hawaiian plume. However, most studies generally interpret differences in major elements to reflect variable degrees of melting of a source homogeneous in its bulk chemistry (e.g., Frey and Rhodes, 1993; Frey et al., 1994; Yang et al., 1996).

To infer the parental magma composition of Kauai lavas, we corrected the major element data for olivine fractionation. The MgO content of primary Hawaiian magmas is between 16 and 18 wt % (Garcia et al., 1995; Yang et al., 1996; Hauri 1996) and, hence, we adjusted the major element data to an MgO content of 17 wt % by adding or subtracting olivine in 1% increments (see Yang et al., 1996 for details). Only samples with $K_2O/P_2O_5 > 1$ were subjected to this correction. Note that using alternative methods to correct for olivine fractionation, such as recalculating the major elements to a constant $Mg/(Mg+Fe^{2+})$ ratio (Mg#) (Hauri, 1996), do not significantly alter the results.

The olivine fractionation corrected data are presented in Table 5. It should be noted that because of the very small data set the results should be treated as tentative. There are small but systematic difference in the major element data between West, Central and East Kauai. For example, West Kauai lavas have lower SiO_2, CaO, Al_2O_3 and higher FeO contents than Central and East Kauai lavas (Table 5). Major element differences between East and West Kauai tholeiites can also be inferred from CaO/Al_2O_3 ratios. Tholeiites from East Kauai have systematically lower CaO/Al_2O_3 ratios than those from West Kauai. While weathering may have decreases CaO/Al_2O_3 ratios in East Kauai lavas, the correlation between CaO/Al_2O_3 and Zr/Nb ratios (Fig. 16) argue against such an interpretation because Zr and Nb are immobile during post-eruptive alteration (e.g.,

Lipman et al., 1990; Frey et al., 1994). Furthermore, correlations between radiogenic isotope ratios and CaO/Al_2O_3 ratios in individual samples (Fig. 16) suggest that CaO/Al_2O_3 ratios reflect magmatic values.

SiO_2 and FeO contents in basalts are sensitive indicators of the degree and mean pressures of melting (e.g., Klein and Langmuir, 1987). For example, higher extent of melting leads to higher SiO_2 and lower FeO contents in the melt (e.g., Klein and Langmuir, 1987; Frey et al., 1994; Yang et al., 1996). In Hawaiian lavas, mean pressure of melt segregation and extent of melting are inversely correlated (Frey et al., 1994; Yang et al., 1996). The SiO_2 and FeO contents in Kauai tholeiites (Fig. 15) indicate that East Kauai lavas are derived from lower mean pressures and higher degrees of melting than West Kauai lavas. However, variable degrees of melting of a source, homogenous in its mineralogy and bulk chemistry, cannot explain all the differences in major element composition of Kauai lavas. First, since Al_2O_3 contents increase with decreasing pressure of melting and Ca/Al ratios increase with the degree of melting (Herzberg and Zhang, 1996; Walter 1998), East Kauai lavas should also have higher Al_2O_3 contents and Ca/Al ratios than West Kauai lavas. While lavas from East Kauai have higher Al_2O_3 contents they have lower Ca/Al ratios compared to West Kauai lavas (Figs. 15 and 16). Fractionation of clinopyroxene is not a feasible explanation for the lower Ca/Al ratios in East Kauai lavas, since this would lead to a higher FeO content (Klein and Langmuir, 1987). In addition, because Sc is compatible in clinopyroxene, the correlation between Sc and MgO (Fig. 3) also argues against clinopyroxene fractionation. Second, in Hawaiian lavas Zr/Nb ratios increase with increasing degree of melting (e.g., Frey et al., 1994;

Yang et al., 1996) and, as a result, the inverse correlation between Ca/Al and Zr/Nb (Fig. 16) is not likely to reflect a melting trend.

The correlations between isotope ratios and major elements (Figs. 15 and 16) in Kauai lavas indicate that the different mantle components in the Hawaiian plume may be associated with distinctive bulk chemistry and mineralogy (also see Hauri and Kurz, 1997). Both the MELTS algorithm (Ghiorso and Sack, 1995) and experiments on depleted peridotites show that, for a given degree of melting, depleted peridotites generate melts with higher Ca/Al, lower SiO_2, and higher FeO contents (Hirschmann et al., 1999; Wasylenki, 1998) than fertile peridotites. Thus, mixing between melts generated from fertile and depleted peridotites may explain the major element variability in Kauai lavas. This would imply that the source of West Kauai lavas sampled a higher proportion of the depleted peridotite component, consistent with the more depleted isotopic signature in West Kauai lavas (Figs. 8 and 14).

Variability in major element chemistry of Kauai lavas may alternatively be explained by melting of a fertile peridotite mixed with varying proportions of eclogite or pyroxenite component. The presence of a recycled eclogite or pyroxenite component in the Hawaiian plume has been suggested to explain the major element chemistry and enriched isotopic signatures of some Hawaiian lavas, particularly those from Koolau (Hauri, 1996; Lassiter and Hauri, 1998). Partial melting of pyroxenite with MORB-like bulk composition at 3 GPa produces basaltic andesites rich in SiO_2 and low in FeO and CaO/Al_2O_3 ratios (Pertermann and Hirschmann, 1998). Furthermore, the major element composition of melts derived from pyroxenites or eclogites will be associated with the enriched isotopic signatures of recycled material (Hauri, 1996). Thus, the higher SiO_2

content, the lower Ca/Al ratio, and the enriched isotopic signature in East Kauai lavas compared to lavas from West Kauai is consistent with a larger contribution from a pyroxenite/eclogite component. Rare earth element data can more rigorously test the two hypotheses we have suggested to explain the difference in major element chemistry between East and West Kauai lavas and the correlation between Ca/Al and radiogenic isotope ratios. For example, for similar degrees of melting, melts derived from pyroxenites would have larger Lu-Hf and smaller Sm-Nd fractionation compared to peridotite melts (e.g., Stracke et al. 1999). Irrespective of whether the difference in major element composition between East and West Kauai lavas reflects source depletion or presence of pyroxenite, the Kauai data strongly support major element heterogeneity in the Hawaiian plume.

4.2. Spatial and Temporal Isotopic Variability of Kauai Lavas

The high $^{3}He/^{4}He$ ratios in Kauai lavas can be attributed to the presence of the Loihi component in the source of Kauai shield lavas (Figs. 8 and 14). The isotope ratios of Sr, Nd, Pb and Os indicate that West Kauai lavas have a larger proportion of the Loihi component, while East Kauai lavas are more 'Mauna Loa-like', reflecting a larger contribution from the Koolau component (Figs. 7-10 and 14). The systematic variation in isotopic composition between West, Central and East Kauai may represent a change in the mantle sources from more Loihi-like to more Koolau-like as the locus of volcanism moved from west to east. A transition from Loihi-like to Koolau-like composition with time has been observed at Mauna Loa and has been interpreted to reflect the translation of the volcano over a radially zoned Hawaiian plume (Kurz et al., 1995; Hauri and Kurz,

1997). However, the possibility that the geochemical variations at Mauna Loa (and possibly at Kauai) are due to heterogeneities in the vertical dimension of the plume cannot be ruled out.

Alternatively, East and West Kauai may be two different shield volcanoes (Holcomb et al. 1997). The systematic differences in West and East Kauai lavas then imply that magma sources and plumbing systems of the two shields were distinct. Previous studies (e.g., Frey and Rhodes, 1993; Frey et al., 1994; Lassiter et al., 1996; Hauri and Kurz, 1997) have attributed the lateral variations in isotopic composition of Hawaiian lavas to the length scales of geochemical heterogeneities in the Hawaiian plume. If so, the source region of Kauai lavas must have been heterogeneous on length scales of ~20-25 km, and East and West Kauai must have maintained distinct magmatic plumbing systems. These length scales are consistent with previous suggestions from other Hawaiian shield volcanoes (e.g., Frey and Rhodes, 1993).

On the Kauai shield, geochemical variations are erratic and occur on timescales of 100 years (Fig. 6a). The magnitudes and timescales of the isotopic variability from Kauai are similar to that documented from Kilauea (Pietruszka and Garcia, 1999a). In comparison, there are no large variations in the isotopic composition of tholeiites in the last 200 kyr of the shield building stage from Mauna Kea (Hauri et al., 1996; Kurz et al., 1996; Lassiter et al., 1996), while at Mauna Loa geochemical variations are present on timescales of 10^3 years but appear to be monotonic (Kurz et al., 1995). The erratic geochemical variations in Kauai shield lavas likely reflect rapid changes in the composition of the parental magma supplying the magma reservoir. Variations in the parental magma composition can appear in the chemistry of the erupted lavas as a result

of a small magma reservoir size. In general, lavas that tap a small-volume magma reservoir can record the variations in composition of the parental magma supplying the reservoir in contrast to lavas that sample relatively large magma bodies, where the geochemical variations will be strongly damped (Albarède 1993).

Following the approach of Pietruszka and Garcia (1999b) we have estimated the magma residence time from variations in Sr isotope ratios in West Kauai lavas. The magma residence time (τ_m) is defined as:

$$\tau_m \cong \frac{C_{Sr}^{in}}{C_{Sr}^{res}} \frac{R_{Sr}^{in} - R_{Sr}^{res}}{dR_{Sr}/dt}$$

The superscript 'in' and 'res' refer to the input magma and reservoir magma respectively. The variable C represents the concentration, R the isotope ratio and dR/dt the rate of change of this ratio in the lavas. The decrease in $^{87}Sr/^{86}Sr$ from 0.70365 to 0.70345 occurs over ~500 years (based on vector group timescale). Assuming that the input magma had an $^{87}Sr/^{86}Sr$ ratio and Sr concentration comparable to Hawaiian post-erosional lavas (0.703 and 500 ppm respectively; e.g., Reiners and Nelson, 1998), the residence time in the magma reservoir is ~1450 years. The calculated residence time is comparable to the estimates from the Kilauea east rift zone (Cooper et al., 2001). Since $V = \tau_m \times Q^{in}$, where V is the volume of the magma reservoir and Q^{in} is the magma supply rate, an estimate of the magma residence time allows us to compute the approximate volume of the crustal magma reservoir. On Kilauea the average magma supply rate in the 20th century was ~0.1 km^3/yr (Denlinger, 1997). Assuming magma supply rates at Kauai were comparable, the volume of the magma reservoir on Kauai would be ~150 km^3, similar to estimates of 160-270 km^3 for Kilauea (Ryan 1988; Denlinger 1997). Therefore, the lack of large non-

monotonic variations at Mauna Kea and Mauna Loa may be related to a larger magma reservoir compared to Kauai or Kilauea, which significantly damped the chemical variations in the composition of the parental magma. Alternatively, Mauna Kea (at least the last 200 kyr of the shield stage) and Mauna Loa magmas may have been derived from well-mixed sources. Geochemical data from a longer stratigraphic section are required to determine whether the large isotopic variations we document were characteristic during the entire evolution of the Kauai shield.

4.3. Implications for the Hawaiian Plume

Models for the Hawaiian plume are often based on the notion that the highest $^3He/^4He$ ratios occur in the oldest tholeiites (e.g., Kurz et al., 1995; Kurz et al., 1996; Valbracht et al., 1996). To explain this observation, Valbracht et al. (1996) proposed a model that invokes an early separation of a CO_2 dominated melt phase from the plume at depths of about 100 km. The noble gases, but not the lithophile tracers, partition into this gas-rich melt. The melt phase migrates ahead of the buoyantly upwelling plume and metasomatises the lithosphere. Conductive heating by the ascending plume then induces melting of the metasomatised lithosphere forming the pre-shield Loihi stage, characterized by high $^3He/^4He$ ratios (30 R_A) and depleted Sr and Nd isotopic composition. Subsequent melting of the helium-depleted plume and mixing with asthenospheric material then yields the shield stage tholeiites dominated by lower $^3He/^4He$ (< 20 R_A) and more enriched Sr, Nd and Pb isotopic composition manifested in lavas from Mauna Loa and Koolau. However, our new $^3He/^4He$ data from the shield building stage of Kauai do not support this hypothesis. $^3He/^4He$ ratios of 17-28 R_A

observed in Kauai tholeiites demonstrate that high $^{3}He/^{4}He$ ratios are not restricted to the pre-shield (Loihi) stage of Hawaiian volcanism and can be sampled during the shield building stage. In addition, the model by Valbracht et al. (1996) suggests decoupling of helium from other lithophile tracers but is not supported by He, Sr, Nd and Pb isotopic ratios from most Hawaiian volcanoes (e.g., Kurz et al., 1995; Eiler et al., 1996). Therefore, we rule out the model of Valbracht et al. (1996) as a major process in Hawaiian magmatism.

Passage of the Pacific lithosphere over a radially zoned Hawaiian plume may explain the temporal geochemical variability of Hawaiian shield volcanoes (e.g., Kurz et al., 1995; Hauri et al., 1996; Lassiter et al., 1996). Kurz et al. (1995) suggested that primitive undegassed mantle (Loihi-component) is the plume source material, which entrains passively upwelling mantle material. He, Sr, Nd, and Pb are incompatible elements and due to melting of the buoyantly upwelling plume become increasingly depleted in the plume material at shallower depths. The geochemical difference between lavas at Loihi, Kilauea, and recent Mauna Loa result from tapping the plume at progressively shallower depths and by dilution of the plume signal by melts from entrained mantle and asthenosphere. The model by Kurz et al. (1995) suggests a steady decrease in the isotopic signatures of the Loihi-component during the evolution of a single volcano. For example, $^{3}He/^{4}He$ ratios would be highest in the pre-shield stage (Loihi; 20-30 R_A), intermediate in the shield stage (Kilauea; 10-20 R_A), and decreasing to MORB values of 8 R_A at the end of the shield building stage (recent Mauna Loa lavas). Because only the last 10-15% of a volcano's history is exposed subaerially (Stolper et al.

1996) the model by Kurz et al. (1995) would not predict Loihi-like $^{3}He/^{4}He$ ratios to be present in subaerial Kauai shield lavas.

Hauri et al. (1996) and Lassiter et al. (1996) suggested an alternative distribution of the components in the Hawaiian plume. They proposed that the Koolau component comprises the core of the plume and is surrounded by entrained lower mantle material (Loihi component). However, models that suggest that the mantle components are distributed radially predict smooth and systematic changes in the isotopic composition of the lavas with time. The rapid excursions in isotopic composition of Kauai lavas (Fig. 2) indicate that the different mantle components were not sampled systematically during the evolution of the Kauai shield and, thus, cannot be explained by any of the radially zoned plume models (e.g., Kurz et al., 1995; Hauri et al., 1996; Lassiter et al., 1996). In addition, the HSDP drill hole data at Mauna Kea demonstrates that shield lavas need not be dominated by Loihi-like $^{3}He/^{4}He$ ratios (Kurz and Curtice, 2000). Thus, each shield may be characterized by distinctive geochemical patterns. In summary, although entrainment of ambient mantle by rising plumes might produce heterogeneities in the plume, a radially zoned plume that has remained in steady state, cannot explain the temporal evolution of all Hawaiian volcanoes.

The isotopic compositions of Kauai lavas suggest that the proportion of the Loihi component in the Hawaiian plume has varied with time (Fig 14). While progressive depletion of incompatible elements in the plume probably occurs during the evolution of a single volcano (Kurz et al., 1995), variations in the vertical distribution of mantle components in the Hawaiian plume may be the major contributor to temporal geochemical variability and inter-shield isotopic differences. Such variations could result

from heterogeneities in D'' from where the Hawaiian plume might originate (Fouch et al., 2001) or through time-varying entrainment of ambient mantle by the upwelling plume. Seismic velocity anomalies and anisotropies reflect thermal, and possibly chemical, heterogeneities in deep mantle layers such as D'' (Sidorin et al., 1999; Fouch et al., 2001). Since the rate of entrainment of material by an upwelling plume is proportional to the temperature difference between the plume head and ambient mantle and inversely proportional to the viscosity of the plume material (Griffiths and Campbell, 1990), a consequence of the thermal heterogeneities in the plume would be *variable* entrainment of ambient mantle by the upwelling plume. Thus, the proportion and vertical distribution of the components in the Hawaiian plume would be expected to change with time.

5. Conclusion

We measured He, Sr, Nd, Pb, Os and major and trace elements in stratigraphically controlled lavas from Kauai. Based on our data we conclude:

- High $^{3}He/^{4}He$ ratios (> $20R_A$) are present during the shield building stage of Hawaiian volcanism. This observation strongly argues against helium depletion in the plume by early melts that are sampled during the pre-shield stage of Hawaiian volcanism (e.g., Valbracht et al., 1996).
- Mixing between the Koolau, Kea, and Loihi components (e.g., Eiler et al., 1996; Hauri 1996) does not explain isotopic variability in Kauai shield lavas. Addition of a fourth component with the isotopic characteristic of Hawaiian post-shield and post-erosional basalts can explain the isotopic composition of Kauai shield lavas.

- Correlated shifts in isotopic ratios and Ca/Al ratios in Kauai tholeiites support the hypothesis that the sources of Hawaiian lavas are heterogeneous in their major element chemistry (Hauri, 1996; Hauri and Kurz, 1997).
- Systematic differences in geochemistry of East and West Kauai lavas may reflect a progressive sampling from the Loihi-component to the Koolau component, which has previously been attributed to the spatial distribution of the mantle components in the Hawaiian plume (e.g., Hauri and Kurz, 1997). Alternately, East and West Kauai are two distinct shield volcanoes (Holcomb et al., 1997) that maintained different magma sources and plumbing systems.
- The erratic geochemical variations in Kauai shield lavas compared to Mauna Kea or Mauna Loa may be the result of a smaller magma reservoir on Kauai.
- The vertical distribution, particularly of the high $^{3}He/^{4}He$ component, has changed significantly over the evolution of the Hawaiian plume. Coupled with the rapid variation in geochemical variations seen in West Kauai, our data require complex geochemical heterogeneities that are not accounted for in the radially zoned plume models.

References

Abouchami W., Hofmann A. W., and Galer S. J. G. (2000) High precision lead isotope anatomy of Mauna Loa and Mauna Kea. *Chem. Geol.* **169**, 187-209.

Albarède F. (1993) Residence time analysis of geochemical fluctuations in volcanic series. *Geochim. Cosmochim. Acta* **57** 615-621.

Bogue S. W. and Coe R. S. (1984) Transitional paleointensities from Kauai, Hawaii, and geomagnetic reversal model. *J. Geophys. Res.* **89**, 10341-10354.

Bogue S. W. (2001) Geomagnetic field behavior before and after the Kauai reverse-normal polarity transition. *J. Geophys. Res.* **106**, 447-461.

Cande S. C. and Kent D.V. (1995) Revised calibration of the geomagnetic polarity timescale for the Late Cretaceous and Cenozoic. *J. Geophy. Res.* **100**, 6093-6095.

Chen C. –Y. and Frey F. A. (1985) Trace element and isotopic geochemistry of lavas from Haleakala volcano, East Maui, Hawaii: implications for the origin of Hawaiian lavas. *J. Geophys. Res.* **90**, 8743-8768.

Clague D. A. and Dalrymple G. B. (1988) Age and petrology of alkalic postshield and rejuvenated-stage lava from Kauai, Hawaii. *Contrib. Mineral Petrol.* **99**, 202-218.

Clague D. A. and Dalrymple G. B. (1989) Tectonics, geochronology, and origin of the Hawaiian-Emperor chain. In *The Geology of North America: The Eastern Pacific Ocean and Hawaii.* (eds. E. L. Wintere, D. M. Hussong, R. W. Decker), Geol. Soc. Am., Boulder, CO, pp188-217.

Condomines M., Gonvold K., Hooker P. J., Muehlenbachs K., O'Nions R. K., Oskarsson N., and Oxburg E. R. (1983) Helium, oxygen, strontium and neodymium isotopic relationships in Icelandic volcanics. *Earth Planet. Sci. Lett.* **66**, 125-136.

Cooper K. M., Reid M. R., Murrell M.T., and Clague D. A. (2001) Crystal and magma residence at Kilauea Volcano, Hawaii: ^{230}Th-^{226}Ra dating of the 1955 east rift eruption. *Earth Planet. Sci. Lett.* **184**, 703-718.

Denlinger R. P. (1997) A dynamic balcance between magma supply and eruption rate at Kilauea Volcano, Hawaii. *J. Geophys. Res.* **102**, 18091-18100.

DePaolo D. J. (1996) High-frequency isotopic variations in the Mauna Kea tholeiitic basalt sequence: Melt zone dispersivity and chromatography. *J. Geophys. Res.* **101**, 11855-11864.

Eiler J. M., Farley K. A., Valley J. W., Hofmann A.W., and Stolper E.M. (1996) Oxygen isotope constraints on the sources of Hawaiian volcanism. *Earth Planet. Sci. Lett.* **144**, 453-467.

Eiler J. M., Farley K. A., and Stolper E. M. (1998) Correlated helium and lead isotope variations in Hawaiian lavas. *Geochim. Cosmochim. Acta* **62**, 1977-1984.

Farley K. A. and Neroda E. (1998) Noble gases in the Earth's mantle. *Annu. Rev. Earth Planet. Sci.* **26**, 189-218.

Farley K. A., Natland J. H., and Craig H. (1992) Binary mixing of enriched and undegassed (primitive?) mantle components (He, Sr, Nd, Pb) in Samoan lavas. *Earth Planet. Sci. Lett.* **111**, 183-199.

Fouch M. J., Fischer K. M., and Wysession M. E. (2001) Lowermost mantle anisotropy beneath the Pacific: Imaging the source of the Hawaiian plume. *Earth Planet. Sci. Lett.* **190**, 167-180.

Frey F. A. and Rhodes J. M. (1993) Intershield geochemical differences among Hawaiian volcanoes: Implications for source compositions, melting processes, and magma ascent paths. *Royal Soc. Lond. Philo. Trans., ser. A.* **342**, 121-136.

Frey F. A., Garcia M. O., and Roden M. F. (1994) Geochemical characteristics of Koolau volcano: Implications for intershield geochemical differences among Hawaiian Volcanoes. *Geochim. Cosmochim. Acta* **68**, 1441-1462.

Ghiorso M. S. and Sack R. O. (1995) Chemical mass-transfer in magmatic process. 4. A revised and internally consistent thermodynamic model for the interpolation and extrapolation of liquid-solid equilibria in magmatic systems at elevated temperatures and pressures. *Contrib. Mineral. Petrol.* **119**, 197-212.

Graham D. W., Castillo P. R., Lupton J. E., and Batiza R. (1996) Correlated He and Sr isotope ratios in south Atlantic near-ridge seamounts and implications for mantle dynamics. *Earth Planet. Sci. Lett.* **144**, 491-503.

Graham D. W., Jenkins W. J., Schilling J. G., Thompson G., Kurz M. D., and Humphris S. E. (1992) Helium isotope geochemistry of mid-ocean ridge basalts from the South Atlantic. *Earth Planet. Sci. Lett.* **110**, 133-148.

Griffiths R. W. and Campbell I. H. (1990) Stirring and structure in mantle plumes. *Earth Planet. Sci. Lett.* **99**, 66-78.

Hauri E. K. (1996) Major-element variability in the Hawaiian mantle plume. *Nature* **382**, 415-419.

Hauri E. H. and Kurz M. D. (1997) Melt migration and mantle chromatography: a time-series Os isotope study of Mauna Loa Volcano, Hawaii. *Earth Planet. Sci. Lett.* **144**, 93-108.

Hauri E. H., Lassiter J. C., and DePaolo D. J. (1996) Osmium isotope systematics of drilled lavas from Mauna Loa, Hawaii. *J. Geophys. Res.* **101**, 11793-11806.

Herzberg C. and Zhang J. (1996) Melting experiments on anhydrous peridotite KLB-1: composition of magmas in the upper mantle and transition zone. *J. Geophys. Res.* **1010**, 8271-8295.

Hilton D. R., Barling J., and Wheller G. E. (1995) Effect of shallow level contamination on the helium isotopic systematics of ocean-island lavas. *Nature* **373**, 330-333.

Hilton D. R., Hammerschmidt K., Teufel S., and Friedrichsen H. (1993) Helium isotope characteristic of Andean geothermal fluids and lavas. *Earth Planet. Sci. Lett.* **120**, 265-282.

Hirschmann M. M. and Stolper E. M. (1996) A possible role for garnet pyroxenite in the origin of the 'garnet signature' in MORB. *Contrib. Mineral. Petrol.* **124**, 185-208.

Hirschmann M. M., Ghiorso M. S., and Stolper E. M. (1999) Calculation of peridotite partial melting from thermodynamic models of minerals and melts. II. Isobaric variations in melts near the solidus and owing to variable source composition. *J. Petrol.* **40**, 297-313.

Hofmann A. W., Jochum K. P., Seufert M., and White W. M. (1986) Nb and Pb in oceanic basalts – new constraints on mantle evolution. *Earth Planet. Sci. Lett.* **79**, 33-45.

Holcomb R. T., Champion D., and McWIlliams M. (1986) Dating recent Hawaiian lava flowa using secular variation. *Geol. Soc. Am. Bull.* **97**, 829-839.

Holcomb R. T., Reiners P. W., Nelson B. K., and Sawyer N. E. (1997) Evidence for two shield volcanoes exposed on the island of Kauai, Hawaii. *Geology* **25**, 811-814.

Ito E., White W. M., and Gopel C. (1987) The O, Sr, Nd, and Pb isotope geochemistry of MORB. *Chem. Geol.* **62**, 157-176.

Klein E. M. and Langmuir C. H. (1987) Global correlations of ocean ridge basalt chemistry with axial depth and crustal thickness. *J. Geophys. Res.* **92**, 8089-8115.

Kurz M. D. (1986) Cosmogenic helium in a terrestrial igneous rock. *Nature* **320**, 435-439.

Kurz M. D. and Curtice J. M. (2000) Helium isotopic evolution of Mauna Kea Volcano: New results from the 3 km drill core. *EOS* **81**, F1343.

Kurz M. D. and Geist D. (1999) Dynamics of the Galapagos hotspot from helium isotope geochemistry. *Geochim. Cosmochim. Acta* **63**, 4139-4156.

Kurz M. D., Jenkins W. J., Schilling J. G., and Hart S. R. (1982) Helium isotopic systematics of ocean islands and mantle heterogeneity. *Nature* **297**, 43-47.

Kurz M. D., Jenkins W. J., Hart S. R., and Clague D. A. (1983) Helium isotopic variations in volcanic rocks from Loihi Seamount and the Island of Hawaii. *Earth Planet. Sci. Lett.* **66**, 388-406.

Kurz M. D., Meyer P. S., and Sigurdsson H. (1985) Helium isotopic systematics within the neovolcanic zones of Iceland. *Earth Planet. Sci. Lett.* **74**, 291-305.

Kurz M. D., Garcia M. O., Frey F. A., and O'Brien P. A. (1987) Temporal helium isotopic variations within Hawaiian volcanoes: Basalts from Mauna Loa and Haleakala. *Geochim. Cosmochim. Acta* **51**, 2905-2914.

Kurz M. D., Kenna T. C., Kammer D. P., Rhodes J. M., and Garcia M. O. (1995) Isotopic evolution of Mauna Loa Volcano: A view from the submarine southwest rift zone.

In *Mauna Loa revealed* (eds J. M. Rhodes and J. P. Lockwood J. P), American Geophysical Union Monograph 92, 289-306.

Kurz M. D., Kenna T. C., Lassiter J. C., and DePaolo D. J. (1996) Helium isotopic evolution of Mauna Kea volcano: First results from the 1-km drill core. *J. Geophys. Res.* **101**, 11781-11791.

Lassiter J. C. and Hauri E. H. (1998) Osmium-isotope variations in Hawaiian lavas: evidence for recycled oceanic lithosphere in the Hawaiian plume. *Earth Planet. Sci. Lett.* **164**, 483-496.

Lassiter J. C., DePaolo D. J., and Tatsumoto M. (1996) Isotopic evolution of Mauna Kea Volcano: Results from the initial phase of the Hawaii Scientific Drilling Project. *J. Geophys. Res.* **101**, 11769-11780.

Lassiter J. C., Hauri E. H., Reiners P. W., and Garcia M. O. (2000) Generation of Hawaiian post-erosional lavas by melting of a mixed lherzolite/pyroxenite source. *Earth Planet. Sci. Lett.* **178**, 269-284.

Lipman P. W., Rhodes J. M., and Dalrymple G. B. (1990) The Ninole basalt – Implications for the structural evolution of Mauna Loa Volcano. *Hawaii. Bull. Volcanol.* **53**, 1-19.

Macdonald G. A., Davis D. A., and Cox D. C. (1960) Geolgoy and ground-water resources of the Island of Kauai, Hawaii. *Hawaii Division of Hydrography Bulletin* **13**, 212p

McDougall I. (1979) Age of shield-building volcanism of Kauai and linear migration of volcanism in the Hawaiian island chain. *Earth Planet. Sci. Lett.* **46**, 31-42.

McKenzie D. P. and O'Nions R. K. (1991) Partial melt distributions from inversion of rare earth element concentrations. *J. Petrol.* **32**, 1021-1091.

Morgan W. J. (1971) Convection plumes in the lower mantle. *Nature* **230**, 42-43.

Patterson D. B., Farley K. A., and McInnes B. I. A. (1997) Helium isotopic composition of the Tabar-Lihir-Tanga-Feni island arc, Papua New Guinea. *Geochim. Cosmochim. Acta* **61**, 2485-2496.

Pertermann M. and Hirschmann M. M. (1999) Partial melting experiments on a MORB-like pyroxenite at 3.0 GPa and 1300°C-1500°C. *EOS* **80**, 1112.

Pietruszka A. J. and Garcia M. O. (1999a) A rapid fluctuation in the mantle source and melting history of Kilauea Volcano inferred from the geochemistry of its historical summit lavas (1790-1982). *J. Petrol.* **40**, 1321-1342.

Pietruszka A. J. and Garcia M. O. (1999b) The size and shape of Kilauea Volcano's summit magma storage reservoir: a geochemical probe. *Earth Planet. Sci. Lett.* **167**, 311-320.

Reiners P. W. and Nelson B. K. (1998) Temporal–compositional-isotopic trends in rejuvenated-stage magmas of Kauai, Hawaii, and implications for mantle melting process. *Geochem. Cosmochim. Acta* **62**, 2347-2368.

Reiners P. W., Nelson B. K., and Izuka S. K. (1998) Structural and petrologic evolution of the Lihue basin and eastern Kauai, Hawaii. *Geol. Soc. Am. Bull.* **111**, 674-685.

Rison W. and Craig H. (1983) Helium isotopes and mantle volatiles in Loihi Seamount and Hawaiian Island basalts and xenoliths. *Earth Planet. Sci. Lett.* **66**, 407-426.

Ryan M. P. (1988) The mechanics and three-dimensional internal structure of active magmatic systems: Kilauea Volcano, Hawaii. *J. Geophys. Res.* **93**, 4213-4248.

Scarsi P. (2000) Fractional extraction of helium by crushing of olivine and clinopyroxene phenocrysts: Effects of the $^{3}He/^{4}He$ measured ratio. *Geochim. Cosmochim. Acta* **64**, 3751-3762.

Schilling J. G. (1973) Iceland mantle plume: geochemical evidence along Reykjanes Ridge. *Nature* **242**, 565-571.

Sharp W. D., Turrin B. D., Renne P. R., and Lanphere M. A. (1996) The 40Ar/39Ar and K/Ar dating of lavas from the Hilo 1-km core hole, Hawaii Scientific Drilling Project. *J. Geophys. Res.* **101**, 11607-11616.

Sidorin I., Gurnis M., and Helmberger D. V. (1999) Dynamics of a phase change at the base of the mantle consistent with seismological observations. *J. Geophys. Res.* **104**, 15005-15023.

Staudigel H., Zindler A., Hart S. R., Leslie T., Chen C. Y., and Clague D. (1984) The isotope systematics of a juvenile intra-plate volcano: Pb, Nd, and Sr isotope ratios of basalts from Loihi Seamount. *Earth Planet. Sci. Lett.* **69**, 13-29.

Stille P., Unruh D. M., and Tatsumoto M. (1986) Pb, Sr, Nd, and Hf isotopic constrains on the origin of Hawaiian basalts and evidence for a unique mantle source. *Geochim. Cosmochim. Acta* **62**, 2303-2319.

Stolper, E.M., D.J. DePaolo, and D.M. Thomas (1996) The Hawaii Scientific Drilling Project: Introduction to the special section. *J. Geophys. Res.* **101**, 11,593-11,598.

Stracke A., Salters V. J. M., and Sims K. W. W. (1999) Assessing the presence of garnet-pyroxenite in the mantle sources of basalts through combined hafnium-neodymium-thorium isotope systematics. *G^3*, 1999GC000013.

Todt W., Cliff R. A., Hanser A., and Hofmann A. W. (1996) Evaluation of a 202Pb-205Pb double spike for high-precision lead isotope analysis In *Earth Process: Reading the isotopic code* (eds A.R. Basu and S. R. Hart), American Geophysical Union Monograph 95 429-437.

Valbracht P. J., Staudigel H., Honda M., McDougall I., and Davies G. R. (1996) Isotopic tracing of volcanic source regions from Hawaii: decoupling of gaseous from lithophile magma components. *Earth Planet. Sci. Lett.* **144**, 185-198.

Walter M. J. (1998) Melting of garnet peridotite and the origin of komatiite and depleted lithosphere. *J. Petrol.* **39**, 29-60.

Wasylenki L. E. (1999) Partial melting of depleted peridotite in the Earth's upper mantle and implications for generation of Mid-Ocean-Ridge basalts. Ph.D. Thesis, California Institute of Technology.

West H. B., Gerlach D. C., Leeman W. P., and Garcia M. O. (1987) Isotopic constraints on the origin of Hawaiian lavas from the Maui volcanic complex, Hawaii. *Nature* **330**, 216-220.

Wilson J. T. (1963) A possible origin of the Hawaiian Island. *Can. J. Phys.* **41**, 863-870.

Yang H. J., Frey F. A., Rhodes J. M., and Garcia M. O. (1996) Evolution of Mauna Kea Volcano: Inferences from lava compositions recovered in the Hawaii Scientific Drilling Project. *J. Geophys. Res.* **101**, 11747-11767.

Zindler A. and Hart S. R. (1986) Helium- problematic primordial signals. *Earth Planet. Sci. Lett.* **79**, 1-8.

Appendix: Complied Sr, Nd, Pb, and He data for Hawaiian shield lavas.

Island	$^{87}Sr/^{86}Sr$	εNd	$^{206}Pb/^{204}Pb$	$^{207}Pb/^{204}Pb$	$^{208}Pb/^{204}Pb$	$^{3}He/^{4}He$
Loihi	0.70353	6.01	18.22	15.48	38.09	30.1
	0.70352	6.16	18.35	15.47	38.14	26.7
	0.70354	6.81	18.43	15.49	38.16	23.1
	0.70358	6.42	18.27	15.47	38.02	27.5
	0.70368	5.99	18.45	15.48	38.19	32.1
	0.70365	6.11	18.42	15.48	38.12	22.6
	0.70353	8.10	18.38	15.49	38.11	22.7
	0.70341	6.79	18.37	15.50	38.16	24.1
	0.70335	8.08	18.26	15.48	38.05	20.9
	0.70351	8.04	18.45	15.49	38.18	24.1
	0.70355	5.25	18.37	15.46	38.14	24.1
	0.70359	6.16	18.39	15.46	38.12	20.3
Koolau	0.70439	-0.55	17.86	15.44	37.93	14.2
Mauna Kea	0.70351	7.50	18.41	15.52	38.04	7.6
	0.70352	7.35	18.49	15.46	37.97	6.0
	0.70351	7.50	18.46	15.48	37.95	8.7
	0.70356	7.45	18.41	15.46	38.00	8.2
	0.70358	7.71	18.43	15.45	37.90	7.6
	0.70354	7.47	18.46	15.45	37.95	7.2
	0.70359	7.21	18.51	15.44	37.96	7.7
	0.70362	7.42	18.50	15.43	37.96	8.8
	0.70355	7.68	18.57	15.48	38.08	10.1
	0.70352	7.19	18.60	15.48	38.09	10.1
	0.70350	7.10	18.50	15.45	38.03	11.3
	0.70360	6.92	18.47	15.47	38.01	11.0
	0.70363	7.15	18.45	15.43	37.96	11.5
	0.70354	6.99	18.55	15.45	38.04	10.7
Mauna Loa	0.70384	4.49	18.07	15.43	37.82	13.1
	0.70378	4.39	18.09	15.45	37.84	11.0
	0.70369	3.76	18.17	15.46	37.93	18.0
	0.70369	5.40	18.17	15.45	37.91	14.8
	0.70374	5.50	18.19	15.45	37.95	20.0
	0.70372	5.60	18.20	15.43	37.92	15.7
	0.70368	5.85	18.13	15.43	37.84	16.0
	0.70369	5.44	18.20	15.45	37.96	15.4
	0.70376	4.90	18.18	15.43	37.93	18.5
	0.70369	5.74	18.18	15.46	37.96	17.2
	0.70368	5.33	18.25	15.45	37.97	18.9
	0.70366	5.36	18.24	15.43	37.94	20.0
	0.70365	5.66	18.33	15.52	38.16	19.1
	0.70368	5.40	18.25	15.46	38.02	16.6
	0.70369	5.31	18.15	15.43	37.89	18.7
	0.70368	5.33	18.19	15.43	37.89	19.9
	0.70362	5.44	18.23	15.46	38.00	13.3

(continued)

Island	$^{87}Sr/^{86}Sr$	εNd	$^{206}Pb/^{204}Pb$	$^{207}Pb/^{204}Pb$	$^{208}Pb/^{204}Pb$	$^{3}He/^{4}He$
	0.70365	5.83	18.29	15.47	38.03	15.9
	0.70361	5.66	18.28	15.45	37.98	17.2
	0.70368	5.34	18.19	15.46	37.98	18.3
	0.70374	4.70	18.31	15.51	38.21	16.9
	0.70365	4.72	18.18	15.47	37.99	16.4
Kauai	0.70365	6.53	18.32	15.45	38.00	27.3
	0.70351	7.37	18.29	15.44	37.88	19.7
	0.70345	7.39	18.26	15.45	37.85	17.9
	0.70368	7.65	18.37	15.46	38.02	24.9
	0.70364	6.77	18.30	15.45	37.96	22.3
	0.70364	6.85	18.38	15.45	38.01	24.0
	0.70363	6.98	18.37	15.44	37.96	26.8
	0.70367	6.67	18.25	15.44	37.90	25.7
	0.70370	5.83	18.20	15.44	37.89	22.9
	0.70369	6.46	18.22	15.44	37.92	21.4
	0.70371	6.30	18.16	15.44	37.87	19.9
	0.70379	6.22	18.22	15.45	37.91	21.4
	0.70373	6.20	18.14	15.43	37.84	26.8

References: Hauri et al., 1996; Lassiter et al., 1996;Kurz et al., 1983; 1995; 1996; Roden et al., 1994; Staudigel et al., 1984; Kauai data is from this work.

Summary

(I) ^{3}He in the sedimentary record

To understand the delivery history of IDPs over geologic time and its relationship to terrestrial impacts, we measured He abundance and isotopic composition of a suite of pelagic limestones exposed in the Italian Apennines that were deposited between ~74 to ~39 Ma. Our results indicate that the IDP accretion rate in the Maastrichtian was fairly constant, except for probable but minor increases between ~70.5 Ma and 68 Ma, and at ~66 Ma. These increases are not likely to be related to showers of long-period comets, but may reflect random events in the asteroid or Kuiper belts.

High-resolution ^{3}He data across the K/T boundary (63.9 to 65.4 Ma) indicate a low and invariant IDP accretion rate. Thus, the K/T impactor was not associated with enhanced solar system dustiness and, hence, not a member of a comet shower. Instead, the K/T impactor is more likely to have been a single earth-crossing asteroid or comet. Using ^{3}He as a constant-flux proxy of sedimentation rate implies deposition of the K/T boundary clay in 10 ± 2 kyr and the impact ejecta layer in 60 years. These results indicate that the mass-extinction at the K/T boundary was catastrophic, ruling out volcanism and sea level changes as important factors and requiring an extremely rapid faunal turnover rate.

We observe a 2-4 fold increase in the IDP accretion rate close to the P/E boundary followed by a factor of three decay over a ~4-5 Myr period. This increase does not exhibit the temporal pattern expected from a comet shower arising from a gravitational perturbation of the Oort cloud. Instead, our data are more consistent with an increase in

IDP accretion resulting from a major collision in the asteroid belt or, alternatively, the Kuiper belt.

The absence of appropriate peaks in the ^{3}He accretion rate between 74 to 39 Ma provide strong evidence against recurrent comet showers with periods less than 38 Myrs. In general, ^{3}He measurements from the Apennine sedimentary rocks do not support the hypothesis that periodic impacts drive terrestrial mass extinction events.

Along with the ^{3}He measurements from the Apennine limestones we also obtained ^{4}He concentrations, which record temporal changes in the flux or composition of terrigenous matter. In the last 4 Myrs of the Cretaceous, the concentration of ^{4}He in the detrital component rises by 300%. This rise tracks an increase in the seawater $^{87}Sr/^{86}Sr$ ratio, suggesting a globally significant change in the composition of continental detritus delivered to the oceans, possibly arising from increased continental weathering.

The work presented in this dissertation, along with previous studies (e.g., Patterson et al., 1998), demonstrates the retention of ^{3}He in sediments over geologic time. To better characterize the ^{3}He carrier(s) responsible for the long-term retention of ^{3}He in sediments, we performed chemical leaching, stepped heating, and sieving experiments. Our results suggest that organic matter (including fullerenes), diamonds, spinels, SiC, graphite, and amorphous carbon are not the primary carrier phase(s) of ^{3}He, although they may account for up to ~10% of the total ^{3}He. However, our data are consistent with either extraterrestrial silicates, ilmentite, or Fe-Ni sulfides as the principal carrier phase(s) of extraterrestrial ^{3}He.

Stepped heating experiments indicate that the ^{3}He release profiles as a function of temperature in both the magnetic and non-magnetic fractions in sediments are similar,

suggesting a single carrier phase that may be magnetite or more probably associated with magnetite. Magnetite could be associated with the ^{3}He carrier phase(s) either as composite grains, inclusions, or nm thick rims around the grains. Further, if we assume that ^{3}He is homogeneously distributed in IDPs, our stepped heating experiments indicate that ~80% of the ^{3}He might be retained in seafloor sediments after 50 Myrs while only 35% will remain in sedimentary rocks exposed on the Earth's surface. Although the absolute values of the ^{3}He loss will likely depend upon the ^{3}He concentration profile within the IDPs, our results qualitatively indicate that continental sections will have lost systematically more ^{3}He than deep-sea sediments. This conclusion should be taken into account while comparing ^{3}He flux computed from different stratigraphic sections that have been subjected to distinct burial temperatures.

(II) Geochemistry of shield-stage lavas from Kauai, Hawaii

To investigate the sources of Hawaiian magmatism and the chemical evolution of the Hawaiian plume, we carried out the first systematic isotopic (He, Sr, Nd, Pb, and Os) and major and trace element study of stratigraphically controlled lavas from the oldest of the main Hawaiian islands, Kauai. Based on our data we conclude that high $^{3}He/^{4}He$ ratios ($> 20R_A$) are present during the shield building stage and not just restricted to the pre-shield stage of Hawaiian volcanism. This observation strongly argues against helium depletion in the plume by early melts that are sampled during the pre-shield stage. Further, analyses of the Kauai data suggest that source(s) of Hawaiian post-shield and post-erosional basalts are involved in the genesis of Kauai shield lavas.

There are systematic differences in geochemistry of East and West Kauai lavas that may reflect a progressive sampling from the Loihi-component to the Koolau component, previously attributed to the translation of the Pacific plate over a radially zoned Hawaiian plume. Alternatively, East and West Kauai are two distinct shield volcanoes (Holcomb et al., 1997) that maintained different magma sources and plumbing systems. Calculated magma residence time and magma reservoir volume for Kauai is similar to values from Kilauea. This computation also suggests that the erratic geochemical variations in Kauai shield lavas compared to Mauna Kea or Mauna Loa may be the result of a smaller magma reservoir on Kauai.

The vertical distribution, particularly of the high $^{3}He/^{4}He$ component, has changed significantly over the evolution of the Hawaiian plume. Coupled with the rapid variation in geochemical variations seen in West Kauai, our data require complex geochemical heterogeneities that are not accounted for in the radially zoned plume models.